UNIVERSITÀ
degli STUDI
di CATANIA

Dipartimento di Scienze Biologiche, Geologiche e Ambientali

Dottorato di Ricerca in Scienze Geologiche Biologiche e Ambientali

Laura Borzì

———

Shoreline evolution in the Gulf of Gela (Southern Sicily):

diachronic and environmental analysis of two study cases by GIS tools

_____

Ph.D. Thesis
_____

SUPERVISOR

Professor Agata Di Stefano

CO- SUPERVISOR

Dr. Domenico Chiarella

COORDINATOR

Professor Agata Di Stefano

XXXII CYCLE (2016 – 2019)

Acknowledgements

CONTENTS

List of Tables

List of figures

Research highlights

- The Gulf of Gela (Southern Sicily, Italy) plays a key role in the economic strategies of the regional management;

- The Gulf of Gela coincides with the coastal sub-cell of II-order n. 4.2 identified by the Regional Plain against Coastal Erosion (Regione Siciliana, 2020) and the shoreline and environmental changes are the study object of the present research work;

- A combined methodology has been used for the first time to study the shoreline evolution of the sub-cell n. 4.2 over mid- and long-term period;

- A negative coastline evolution trend has been mainly found within the Gulf of Gela;

- Significant erosion phenomena have been detected nearby the Licata harbour, where the Southern Imera river mouth has profoundly changed, retreating up to hundreds of meters;

- Erosional phenomena have been mainly detected where high coastal armouring impact and high level of fragmentation have been found;

Extended abstract

The aim of this Ph.D. thesis was to investigate the evolution of the coastline within the Gulf of Gela (Southern Sicily, Italy), applying, for the first time, a combined methodology that outlines, on one hand, the shoreline changes and, on the other hand, allows to assess the main environmental variations, as the fragmentation or disappearance of dune systems and the implementation of maritime structures insisting on the coast. Some previous works have studied the shoreline evolution within the Gulf, but an obsolete methodology has been adopted or an incomplete analysis has been performed due to the lack of data on the entire stretch of coast.

The Gulf of Gela coincides with the second order coastal sub-cell n. 4.2 identified by the Regional Plan against Coastal Erosion and falling within the first order coastal sub-cell that extends from Capo Passero Island to Capo San Marco (Regione Siciliana, 2020). The physiographic limits of the second order physiographic unit n. 4.2 are represented by the port of Licata (AG) and Punta Braccetto (RG). The study area was divided into 5 sectors: 1) it extends from the Licata harbour to the promontory where there is the Falconara Castle, a stretch of coast mainly characterised by sandy beaches; 2) from the Falconara Castle to the port of Gela, with a predominantly low and sandy coast, except for the cliff where the Manfria Tower is set; 3) the area that goes from the Gela harbour to the Scoglitti one, it is the longest sector that has been studied and the coastline is mainly low and sandy; 4) from the Scoglitti harbou to the Randello promontory, where high and low sandy coasts alternate; 5) from the Randello promontory to Punta Braccetto cape, where there is a beach 2 km wide, and a well-preserved and wide dune system still resists. The study focused on the analysis of the shoreline variations, but the investigation of the environmental changes that have affected the coastal area has been performed, considering the progressive fragmentation of the dune systems and the impact of coastal works. The present work methodology therefore included the analysis of shoreline variations over the long and medium term, covering a total time span of about 60 years, the application of the coefficient of technogenous impact of coastal maritime works (coefficient of technogenous impact, Aybulatov & Artyukhin, 1993), the assessment of the level of fragmentation of dune systems carried out through the calculation of the fragmentation index (Molina et al, 2020), and the grain-size and textural analysis of beach sediments to investigate the current evolutionary state of the studied coastlines.

The cartographic dataset counts: i) photographs of IGM areas (1955, 1966), ii) orthophotos of the National Geoportal (1989, 2000, 2006, 2012), iii) UAV (Unmanned Aerial Vehicle) image acquired in 2018 in the area of sector n. 5. The shorelines were drawn for each image and the statistical indexes (SCE, NSM, WLR) were computed using the Digital Shoreline Analysis System (DSAS), an application of the ESRI ArcGIS© software.

The coefficient of technogenuous impact is the ratio between the total length of the shoreline and the length of all the maritime infrastructures insisting on that given stretch of coast. The coefficient is expressed through qualitative classes that vary from minimum to extreme.

The fragmentation index (F) was first proposed by Molina et al. (2020) and vaguely inspired by the coefficient of technogenuous impact. It is computed as the ratio between the breaks within each identified dune system and the total length of the system. As for the impact coefficient of coastal maritime works, the index is expressed with qualitative classes that vary from zero fragmentation to very high level of fragmentation.

Sedimentological analyses were carried out on sediment samples taken in summer and winter for three consecutive years, in correspondence with the main and recognizable morphological elements of the beach. The samples were collected at two beaches chosen along the coast between Licata and Gela, and along a transect at Punta Braccetto beach. The statistical parameters used to describe the granulometric characteristics of the samples are those proposed by Folk & Ward (1957).

The shoreline change analysis shown that within sector 1, from the port of Licata to the Castle of Falconara, the evolutionary trend over the medium term is mainly negative. It is worth to note that significant retreat has been recorded between the Licata harbour and the breakwaters located eastward Southern Imera river mouth, with a maximum negative rate of – 3,15 m/year. The scenario described over the medium-term was also confirmed by the analysis performed over the long-term period, with a maximum retreat rate of -6,7 m/year observed again eastward the Southern Imera river mouth. Significant accretion has been registered where eleven breakwaters are set, even though the Shoreline Change Envelope (SCE) index showed that the main depositional phenomena occurred during the decade between 1955 and 1966, whereas progressive and constant landward migration has been observed between 1966 and 1989. Sector n. 2 and 3 showed mainly a stable trend, even if the described curve is asymmetrically negative. Significant depositional phenomena

were found up-drift the Scoglitti harbour, the northern dike has been repeatedly implemented between the 1970s and 1980s and fnished in 2008. It could be assumed that this work modified the sediment littoral transport affecting the evolution of the coastline within sector no. 5, located a few kilometres southward the Scoglitti harbour. Within sector n. 5 the medium-term analysis showed mainly a stable trend, and, partly, erosive phenomena have been detected, but the long-term analysis and the SCE index revealed that this sector did not face any retreat over the period between 1955 and 2012, and it experienced a stability state and minimal moderate accretion over the period between 1955 and 1989 and the trend has changed between 1989 and 2012, when slight erosion phenomena have been recorded.

The analysis of beach sediments confirmed what emerged from the analysis of shoreline variations, i.e. a currently unstable beach profile with a tendency to erosion within sector 1, and a substantially stable beach profile in those sectors where there is still a well-preserved dune ridge of significant size.

The study showed that the areas most affected by the most intense erosion phenomena are those where the highest levels of fragmentation of dune systems have been recorded and where the coefficient of technogenuos impact is higher.

The combined approach used to understand the evolution of the Gulf of Gela has filled the lack of updated data and obtained through an integrated methodology widely used and recognised within the scientific community. In fact, the need has emerged to adopt a shared methodology at regional level in the study of complex coastal systems. Moreover, to complete and support what has emerged here, bathymetric and granulometric analysis of the submerged beach and analysis of the transport of coastal sediments would allow to deepen and frame the coastal dynamics and support the data obtained from this thesis work.

Keywords: shoreline evolution, dune fragmentation, DSAS, coastal armouring

Extended abstract (Italian language)

EVOLUZIONE DELLA LINEA DI COSTA NEL GOLFO DI GELA (SICILIA MERIDIONALE): ANALISI DIACRONICA ED AMBIENTALE DI DUE CASI STUDIO TRAMITE SOFTWARE GIS

Il presente lavoro di tesi di Dottorato ha avuto come obiettivo quello di investigare l'evoluzione della linea di costa all'interno del Golfo di Gela (Sicilia Meridionale, Italia), applicando, per la prima volta, una metodologia combinata che delinea, da un lato, l'avanzamento e/o l'arretramento del litorale in esame, e dall'altro, consente di valutare le principali variazioni ambientali, come la frammentazione o la scomparsa di sistemi dunali e/o la realizzazione di opere marittime che hanno interessato la fascia costiera studiata, ed è stata applicata sull'intero tratto di costa. Alcuni lavori precedenti hanno in parte affrontato lo studio del litorale, o di alcune zone ricadenti all'interno dell'area, ma risultano, ad oggi, obsoleti per la metodologia adottata o incompleti per la mancanza di dati sull'intero tratto di costa.

Il Golfo di Gela coincide con l'unità fisiografica di secondo ordine individuata dal Piano Regionale contro l'Erosione Costiera e ricadente all'interno dell'unità fisiografica di primo ordine che si estende da Isola di Capo Passero a Capo San Marco. I limiti fisiografici dell'unità fisiografica di secondo ordine n. 4.2 sono rappresentati dal porto di Licata (AG) e da capo di Punta Braccetto (RG). L'area di studio è stata a sua volta suddivisa in 5 settori: 1) si estende dal porto di Licata al promontorio dove è presente il Castello di Falconara, tratto di costa prevalentemente caratterizzato da spiagge sabbiose; 2) dal Castello di Falconara al porto di Gela, con costa prevalentemente bassa e sabbiosa, ad eccezione del tratto a falesia in corrispondenza dell'area dominata da Torre Manfria; 3) l'area che va dal porto di Gela al porto di Scoglitti, è il tratto di costa esaminato con estensione maggiore e il litorale si presenta esclusivamente basso e sabbioso; 4) dal porto di Scoglitti al promontorio di cava Randello, in cui si alternano coste alte e basse e sabbiose; 5) dal promontorio di cava Randello a capo di Punta Braccetto, dove è localizzata una spiaggia di ca. 2 km alle cui spalle si estende un sistema dunale ben conservato e ampio. Lo studio è stato focalizzato sull'analisi delle variazioni della linea di riva, ma ha incluso un'indagine sui cambiamenti ambientali che hanno interessato la zona costiera, considerando la progressiva frammentazione dei sistemi dunali e l'impatto delle opere costiere. Il lavoro ha previsto, quindi, l'analisi delle variazioni della linea di riva su lungo e medio termine, coprendo un arco temporale totale di circa 60 anni, l'applicazione del coefficiente di impatto delle opere marittime costiere (*coefficient of technogenous impact*, Aybulatov & Artyukhin, 1993), la valutazione del livello di

frammentazione dei sistemi dunali effettuato tramite il calcolo dell'indice di frammentazione (Molina et al., 2020), e lo studio delle caratteristiche granulometriche e tessiturali dei sedimenti di spiaggia per indagare sullo stato evolutivo attuale dei tratti di costa studiati.

Per l'analisi dell'evoluzione della linea di riva, il materiale cartografico utilizzato comprende: i) *fotografie aree IGM (1955, 1966), ii) ortofoto del Geoportale Nazionale (1989, 2000, 2006, 2012), iii) immagine UAV (Unmanned Aerial Vehicle)* acquisita nel 2018 in corrispondenza dell'area del settore n. 5. Le linee di riva sono state tracciate per ciascuna immagine e gli indici statistici (SCE, NSM, WLR) sono stati calcolati tramite il Digital Shoreline Analysis System (DSAS), applicativo dei software ESRI ArcGIS©.

Il coefficiente d'impatto delle opere marittime costiere viene calcolato come il rapporto tra la lunghezza totale della linea di riva e la lunghezza di tutte le infrastrutture marittime che insistono su quel dato tratto di costa. Il coefficiente viene espresso tramite classi qualitative che variano da minimo ad estremo.

L'indice di frammentazione (F) è stato per la prima volta proposto da Molina et al. (2020) e vagamente ispirato al coefficiente d'impatto delle opere marittime costiere. Difatti, l'indice viene computato come il rapporto tra le interruzioni identificate all'interno di ogni singolo sistema dunale identificato e la lunghezza totale del sistema. Come per il coefficiente di impatto delle opere marittime costiere, l'indice viene espresso con delle classi qualitative che variano da frammentazione nulla a livelli di frammentazione molto alta.

Le analisi sedimentologiche sono state eseguite su campioni di sedimento prelevati in estate e in inverno per tre anni consecutivi, in corrispondenza dei principali e riconoscibili elementi morfologici della spiaggia. I campioni sono stati raccolti presso due spiagge scelte lungo il litorale tra Licata e Gela, e lungo un transetto presso la spiaggia di Punta Braccetto. I parametri statistici utilizzati per descrivere le caratteristiche granulometriche dei campioni sono quelli proposti da Folk & Ward (1957).

Dall'analisi dell'evoluzione della linea di riva è emerso che all'interno del settore 1, dal porto di Licata al Castello di Falconara, la tendenza evolutiva su medio periodo è prevalentemente negativa. In particolar modo, tra il porto di Licata e i frangiflutti posti ad est della foce del fiume Imera Meridionale, è stato registrato un arretramento significativo della linea di costa, con un tasso di arretramento massimo osservato pari a – m/year. Lo scenario descritto su medio periodo ha trovato riscontro anche su lungo

periodo, con un tasso di arretramento massimo ottenuto subito ad est della foce del fiume Imera Meridionale (- m/year). Significativa l'accrezione registrata nell'area dove è stata ubicata una barriera emersa composta da undici frangiflutti (WLR massimo pari a m/year), anche se dal calcolo dell'indice SCE è emerso che i principali fenomeni deposizionali si sono verificati durante il decennio tra il 1955 e il 1966, e tra il 1966 e il 1989 è stato invece osservato un progressivo e costante arretramento della costa. Il tratto di costa dei settori 2 e 3, incluso tra il Castello di Falconara e il porto di Scoglitti, ha mostrato un andamento prevalentemente stabile, anche se la curva descritta risulta asimmetricamente negativa. Fenomeni deposizionali rilevanti sono stati rilevati nell'area sovraflutto il porto di Scoglitti, di cui la diga settentrionale è stata ripetutamente implementata tra gli anni settanta e ottanta e definitivamente completata nel 2008. E' probabile che questa opera abbia modificato il trasporto litoraneo dei sedimenti in modo tale da influire sull'evoluzione della linea di costa all'interno del settore n. 5, situato pochi chilometri a sud del porto di Scoglitti, dove l'analisi su medio periodo ha evidenziato un trend stabile e, in alcune parti, erosivo, diversamente da quanto è stato messo in evidenza dall'analisi su lungo periodo e dal calcolo dell'indice SCE, da cui è emerso che il settore n. 5 è rimasto prevalentemente stabile e, in alcune zone, tendente ad una moderata accrezione, nell'arco temporale tra il 1955 e il 1989, ma il trend ha subito un'inversione di tendenza tra il 1989 e il 2012, registrando anche lievi fenomeni erosivi.

L'analisi dei sedimenti di spiaggia ha confermato quanto emerso dall'analisi delle variazioni della linea di riva, ovvero un profilo di spiaggia attualmente instabile con tendenza all'erosione all'interno del settore 1, e di un profilo di spiaggia sostanzialmente stabile in corrispondenza di quei settori dove è ancora presente un cordone dunale ben conservato e di dimensioni significative.

Dallo studio, è emerso che le aree maggiormente colpite da fenomeni erosivi più intensi sono quelle in cui sono stati registrati i maggiori livelli di frammentazione dei sistemi dunali e dove il coefficiente di impatto delle opere marittime costiere è più alto.

L'approccio combinato utilizzato per comprendere l'evoluzione del Golfo di Gela ha colmato la mancanza di dati aggiornati e ottenuti inoltre mediante una metodologia integrata e largamente utilizzata e riconosciuta all'interno della comunità scientifica. Difatti, è emersa l'esigenza adottare una metodologia condivisa a livello regionale nello studio dei complessi sistemi costieri. Inoltre, a completamento e a supporto di quanto qui emerso, l'analisi batimetrica e granulometrica della spiaggia sommersa e l'analisi del

trasporto di sedimenti litoraneo consentirebbero di approfondire e inquadrare la dinamica costiera e supportare i dati ottenuti dal presente lavoro di tesi.

Parole chiave: evoluzione linea di costa, frammentazione sistemi dunali, DSAS, impatto opere costiere

1 INTRODUCTION

1.1 BACKGROUND

Coastal zones can be defined as the transition areas that connect terrestrial and marine environments. They are planet's most productive and valued ecosystems (Crossland et al., 2005). Sixty percent of the world's major cities are in coastal regions, and 40% of all people on the planet live within 100 km of a coastal zone (Nicholls et al., 2007).

Shorelines are dynamic in nature and coastal behaviour is the complex result of multiple processes occurring and interacting on a variety of time and spatial scales. Some physical processes that drive shoreline change include waves, currents, tides, storm surges, seasonal fluctuations, aeolian transport, and relative changes in sea level (Komar, 1998). There is a delicate balance between the forces that erode the beach by carrying away the sand and the forces that tend to move sand onto the beach from other areas.

Coastal communities are often planned with insufficient thought for natural hazards such as coastal erosion, and coastal structures built too close to eroding shorelines experience wave inundation and damage. In response, sea walls and other structures are built to protect coastal homes, hotels, and infrastructure; but these structures can lead to the total loss of the beaches that once fronted them (Romine & Fletcher, 2012). As a result, numerous shoreline studies aim to quantify trends in shoreline migration (e.g., Crowell et al., 1991; Galgano et al., 1998; Romine & Fletcher, 2012). Shoreline studies are thus vital to the early stages of the decision-making process for planned coastal developments to mitigate the potential loss of buildings, infrastructure, and beaches. Long-term trends in data are of particular interest because coastal planning projects tend to be longstanding.

Therefore, coastal evolution has become one of the most sensitive issue for Governments, that have been forced to take into more consideration in their political decision.

In 2004, the EUROSION study has been commissioned by the Environment European Commission, following an initiative by the European Parliament, in order to quantify the status, impact and trends of coastal erosion in Europe and assess needs for action at EU, Member State and regional levels. The report showed that about twenty thousand kilometres of coasts, corresponding to 20% of the whole European coast length, face serious impacts and 15,100 km are actively retreating, some of them despite the coastal protection works that have been emplased there. The area seriously impacted by erosion is estimated to be 15

km² per year. Houses market value has decreased by at least 10% and houses have been abandoned as a result of imminent coastal erosion risk (Salman et al., 2004).

The EUROSION study also pointed out that 218 km of the total Sicilian coastline length (ca. 1,531.6 km) have been eroding. Sicily is one of the regions with the highest coastal urban development in Europe, about 900,000 inhabitants live within the area of influence of coastal erosion (Salman et al., 2004).

1.2   PURPOSE

The Gulf of Gela, over 70 km long in Southern Sicily, has seen an increasing human development over last decades, but any actions have been implemented to reduce the negative impact of human works on the coast except for few natural protection areas, already established in the fifties and the sixties that partly mitigated the effect of human impact on the coastal evolution. The main purpose of the present Ph.D. thesis was to apply for the first time a multimethodology research to study the shoreline evolution within the Gulf of Gela and assess how the coast evolved in response to the environmental changes.

The Gulf of Gela is identified as second-order coastal sub-cell (n. 4.2) whose physiographic limits are the Licata Harbour at NW and the cape Punto Braccetto at SE. The sub-cell n. 4.2 falls within the first-order coastal sub-cell n. 4 and it has also been subdivided into two third-order sub-cell, the cell n. 4.2.1, from cape Punta Braccetto to the Gela harbour, and the cell n. 4.2.2, from the Gela harbour to the Licata one (Regione Siciliana, 2020; Fig. 1).

To the purpose of this work, the study area has been split into 5 sectors, partly based on the coastal sub-cell classification proposed by the Sicilian Region and choosing as their delimitation the main coastal physiographic structures or the main manmade works (Regione Siciliana, 2020). The first sector (S1) is ca. 10 km long from the Licata harbour to the Falconara Castle, the second one (S2) falls within the Falconara Castle and the Gela harbour, the third sector (S3) is ca. 27 km length of coastline between the Gela harbour and the Scoglitti one, the fourth sector (S4) is from the Scoglitti harbour and the Randello promontory and the sector n. 5 (S5) is from the previous physiographic limit and cape Punta Braccetto (Fig. 2).
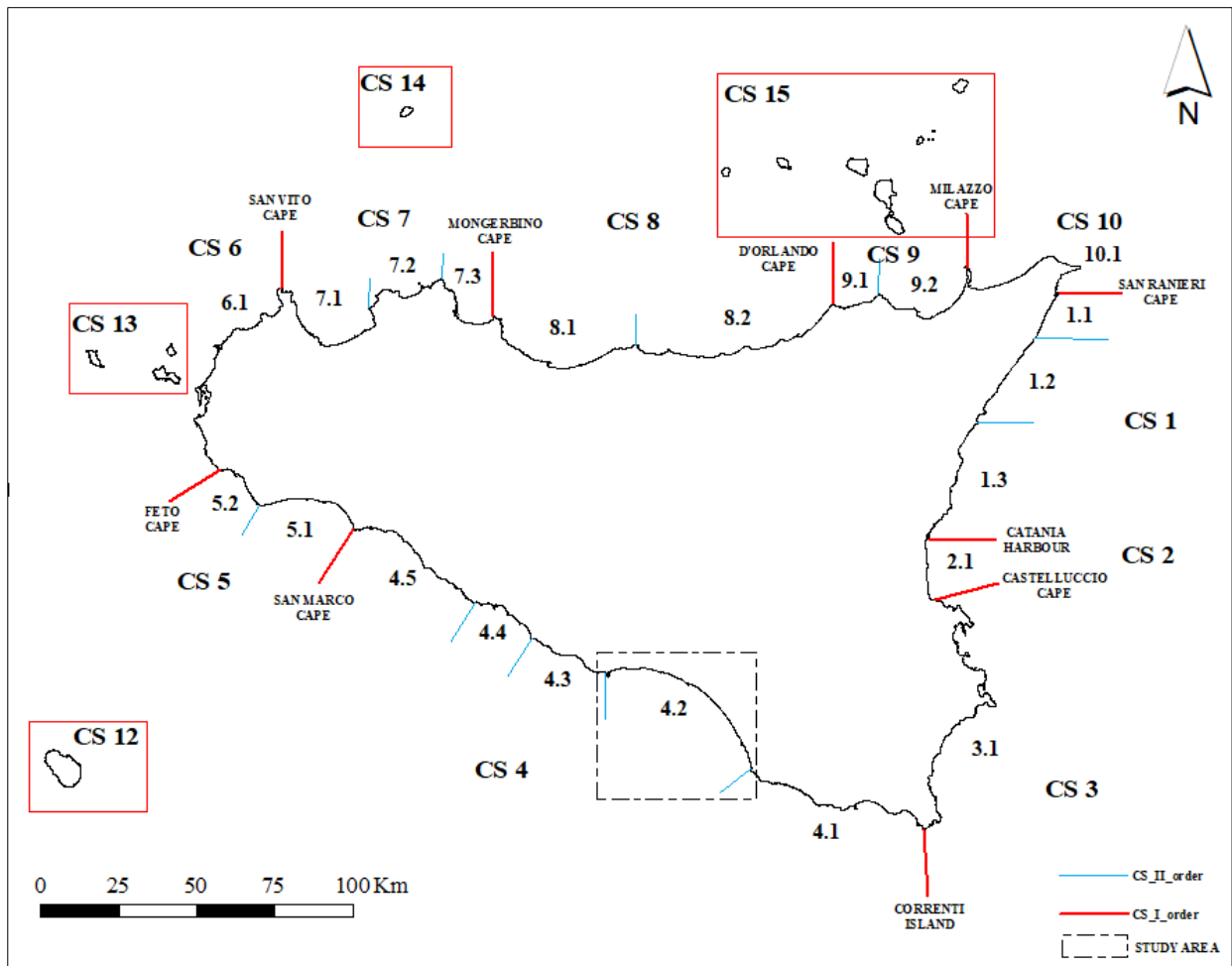
Fig. 1 - Coastal sub-cells of I- and II-order of Sicily, in the dashed square the study area (cell n. 4.2; modified from Regione Siciliana, 2020).

Fig. 2 – The five coastal sectors the study area has been split into and their limits.

For each sector, the shoreline change analysis on medium-term period has been performed, covering a time span of 23 years (1989 to 2012); for sectors S1, S2 and S5, shoreline change analysis has been even carried out on long-term period, since 1955 to 2012 for sectors S1 and S2, between 1955 and 2018 for sector S5. The shoreline change analysis has been based on the integration of remote sensing and geographic information system (GIS) techniques. Shorelines have been traced from aerial photographs, ortophotos and UAV image and analyzed by the Digital Shoreline Analysis System (DSAS), which is a software extension to ESRI ArcGIS© that can calculate the shoreline rate-of-change statistics starting from multiple historical shoreline positions (Thieler et al., 2009).

The coastal armouring analysis has been conducted to assess the maritime structures impact on the shoreline evolution. The *coefficient of technogenous impact* (K) is generally applied and represents the ratio between the total length of the shoreline and the length of all maritime hydraulic structures that insist on the coast (Aybulatov & Artyukhin, 1993).

The dune fragmentation index (F) has been applied to all available image for each sector and it has been computed as the ratio between the length of all breaks and the whole dune toe length at each dune

system and year. The proxy chosen to map the dune toe was the seaward dune vegetation line (Molina et al., 2020).

The grain-size and textural analysis measures the individual particle sizes to determine their frequency distribution and to calculate a statistical report that effectively characterizes the samples. Three beaches have been chosen within the study area and 4 transect have been casted for each. The statistical parameters proposed by Folk & Ward (1957) have been used to describe the sediment samples.

1.3   ROAD MAP THESIS

Coastal dynamic should be known and understand to investigate and assess the shoreline evolution. Chapter 2 describes the main shoreline and coastal dynamic processes that supply sediments to the coastal system and those ones that move sediments away, and it is clarified that coast and shoreline have different meanings and are not used as synonyms, even if they seem to be interchangeable in many studies. The current knowledge on the most common methods used to investigate the shoreline evolution are here also presented.

In Chapter 3 the Sicilian Foreland system and the regional geological setting is examined.

The climate, oceanographic and environmental characteristics of the study area are discussed in Chapter 4 and previous shoreline evolution studies on the Gulf of Gela are here presented.

Materials, methods and the used workflow are described in Chapter 5.

The results obtained by the analyses performed for the present work are shown in Chapter 6, including the shoreline rate-of-change, the grain-size and textural characterization of the sediment beach, the evolution of the coastal works and the dune fragmentation evolution.

Chapter 7 discusses the main findings and insights emerged from the performed analyses and results are interpreted in relation to the main topic of the research.

Finally, Chapter 8 outlines the main conclusions pointed out from the study and identifies recommendations for further research.

2   SHORELINE AND COASTAL DYNAMICS

The coasts of the world are the margins separating 29% of the earth that is land from the 71% that is water. Coastal landscape modelling is an interactive complex phenomenon ruled by several dynamic processes, all linked in a non-linear way. Land margins are generally eroded and reworked by wind and waves, fluvial sediments are transported by rivers and reach the ocean water and the marine currents can carry large amounts of sediment alongshore or offshore. Thus, many natural and human factors affect shorelines and all of them are different and specific for each area.

There is significant natural diversity in shore types throughout the world and coastal managers and planners need to be aware of coastal diversity for many reasons:

- The coast is dynamic and constantly evolving to new condition;

- The balance and the interaction of processes are delicate and different in various areas;

- Different settings imply different erosion and accretion sediment patterns.

Coastal dynamic should be known and understand to investigate and assess the shoreline evolution of the study area. The following briefly describes the main processes that supply sediments to the coastal system and those ones that move sediments away.

For clarity, coast and shoreline have different meanings and are not used as synonyms, even if they seem to be interchangeable in many studies.

The coast is broad zone that reaches from the landward limit of marine processes to the seaward limit of alluvial and shoreline processes. It includes all those parts of the coastal plain affected by the proximity of a shoreline, not only deltas, beaches, barrier islands, tidal flats, tidal inlets, estuaries and cheniers (Summerfield, 1991).

The shoreline is a line of a demarcation between sea water and an exposed beach (Komar, 1976). It is therefore a local and transient feature.

2.1   SEDIMENT BUDGET

Shoreline morphology essentially reflects the sediment budget of the coastal system, as the result of the interaction between the sediment supply and the basinal reworking processes (Fig. 3). The main inputs (sediment supply) and outputs (natural forces that move sediment away) can be briefly summed up as follow:

- Sediment river load is generally the main source of sediment input into the coastal sediment budget. The amount, the grain-size and the composition of the sediments depend on the geology and geomorphology of the drainage basin;

- Cliff and dune erosion are produced by winnowing action (rainfall, wind), wave attack and groundwater seepage. It is another source of sediment to the system. Cliff erosion can be influenced by rising sea levels and is magnified with storm surge events;

- Ocean waves are generated by the wind and they can move large amount of sediment. Waves motion can be explained by different mathematical theories, that are going to be briefly described later. For the purpose of this Ph.D. thesis, wave setup and wave runup, that directly affect the shoreline, are going to be taken into account and described;

- Currents are continuous, directed movement of sea water generated by a number of forces and may be directed offshore (rip currents), parallel to the shore (longshore currents), obliquely (cross-shore currents). They can move huge amount of sediment as well;

- Tides are the daily rise and fall of the sea level. They induce the shifting of the site of wave action but also influence the biology of nearshore zone. They also generate currents as large volumes of water move between the sea and the coastal plain, lagoons and estuaries via inlets and delta distributaries;

- Wind is one mechanism by which sediment can be moved. Different grain-size particles can be blown away, both onshore and offshore.
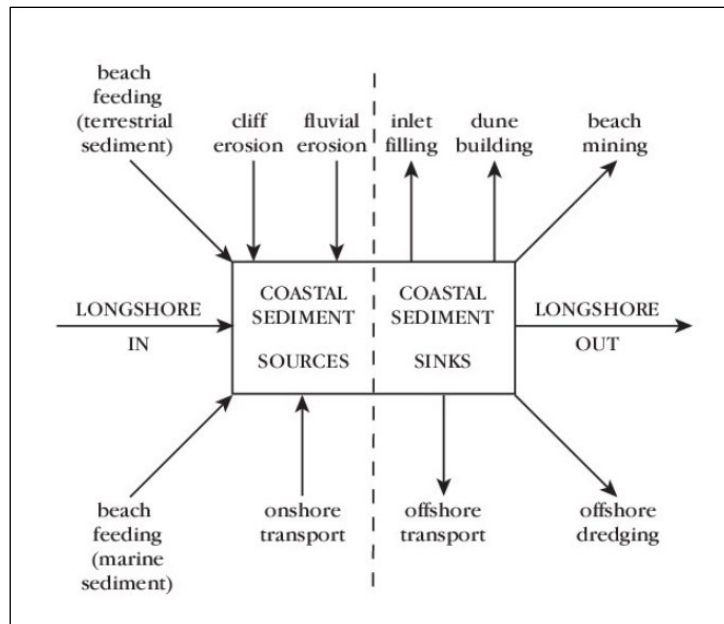
Fig. 3 - Scheme of the sediment budget with the main inputs and outputs in a coastal system (from May & Hansom, 2003).

2.1.1 *NATURAL PROCESSES*

2.1.1.1 *Waves*

Beach morphology and shape are mainly affected and modelled by waves, which dissipate a significant quantity of their energy in the nearshore region. Wind is the main generating force for waves motion. Wave can be described by the following parameters (Fig. 4):

- wave crest, that is the high water level reached by the free surface;

- wave trough, that is the low water level;

- wave height (H), defined as the vertical distance between the crest and the trough;

- wavelength (L), that is the distance over which the wave pattern repeats itself;

- wave celerity or speed (C) is the velocity of a single wave;

- wave period (T) is the time required for a wave to complete a cycle;

- wave frequency (f) is the inverse of the period.
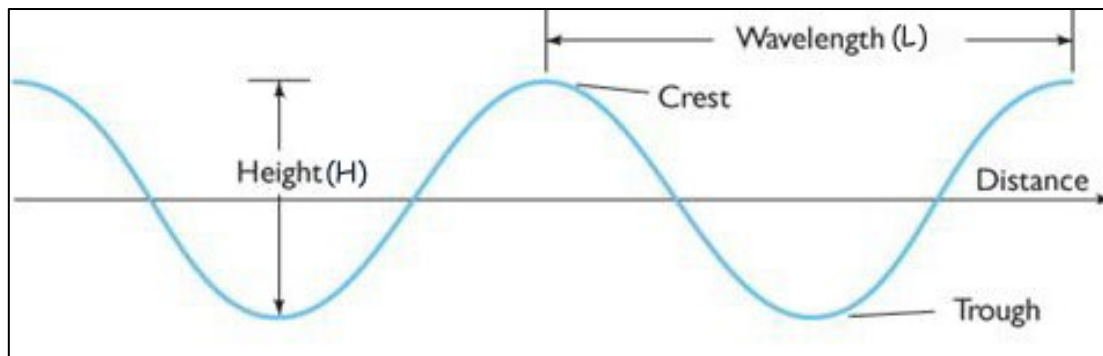
Fig. 4 - Wave parameters (Pinet, 2006)

Waves can be classified in short and long waves. The formers have period lower 20s, the latters have period between 30s and 40min. Water-level oscillations with a period longer than 1 hour are the astronomical currents and storms surge, they are related to water-level variations. Short waves are divided in two groups (Kinsman, 1965):

- Wind or sea waves, generated by the local wind field. They are generally steep (high and short), irregular and directional waves. Wave height, period, direction depend on the wind field (speed, direction and duration, on the meteorological fetch and the geographical fetch) and on the water depth in the wave generation area;

- Swell waves travel long distances away from their generation area and are more regular and unidirectional than wind waves. A portion of wave energy is lost during the propagation in deep water due to dissipation phenomena, which results in long period waves.

Wave height and period are closely related to wind conditions, from which they are estimated. The analysis of historical measured wind records is useful to reconstruct wave climate at a site. Such a computation is known as wave hindcasting. Forecast wind conditions are used to perform the wave forecasting.

The simplest theory to describe wave motion is the linear one, that gives a reasonable approximation of wave characteristics for a wide range of wave parameters. The linear theory is valid when waves and their motion are infinitesimally smalls and provides some insight for finite-amplitude periodic waves. When waves become larger or travel toward shore into shallow water, higher-order wave theories (nonlinear theories) are often required to describe wave phenomena (Coastal Engineering Research Center, 2001).

Regular waves theory assumes that ocean waves are two-dimensional (2D), small in amplitude, sinusoidal, and progressively definable by their wave height and period given by water depth. When wave

17

height becomes larger, the simple treatment may not be adequate and a 2-D approximation of the ocean surface to deviate from a pure sinusoid should be considered. This kind of theories becomes nonlinear and allow formulation of waves that are not of purely sinusoidal in shape (Coastal Engineering Research Center, 2001).

Irregular waves theory describes the natural time-dependent three-dimensional (3D) characteristics of real wave systems. A 3D representation of ocean waves requires considering the sea surface as an irregular wave train with random characteristics. To quantify this randomness of ocean waves, this theory employs statistical and probabilistic theories (Coastal Engineering Research Center, 2001).

A statistical description of waves is necessary in order to make a correct analysis of the wave climate and of the littoral transport. This statistical description is based on the directional distribution of the following wave characteristics (Benassai, 2006):

- The *significant wave height* H_s, defined as the mean of the highest third of the waves in a time-series of waves representing a certain sea state (H_s computed on the basis of a spectrum is referred to as H_{m0});

- The *mean wave period* T_m, described as the mean of all wave periods in a time-series representing a certain sea state;

- The *peak wave period* T_p, which is the wave period with the highest energy. The analysis of the distribution of the wave energy as a function of wave frequency for a time-series of individual waves is referred to as a spectral analysis. The peak wave period is extracted from the spectra;

- The *mean wave direction* θ_m that is the mean of all the individual wave directions in a time-series representing a certain sea state.

These parameters are often calculated from a time-series of the surface elevations. The time-series is thereafter statistically analysed to arrive at a synthetic description of the wave conditions. The aim is, on one hand, to find the occurrence probability of the extreme wave events, generally expressed as the percentage of exceedance of the wave height H_s, and, on the other hand, to identify the wave climate for the computation of coastal dynamics processes and expressed as directional distribution of the wave heights, often presented in the form of a wave rose or scatter diagram of T_p, versus H_s.

Two other important parameters should be defined to determine the active portion of the beach profile: the wave setup and the wave runup (Fig. 5).
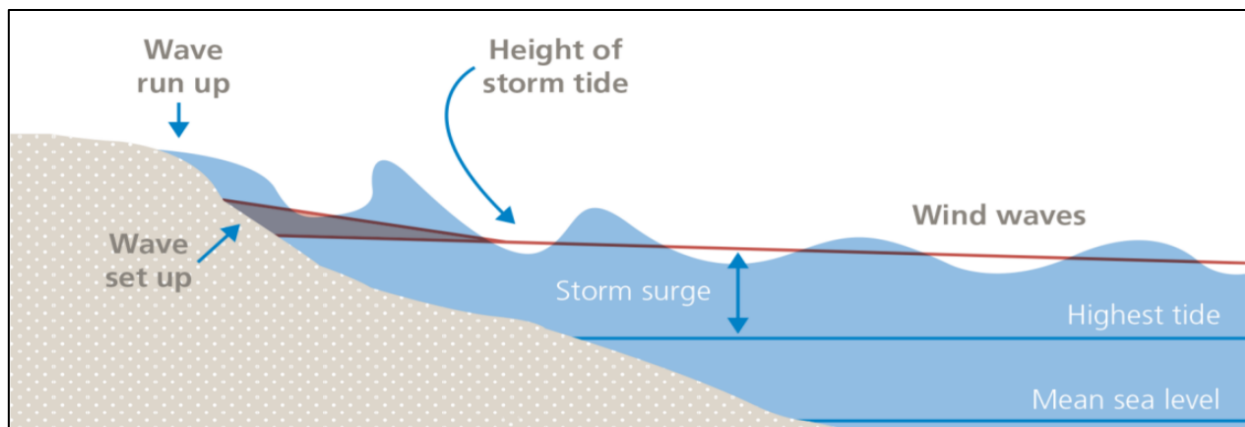
Fig. 5 - Scheme of the surf zone showing principal contributors to the coastal water level (modified from Hughes, 2016).

Wave setup is the superelevation of mean water level caused by wave action. Total water depth is a sum of still-water depth and setup

$$d = h + \bar{\eta}$$

where

h = still-water depth

$\bar{\eta}$ = mean water surface elevation about still-water level

Wave setup balances the gradient in the cross-shore directed radiation stress, the pressure gradient of the mean sloping water surface balances the gradient of the incoming momentum. Nondimensional wave setup increases with decreasing deepwater wave steepness. The beach slope is predicted to have a relatively small influence on setup for irregular waves.

Wave runup is the maximum elevation of wave uprush above still-water level. Wave uprush consists of two components: superlevation of the mean water level due to wave action (setup) and fluctuations about that mean (swash). Runup (R) is defined as a local maximum or peak in the instantaneous water elevation, η, at the shoreline. Difficulties inherent in runup prediction include nonlinear wave transformation, wave reflection, three-dimensional effects, porosity, roughness, permeability, and groundwater elevation.

In 1959, Hunt empirically determined runup for regular waves as a function of beach slope, incident wave height, and wave steepness based on laboratory data. Hunt's formula, given in nondimensional form (Battjes, 1974) is:

$$\frac{R}{H_0} = \varepsilon_0 \quad \text{for } 0.1 < \varepsilon_0 < 2.3 \text{ f}$$

for uniform, smooth, impermeable slopes.

ε_0 is the surf similarity parameter or Iribarren number. It is a dimensionless parameter used to model several effects of (breaking) surface gravity waves on beaches and coastal structures. It is expressed as (Battjes, 1974):

$$\varepsilon_0 = \frac{tan\alpha}{\sqrt{H/L_0}}, \text{ with } L_0 = \frac{g}{2\pi}T^2$$

where

α = the angle of the seaward slope of a structure

H = the wave height

L_0 = the deep-water wavelength

T = the period

g = the gravitational acceleration

Walton et al. (1989) modified the previous equation to extend the application to steep slopes by replacing tanβ in the surf similarity parameter, which becomes infinite as β approaches π/2, with sinβ. The modified formula was verified with laboratory data from Saville (1956) and Savage (1958) for slopes of 1/10 to vertical.

The nonbreaking upper limit of runup on a uniform slope is given by

$$\frac{R}{H_0} = (2\pi)^{1/2}\left(\frac{\pi}{2\beta}\right)^{1/4}$$

Based on criteria developed by Miche (1951) and Keller (1961) (Walton et al., 1989).

Irregular wave runup has been found to be a function of the surf similarity parameter (Holman & Sallenger, 1985; Mase, 1988; Nielsen & Hanslow, 1991), but differs from regular wave runup due to the interaction between individual runup bores. Uprush may be halted by a large backrush from the previous wave or uprush may be overtaken by a subsequent large bore. The ratio of the number of runup crests to the number of incident waves increases with increased surf similarity parameter (ratios range from 0.2 to 1.0 for ε_0 of 1.5 to 3.0) (Mase, 1988; Holman, 1986). Thus, low-frequency energy dominates runup for low values of ε_0.

Mase (1988) presents predictive equations for irregular runup on plane, impermeable beaches (slopes 1/5 to 1/30) based on laboratory data. Mase's expressions for the maximum runup (R_{max}), the runup exceeded by 2% of the runup crests ($R_{2\%}$), the average of the highest 1/10 of the runups ($R_{1/10}$), the average of the highest 1/3 of the runups ($R1/3$) and the mean runup ($\bar{R}$) are given by

$$\frac{R_{max}}{H_0} = 2.32 \, \varepsilon_0^{0.77}$$

$$\frac{R_{2\%}}{H_0} = 1.86 \, \varepsilon_0^{0.71}$$

$$\frac{R_{1/10}}{H_0} = 1.70 \, \varepsilon_0^{0.71}$$

$$\frac{R_{1/3}}{H_0} = 1.38 \, \varepsilon_0^{0.70}$$

$$\frac{\bar{R}}{H_0} = 0.88 \, \varepsilon_0^{0.69}$$

For $1/30 \leq \tan\beta \leq 1/5$ and $H_0/L_0 \geq 0.007$, where H_0 is the significant deepwater wave height and ε_0 is calculated from the deepwater significant wave height and length. The appropriate slope for natural beaches is the slope of the beach face (Holman, 1986; Mase, 1988). Wave setup is also included. The effects of tide and wind setup must be calculated independently. Walton (1992) extended Mase's (1988) analysis to predict runup statistics for any percent exceedance under the assumption that runup follows the Rayleigh probability distribution.

Actually, field measurements of runup (Holman, 1986; Nielsen & Hanslow, 1991) are consistently lower that values obtained by the previous equations. For example, the equation for the runup exceeded by 2% of the runup crests overpredicts the best fit to $R_{2\%}$ by a factor of two for Holman's data, which used the beach face slope, but is a roughly an upper envelope of the data scatter.

2.1.1.2 Tides

Tides result from the gravitational attraction exerted on oceanic or lake waters by the moon and the sun. A water mass rises and falls twice daily along most coasts, to produce semi-diurnal tides (Ross, 1995). High tide occurs about every 12 h 26 min, a little bit more than solar day because the lunar one is longer, hence high tide gets progressively later by about 50 min each day (Thurman, 1991). However, there may be

diurnal tides with one high and one low a day along some coasts due to the configuration of the generating basins and complexities of the shoreline, or a mixed tide with highs and lows different magnitudes.

When the sun and moon are aligned, tides are about 20% higher than normal and known as spring tides. When the sun and moon are at right angles relative to the Earth, the tides are about 20% lower than normal and are called neap tides (Fig. 6). This cycle extends over 14 days (Reading, 1996).
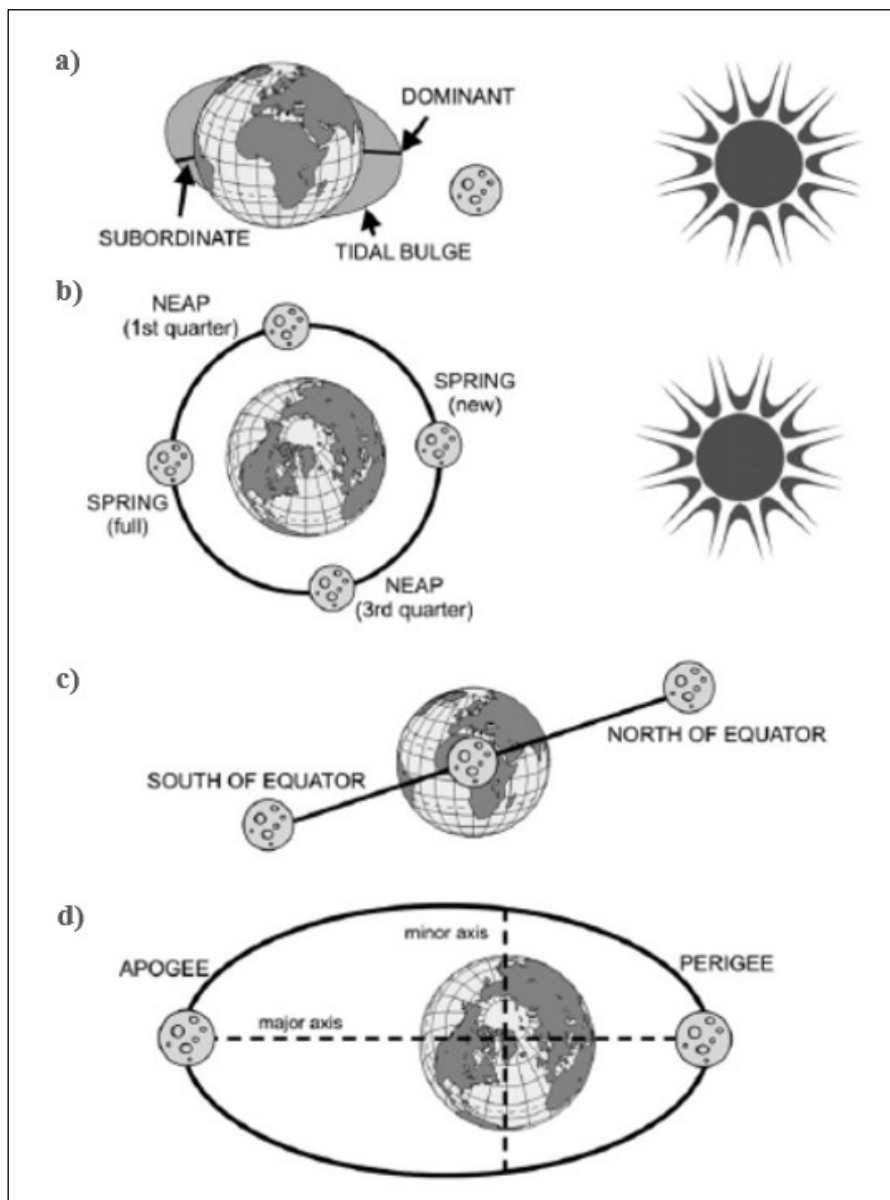
Fig. 6 – a) Idealized equilibrium tidal models that illustrate semidiurnal tides, (b) relative position of the Earth and Moon system around the Sun with Spring and Neap periods, c) the tropical month, and d) apogee and perigee (from Kvale., 2006).

Although the tidal range of open ocean is small, it increases when the tidal bulge reaches shallow water. Tides have less effect on the sediment load and on coastal morphology than waves, but they govern, on one side, the strength and flow pattern of the regularly fluctuating tidal currents, and, on the other side, the amount and timing of tidal rise and fall.

Vertical tidal fluctuations disturb the coastline by regularly submerging and exposing the beach and intertidal flats. The different zones of the beach and shoreface are subjected to varying degrees of wave energy and populations of specialized organisms have evolved to tolerate the high levels of stress that these changes cause. In semi-arid and arid climates plant life develops complex structures, while, in the humid tropics, mangroves have adjusted to the rise and fall of the tide. In most temperate areas, beaches are lacking vegetation and are a source of wind-blown sand, especially in areas of high tidal range (Reading, 1996).

2.1.1.3 Winds

Wind is the main agent that generate waves, but it can directly disturb and shape coastal morphology. Strong winds erode the beach, finer sediments can be moved both offshore and, more commonly, onshore, where they form extensive complexes of aeolian dunes, which in turn supply sediment to adjacent lagoons and coastal plains.

2.1.1.4 Currents

Currents are constant sea water movement generated by many forces working upon the water. They occur within the deep ocean, over the continental shelf and within the offshore and nearshore zones. They may be quasi-steady and persist for several hours to several weeks (ocean and shelf currents), or they may be oscillatory with periods of seconds (currents under waves). They may be limited to the surface or to the seabed, or they may extend over the full depth of water.

A partial currents classification based on the water depth divides the currents into the ocean, shelf and nearshore currents. The ocean currents are the largest and are driven by global scale interactions between the atmosphere and the sea. The continental shelf can extend between 1 and several kilometres from the coast. Continental shelf currents are made up of internal waves, coastal trapped waves, tides and local wind induced currents. Shelf and ocean currents are generally of little significance within the shallower waters of the nearshore zone.

Nearshore currents are mainly caused by surface waves breaking on a beach. In fact, when surface waves break on a beach, wave energy is lost to turbulence generated in the process of breaking, and wave momentum is transferred into the water column generating nearshore currents. There are two current systems whose flow structures are predominantly horizontal, alongshore currents caused by obliquely incident waves

and cell-like circulations, which can occur when waves are nearly at normal incidence. The nearshore currents system can be divided in *longshore currents*, *cross-shore currents* and *rip currents*.

Wave- and wind-induced *longshore currents* (Fig. 7) flow parallel to the shoreline and are strongest in the surf zone, decaying rapidly seaward of the breakers. Typically, longshore currents have mean values of 0.3 m/sec or less, but value exceeding 1 m/sec can occur in storms. The velocities are relatively constant over depth (Visser, 1991). These currents, which is parallel to the shoreline, carries the sediments alongshore.

Unlike the longshore currents, the *cross-shore current* is not constant over depth. The mass transport carried toward the beach due to waves is concentrated between the wave trough and the wave crest elevations. Because there is no net flux through the beach, the wave induced mass transport above the trough is largely balanced by a reverse flow or undertow below the trough. The vertical profile of the undertow is determined as a balance between radiation stresses, the pressure gradient from the sloping mean water surface, and vertical mixing (Dally & Dean, 1984; Hansen & Svendesn, 1984; Stive & Wind, 1986; Svendsen et al., 1987). *Rip currents* are features of highly three-dimensional current patterns. They are fed by longshore-directed surf zone currents, which increase from zero between two neighboring rips, to a maximum before turning seaward to form a rip current (Fig. 7). They often occur periodically along the beach, forming circulation cells. *Rip currents* cause a seaward transport of beach sand, hence have direct impacts on beach morphology. Recent studies (Yu & Slinn, 2003) show that the offshore directed rip currents interact with the incident waves to produce a negative feedback on the wave forcing, reducing the strength and offshore extent of the currents.
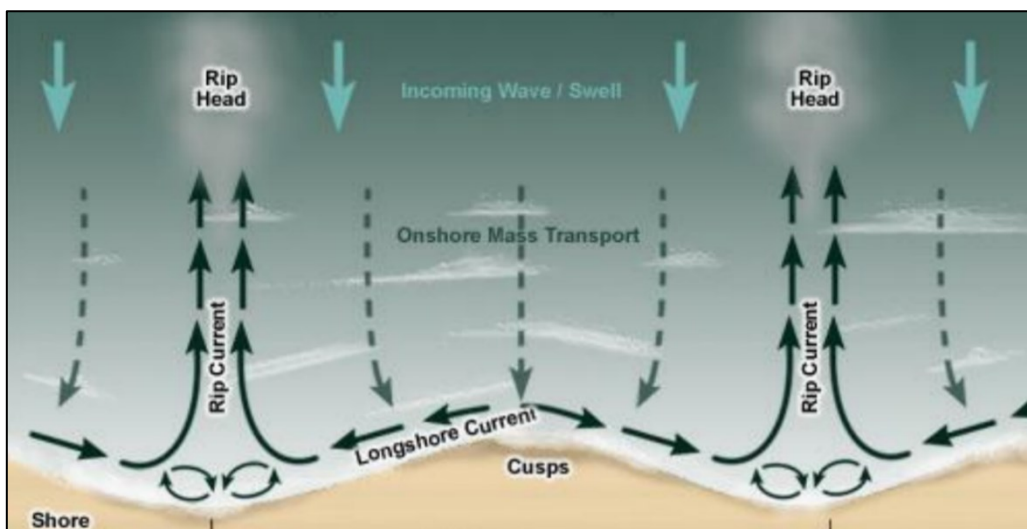
Fig. 7 - Scheme of cross-shore, longshore and rip currents (from COMET program).

2.1.1.5 Sediment supply

Globally, 7 x 10^9 tons of suspended sediment are supplied by fluvial systems to the ocean yearly; about 5 – 10% come from erosion of cliffs, mostly made up of soft sediment and including every rocky type (Milliman & Meade, 1983). Sometimes, beaches are even supplied from sediment deriving from longshore drift, erosion at the shoreline and from the shelf.

As mentioned earlier, the nature and volume of sediment are determined by the alluvial catchment area, and thus depend on its size, relief, tectonics, climate, vegetation and the character of its bedrock and superficial deposits. These factors govern the amount, grain size and manner of delivery of the sediment to the shoreline. Larger catchment areas are associated with greater sediment volumes, generally finer-grained material, more steady water and sediment discharge and lower coastal-plain gradients. Small catchment areas tend to supply coarser sediment, typically gravel and sand. However, many local catchment areas only reach a short distance inland, sometimes within the coastal plain, and may yield and type of sediment. In semi-arid regions sand is more abundant. In humid tropical regions silt and clay are nearly always dominant, except where a granitic basement provides abundant sands (Reading, 1996).

Terrigenous sediments hardly pass out onto the shelf, because there is a littoral energy fence at the shoreline, where shoaling and breaking waves have the potential to move more sediment landward than seaward (Allen, 1970). Sediment can bypass this fence and reach the shelf by one of three methods: river-mouth-bypassing, where deltas enter the sea and especially during the flood stages of the rivers; estuary-mouth-bypassing, mainly by ebb-tide enhanced currents; and shoreface-bypassing by which shoreface sediments are removed as the shoreface is eroded by wave/storm processes.

Cliff erosion is generated by two processes: notching at the base of the cliff by marine processes, and collapse and denudation of the entire cliff face by a combination of atmospheric and marine processes. Concentration of wave attack at the cliff base accelerates erosion, permitting collapse or movement of the overlying material. This debris is subsequently removed by wave action, and the marine attack continues at the base (Short, 1982).

2.2   HUMAN IMPACT ON SEDIMENT BUDGET

Shoreline landward migration occurs when the erosional processes overcome the sediment supply. Decreasing sediment river load appears to be a pivotal factor in coastal retreat and man-made works along the rivers can be the main cause of the reduction of the fluvial sediment (Bird, 1993).

Di Stefano et al. (2013) studied the shoreline evolution of the Gulf of Catania (eastern Sicily) over the last four decades and pointed out that the landward migrations were strictly governed by the hydrological parameters of the Simeto river. The authors applied a combined methodology analysing the historical and recent variations of the coastline position, with quantitative estimations of the coastal retreat and of the displacement velocities, assessing changes of the solid and liquid discharge and examined pluviometric data and the wave regime. They observed that the drastic reduction of the solid and liquid discharge occurred when the several hydraulic works along the river (dams, fluvial barrages and artificial embankments) have begun to come into operation after the 1950s. The statistical analysis of the rainfall data indicated an almost steady trend over the last century which could not have produced any relevant effect and any variation in the wave regime have triggered more intense erosional processes along the shoreline, as no significant change is observable in the wave parameters either. These insights led the authors to relate the sediment supply reduction to the installation of hydraulic works along the Simeto river, which coupled with the progressive destruction of the coastal dune belt due to human building activities, caused the consequent coastline retreating.

2.2.1 COASTAL ARMOURING

Coastline armouring is defined as the protection of coasts using hard defence structures, it is a very common engineering solution against erosion and waves (Griggs, 2005; Charlier et al., 2005). It includes traditional onshore structures, as seawalls, dikes/revetments, but also port and harbour developments. During the past decade, the expanded level of coastal armouring has arisen as one of the most critical problems all over the world. The increasing of coastal armouring has been accompanied by a crescent concern on the cumulative impacts of protection structures and the artificial stabilization of natural coastline. Often, there are a number of adverse influence, including disturbance of cross- and long-shore sediment transport, and associated downdrift beach reduction, accelerated bottom erosion in front of structures, restricted public

access to the beach, potential risks for bathers, anaesthetic visual effects on the seaside landscape, etc. (Griggs, 2005; European Environment Agency, 2006; Stancheva & Marinski, 2007).

As partly mentioned above, coastline armouring includes:

- Groynes or similar shore normal structures;

- Ports;

- Inlet jetties at river mouths;

- Breakwaters;

- Seawalls, seadikes and revetments.

Groynes are long and narrow structures perpendicular or slightly oblique to the shoreline extending into the surf zone to reduce the longshore currents and hence the littoral drift in the inner surf zone, to retain the beach sand between the groynes, to stabilize and widen the beach or to extend the lifetime of beach fills. A series of similar groynes (groyne field) may be constructed to protect a stretch of coast against erosion. These structures are known as beach groynes. Summarizing, groynes are built to serve three main purposes:

- to stabilize or widen the beach by trapping sand from the littoral drift; a groyne acts as a partial dam that intercepts a portion of the littoral drift; sediment material is impounded on the updrift side and erosion is caused on the downdrift side (often increased erosion due to generation of additional turbulence at the groyne tip); to reduce downdrift impacts these types of groynes should be relatively short and/or permeable and have relatively low crest levels;

- to stabilize the placement of beach fill material (nourished beaches); often these types of groynes are constructed to stabilize artificial beaches along heavily armored made-land shores without any updrift supply of sediment (no or almost zero longshore drift; sediment-starved shores; Chrzastowski, 2004);

- to prevent the movement of littoral material out of an area (at terminus of littoral cell close to an inlet or other sediment sink); these groynes should be relatively long and and have high crest levels above the prevailing high tide levels and normal wave run-up levels.

The primary purpose of a *port* is to provide safe mooring and navigation for vessels but when built on the shoreline it interferes with littoral drift budget and the results are sedimentation and shoreline impact. Like groyne, the port acts as a blockage of the littoral transport, whereby it causes trapping of the sand on the

upstream side in the form of an accumulating sand filet, and the possible bypass causes sedimentation in the entrance. The sedimentation requires maintenance dredging and deposition of the dredged sand. The result is a deficit in the littoral drift budget which causes lee side erosion on the adjacent shoreline.

Jetties are long, narrow, dam-like structures that are built more or less perpendicular to the coast to prevent the shoaling and migration of inlet channels or navigation channels and to protect the channel entrance against storm waves. Jetties generally extend through the surf zone to beyond the outer breaker line; jetties may increase the tidal current velocities in the inlet channel, resulting in deepening of the channel. The ebb shoal may be pushed to a more offshore position. Sand accumulation will take place on the updrift side and erosion on the downdrift side of the inlet; the latter may be on a relatively large scale as jetties are usually relatively long. Mechanical bypassing of sand may be required to reduce downdrift erosion. Significant deepening of the inlet channel through the bars and shoals on the seaward side will alter the sediment bypassing mechanism and thereby the response of the downdrift beaches. Lee-side erosion will increase with deepening of the channel, as more sediment will move into the back-barrier basin and less sediment will be bypassed to the downdrift beach. Other problems are channel deposition and migration of shoals within the inlet and scour near the jetty tips. Inlets without jetties may also suffer from bank erosion (often related to the migrational tendencies of the inlets) (Van Rijn, 2013).

Harbour breakwaters are structures perpendicular and/or oblique to the shore, forming a shield to harbours and boat anchorages and protecting a portion of the shoreline from the waves (blocking of incident wave energy). They are generally attached to the shore at one or both ends, often with a gap for boat entrance and extend outward through the surf zone. If the jetty or breakwater is not long enough, sand will be carried along the tip of the jetty into the entrance of the harbour forming a localized spit in the entrance (Van Rijn, 2013).

Detached breakwaters are built as offshore barriers parallel or occasionally obliquely positioned to the shore protecting a section of the shoreline by forming a shield to the waves. There can be many variants in the design of detached breakwaters, including single or segmented, emerged, if the crest is roughly 2 m above high water line, or submerged, when the crest is below water surface, narrow or broad-crested, etc. Submerged breakwaters are also known as reef-type breakwaters. Three basic types can be used: (1) rubble mound with trapezoidal cross-section of rock or conctre units, (2) prefabricated units of triangular shape of

concrete and (3) flexible membrane (geotextile) units constructed of sand-filled containers. Low submerged breakwaters can also be used as sills to support the seaward toe of beach fills. Detached breakwaters can be designed in such a way that not all longshore transport is blocked by the structure, reducing potential lee-side erosion of adjacent beaches (Van Rijn, 2013).

Seawalls, *seadikes* and *revetments* are shore-parallel structures armouring the shore to protect the land behind it against episodic storm-induced erosion and/or long-term chronic erosion by the sea. In the latter case, they usually are not very effective, because these types of structures hardly change the longshore transport gradients. Furthermore, beach and shoreface erosion will ultimately lead to an increased wave attack intensifying the transport capacity and hence intensified erosion (negative feed-back system). A *seawall* is a vertical retaining wall with the purpose of coastal protection against heavy wave-induced scour; it is not built to protect or stabilize the beach or shoreface in front of or adjacent to the structure. Thus, chronic erosion due to gradients of longshore transport will not be reduced. A *seadike* is an artificial sand dune that is protected on both sides by armour layers and filter layers to prevent erosion of sand. Groynes are often constructed to reduce scour at the toe of the dike by deflecting nearshore currents. Seabed protection may be necessary in case of strong tidal currents passing the structure. A *revetment* is an armour protection layer, consisting of light to heavy armour layer, underlying filter layer and toe protection, to protect the adjacent upland against wave scour by current and wave action.

For quantitative assessment of the impact of maritime structures on the coastline, the so-called coefficient of technogenous impact K is generally used. This coefficient represents the ratio between the total length of all maritime hydraulic structures and objects and total length of the coastal area studied. K is defined through the following simple equation (Aybulatov & Artyukhin, 1993).

$$K = l/L$$

where l includes the linear sizes of all structures and objects; and L represents the total length of the coastline. According to this methodology the extent of technogenous impact is considered as minimal at K = 0.0001−0.1; averaged when K = 0.11−0.5; maximal at K = 0.51−1.0 and extreme if K > 1.0.

The coefficient K can be useful as an indicator for the extent of human impact and would allow quantifying coastline modifications related to maritime structures (port and coast-protection).

2.3   RESULTING BEACH MORPHOLOGY AND CLASSIFICATION

Beach morphology is a difficult aspect to be documented and described because many structures and features are temporally and spatially transient. Moreover, different definitions are used by researchers to describe elements and characteristics of a coast. Nevertheless, the Coastal Engineering Research Center (1995) present a general definition of coastal zone based on geological criteria, which defines three subzones (Fig. 8):

- *Shore*;

- *Shoreface*;

- *Continental Shelf* (offshore).

The *shore* zone is a sloping area where unconsolidated sediments are subject to wave action. The term "*backshore*" is used for the zone above the limit of the swash of normal high spring tide, and it is exceptionally under the direct influence of waves. On a rocky coast it includes the cliffs, while a low coast may consist of sand dunes or mature salt marsh. The "*foreshore*" zone is a sloping portion of the beach including all that part of the beach which is regularly covered and uncovered by the tide. On a tideless beach this zone will be narrow, only covering the distance between the limit of the swash and backwash of the larger waves. The *foreshore* zone includes the *surf zone*, extending between the wave breakpoint and the maximum run-up of the swash, and a *swash zone*, where waves swash and backwash foreshore. The "*berm*" is a terrace formed in the backshore zone above the limit of the swash at high tide to form a flat terrace or a ridge with a reverse slope.

The *shoreface* is a narrow sloping zone between the continental shelf and the low water limit, where unconsolidated sediments are subject to vigorous transport. Below low water the positive features on the sandy floor in the offshore zone are called "*submarine bars*". The hollows found on the landward side of the submarine bars of sandy beaches are termed "*troughs*".
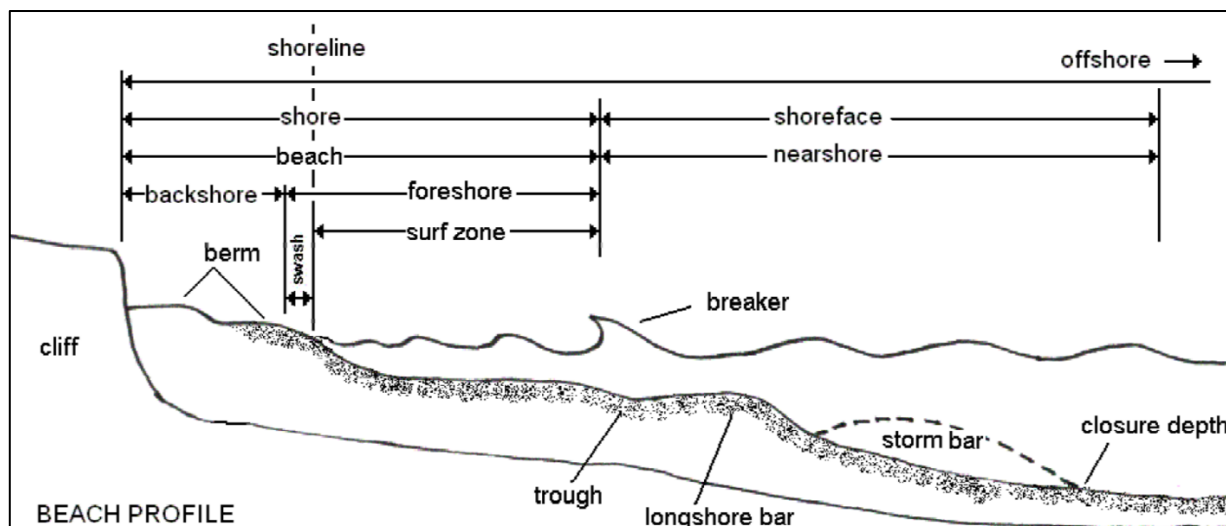
Fig. 8 - Scheme of the beach profile proposed by Coastal Engineering Research Center (1995).

The *continental shelf* is a slightly sloping zone of submerged continental margin extending from the offshore limit of shoreface to the slope of shelf break.

The *surf zone* is an area where breaking processes cause energy dissipation and produce vortices and turbulence phenomena. Breaking mechanisms are usually divided into two groups: spilling and plunging. Spilling occurs when steep waves advance up a gentle beach, the energy is gradually released over a considerable distance, and wave deformations are smaller than in plunging breakers. Suspended sediments are transported offshore by undertow currents or superficial currents associated with breaking. Plunging usually occurs on slightly steeper beaches, so the crest becomes faster than the wave base, curls and violently descends into the wave trough. A considerable amount of energy is released into a downwardly directed mass of water and the turbulence reaches the area beyond the breaking zone. Bottom materials are suspended and transported offshore by undertow currents. A large bore is formed and becomes deeper and deeper until the energy is completely exausted. Ahead of the bore, a sediment accumulation is formed, localized between the breaking point and the deepest zone reached by vorticity. The *swash zone* is characterized by the fluctuation of coastline associated with sediment transport which occurs when the energy of the waves advancing up the beach is not completely exhausted. Swash dynamics depend on the frequency oscillations. At low frequencies, if the beach is permeable and the sand is not saturated, the water percolates through the substrate and the backrush decreases. An amount of sediment is accumulated on the beach in the *swash zone* and the beach slope increases. The result is a convex beach profile. Storm waves and saturated substrate

generate a sediment transport associated with backrush, which is greater than uprush, and produce concave beach profile.

The beach slope is even related to the grain-size particles. Larger grain sizes generate steeper beaches (Coastal Engineering Research Center, 1984). During the winter storm waves move sand offshore, while the summer waves move sand onto the beach. Kamphuis (2010) showed that beach slopes are function of the ratio H/D, which represents the ratio of disturbing wave forces to restoring particle forces. During the action of larger waves the beach material is redistributed offshore to become a longshore bar or sandbar, generally visible at low tide. The bars are defined as accumulation of material near the point of breaking waves and are considered offshore features of a beach (Kamphuis, 2010). Bars are formed near the breaking point because the breaking waves set up a shoreward current with a compensating counter-current along the bottom. Sand carried by the offshore moving bottom current is deposited where the current reaches the wave break (Kamphuis, 2010). Berms form as a result of preferential shoreward transport within the swash. They are generally preserved (left behind) after a highwater event. The berm is periodically overtopped during storms or extreme high tides. On sandy and shingle beaches berms build seaward through the multiple accretion of bars to the beach face. Vertical accretion to the berm is accomplished by swash, which is influenced by wave height. A beach may have more than one berm or none at all.

The *equilibrium beach profile* results from steady wave forcing during the seasonal cycle. As described above, summer wave conditions move sand onto the beach, while winter storm waves move sand offshore. Beach profiles fluctuate with the seasonal cycle of wave energy: storms cause larger and more energetic waves in winter than in summer. As a result, the winter profile is characterized by the presence of a bar or by a berm on the foreshore (Fig. 9).
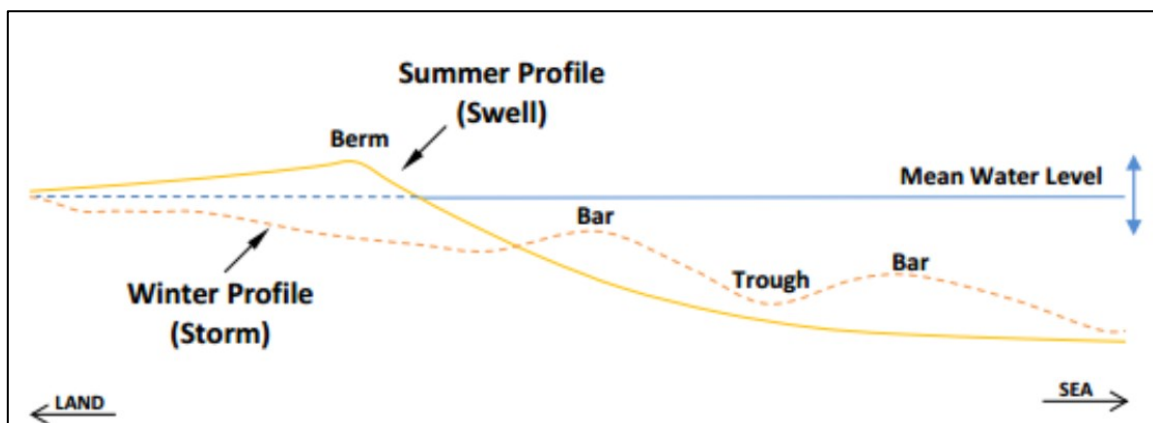
Fig. 9 - Seasonally variations in beach profiles in response to changing energy conditions (after Komar, 1983).

Beach can be classified on the base of wave energy action at the shoreline. It depends on deepwater wave energy and the water depth of the basin, but also on the frictional attenuation that occurs on the shelf as eave power is transmitted from deeper water to the shoreline. Frictional attenuation is a function of the gradient of the sea floor which itself depends on the nature and width of the shelf and the rate and type of sediment supply to the nearshore zone. Thus, two types of wave-influenced shoreline are recognized: *reflective* and *dissipative* (Wright et al., 1979; Short, 1982; Wright & Short, 1984; Fig. 10).

Reflective shorelines have smooth, steep beach/shoreface profiles. Although offshore wave energy may not be high, most waves break directly against the beach. Wave energy is reflected from the beach and often refracted alongshore. Beach cusps form, but bar and trough topography and swash bars are absent. *Reflective* shorelines develop where gravel is the dominant sediment because the swash percolates into the foreshore sediments and there is virtually no backwash. Thus, landward-directed processes predominate. Most of the sediment accumulates on the upper foreshore to form a high berm, while the coarsest gravels accumulate on the lower foreshore (Dabrio, 1990). Below the berm the foreshore is steep, occasionally reaching almost the angle repose. However, deposition by waves and erosion by storms tend to smooth the foreshore profile. At the base of the foreshore there is a sharp change in slope as the relatively steep foreshore passes basinwards into a relatively gently inclined shoreface.

Dissipative shorelines have an irregular, gentler profile with high energy waves breaking a considerable distance from the shore. The width of the surf zone can range from 50 to 500 m depending on wave strength and the grain size. If sand is the predominant grain-size sediment then the surf zone develops a pattern bars, separated by troughs. A complex three-dimensional topography occurs where longshore bars are cut by rip current channels. Percolation of swash is limited by the sediment texture and backwash carries the highly mobile sediment seaward across the gently dipping shoreface, thus dissipating wave energy and further reducing the wave power at the beach. When sand and gravel are available, a steep gravelly reflective foreshore may lie landward of a gentler finer-grained more dissipative shoreface. Where mud is the predominant sediment and is transported in suspension, the soft unconsolidated bottom and subacqueous fluid mud shoals can completely attenuate wave energy and protect the coastline from erosion. Continual landward motion of water carries mud particles landward, with no counterbalancing offshore movement so that muds are trapped in the nearshore zone.
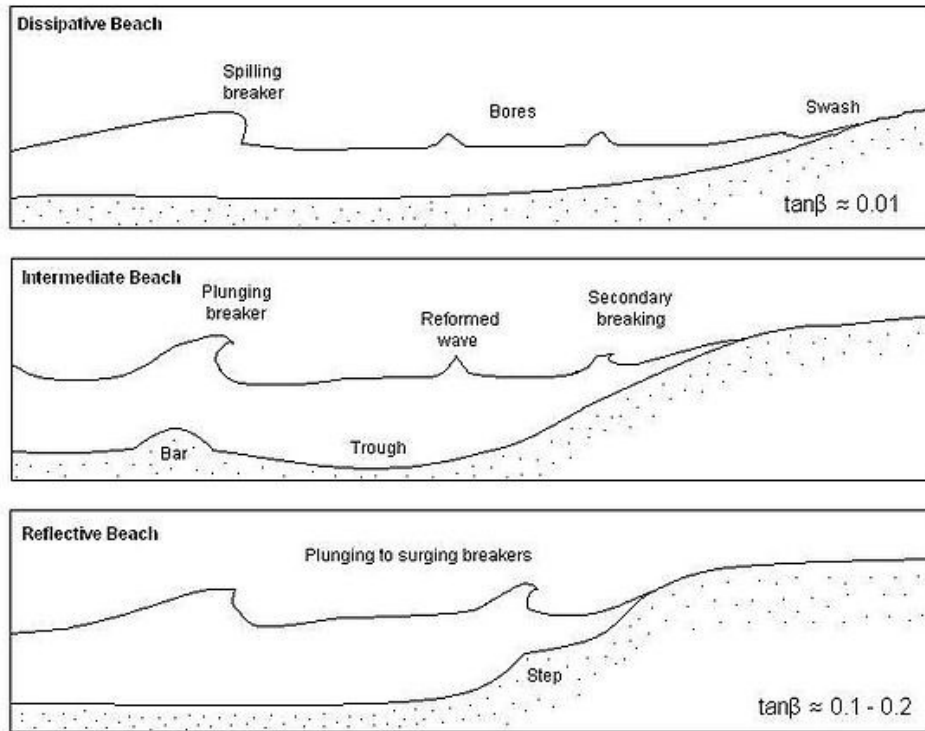
Fig. 10 - Beach classification after Wright and Short (1984) showing dissipative, intermediate, and reflective beaches.

Tides and waves are dominant forces driving littoral processes on open coasts because they sort the sediment and move it alongshore. Davies (1964) applied an energy-based classification to coastal morphology by dividing the world's shores according to tide range. Hayes (1979) expanded this classification, defining five tidal coastlines categories:

- microtidal < 1m;

- low-mesotidal, 1-2 m;

- high-mesotidal, 2-3.5 m;

- low macrotidal, 3.5-5 m;

- macrotidal > 5 m.

Ainsworth (2003) and Ainsworth et al. (2008) coupled the impacts of coastal morphology with the concepts of accommodation-to-sediment supply A/S ratios to predict the occurrence of primary and secondary processes in mixed-process systems along both fluviatile and non-fluviatile shorelines in settings where tidal influence was predominantly driven by shoreline morphology.

In this classification scheme, depositional systems are initially defined based on the relative influence of tidal, wave, and fluvial processes that acted on the sediments as they were deposited. Thus, coastlines are routinely classified as *wave-*, *tide-*, or *fluvial-dominated*.

Wave-dominated shorelines are those where wave action causes significant sediment transport and predominates over the effects of tides (Heward, 1981). Tides play an important role in defining the geomorphology of depositional shores, namely coastal and deltaic plains. On such shores, it is the ratio of tidal energy, usually dictated by tidal range, to wave energy, a function of average wave height, that determine the morphology of the coast, with sediment supply being an important modifier near major river mouths. As a generalization, coasts with small tidal ranges (Davies, 1964) are *wave-dominated*. On the other hand, coasts with large tidal ranges are typically dominated by tidal energy and are termed *tide-dominated* coasts.

The Ainsworth classification uses discrete categories that are based on a dominant process, as well as a secondary and tertiary process. A non-fluviatile coastline can be wave dominated (W); wave dominated tide influenced (Wt); wave and tide influenced (when wave and tidal processes are equal [wt]); tide dominated, wave influenced (Tw); or tide dominated (T). When this approach is expanded to include fluvial influence, additional different combinations of fluvial, tidal, and wave processes are introduced. Where three processes are involved, the most important process is said to "dominate," the second most important process is said to "influence," and the third most important process is said to "affect" deposition. For example, a system may be classified as fluvial dominated, tide influenced, wave affected (Ftw). Figure 11 shows schematic but representative plan-view geometries of systems. Note the distinct differences in coastal geometries that result from the different combinations of processes.
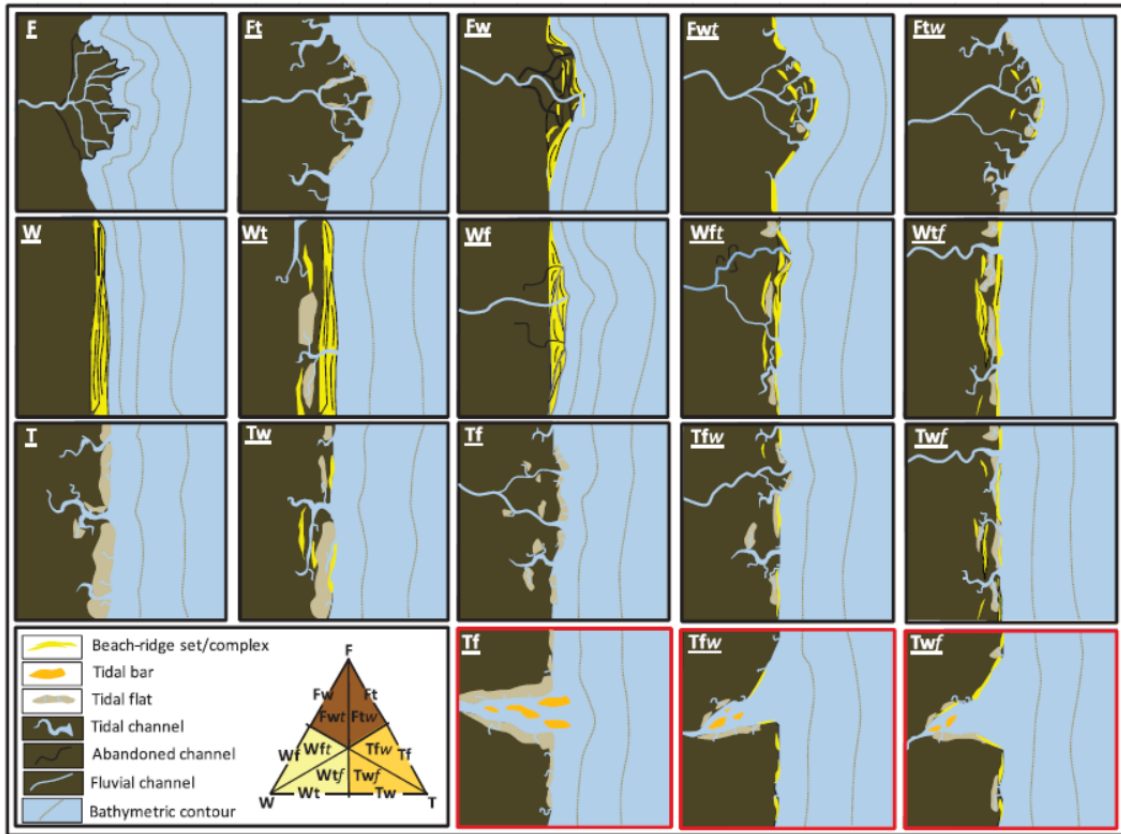
Fig. 11 - Representative schematic plan view models of the classification categories. The figure was developed from analysis of architectures of modern systems. Note differences in geometries and depositional elements in the different categories. Red boxes around the Tf, Tfw, and Twf (bottom right) represent differences in architecture of these categories when part of an embayed shoreline. Categories T and Tw can occur along stretches of shoreline within the embayed Tf, Tfw, and Twf categories. Map scales and labels of bathymetric contours have purposefully been omitted to keep the models generic (from Ainsworth et al., 2011).

36

2.4   SHORELINE CHANGE STUDY

Shoreline location and changes are important to coastal scientists and engineers to manage the coastal areas (Douglas & Crowell, 2000; National Research Council, 1990). Coastal management and engineering design require information about shoreline variations over time and even about the future trend. A shoreline change analysis is needed to (i) plan coastal protection (Coastal Engineering Research Center, 1984), (ii) calibrate and verify numerical models (Hanson et al., 1989), (iii) assess sea-level rise (Leatherman, 2001), (iv) develop hazard zones (Bellomo et al., 1999; Douglas et al., 1998), (v) formulate policies to regulate coastal development (National Research Council, 1990), (vi) assist with legal property boundary definition (Morton & Speed, 1998), and (vii) coastal research and monitoring (Smith & Jackson, 1992). The location of the shoreline can provide information in regard to shoreline reorientation adjacent to structures (Komar, 1998) and beach width and volume (Smith & Jackson, 1992), and it is used to quantify historical rates of change (Dolan et al., 1991; Moore, 2000).

2.4.1 SHORELINE: WHAT'S THE TRUTH?

Shoreline is a transient boundary that changes rapidly in time and it is affected by many factors. Thus, a functional definition is required to analyse the variability of the shoreline both in a temporal and spatial sense.

An idealized definition of shoreline is that it coincides with the physical interface of land and water (Dolan et al., 1980). This definition is apparently simple, but it is a challenge to apply. In order to investigate the idealized shoreline boundary variations, coastal scientists have typically adopted the use of shoreline indicators. A shoreline indicator is defined as a feature that represent the "true" shoreline position (Boak & Turner, 2005).

Individual shoreline indicators generally fall into one of three categories (Boak & Turner, 2005):

- Indicators that are visually discernible coastal feature and can be physically seen. The *high-tide line* or the *wet/dry boundary* are part of this group (Fig. 12);

- Tidal datum–based shoreline indicators, that are determined by the intersection of the coastal profile with a specific vertical elevation, defined by the tidal constituents of a specific area. Examples are the *Mean High Water* (MHW) or *Mean Sea Level* (Fig. 12);

- The third category is based on the application of image processing techniques to extract proxy shoreline features from digital coastal images that are not always visible to the human eye (Aarninkhof et al., 2001).

KEY
A Bluff top/cliff top
B Base of bluff/cliff
C Landward edge of shore protection structure
D Seaward stable dune vegetation line
E Seaward dune vegetation line
F Erosion scarp
G Storm/debris line
H An old high tide water level
I Previous high tide high water level
J Mean high water (datum referenced)
K Wet/dry line or runup maxima
L Groundwater exit point
M Instantaneous water line
N Shorebreak maximum intensity
O Mean lower low water line (datum referenced)
P Beach toe/crest of beach step

Fig. 12 - Sketch of the spatial relationship between many of the commonly used shoreline indicators (Boak & Turner, 2005).

Visually discernible indicators can be grouped into three types. The first one is based on the alignment of man-made structures, e.g. the landward edge of a revetment structure. The second type is based on a morphological feature, e.g. an erosion scarp. The third type includes those based on the position of a selected waterline, e.g. previous high tide High Water Level (Boak & Turner, 2005).

Many authors refer to the discernible indicators as High-Water Line (HWL). Commonly, the HWL is visually determined as a change in tone left by the maximum runup from a preceding high tide (Anders &

Byrnes, 1991; Crowell et al., 1991; Smith & Zarillo, 1990). Nevertheless, the definition provided by the several and different authors is often ambiguous and varies considerably between studies. Many studies (Anders & Byrnes, 1991; Moore, 2000; Pajak & Leatherman, 2002; Stockdon et al., 2002) has shown that the interpretation itself of the HWL from aerial photographs can be a significant source of error for shoreline mapping. For example, the HWL may not appear as a distinct line but instead may appear as a transitional zone or may not be visible at all (Crowell et al., 1991). McBeth (1956) suggested that the previous high tide HWL will appear as a static, shore-parallel band, even after the tide has receded and the shore has been exposed to drying from the sun. Crowell et al. (1991), Leatherman (1983), Stafford & Langfelder (1971) also use the term wet/dry line to describe this feature; it may introduce a further source of potential uncertainty, because Dolan et al. (1978), Dolan et al. (1980) and Overton et al. (1999) consider the wet/dry line to be the rising maximum runup limit on a flooding tide, and the landward extent of the falling ''wetted'' beach during tidal ebb. Inspection of an aerial photograph will often reveal multiple shore-aligned bands around the waterline (Pajak & Leatherman, 2002). These shore-aligned bands may be interpreted by different researchers as any one of several shoreline indicators, including the previous HWL, the debris line, a prior HWL, vehicle tracks, or erosion scarps (Moore, 2000; Pajak & Leatherman, 2002).

Of some concern is that many of indicator features may not take account of the spatial and temporal influences in shoreline position; for example, they do not consider the prevailing tide and wave conditions at the time the "shoreline" was mapped. For example, on a low, sloping beach, the horizontal offset of a shoreline indicator feature due to wave, tide, or wind effects can be on the order of several tens of meters (Thieler & Danforth, 1994). Seasonal influences may also significantly affect the position of the shoreline indicator relative to the land–water interface (Moore, 2000; Smith & Zarillo, 1990). Storminess and short-term shoreline variability are also significant factors that need to be taken into account when assessing longer-term trends of shoreline change (Crowell et al., 1993; Fenster et al., 2001; Honeycutt et al., 2001; List & Farris, 1999; Morton, 1991; Smith & Zarillo, 1990; Zhang et al., 2002).

Ideally, the selection and definition of the preferred proxy shoreline feature would be determined by the context of the specific investigation. Which shoreline indicator can be used at a specific location is often related to data availability (Boak & Turner, 2005).

However, the most common proxies are the wet/dry line (Crowell et al., 1991), the vegetation line (Garcia et al., 2010), the dune toe (Schwarzer et al., 2003) and the cliff top (Moore & Griggs, 2002). The wet/dry line is generally deemed as a valid indicator of shoreline position (Gorman et al., 1998). In fact, in some cases, the wet/dry line is the only indicator available, as occurs in highly developed coasts where the beach is backed by a seawall, revetment or other artificial structure. The dune toe is considered as the contact between backshore and foredune and it is usually chosen as shoreline proxy when the dune is present, with the aim of using an indicator that is independent of meteorological conditions, waves, tides and beach profile shape (Moore & Griggs, 2002; Schwarzer et al., 2003).

2.4.2 DATA SOURCE

Different kinds of data can be used as sources to examine the position of the shoreline, even though there is often a lack on historical data for the great majority of coastal sites. Therefore, the choice of what data to use is generally determined by the availability of data for the specific study area. This often means that different sources are used in a single study to achieve the desired temporal coverage, introducing additional potential uncertainty. There are many data sources that could be used by the researchers:

- *Historical Land-Based Photographs*, that provide general background information to the coastal investigator, such as the presence of a specific morphological feature such as a sand spit or channel entrance. However, most land-based photos are by definition very oblique, with limited information available of scale or ground control points, and there is usually no information about the sea conditions at the time the photograph was taken (Dolan et al., 1980). For these reasons, most historical photographs are of limited value for application to quantitative mapping of past shorelines;

- *Coastal Maps* and *Charts*, that are generally more focused on decoration than on content, with minimal information recorded, as the specific shoreline feature selected, and assessments of accuracy (Carr, 1962). Mapping and charting techniques became more reliable in the late 18th century (Carr, 1962), and these maps and charts can be useful for shoreline change investigations. Maps and charts provide good spatial coverage, but temporal coverage can be restricted, and is most often very site specific (Dolan et al., 1980). Potential errors associated with historical coastal maps and charts include errors in scale, datum changes, distortions from uneven shrinkage, stretching, creases, tears, and folds, different surveying standards, different publication standards, projection

errors and partial revision (Anders & Byrnes, 1991; Carr, 1962, 1980; Crowell et al., 1991; Moore, 2000). However, their advantage is being able to provide a historic record that is not available from other data sources. The shoreline obtained by historical maps and charts is generally assumed to have been associated with some type of visibly discernible features;

- *Aerial Photography*. Coastline vertical aerial photographs began to be collected around the world in the 1920s (Anders & Byrnes, 1991; Crowell et al., 1999), but reasonable-quality stereo aerial photos became available just in the late 1930s (Anders & Byrnes, 1991). By definition, the shoreline obtained from aerial photography is based on a visually discernible feature. Aerial photographs provide good spatial coverage of the coast (Dolan et al., 1980), but temporal coverage is site specific. They can only be taken on daylight and through clear skies, which make them weather dependent, and requiring rectification to compensate image distortions. Common distortions include radial distortion, relief distortion, tilt and pitch of the aircraft, and scale variations caused by changes in altitude along a flight line (Anders & Byrnes, 1991; Crowell et al., 1991; Moore, 2000; Thieler & Danforth, 1994). Modern softcopy photogrammetry allows a digitally scanned pair of aerial photos to be converted into a three-dimensional digital terrain model and a georectified orthophoto (Hapke & Richmond, 2000; Overton & Fisher, 1996). The addition of datum-referenced elevation information allows tidal datum–based shorelines to be easily and accurately determined. Where it is available, aerial photography is the most common data source for determining past shoreline positions;

- *Beach Surveys* data can be an accurate source of shoreline information (Dolan et al., 1980; Goldsmith & Oertel, 1978), but the high costs of the labor-intensive method of sending survey make them to be limited both spatially (Morton, 1991) and temporally (Dolan et al., 1980; Goldsmith & Oertel, 1978; Smith & Jackson, 1992). A shoreline can be compiled by interpolating between a series of discrete shore-normal beach profiles. Often the alongshore distance between adjacent profiles is relatively large, so alongshore accuracy of shoreline location is diminished accordingly (Morton, 1991). If sufficient beach profiling data are available for a specific site, tidal datum-based shorelines, such as MHW, are easily and accurately determined;

- *GPS Shorelines* is a recent method of mapping the shoreline. A kinematic differential GPS mounted on a four-wheel-drive vehicle is driven at a constant speed along the visibly discernible line of interest (Morton et al., 1993). The benefits of this method are that it is relatively rapid, low cost, and highly accurate (Morton & Speed, 1998). With modern GPS equipment, the greatest errors associated with this method are caused by the visual determination of the line of interest by the operator, rather than error from the GPS measurements;

- *Remote Sensing*: a range of airborne, satellite, and land-based remote sensing techniques have become more generally available to the coastal scientist. The derived shorelines may be based on the use of visually discernible coastal features, digital image-processing analysis, or a specified tidal datum. Multispectral/Hyperspectral Imaging Satellites provide near-continuous monitoring of many of the world's shorelines (Morton, 1991). Traditional multispectral satellite-flown instruments, such as Landsat, SPOT, etc., generate a discrete signal in a limited number of broadbands (Cracknell, 1999). Hyperspectral imaging provides wide and continuous spectral coverage (Richards & Jia, 1999). The main limitations of this data source are the pixel resolution and cost (Cracknell, 1999). The advantages of multispectral/hyperspectral imagery are the large areas that can be covered, and the detailed spectral information provided. Shorelines may be derived from visibly discernible coastal features (using true- or false-color imagery) or by the application of digital image-processing techniques. Airborne Light Detection and Ranging Technology Airborne light detection and ranging technology (LIDAR) has the ability to cover hundreds of kilometers of coast in a relatively short period (Stockdon et al., 2002). LIDAR is based on the measurement of the time it takes a laser beam, from leaving the instrument to return after reflection (Cracknell, 1999). Knowledge of the speed of light allows a distance to be calculated, and the use of differential GPS specifies an exact location. Tidal datum-based shorelines, such as MHW, can then be found by fitting a function to cross-shore profiles of LIDAR data (Stockdon et al., 2002). This data source is generally limited in its temporal and spatial availability because of cost. The main advantage of LIDAR data is that it can cover large areas very quickly. Microwave Sensors Data from the microwave range of wavelengths can be collected using airborne side-looking airborne radar or spaceborne synthetic aperture radar. Information about the point on the ground is calculated based on the return period of the signal and

signal strength (Richards & Jia, 1999). Large spatial areas can be covered using radar technology, but the cost is high (Richards & Jia, 1999). Data can be easily converted into a digital terrain model (Cracknell, 1999), providing good determination of tidal datum-based shorelines;

- *Video Imaging*. These systems have the capability to monitor detailed changes in the coastal system, as well as providing long-term shoreline change information. One example is the Argus coastal imaging system (Holman et al., 1993) that consists of one or more cameras pointed obliquely along the coastline. The cameras are connected to an automated computer, which controls the capture and pre-processing of the images. The original images are oblique and need to be corrected before they can be used to determine a shoreline. The fixed location of the sensor means that only the lens characteristics (radial distortion) and ground control points are required to create a georectified image (Holland et al., 1997). The system has the ability to collect time-averaged images as well as instantaneous images. All other data sources discussed above collect only an instantaneous record. These types of systems provide temporally dense but spatially limited data sets. It means that the density of data can be useful to resolve the short-term fluctuations.

2.4.3 TECHNIQUE TO DETECT SHORELINE

First step to detect shoreline from data source is to choose a unique shoreline indicator that will act as a proxy for the land-water interface. Then, the operator detects the chosen shoreline indicator within the available data source. Most of the detection techniques are subject to induce error when estimating a shoreline position (Stockdon et al., 2002). Various data acquisition techniques have been developed to map the position and shape of shoreline over time (Thieler & Danforth, 1994). The most common shoreline detection technique applied to visibly discernible shoreline features is manual visual interpretation, in the field or from aerial photography. In the field, a GPS is used to digitize the visible shoreline feature in situ, as determined by the operator. Aerial photographs are generally corrected for distortions, adjusted to the correct scale and then a shoreline is traced directly or scanned into a computer, corrected, adjusted for scale, and digitized. Nevertheless, these methods are subjective and often rely on the individual skills of the interpreter or photogrammetrist (Anders & Byrnes, 1991; Byrnes et al., 1991; Dolan et al., 1980; MCbeth, 1956). It also means that it would be better if the operator is familiar with the specific location, including knowledge of factors that may have affected the position of the shoreline, such as hurricanes, beach replenishment, etc.

(Byrnes et al., 1991). Some authors suggested that the detection of a chosen visible shoreline indicator feature from aerial photographs may be more subjective and less accurate than in situ detection in the field (Crowell et al., 1991; Pajak & Leatherman, 2002). Many of the features indicating the position of the shoreline indicator may be remnants of previous high-water events and may not represent the true position of the most recent maximum runup limit. An individual HWL has no reference to a tidal datum or a fixed elevation; instead, it may represent a combination of several factors, including pre-existing beach face morphology, atmospheric conditions, and the prevailing hydrodynamic conditions.

In the light of the above, many authors recognized the need to improve the accuracy of shoreline mapping (Morton, 1991) and to find an objective, robust, and repeatable detection techniques (Boak & Turner, 2005). Softcopy photogrammetry (Hapke & Richmond, 2000; Overton & Fisher, 1996), LIDAR topographic data (Stockdon et al., 2002), and survey data can be used to create a digital terrain model of the coastline, from which a tidal datum-based indicator can be determined. Tidal datum shoreline indicators seem to meet the needs described above, but their applicability to the analysis of historical trends is more limited.

Aerial photographs and softcopy photogrammetry can allow coastal scientists to generate a tidal datum-based historical shoreline, but good-quality stereo pairs and accurate ground control points are needed (Brown & Arbogast, 1999). Otherwise, it is necessary to integrate subjective historical shorelines with modern objective analysis. The differing accuracy and potential offset between the two data sets must be carefully considered. Objective detection methods for application to visual shoreline features have recently been developed using supervised and unsupervised classification techniques. These types of objective shoreline detection techniques utilize the colour information contained in digital images (i.e., red, green, and blue). In a physical sense, as light penetrates a water surface, wavelengths from the red range (~0.7 mm) of the electromagnetic spectrum are attenuated more rapidly than those from the blue range (~0.4 mm). This results in a pixel corresponding to the "wet" state and being predominantly blue and green (because the red component has been absorbed), whereas a "dry" beach pixel exhibits all three components. Each of these techniques manipulates this optical information in a slightly different manner to objectively define a proxy shoreline feature. The objective detection techniques just described, along with other comparable digital image-processing methodologies, can be used to identify a robust and repeatable shoreline indicator feature

for shoreline investigation. However, a fundamental shortcoming of these new objective methods is that they still do not resolve the basic question of the relation of the specific shoreline indicator feature to the land–water interface.

2.4.4 SHORELINE CHANGE RATE

The shoreline rate of change statistic is expected to reflect a cumulative summary of the processes which have impacted the coast through time. The precision with which rate of change values reflect this "summary" is dependent on:

- accuracy of the shoreline measurements;

- temporal variability of the shoreline;

- number of data points, thus measured shoreline positions, used in calculating the rate;

- proximity of each observation to the time of an actual change in the trend of shoreline movement;

- period of time between the shoreline measurements;

- total time span of shoreline data;

- method used to calculate the rate.

The movement of the shoreline over time usually consists of a predictable component of variation that can be regarded as the signal, and short-term variation, or noise. Long-term phenomena, such as a rise in sea level or the shift in natural sediment supply, occur over periods of decades to centuries and produce the more predictable trends. Generally, short-term variation is introduced over periods ranging from days to seasons (National Research Council, 1990). This suggests that both the long- and short-term trends are discernible, but it may be hard to understand if the processes responsible for these changes function independently or dependently. Furthermore, the definition of long-term depends on the purpose of the investigation, the availability of data, and the temporal variability of the shoreline under study. If a shoreline is undergoing change at a constant and uniform rate, the time interval is not an important consideration and the precision of the estimates of change would be high. In reality, few shorelines behave in this manner. When developing statistics for predicting shoreline change from highly variable shoreline data, the reliability of the data used is a fundamental issue. The first step in calculating rates of shoreline change is to measure the position of the shoreline as accurately as possible (Dolan et al., 1991).

Following several shoreline rate of change statistics will be described and their reliability is going to be also discussed.

The *End Point Rate* (EPR) method is a simple calculation of the distance of total shoreline movement divided by the time elapsed between the measurements (Fig. 13). Usually, the earliest and latest dates are used, but if several shoreline positions are available, combinations of EPRs can be calculated. The primary advantages of the EPR method are the ease of computation and its widespread use. The main disadvantages are that in some cases, available data, which record shoreline changes, are not used in the analysis of the shoreline's dynamics and, in using only two data points, spurious data can have a strong influence on the results. When data that are available in the record are not used in the analysis, important trends or changes in trend may not be detected or incorporated into the results. Naturally, as the temporal variation increases, the likelihood of omitting important trends also increases (Crowell et al.,1997; Dolan et al., 1991).
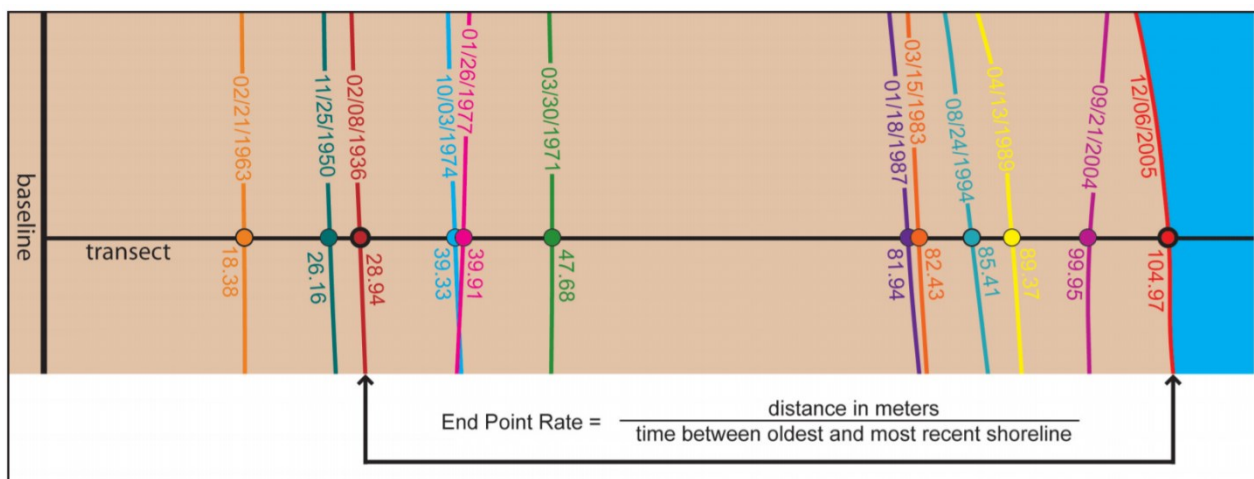
Fig. 13 - The End Point Rate is graphically and mathematically shown. It is computed as the distance between the oldest and the youngest shorelines divided by the span of time elapsed between the two shoreline positions. All other shoreline data are ignored in this computation (Thieler et al., 2005).

Another approach is to calculate a best fit line, using the method of *Least Squares*, through the entire sample of shoreline positions; the slope of the line is an estimate of the shoreline rate-of change. *Linear regression rate* (LRR) is purely computational (i.e., requires no a priori analysis), is based on accepted statistical concepts, and is easy to employ (
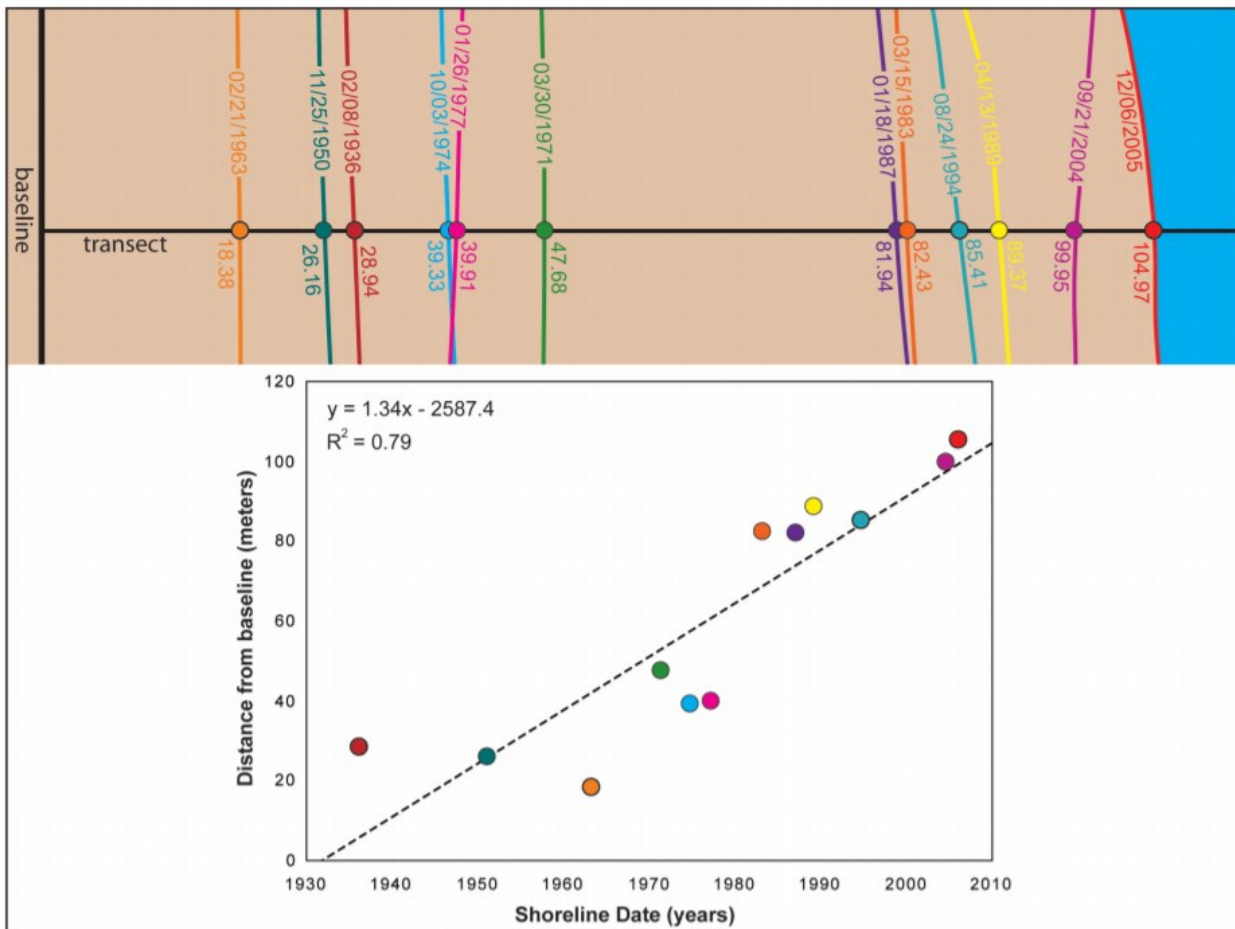
Fig. **14**). In addition, LRR uses all the data to calculate the rates (Dolan et al., 1991). One of the main problems with LRR is that, when the shoreline positions are clustered, some dates will have more influence on the regression than others. For example, many long-term data sets consist of at least one early shoreline position, obtained from a T-sheet, and a cluster of modern positions, obtained from aerial photographs. Regressions computed from these data result in rates that may be an unreliable balance between the old date and a cluster of modern dates, especially when the modern dates contain information on more recent trends in shoreline change (Genz et al., 2007).
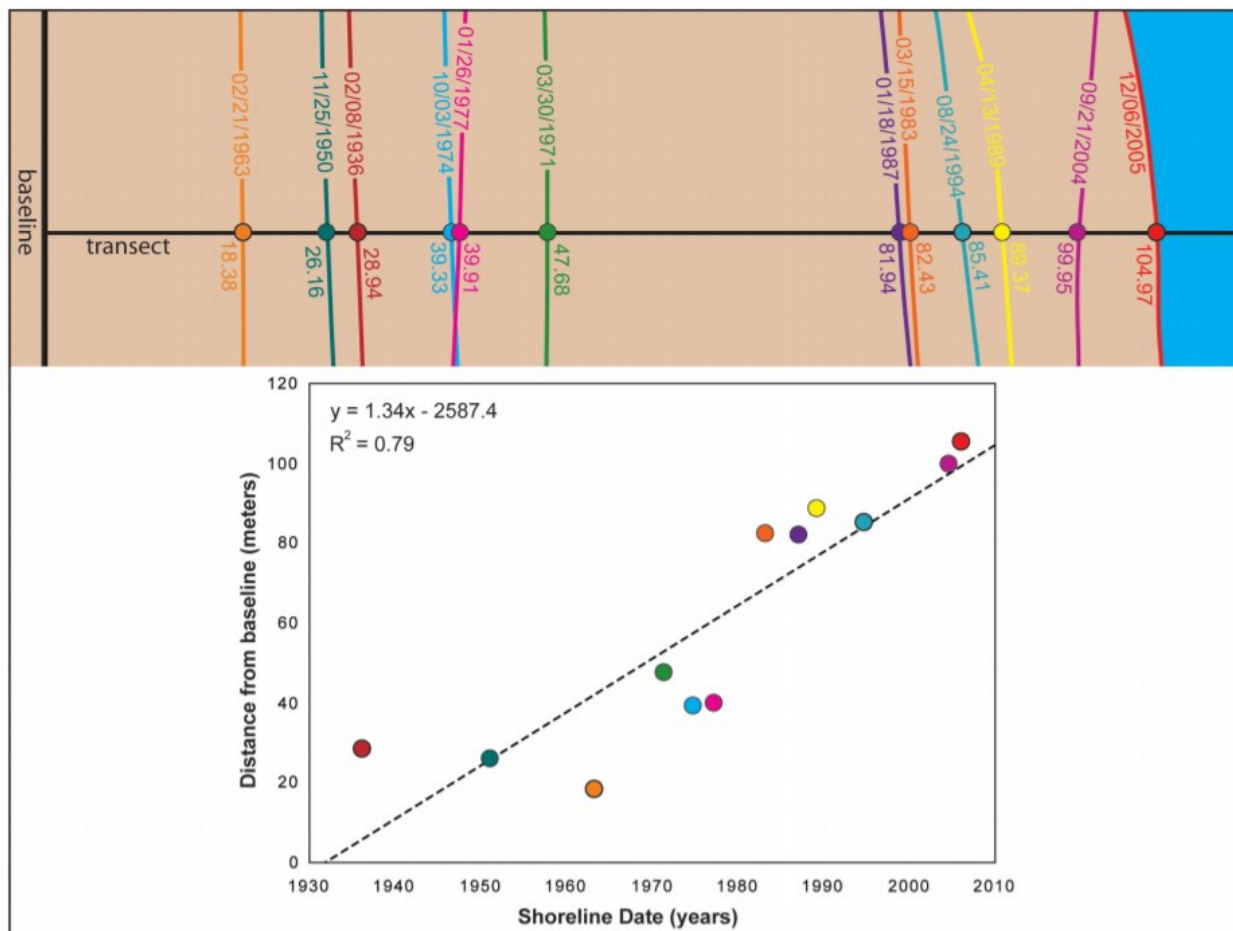
Fig. 14 - The linear regression rate is shown. It is determined by plotting the shoreline positions with respect to time and calculating the linear regression equation. The slope of the equation describing the line is the rate (Thieler et al., 2005).

Foster & Savage (1989) developed the *Average Of Rates* (AOR) method to average the long-term change, excluding changes due to measurement errors. To do this, they created a minimum time criterion that filters out any changes due to short time spans or measurement errors. EPRs are determined between all data point pairs and are removed if the time interval is less than a specified minimum. All EPRs that pass the criterion are averaged to determine the shoreline change rate (Dolan et al., 1991; Foster & Savage, 1989). One drawback is that the minimum time criterion can be affected by large errors or small EPRs, resulting in potentially misleading results (Dolan et al., 1991). AOR also gives more influence on EPR rates of short time spans (Fenster et al., 1993).

Since short-term changes may affect long-term trends, Fenster et al. (1993) proposed a simplified form of the *Minimum Description Length* (MDL) method to help identify influential short-term changes. Assuming Gaussian errors, MDL uses an error component and a complexity penalty to select the best model fit, whether it is a constant, line, quadratic, etc. If the resulting model is quadratic or higher, two lines are

produced— the zero-weight line (MDL ZERO), which uses only recent data, and the low-weight line (MDL LOW), which assigns weights to older data. MDL rates based on nonlinear models tend to result in variable or highly inaccurate forecasts, though the MDL criterion can help identify physical changes within a beach (Crowell et al., 1997).

The *Jackknifing* (JK) method uses multiple LS fits to determine the shoreline change rate. A different point for each line is omitted, resulting in a different slope for each line. The slopes are averaged to provide a shoreline change rate. Jackknifing has the advantage of decreasing the influence of clustered data and extreme data points. However, computing all possible linear trends is not efficient (Dolan et al., 1991).

Reweighted Least Squares (RLS) helps identify the true trend of shoreline change data by removing statistical outliers in the data. This two-step method first identifies outliers at a cut-off value ($\hat{\sigma}$) using the least median of squares regression (Rousseeuw & Leroy, 1987). Points identified as statistical outliers are given a weight of 0, and all other points are assigned a weight of 1. A LS fit then finds the trend with all data points of weights equal to 1. Unlike LS, RLS is more robust and not as sensitive to outliers. RLS has a breakdown of 50%, thus, if 50% of the data are outliers, the trend of the data can still be identified accurately (Rousseeuw & Leroy, 1987).

Genz et al. (2007) reviewed most studies of shoreline changes and other studies that determine the most appropriate method based on either a comparative approach or the prediction of known positions. They mentioned the paper of Dolan et al. (1991), which compared long-term and short-term erosion rates. They focused on methods such as End Point Rate (EPR), Linear Regression Rate (LRR), Jackknifing (JK), and Average Of Rates (AOR). By plotting the rates from one method vs. the rates of another method, they concluded that AOR is most variable, while LRR and JK share a high degree of similarity. They stressed that the best method depends on the objective and the temporal variables of the research. In 1995, Thieler, et al. calculated erosion rates using EPR, LRR, JK, and AOR in the Digital Shoreline Analysis System (DSAS), an ArcGIS extension that provides an automated method to perform rate calculation. They divided their study site into four separate areas and calculated an average shoreline change rate at each section for each of the four methods. All four methods resulted in similar rates, but AOR was identified as the most appropriate shoreline change rate method. Dean & Malakar (1999) considered the LRR, EPR, and AOR methods to map Florida's hazard zones. They calculated correlation coefficients to compare the three methods. All three

methods agreed with each other; however, EPR and LRR correlated better with each other than either did with AOR. The authors chose LRR as their preferred method. Crowell et al. (1997) compared predicted values from the MDL and LRR methods to actual values using sea-level data as a proxy for historical shoreline data. They concluded that LRR provides equal results for shorelines without any physical modifications. Differing from Crowell et al. (1997), Honeycutt et al. (2001) compared EPR to LRR by predicting known historical shoreline data to determine the accuracy of the methods. Using a priori knowledge of major storms, they confirmed the findings of Galgano et al. (1998) and Galgano & Douglas (2000), which showed that the accuracy of shoreline change rates improves without storm-influenced data points. They concluded that LRR better predicts shorelines than EPR.

Most shoreline change rate methods assume shoreline change is linear through time, with any nonlinearity attributed to mapping and measurement errors, but shoreline evolution is not generally uniform (Douglas et al., 1998; Fenster & Dolan, 1994; Fenster et al., 1993; Morton, 1991).

This is the reason why Genz et al. (2007) proposed a new erosion rate method that assumes heteroscedastic uncertainties. It is the Weighted Least Squares (WLS) or Weighted Linear Regression Rate (WLRR), which considered the variance associated with each shoreline position (Y component) is not necessarily the same at each time (X component) (e.g., Kleinbaum et al., 1988). If the variance (σ^2) or standard deviation (σ) for each Y component is known, the weight (w) is defined as

$$w = 1/ (\sigma^2)$$

Data points with large variance will have less of an influence on the trend line than data points with smaller variance (Graybill & Iyer, 1994). For example, early shoreline data have larger uncertainties associated with them than recent shorelines. WLS will put more weight on the recent data. In order to apply this method, it is necessary for researchers to estimate all uncertainties associated with their study. A disadvantage of this method that it is sensitive to outliers even if their weights are small. Hence, a priori knowledge is also important. If the calculated uncertainties at each shoreline position do not accurately express the real deviations, then the resulting rate may underestimate or overestimate the true rate.
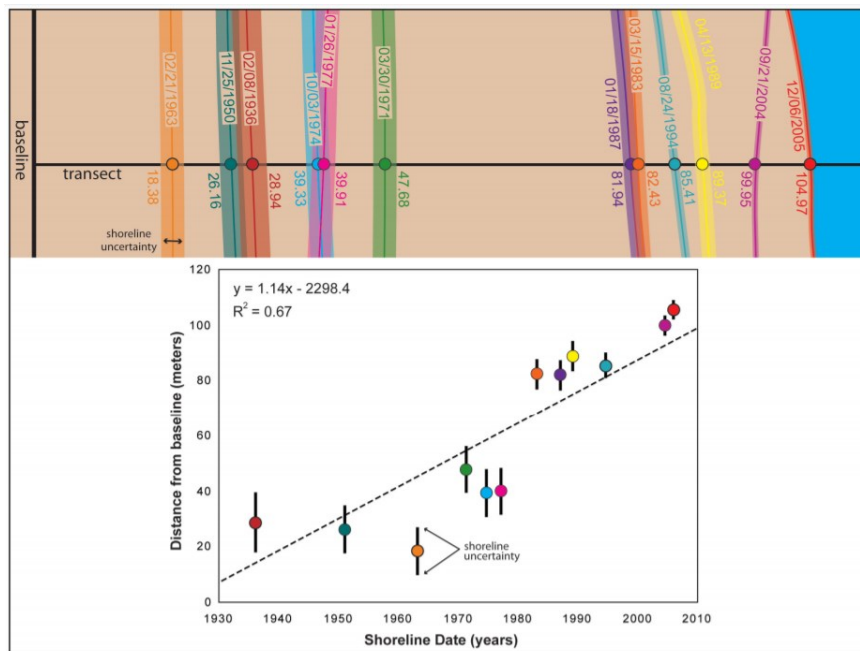
Fig. 15 - The weighted linear regression rate is determined by plotting the shoreline positions with respect to time; these data are exactly the same as in the linear regression example. The shoreline measurement points with smaller positional-uncertainty values had more influence in the regression calculation because of the weighting component in the algorithm. The slope of the regression line is the rate (Thieler et al., 2005).

2.4.5 SHORELINE CHANGE ANALYSIS METHODS

Shoreline change analysis can be led by using different methods:

- GIS-based Analysis of Shoreline Dynamics;

- GIS-based Data Model for Shoreline Representation.

The *GIS-based Analysis of Shoreline Dynamics* is based on the assumptions that the shoreline progresses or recedes along a major direction, which is perpendicular to the main orientation of the coastline. This method involves the use of transects casted from a baseline. In recent times, computers allowed the progressive automation of most of the tasks and a considerable reduction of the processing time. Attempts to automate transect extraction operations can be traced back to Dolan et al. (1978), who used manual measurements, along a baseline and punched the data into computer cards to computerize the calculations. Taking full advantage of progresses in computing, Clow & Leatherman (1984) developed a new technique for the definition of baselines and transects, which substantially increased automated components. Currently, the most user-friendly and powerful tool available is the Digital Shoreline Analysis System (DSAS), created by Thieler & Danforth (1994). This program was originally developed using loosely couple programming technique, while current versions use the ArcView Avenue Macro language. Within an ArcView environment, DSAS can benefit from the other GIS capabilities of ArcView, such as importing shapefiles,

coverages and grids, editing, and changing projections. The latest version of DSAS can be downloaded freely from the USGS web page. GIS systems provide new or improved capabilities to study shoreline dynamics. The GIS vector format can handle accurate geographic positions that allow for detecting a very small displacement of spatial features. More recent software specifically developed for coastal analysis gained increased flexibility by using the vector-based concept of polyline, which can be treated as objects, instead of ASCII or binary files that only contain pairs of coordinates. GIS programs treat shorelines as being constituted by sets of polylines. Each polyline is an ordered collection of paths that can be connected or disjointed (Cadkin, 2002). The paths contain a collection of segments defined by pairs of points (from- and to-points) that must contain x, y values; optional values attributes height, and other properties can also be assigned to each point or line segment.

The *GIS-based Data Model for Shoreline Representation* is built upon the arcs of a line coverage, and allows for the use of real-world coordinates with linear measures. Dynamic segmentation involves three types of elements: routes, sections and events. A section is a set of related arcs in the line coverage, and provides measures to a route system. A route, which is also a linear feature made up by sections, has a unique identifier and measurement system on the m value of attributes, and is treated as a sub-class in line coverages. Events are attribute data such as occurrences and local conditions that are related to the route system by measures of their location. The process of developing a model requires the creation of routes, their measurement, and building event tables. Bartlett et al. (1997) proposed a dynamic segmentation approach to the coast to facilitate the creation of sensitivity maps. The key variables for their dynamic segmented linear model fell under three major types: environmental data (shoreline types, shore structure, sediments), socio-economic and cultural data (population, scientific interest), and mathematical weight values. The model created by Bartlett et al. (1997) not only improved shoreline representations in GIS, but also became the foundation for a coastal zone geographic information system (CZGIS). Morton and Peterson (2003) proposed a schematic model to perform coastal classification. The model is based on a comprehensive list of coastal types based on morphological characteristics that can be easily traced in aerial photographs. The presence of a given characteristic along a sector of the coast can be treated in a GIS environment as an arc and visually represented through colour based codes. The advantage of the Morton and Peterson (2003)

method is that allows for multiple classification of the same segment of the coast when several characteristics are present.

2.4.6 *UNCERTAINTY AND ERRORS*

The accuracy of shoreline change rates depends on the data quality and on the methods by which they are calculated. There are many potential sources of error involved in the process of measuring rates, thus knowing and understanding the errors involved is vital to the successful completion of a project. Errors can be divided into two categories (Moore, 2000):

- those introduced by data sources (historical maps, aerial photography, etc);

- errors introduced by measurement methods, thus related to the shoreline indicator adopted and the detection processes.

Aerial photographs are the most commonly used data source in shoreline mapping. Nevertheless, some studies require to cover a larger time span to reconstruct the shoreline variation, aerial photography can be very site-specific for some areas, thus the use of chart and historical maps in conjunction with aerial photography is needed. When multiple data sources are used in shoreline change studies, the uncertainties must be properly accounted for in order to be able to test the statistical significance of the shoreline change signal. The use of historical maps introduces several potential errors to the coastal mapping process. The severity of these errors depends on the accuracy standards met by each map and on physical changes in each map since publication (Anders & Byrnes, 1991). Map accuracy is influenced by displacements of feature position resulting from changes in the horizontal reference datum. Before detecting shorelines from maps with different projections, ellipsoids and datums, they must be converted to a common projection, ellipsoid and datum. Shoreline coordinates can be converted by specific equations (Clow & Leatherman, 1984; Thieler & Danforth, 1994), digitized coordinates can be converted to an intermediate coordinate system and then projected into a map projection, as in Evenden (1990 and 1991), or Geographic Information System (GIS) software can be employed to convert map data to a common coordinate system (McBride, 1989).

Finally, map shrinkage, stretch and other defects also add error to shoreline change analysis. For example, typical map paper can expand by greater than 1 percent with a humidity increase of 60 percent (Snyder, 1987). Estimates by Knowles & Gorman (1991) of potential change in map paper range from 0.03

to 0.25 mm. At a scale of 1:20,000 this is a ground distance of ±0.6 to 5.0 m. Errors may also result from tears, folds and creases in paper maps.

In Italy, The Italian Geographic Military Institute (IGMI) is the Army's geographic supporting office. It is also the National Cartographic Authority according to the law n° 68/1960 and therefore the high-quality cartography, produced by the institute and used by both public and private entities, is considered the official state cartography. In 1861, after the Italian unification, the IGMI began its activity as the Topographic Office of the Italian Army Staff, inheriting traditions and experiences from the topographic offices of three pre-Unitarian states: the Kingdom of the Two Sicilies, the Kingdom of Sardinia and the Grand-Duchy of Tuscany. Most of the official historical maps are provided by the IGMI and details on map construction processes and accuracy are described.

Vertical aerial photographs introduce the intrinsic distortions affecting the photographs as source of uncertainty. These distortions are due to different causes related to the geometry of the aerial photographs (Gorman et al., 1998; Wolf & Dewitt, 2000):

- Changing altitude of the aircraft along the line of flight due to atmospheric turbulences, causing scale changes between adjacent photographs;

- Camera tilt of the aircraft, producing not truly vertical but slightly oblique aerial photographs and hence distorting the scale of the photographs;

- Terrain relief causes an outward/inward displacement, that is called topographical displacement or relief displacement of the elements located above/below mean ground level, such as cliffs or buildings;

- Lens distortion, producing a radial deformation of the photograph. The two main consequences of these phenomena are scale changes between and within photographs and shifting of objects in the photographs away from true geographical location (Wolf & Dewitt, 2000).

Thus, aerial photographs should not be treated as maps (Anders & Byrnes, 1991) and they must be corrected before using them for the quantification of shoreline changes (Gorman et al., 1998; Moore, 2000; Boak & Turner, 2005). Coastal scientists often have digital orthophotographs available for recent periods and paper photographs for earlier periods. Orthophotographs are truly vertical aerial photographs whose perspective has been changed from central to orthographic by using a high-resolution DEM of the study area,

specific information on the camera used and specialized software (Hapke & Richmond, 2000), resulting in complete removal of the aforementioned distortions. On the other hand, the minimization of distortions in historical aerial photography is achieved by scanning and georeferencing processes. This procedure provides a common geographical reference system that enables digital photograph overlapping and thus coastal change measurements, and the process results in a geometric correction of most of the aforementioned distortions (Hughes et al., 2006), except the highest relief displacements that can only be removed by orthorectification (Moore & Griggs, 2002). Georeferencing of historical photographs is usually accomplished in GIS environment by using polynomic corrections based on ground control points (GCPs) identified on the photograph. The real-world coordinates of the GCPs are derived either from DGPS field surveys or from other mapping sources such as digital maps or orthophotographs from the same area. GCPs must be carefully chosen according to the general criteria of appropriate number, location and distribution established by authors like Moore (2000) or Wolf & Dewitt (2000). This way, on each photograph, an adequate number of GCPs should be identified, evenly distributed across the whole photograph and mostly located on human landscape features such as crossroads. If the photographs are intended to be used for calculating shoreline rates of change as accurate as possible, root-mean-square error (RMSE) for the GCPs should generally be less than one half the pixel size of the image (Vanderstraete et al., 2003). After this process is completed, geometrically corrected photographs and orthophotographs from the same areas are superimposed on GIS environment in order to assess temporal changes in shoreline position.

In addition to deficiencies inherent in maps and air photos, measurement errors associated with interpretation of shoreline proxy and digitization of the shoreline and control points are introduced. On maps, the shoreline is already delineated; on air photos the shoreline must first be detected by an interpreter. However, the precision with which an operator can visualize and move the cursor along a line can lead to much greater errors (Stafford & Langfelder, 1971). Fortunately, improper tracking associated with shoreline digitizing generally is random and may be dampened when averaged over finite distances of shoreline. To evaluate the magnitude of operator error associated with digitizing shoreline position, at least three repetitive measurements should be compared (Byrnes et al., 1989).

Moreover, seasonal and water level differences between successive maps and air photos must be considered. The position of the shoreline can vary significantly from summer to winter and from normal to

storm conditions. Smith & Zarillo (1990) estimate potential errors of up to ±40 m in shoreline position when comparing air photo sets taken during different seasons. Meaningful shoreline change rates demand that original data sources be consistent in conditions affecting the beach. Normal and storm conditions should never be compared if the objective is to examine long-term trends in shoreline change. Even differences in water level from high to low tide on gently sloping beaches with moderate tide range can significantly displace the shoreline. Extreme care should be taken to ensure that all data sets used in a shoreline analysis are approximately consistent with respect to season, water level, and short-term history of incident processes.

All the potential errors should be applied to each individual map or air photo. When making comparisons of shoreline position, error is cumulative because separate maps and air photos are being used (Anders & Byrnes, 1991).

For these reasons, uncertainty must be estimated in the interpretation of shoreline change position and several authors debated on the method to quantify it (Anders & Byrnes, 1991; Crowell et al., 1993; Moore, 2000). Most of them proposed methods to quantify the factors causing error, such as image resolution or short-term shoreline variability, and calculated by summing in quadrature (Coyne et al., 1999; Fletcher et al., 2003; Zviely & Klein, 2004). For example, Fletcher et al. (2003) calculated total uncertainty for the shoreline change rates of the beach of Maui (Hawaii) as following:

$$\text{Ut} = \pm \sqrt{T^2 + S^2 + t^2 + RMS^2 + O^2}$$

where

T = T- sheet uncertainty

S = seasonal positional uncertainty

t = tidal stage uncertainty

RMS = reported uncertainty due to orthorectification accuracy (includes pixel size and DEM uncertainties)

O = uncertainty due to onscreen delineation of the toe of the beach

In Romine et al. (2009), the uncertainties for shoreline change position in Southeast Oahu, Hawaii have been computed as:

$$\text{Et} = \sqrt{E_d^2 + E_p^2 + E_s^2 + E_r^2 + E_{td}^2 + E_{ts}^2 + E_{tc}^2}$$

where

E_d is the digitizing error. The digitizing error is the standard deviation of differences in shoreline position from a group of experienced operators. E_p is the pixel error, thus the resolution of the orthomosaics, factor that limits the ability to resolve the position of a feature. E_s is the seasonal error, the authors surveyed beach profiles summer and winter for 8 years and the seasonal change has been computed as the difference between shoreline positions along a survey transect between summer and winter. A randomly generated uniform distribution (> 10,000 points) is calculated incorporating the standard deviation of the measured seasonal changes. E_r is the rectification error, aerial photographs are orthorectified to reduce displacements caused by lens distortion, earth curvature, camera tilt and terrain relief. RMS error has been calculated by the misfit of the orthorectification model to the master orthorectified image and DEM. E_{td} is the tidal fluctuation error, it is the standard deviation of a randomly generated uniform distribution derived from the standard deviation of the surveyed tidal fluctuations. E_{ts} and E_{tc} are respectively the T-Sheet plotting error and the conversion error for T-Sheets, both related to the use of American T-sheet.

Virdis et al. (2012) examined the shoreline change evolution at two spatiotemporal scales over ca. 18 km of Platamona-Maritza beach (Northwestern Sardinia, Italy). They used as dataset archival aerial photographs, orthophotos, satellite imagery, light detection and ranging data, terrestrial laser scanner, Global Positioning System, and recent and historical topographic maps. The total positional uncertainty (σt) was calculated using the following equation:

$$\sigma_t = \sqrt{\sigma_d^2 + \sigma_p^2 + \sigma_r^2 + \sigma_{cor}^2 + \sigma_{td}^2 + \sigma_{wr}^2 + \sigma_{gps}^2}$$

As for Romine et al. (2009), σ_d is the digitizing error, evaluated by delineating the same feature several times on the same image and calculating the error as the standard deviation of position residuals for that feature, and σ_p is the pixel error, assumed to be equal to the pixel size, in that, theoretically it is not possible to resolve features smaller than this. σ_r is the orthorectification error, obtained as the RMSE for photogrammetric blocks. σ_{cor} is the image coregistration error, calculated from the RMSE of residual misalignment among single pixels from the multitemporal images dataset, obtained by the affine rectification. σ_{td} is the tidal fluctuation error, the authors assessed variations in levels at the tide gauge station located at Porto Torres, less than 20 km from the study area, to estimate the possible influence of tide levels. σ_{wr} is the wave runup error, considered a source of error when the wet/dry boundary is assumed as proxy for

shoreline multitemporal analysis (Ruggiero et al., 2001). This error can be estimated if the runup elevation is known. According to several authors (Moore et al., 2006; Stockdon et al., 2006; Vousdoukas et al., 2009) extreme runup elevation $R_{2\%}$ can be predicted by means of empirical equations based on deep-water significant wave height H_0, wave period T, and beach slope. The authors used and implemented the general expression for natural beaches developed by Stockdon et al. (2006). The authors did not include the seasonal error (σ_s) because they were unable to estimate it and they assumed that it could be considered negligible.

Del Rio and Gracìa (2013) proposed an easy-to-use technique to estimate error involved in the calculation of shoreline changes on aerial photographs, including the three most used types of shoreline indicators, that is, HWL, dune/cliff toe and cliff top. They take in account both the uncertainties related to each shoreline proxy, such as relief in the case of the cliff top or tidal oscillations in the case of the HWL, and the error components related to the dataset (scanning and georeferencing). The method is based on the assumption that the cumulative uncertainty in shoreline position digitized from an aerial photograph is the result of three factors:

1. *scanning error*, represented by the image resolution (R) (Coyne et al. 1999; Catalão et al., 2002);

2. *georeferencing error* (G), represented by the RMSE of the georeferencing process (Shoshany et al., 1996; Morton et al., 2004)

3. a *physical component of the error* (D), related to each shoreline proxy adopted.

The *scanning error* (R) of uncertainty corresponds to the scanning or digital capture processes of the original photographs or orthophotographs. It is represented by image pixel size (Coyne et al. 1999; Catalão et al. 2002), since the larger the pixels, the larger the uncertainty in interpreting shoreline position on the photograph. According to the Shannon sampling theorem, pixel size should be set to at least one half of the minimum spacing that needs to be resolved on the photograph (Weeks, 1996; Lehmbeck & Urbach, 2004). The *georeferencing error* (G) is related to the geometric correction of the photographs, expressed by the RMS error of the process (Shoshany et al., 1996; Morton et al., 2004). As mentioned above, the so called *physical component of the error* (D) depends on the shoreline proxy. In the case of using the HWL, it includes the changing high water level due to alternating spring-neap tides, as well as the horizontal variability of high water mark resulting from changes in beach slope. The position of the HWL is also influenced by waves and storm surges, but most photogrammetric flights are generally performed under

fairweather conditions in spring or summer periods, so it was not included by the authors. Nevertheless, in case that post-storm photography cannot be avoided, then the local variability of the HWL during storms should be estimated and included in error calculations (Moore, 2000). D factor is geometrically calculated as the horizontal variability in shoreline position resulting from a certain tide height (M) on a beach profile with a certain slope (tanβ) (Allan et al., 2003):

$$D_{HWL} = M/\tan\beta$$

If the date and time of the aerial picture is known, M is computed by the specific tide conditions, otherwise it is calculated as half the maximum difference between spring and neap high tide levels in the study area.

In case of using the cliff top as shoreline indicator, the D component of error represents relief displacement, which is partly but not completely removed by geometric correction. The magnitude of relief displacement depends on cliff height, cliff position in the aerial photograph, image scale and characteristics of the georeferencing process (Anders & Byrnes, 1991; Zviely & Klein, 2004). The displacement increases in low altitude aerial photographs. The D component of error is computed as:

$$D_{TOP} = (S \times d \times h/H)/\sqrt{n}$$

where S is image scale, d is the distance from the cliff top to the principal point of the photograph, h is cliff height, H is flight height and n is the number of GCPs used in the georeferencing process. If digital orthophotographs are used, the D factor is zero, as orthorectification removes relief displacement.

Finally, where dune foot or cliff toe is employed as shoreline proxy, the D factor is also considered as zero, due to the relative independence of these indicators from both short-term variability and relief displacement errors.

The total uncertainty in shoreline position on a certain photograph (EP) is computed as the quadratic sum of each component (Coyne et al., 1999; Fletcher et al., 2003) according to the following:

$$E_p = \sqrt{G^2 + R^2 + D^2}$$

This equation is used to calculate the error E_p for each image (P), thus it needs to compute the cumulative error when comparing multiple images (Anders & Byrnes, 1991). It is obtained as follow (Fletcher et al., 2003; Morton et al., 2004):

$$E_{rate} = \sqrt{E_{p1}^2 + E_{p2}^2}/T$$

where E_{p1} and E_{p2} are the error computed for each image used for the analysis and T is the time span between two photographs.

2.5   GRAIN-SIZE AND TEXTURAL SEDIMENT ANALYSIS

Grain-size is one of most significant physical property of sediment and commonly used in order to understand the processes involved in transportation and deposition of sediments (Inman, 1952; Folk & Ward, 1957; Mason & Folk, 1958; Friedman, 1961; Nordstrom, 1977). Grain-size parameters have been proved to be a useful measure of the speed of the depositing flow (McCave, 2008). The objectives of a grain-size analysis are to accurately measure the individual particle sizes to determine their frequency distribution and to calculate a statistical report that effectively characterizes the samples.

Statistical parameters used to describe sediment samples are generally those proposed by Folk & Ward (1957). In order to compare sedimentary environments with each other quantitatively, they adopted and improved precise measures of average size, sorting, and other frequency distribution properties. These properties may be determined either mathematically by the method of moments or graphically by reading selected percentiles off the cumulative curves. They focused their work on the following statistical parameters:

- *Median*;

- *Mean size*;

- *Sorting*;

- *Skewness*;

- *Kurtosis*.

The *Median* (Mz) corresponds to the 50th percentile on a cumulative curve, where half the particles by weight are larger and half are smaller than the median.

The *Mean* S*ize* is the average grain-size and the most inclusive graphically derived value is that given by Folk & Ward (1957):

$$\text{Mz} = \frac{\varphi\,16 + \varphi\,50 + \varphi\,84}{3}$$

where 16, 50, and 84 represent the size at 16, 50, and 84 percent of the sample by weight. Mean is also measured in phi units and is the most widely compared parameter.

Sorting (σ) is a method of measuring the grain-size variation of a sample by encompassing the largest parts of the size distribution as measured from a cumulative curve. Folk & Ward (1957) introduced the "inclusive graphic standard deviation", that is calculated as follows:

$$\sigma = \frac{(\varphi\,84 - \varphi\,16)}{4} + \frac{(\varphi\,95 - \varphi\,5)}{6}$$

where φ 95, φ 84, φ 16 and φ 5 represent the phi values at 84, 16, 95, and 5 percentiles. They also presented a qualitative classification scale for sorting (Table 1).

Very well sorted	s < 0.35
Well sorted	0.35 < s < 0.50
Moderately well sorted	0.50 < s < 0.71
Moderately sorted	0.71 < s < 1.00
Poorly sorted	1.00 < s < 2.00
Very poorly sorted	2.00 < s < 4.00
Extremely poorly sorted	s > 4,00

Table 1 – Folk & Ward (1957) classification of sediments by their standard deviation (s).

The *Skewness* (Sk) measures the degree to which a cumulative curve approaches symmetry. Two samples may have the same average grain size and sorting but may be quite different to their degrees of symmetry. Folk's "inclusive graphic skewness" (1968) is determined by the equation:

$$Sk = \frac{\varphi\,16 + \varphi\,84 - 2\,\varphi\,50)}{2\,(\varphi\,84 - \varphi\,16)} + \frac{(\varphi\,5 + \varphi\,95 - 2\,\varphi\,50)}{2\,(\varphi\,95 - \varphi\,5)}$$

where the phi values represent the same percentages as those for sorting. This formula includes a measure of the tails of the cumulative curve as well as the central portion. Other methods for determining skewness, notably those by Inman (1952) and Trask (1950), do not measure the tails of the curve. Symmetrical curves have a skewness equal to 0.00; those with a large proportion of fine material are

positively skewed; those with a large proportion of coarse material are negatively skewed. A verbal classification for skewness suggested by Folk (1968) includes: from +0.10 to -0.10 as nearly symmetrical; -0.10 to -0.30 as coarse-skewed; and, -0.30 to -1.00 as strongly coarse-skewed (Table 2).

Fine skewed	0.30 < Sk < 0.10
Near symmetrical	0.10 < Sk < -0.10
Coarse skewed	-0.10 < Sk < -0.30
Strongly coarse skewed	-0.30 < Sk < -1.00

Table 2 – Skewness (Sk) classification of sediments by Folk & Ward (1957).

The *Kurtosis* (Kg) is a measure of steepness in a curve. Folk's (1968) formula for kurtosis is:

$$Kg = \frac{(\varphi\ 95 - \varphi\ 5)}{2,44\ (\varphi\ 75 - \varphi\ 25)}$$

where the phi values represent the same percentages as those for sorting. A normal Gaussian distribution has a kurtosis of 1.00 which is a curve with the sorting in the tails equal to the sorting in the central portion. If a sample curve is better sorted in the central part than in the tails, the curve is said to be excessively peaked, or leptokurtic; if the sample curve is better sorted in the tails than in the central portion, the curve is flat peaked or platykurtic. For normal curves = 1.00, leptokurtic curves have >1.00, and platykurtic curves have <1.00 (Folk & Ward, 1957; Table 3).

Very platykurtic	Kg < 0.67
Platykurtic	0.67 < Kg < 0.90
Mesokurtic	0.90< Kg < 1.11
Leptokurtic	1.11< Kg < 1.50
Very leptokurtic	1.50 < Kg < 3.00
Extremely leptokurtic	Kg < 3.00

Table 3 – Kurtosis (Kg) classification of sediments by Folk & Ward (1957).

3 GEOLOGICAL OVERVIEW ON THE SICILIAN OROGENIC SYSTEM

3.1 GENERAL SETTING

The study area falls within the transitional zone between the Gela Nappe and the Hyblean Foreland (Fig. 16), part of a complex "thrust-and-fold" belt in the central Mediterranean area namely known as Sicilian orogenic system. The Sicilian orogenic system consists developed as response to the collision of the leading margin of the African Plate with more internal units of the European province originated in Neogene time up to Pleistocene (Lentini et al., 1990; 1994; 1995; 1996; Grasso, 2001; Elter et al. 2003; Lentini & Carbone, 2014 and references therein).
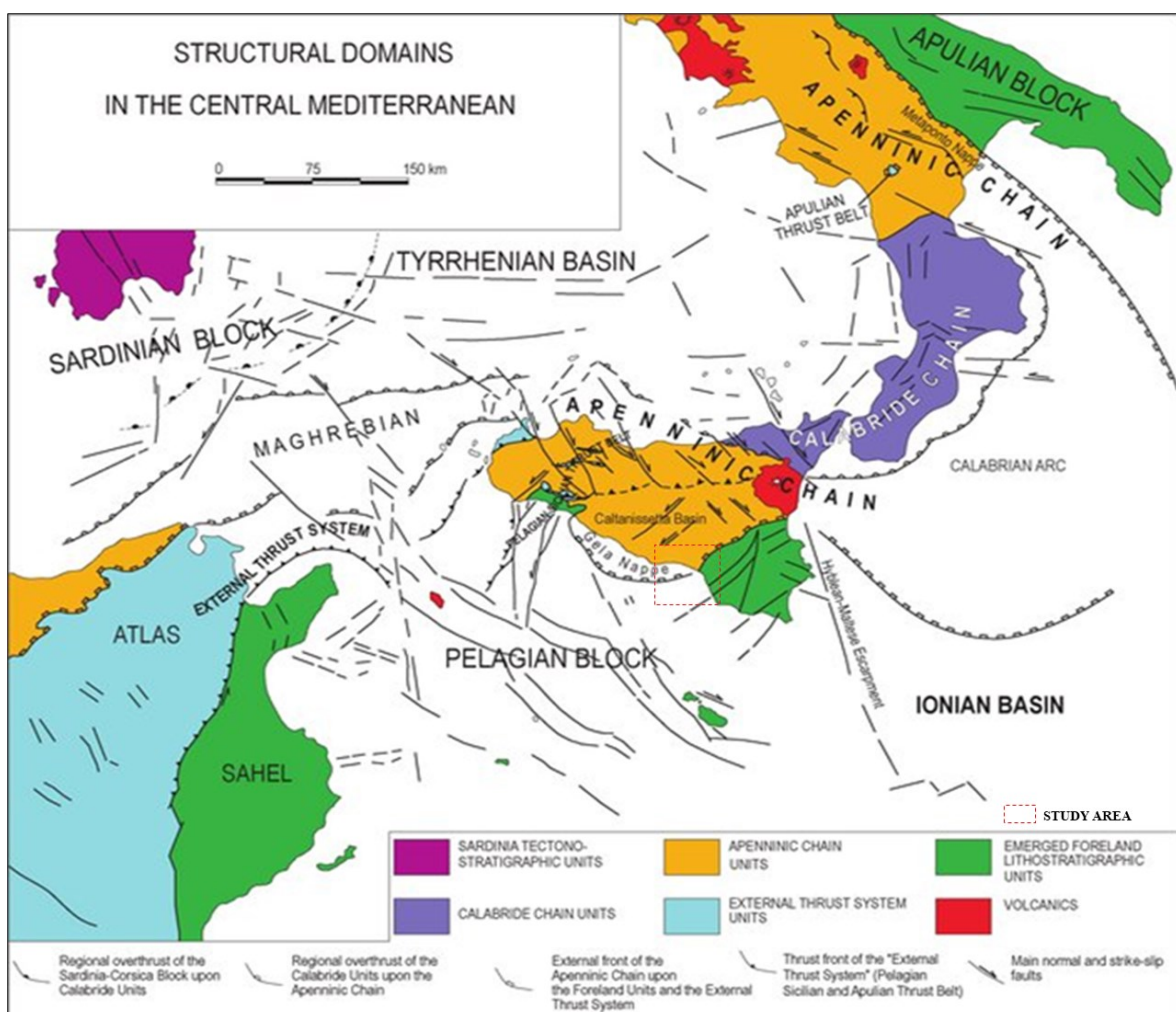
Fig. 16 - Elements of the Sicilian orogenic system in the frame of the central Mediterranean area (after Lentini et al., 1996). In the red square the study area under analysis.

The collisional belt consists of three main distinct elements: i) the Foreland, belonging to the African palaeo-margin, which represents the undeformed margin of the descending African Plate, nowadays occupying the SE sector of Sicily (Hyblean Plateau); ii) the Apenninian-Maghrebian Chain, comprising Meso-Cenozoic units developed in the Tethys, the ocean extending between the African and the European

margins, and evolved as accretionary wedge in the collisional stage, extensively outcropping in central-western Sicliy; iii) the Calabride Chain, composed of basement nappes, representing detached fragments of the original European margin, and represented by the Peloritani Mountains in NE Sicily.

3.2   THE SICILIAN APENNINIC MAGHREBIAN CHAIN

The Apenninic-Maghrebian Chain, widely exposed in central-western Sicily, consists of an allochthonous roof thrust system (Fig. 17), developed since the Late Oligocene, at expense of the Tethyan basinal sequences, which originally floored the oceanic crust, even known as Sicilide Units. Since Middle Miocene the evolution of the system continued by the tectonic denudation of continental crust sectors, due to the orogenic transport of the allochthonous carbonate covers (Panormide Units) onto the Ionian basinal successions (Ionides). The Panormide and Ionides Units are considered the deepest Meso-Cenozoic tectonic units of the chain and the original deposits of the Palaeo-Ionian basin (Finetti et al., 2005a; Lentini & Carbone, 2014).

In the innermost element, compressional deformation and thrusting timing of the Peloritani Units is generally dated as late Palaeogene; their emplacement onto the African continental margin is assumed to be post-late Miocene (Duée , 1969; Amodio Morelli et al., 1976; Bonardi et al., 1980; Giunta et al., 1989; Lentini et al., 1994; Finetti et al., 2005b) According to new recent data, their present-day setting is believed to be the result of a SE tectonic drifting of the Calabrian block following the Tyrrhenian back arc opening; its final docking with Southern Apennines and Sicily is dated to be as old as about 1 Ma.

The intermediate element includes tectonic units emplaced during the Miocene. It comprises many thrust systems. The Sicilidi Thrust System is exposed in NE Sicily and reached its greatest thickness in eastern Sicily. The lnner Carbonate Thrust System comes out in the NW part of the chain. It is extended from the Madonie Mountains to the Palermo ones, and even exposed at the S. Vito Cape Mountains. The main Inner Carbonate Thrust System lithotectonic assemblages derived by the deformation of Mesozoic-Palaeogene units, locally known as Pre-Panormide, Panormide, Imerese and Trapanese units. The carbonate thrust sheets are generally no more 1000 m thickened (Catalano et al., 1995). The Sicanian Thrust System arises in the Sicani Mountains area and it is buried by the Gela Thrust System in Central Sicily. It even crops out southeasternward in the Judica and Scalpello ridges (Roure et al., 1990). In western Sicily, the Sicanian thrust system is bounded to the west by a complex lateral ramp and overthrusts the Outer Carbonate Thrust

System and the Gela Thrust System (Hill & Hayward, 1988). The Sicanian structures derive from deformation of the Sicanian palaeogeographic domain. Compression started in the late Miocene (Catalano & D'Argenio, 1978; Mascle, 1979) or early Pliocene (Oldow et al., 1990) and continued during the Plio-Pleistocene, with folding and reactivation of simultaneously active thrust fronts (Speranza et al., 1999) (Fig. 17).
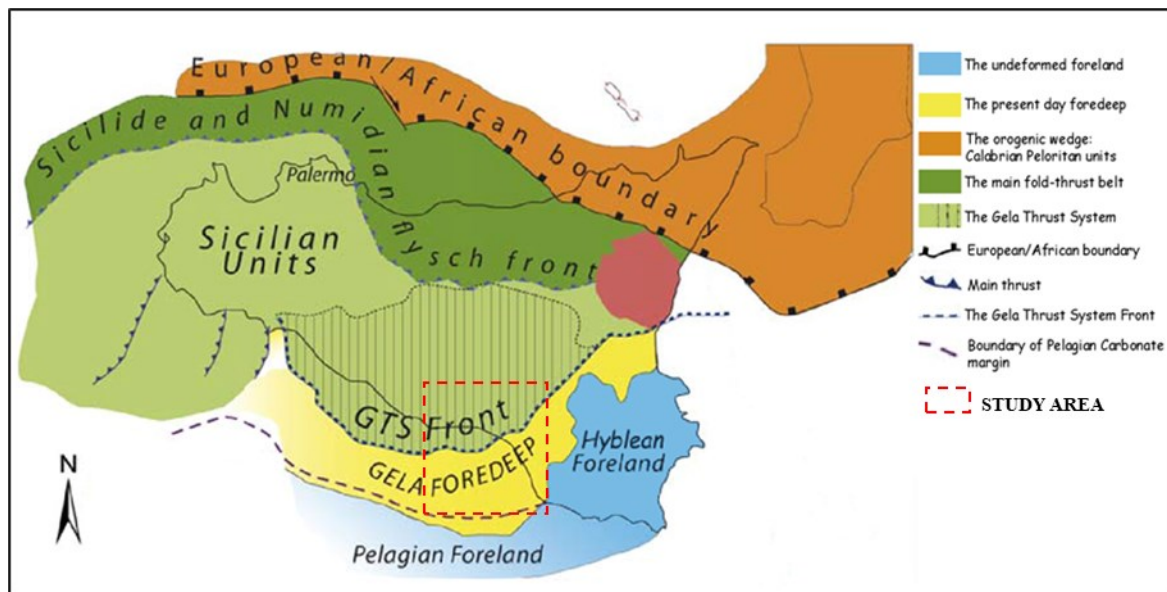
Fig. 17 - Principal Units within the Sicilian orogenic system in outcrop and in offshore areas (after Catalano et al., 2013). In the red square the study area.

The Cenozoic sedimentary covers pertaining to the Sicilian Appenninian-Maghrebian Chain represents elongate regions of sediment accommodation formed on continental crust between contractional orogenic belts and cratons in response to geodynamic processes related to the orogenic belt and its associated subduction system (DeCelles & Giles, 1996).

Seen in detail, the basins associated to a foreland-foredeep-chain system can be divided in four depozones (Fig. 18):

- The wedge-top, where the mass of sediment accumulates on top of the frontal part of the orogenic wedge, including 'piggyback' and 'thrust top' basins.

- The foredeep, filled by the sediment deposited between the structural front of the thrust beltand the proximal flank of the forebulge.

- The forebulge represents the broad region of potential flexural uplift between the foredeep and the back-bulge depozones.

- The backbulge, last part where mass of sediment flows in the shallow but broad zone of potential flexural subsidence cratonward of the forebulge.
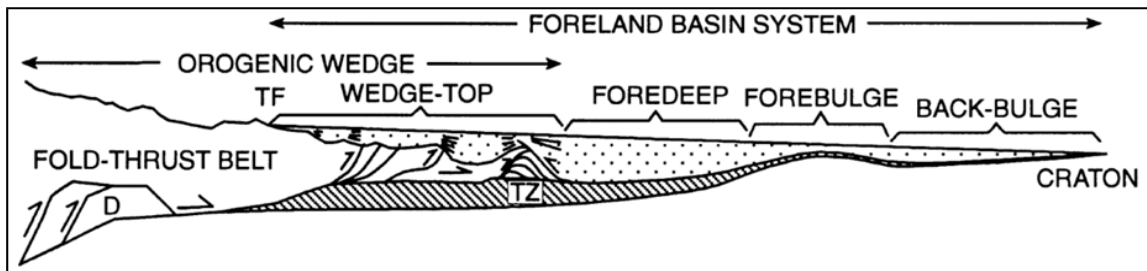
Fig. 18 - Cross-section scheme of chain-foredeep-foreland basin system (De Celles and Giles, 1996).

The evolution of a chain-foreland systems is dominated by contractional structures coupled with extensional structures, both at the chain external-most sector (foredeep) and at the foredeep-foreland transition zone (Dewey, 1988). The main compressional movements in the south-central Mediterranean area, after the Paleogene Alpine orogeny, began with the latest Oligocene-Early Miocene anticlockwise rotation of Corsica and Sardinia and its collision with the African continental margin (Bellon et al., 1977; Channell et al., 1979; Dercourt et al., 1986; Finetti et al., 2005b).

3.3   THE GELA NAPPE AND FOREDEEP

In Sicily, the most advanced front of the orogenic belt is represented by the Gela Nappe (Beneo, 1958; Di Geronimo et al., 1978; Grasso & La Manna, 1993; Lickorish et al., 1999) (Fig. 17, Fig. 19), widely outcropping along the Catania-Gela lineament and in the off-shore sector, partially hidden by the huge volumes of sediments filling the Gela Foredeep, a Plio-Pleistocene foredeep flanking the Hyblean foreland onshore and extending to the Southern and Southwestern part of Sicily offshore, and mainly detected by seismic profiles (Argnani, 1989; Bianchi et al., 1989; Finetti et al., 2005b), which well image the deformed stratigraphy of the Gela Nappe on the undeformed foreland plate (Fig. 17).

The subsiding area corresponding to the Gela Foredeep is weakly deformed, and the NW-dipping foreland ramp has been involved in a very recent slightly compressional and extensional deformation (Ghielmi et al., 2012; Distefano et al., 2019).

In the present study, the first study area (Area 1) is located, from a geological point of view, at the transition between the Gela Nappe and the Hyblean Foreland; thus, more details concerning the geological context are given in Paragraph 6.2.1.
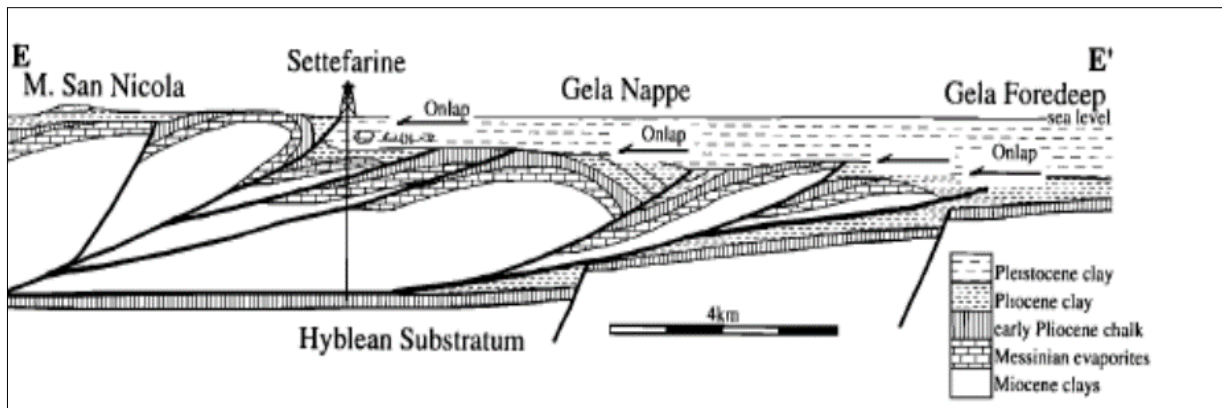
Fig. 19 - Schematic cross-section showing the relationships among the more advanced front of the orocenic belt (Gela Nappe), the Gela Foredeep and the Hyblean undeformed substratum (Lickorish et al., 1999).

3.4 THE HYBLEAN FORELAND

The Hyblean Foreland **(**Fig. 17**,** Fig. 20**)**, part of the Pelagian Block (Burrollet et al., 1978; Ben-Avhraham & Grasso, 1991) emerges onshore in South-Eastern Sicily, and moves offshore southward into the Sicily Channel-Malta area and into the Western Sicily Channel. The Pelagian-Hyblean foreland basement wedge is supposedly dated as pre-Permian. This crust slightly counterclokwise rotated of few degrees during the Plio-Pleistocene (Besse et al., 1984; Cifelli et al., 2007; Maffione et al., 2013;Fig. 21).

The sector is bounded on the East by Ionian crust, consequently the present-day Hyblean Foreland is considered a remnant of a Jurassic or older passive continental margin with its oceanic abyssal plain located in the adjacent Ionian Sea (Catalano et al., 2000, 2001; Chamot-Rooke et al., 2005; Finetti et al., 2005b; Valenti, 2010, 2011; Polonia et al., 2012).

The Pelagian Block represents an E-W segment of the Africa continental margin flexured to the North beneath the orogenic belt. The Hyblean-Maltese Escarpment is a N-S trending fault zone that splits the Pelagian Block to the East from the Ionian Basin. This normal fault system has been active during the Pliocene and Quaternary and plays an important role in the seismotectonic evolution of the area (Lentini & Carbone, 2014).
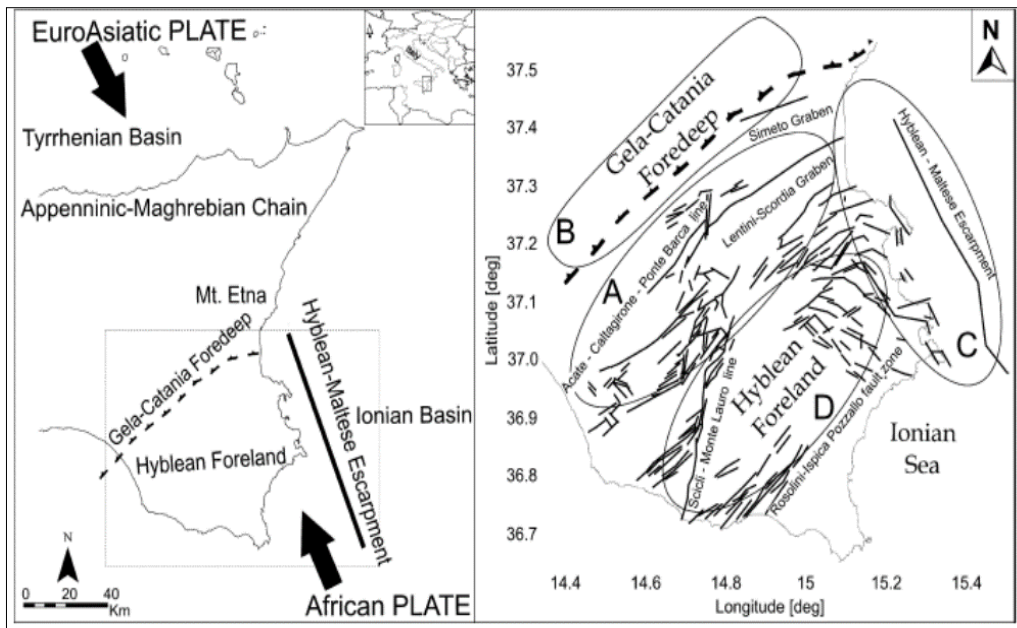
Fig. 20 - The Hyblean Foreland in the framework of the Sicilian orogenic system. The arrows indicate the present direction of convergence of the Euro-Asiatic and African Plates. On the left the structural layout of SE Sicily (after Agostino et al., 2009).

The main foreland flexure gets out in the orogenic areas on the North, where a wide axial depression is recognizable within the chain units and known as "Caltanissetta Basin".

The Hyblean Plateau is characterized by huge volumes of carbonatic sediments of Triassic to Quaternary age, outcropping into a western and an eastern sector, whose stratigraphic features have been widely described by Patacca et al. (1979), Lentini et al., (1987), Cogan et al. (1989), and has been the site of intermittent volcanic activity from the Triassic up to the Early Pleistocene. This activity occurred when to the NW the Hyblean Foreland collapsed and a system of normal faults developed, originating the Gela Foredeep (Lentini & Carbone, 2014).
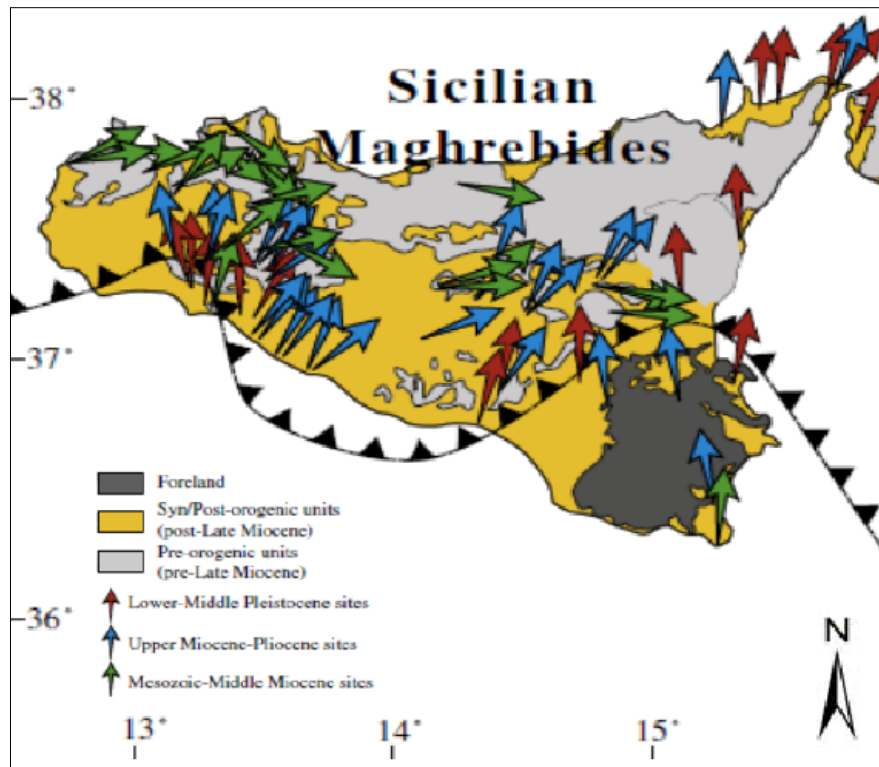
Fig. 21 - Estimated tectonic rotations (colored arrows) with respect to stable Africa computed by Cifelli et al. (2007) (after Maffione et al., 2013)

4 STUDY AREA DESCRIPTION

The Gulf of Gela concides with the second-order coastal sub-cell n. 4.2 of the Regional Plan against the coastal erosion (Regione Siciliana, 2020). It has a total length of 72,595 km and represents a well-defined area of sediment transport. The sub-cell lies within three Sicilian administrative Provinces of Agrigento, Caltanissetta and Ragusa. Westward it falls within the municipal territory of Licata (Agrigento Province, AG), eastward in the province of Caltanissetta, including the municipal territories of Butera and Gela, while the SE part of the cell belongs to the province of Ragusa, including the municipal territories of Acate, Vittoria and Ragusa itself (Table 4).

CS II order	CS III order	Beach/Coastal tract	Municipalities
CS 4.2 Punta Braccetto cape - Licata harbour	4.2.1 Punta Braccetto cape - Gela Harbour	Randello Club Med Orchidea nera Scoglitti Macconi - Marina di Acate Gela east	Ragusa, Vittoria Acate, Gela pp
	4.2.2 Gela Harbour - Licata Harbour	Gela west Femmina Morta, Punta Secco, Lido di Manfria Manfria west Falconara east and west	Gela pp, Butera, Licata pp

Table 4 - Second-order coastal sub-cell n. 4.2 and the third-order coastal sub-cells, the main beaches of the area and the municipalities the cells belong to (modified from Regione Siciliana, 2020).

The main economic activity of the coastal area is nowadays leisure industry, even though industrial and agricultural activities have been carried on over the last fifty years. The Gela refinery is one of the largest petrol-chemical poles in Europe, which has been recently converted in a biorefinery (Fig. 22).
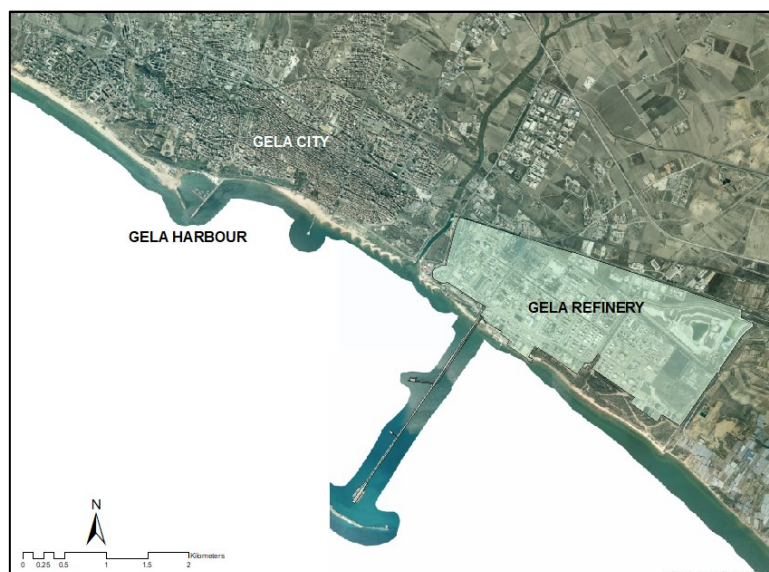
Fig. 22 – Gela refinery, nearby the Gela city.

Three harbours (Licata, Gela, Scoglitti) insist on the coast, the Licata and Scoglitti ones are orchestrated for tourists and commercial uses, the Gela one has been implemented to serve the refinery. Other permanent infrastructures set on the coast are the Kamarina Touristic village (Vittoria municipality) and the province roads that connect the main cities of the gulf.

4.1 DRAINAGE BASINS

Ten catchment basins can be found within the coastal sub-cell n. 4.2. Even though a high number of rivers and torrents face the Gulf, Amore & Randazzo (1997) registered that the fluvial sediment inputs of the sub-cell are minimal, because most of the rivers flows through predominantly chalk catchment, resulting high solute, but low sediment loads. The main rivers are the Southern Imera, the Gela, the Acata-Dirillo and the Ippari (Table 5, Fig. 23).

CODE	NAME	TOTAL AREA (Km²)	MAIN RIVER LENGTH (Km)	MAIN LAND USE	ARTIFICIAL RESERVOIRS
72	Southern Imera River	2,002.50	132	Arable land	Gibbesi, Olivo, Villarosa
77	Gela River	569.00	59	Arable land	Cimia, Disueri
78	Acate-Dirillo River	385.10	54	Arable land	Dirillo
80	Ippari River	195.50	30	Arable land	-

Table 5 – Main river basins within the coastal sub-cell n. 8; the total catchment area expressed in Km², the length of the main stream (Km), the main land use and the artificial reservoirs of each basin are shown. *Code* is the progressive number attributed by the Sicilian Region to each regional catchment basin.
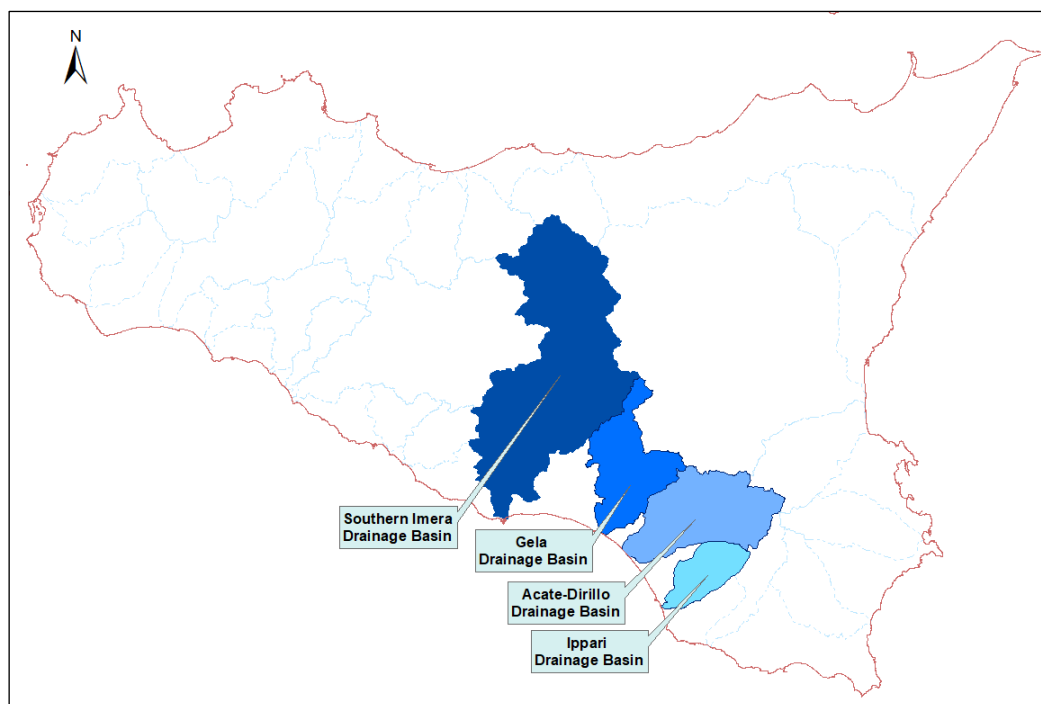
Fig. 23 – Drainage basins of the main rivers (Southern Imera, Gela, Acate-Dirillo, Ippari) within the coastal sub-cell n. 8.

The main stream for length and liquid and solid flow is the Southern Imera river (Code 077) and the namesake basin is the biggest one of the unit (2,002.50 Km^2) and the second largest drainage basin by size in Sicily. The river flows for 132 km southward through the centre of the island and into the Mediterranean Sea at the western end of the Gulf of Gela at the seaport of the town of Licata (AG). The Southern Imera river is eastward bounded by the Simeto river drainage basin and the Gela river drainage basin, westward bordered by the Platani river basin, the Naro river and the Palma river basin, and on the north by the Northern Imera river basin and the Pollina river basin. The main tributaries of the Southern Imera river are the Salso, Morello, Gibbesi and Torcicoda rivers and the Braemi streams. The Southern Imera river feeds the artificial reservoirs Villarosa that blocks the Morello torrent, Olivo, which intercepts the course of the Braemi torrent, and Gibbesi, which is still not in operation. The Villarosa reservoir has been built nearby the town of Villarosa between 1969 and 1973, it has a volume of 17,16 Mm^3 and an estimated burial volume of $5,00 \times 10^6$ m^3. The main destination use is for agricultural irrigation. In 1989, a bathymetric survey recorded a burial volume of $1,37 \times 10^6$ m^3. The Olivo reservoir (Piazza Armerina municipality, EN) has a total volume of 18 Mm^3 and an estimated burial volume of $2,00 \times 10^6$ m^3. (Regione Siciliana, 2008; Fig. 24). Lanza & Randazzo (2011) noted that most of the waterway capacity of the river has been reduced due to the intense draining of superficial ground water used for irrigation. The vegetation is still quite rich within the area of the basin, although the human action partly changed the land use and developed an intensive agricultural system. Most of the land is devoted to a mixed system of tree crops and cultivation mosaics. Pasture farming system is also widespread.
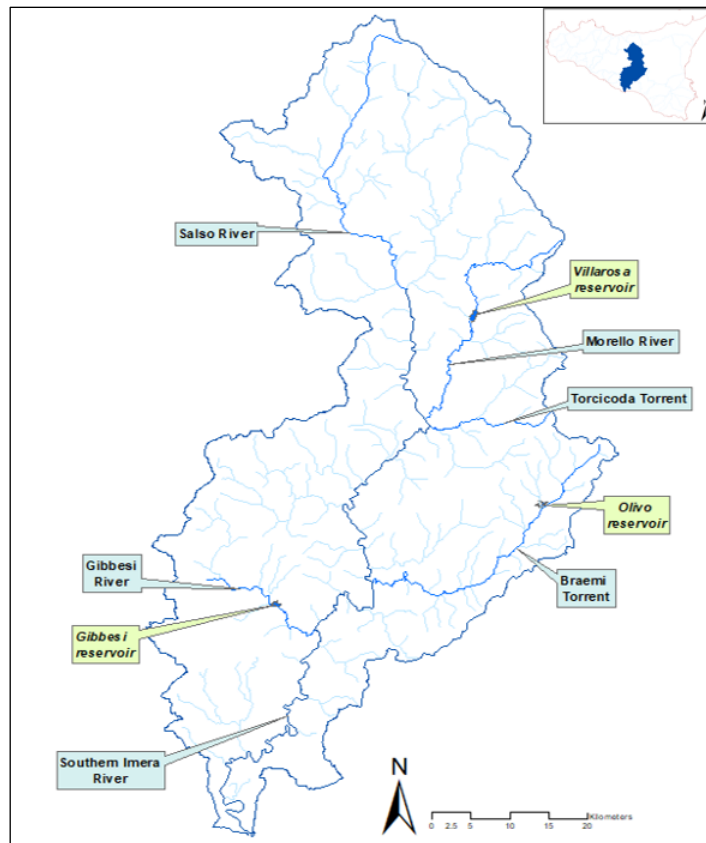
Fig. 24 – Southern Imera drainage basin, its main river, tributaries and artificial reservoirs.

The Gela river drainage basin (Code 077) area is 595.92 km^2. It is N-S shaped and it is bounded at the north by the Southern Imera river basin; at the northeast by the Simeto river Basin and southward by the Acate-Dirillo river Basin and the Comunelli torrent basin. The river flows for 59 km through three Sicilian provinces, Caltanissetta, Catania, Enna. One of the biggest petrochemical poles in Europe is nearby the city of Gela, located within the area between the Gela river basin and the Acate-Dirillo river basin. In the central part of the basin, the Disueri reservoir interrupts the Disueri river, it has built over the forties, but it has been implemented over the nineties and finished in 1997. The reservoir has a volume of 28.2 Mm^3 and its waters are used for irrigation. The Cimia reservoir blocks the waters of the namesake torrent, it falls within the sub-basin of the Maroglio river, the main tributary of the Gela river. The tank has been constructed in 1980 and nowadays it does not result to be significantly buried. The lands of the Gela catchment basin are mainly devoted to agricultural activities, the simple arable lands are the most common, but there are also several specialized crops (Fig. 25).
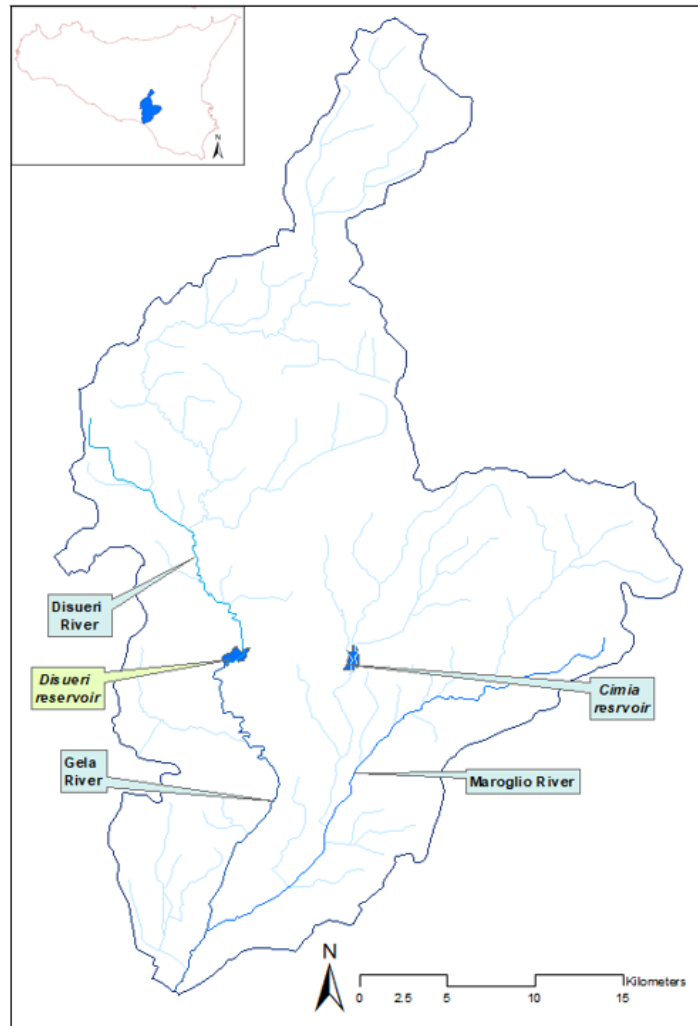
Fig. 25 – Gela drainage basin, its main river, tributaries and artificial reservoirs.

The catchment area of the Acate or Dirillo river (Code 078) is in south-eastern Sicily, on the edge of the vast plain of Vittoria (RG) and near the south-western edge of the Hyblean Plateau. It is 740 km^2 large and the highest peak reaches 986 m above sea level. Four provinces fall within the area of the basin, Caltanissetta, Catania, Siracusa and Ragusa. The Acate-Dirillo basin is bounded at the north by the Simeto river Basin; at the northeast by the Lentini river basin; it borders southward with the Irminio river Basin and with the Ippari river basin. The river course is approximately NE - SW oriented and does not receive huge tributaries, except for the river Mazzarronello and the Terrana torrent. The Dirillo (Ragoleto) artificial reservoir has been implemented between 1961 and 1962, it has a volume of 21.3 Mm^3. Its waters are used by the ENI refinery of Gela and for irrigation and agricultural activities. Since 1963, two bathymetric surveys have been performed to assess the burial volume, in 1980 and 1995, when 1.30x10^6 m^3 and 0.27x10^6 m^3 of sediments have been recorded, respectively (Fig. 26). Most of the area is exploited for agricultural and

zootechnical use, except for some small cities and some uncultivated rocky areas. The greenhouses are even common and mainly widespread along the coast.
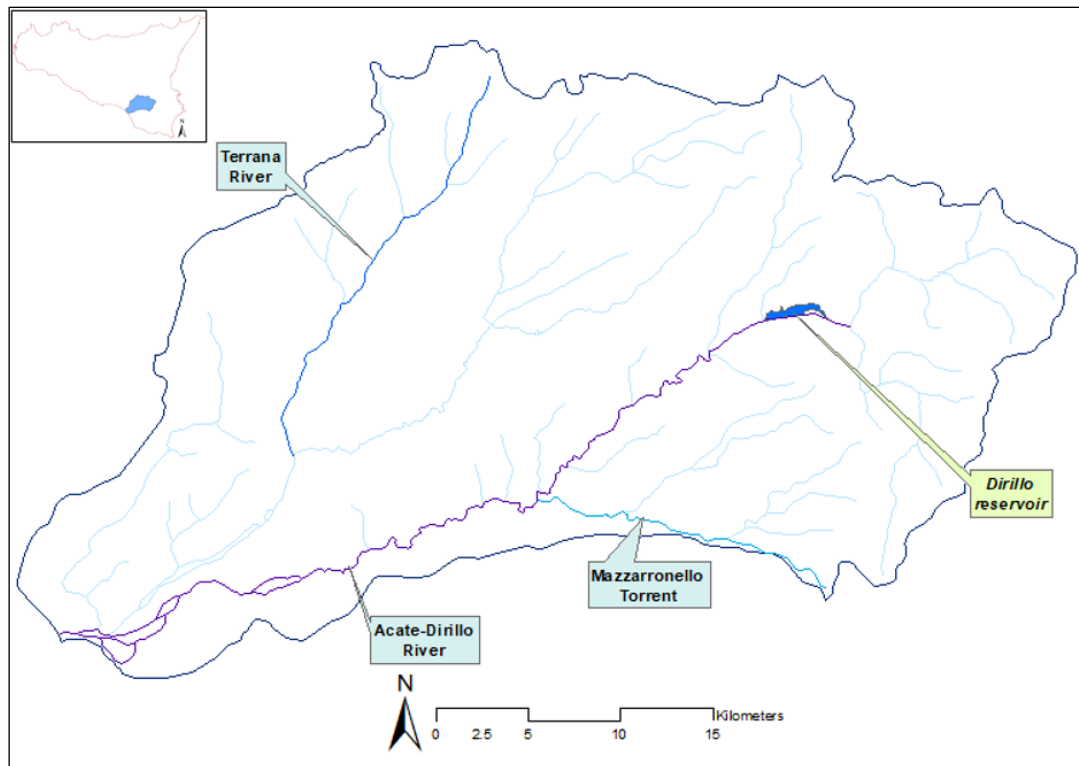
Fig. 26 – Acate-Dirillo drainage basin, its main river, tributaries and artificial reservoirs.

The catchment area of the Ippari river (Code 080) is in south-eastern Sicily, at the south-western limit of the Hyblaean plateau, including entirely the Vittoria - Comiso plain (Fig. 27). It is bounded on the north by the Hyblaean massif and by the Para Para river, to the west and north-west by the Dirillo river basin, to the east and southeast by the first reliefs of the Hyblaean massif and the plateau itself, and finally on the south by the Mediterranean Sea. It is about 195 km^2 and the highest peak reaches 882 m above sea level. The Ippari river length is about 25,8 km and it is mainly sub-dendritic and most of its tributaries springs out on the left bank of the basin, originating from the Hyblean Plateau. Most of the territory is devoted to agricultural activities. Over time, the wide Ippari wetlands have been drained to create agricultural land and many artificial embankments have been built to channel the watercourse. Nowadays, the coastal area is mostly exploited by greenhouses and vineyards cultivations.
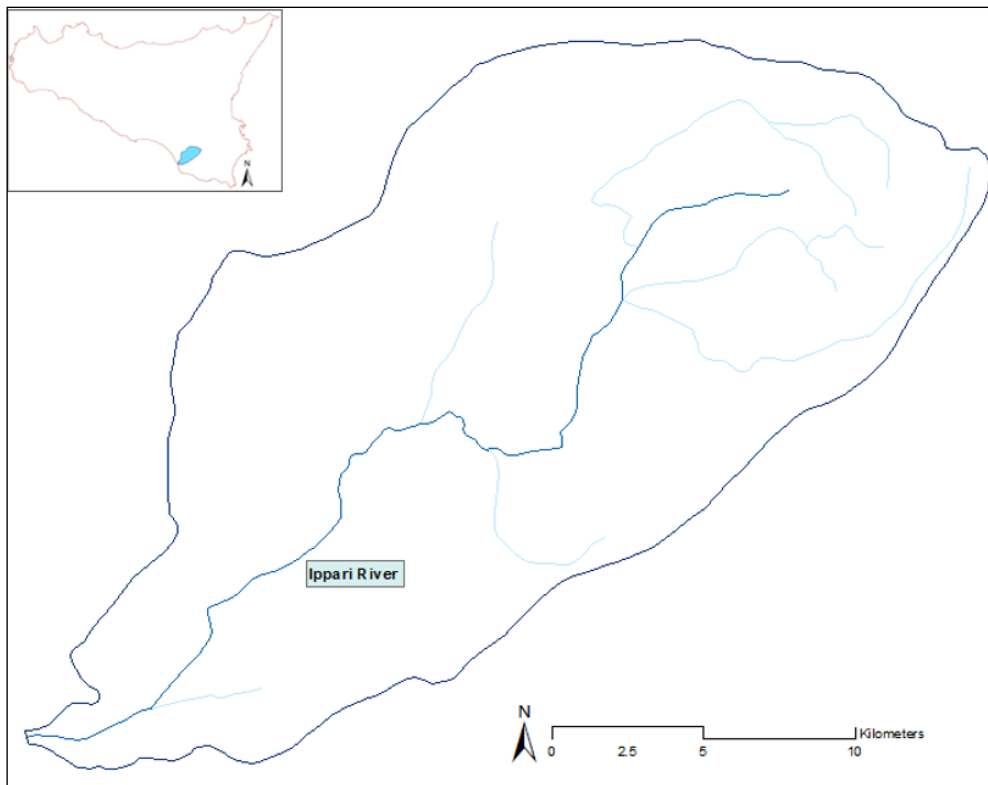
Fig. 27 – Ippari drainage basin, its main river and tributary network.

4.2 WIND AND OCEAN CLIMATE OF THE GULF OF GELA

4.2.1 WINDS

Foti et al. (2010) analyse the wind regime of the Gulf of Gela for the feasibility study of a wind farm. The authors analysed wind data over 38 years (01.08.1965 – 30.09.2003) using the time series of the Meteorological Service of the Italian Air Force at the inland station of Gela. The directional analysis showed that the wind regime is dominated by winds blowing from the 3rd quadrant and partly from the 4th quadrant, both in terms of frequency and in terms of maximum velocity (Fig. 28).
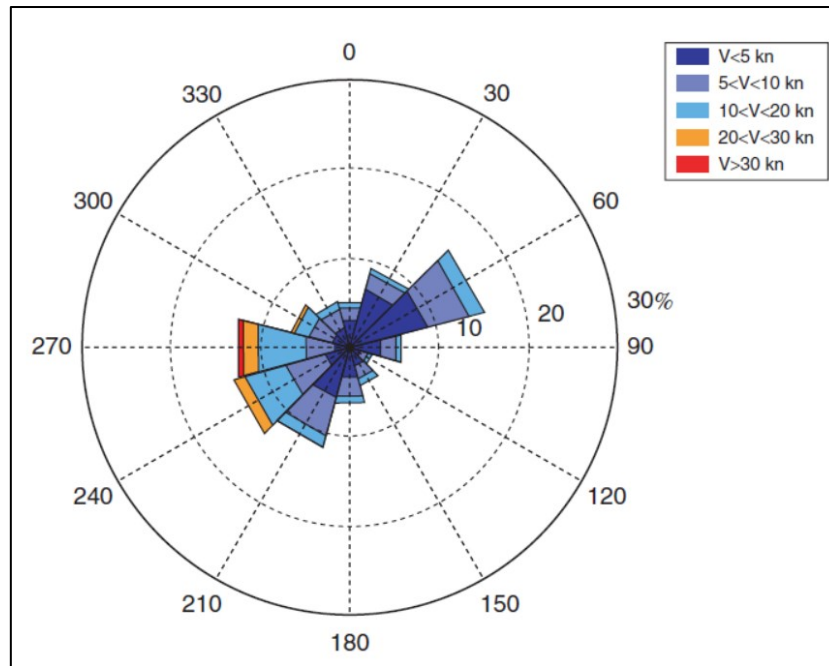
Fig. 28 - Directional distribution of the wind at the Meteorological Service of the Italian Air Force station of Gela, time span from 01.08.1965 to 30.09.2003. Velocities are in knots (Foti et al., 2010).

In the Sicilian Hydrogeology Management System Plan (2007), 1956 to 1999 data from (i) the Gela station of the Meteorological Service of the Italian Air Force, (ii) two stations set outside the coastal sub-cell, in the southern part of Sicily, (iii) the ENAV (Ente Nazionale per l'Assistenza al Volo, National Authority for the Air Assistance) station at Cozzo Spadaro (SR) and (iv) the navy station in Capo Passero (SR), have been analysed. Results indicates that the ENAV station and the navy one described a wind regime that is analogous to the data recorded by the Gela station. In order to cover the entire time span considered in the present study, wind speed and direction data recorded by the Porto Empedocle (AG) station have been downloaded from the National Tide gauge Network. The time range is from 01.01.2010 to 01.01.2019, the computed wind rose diagram shows that winds mainly blow from West-Southwest, accordingly with the data obtained by the previous studies and reports (Fig. 29).
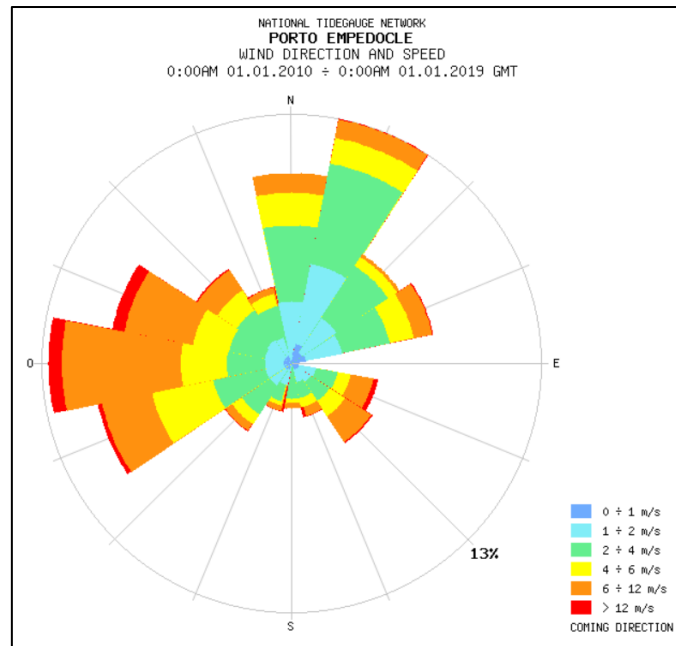
Fig. 29 – Wind speed and direction chart, National Tidegauge Network, Porto Empedocle station, time span 01.01.2010 – 01.01.2019.

4.2.2 CURRENTS

Foti et al. (2010) examined the current regime of the Gulf of Gela. Data derive from the 2000 cruise of the Urania (National Research Council), which surveyed a large portion of the Strait of Sicily, computing the spatial variability of both current and hydrographic characteristics (Gasparini et al., 2004). In the Strait of Sicily, surface circulation is controlled by the Atlantic Ionian Stream (AIS) (Robinson et al., 1999), a segment of the Modified Atlantic Water (MAW). The MAW enters through the Strait of Gibraltar and flows easterly, reaching the Strait of Sicily, here the AIS describes one large cyclonic meander that embraces the Adventure Bank before approaching the shore by the southern coast of Sicily. The AIS detaches the shore in the shelf of Malta and encircles a second cyclonic vortex off Cape Passero. The Gulf of Gela is affected by the Atlantic Ionian Stream (AIS) and by the presence of those large scale cyclonic and anticyclonic structures, since baroclinic waves are trapped by the sea bottom morphology (Gasparini et al., 2004). The residual current is larger over the two shelfs and quite smaller offshore of the Gulf of Gela, with velocities of the order of 0.3 m/s (Foti et al., 2010). They analysed the KNMI data (Leo observations) and observed that the coastal strip between the Acate-Dirillo river mouth and cape Punta Braccetto is mainly affected by waves and storms from the west and a south-eastward littoral drift has been detected, even though sediment load in the opposite direction has been rarely recorded (Anfuso, 1999; Anfuso & Martinez del Pozo, 2005).

Foti et al. (2010) applied two methodologies in order to study the wave regime of the Gulf of Gela. They used wave data recorded since 01.07.1989 to 31.03.2008 by the Italian Sea Wave Network gauge offshore Mazara del Vallo (TP) and extended the results to the study area. They also employed Sverdruv Munk Bretschneider (SMB) method, which allows to predict the significant wave height from wind data. The input dataset derived from the station set in Gela of the Meteorological Service of the Italian Air Force and the period considered was from 01.08.1965 to 30.09.2003. Both analyses pointed out that the wave motion computed is mainly made by waves coming from West-South-West and the most energetic waves come from the West (Fig. 30).
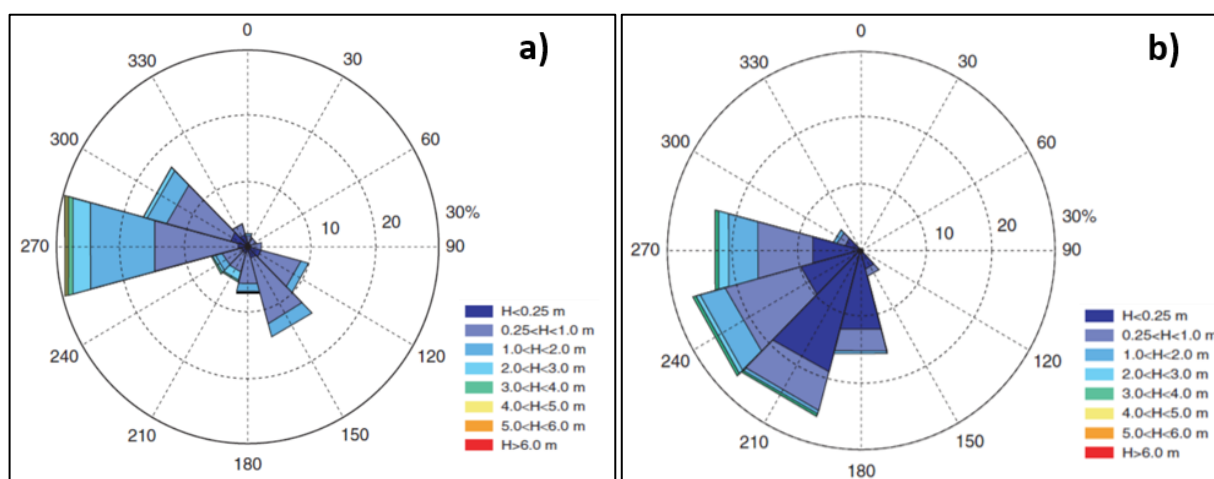
Fig. 30 – a) Directional distribution of the wave persistence in Gela obtained by the geographic transposition of the data recorded during the period 1.7.1989–31.03.2008 by the Italian Sea Wave Network at the wave gauge of Mazara del Vallo; b) Directional distribution of the wave persistence in Gela obtained by applying the SMB method to the wind data recorded at the inland station of Gela during the period 1.8.1965–30.9.2003 by the Meteorological Service of the Italian Air Force. (from Foti et al., 2010).

Anfuso & Martinez del Pozo (2005) investigated the wave motion thanks to the KNMI data (Leo observations). They observed that the largest storms hit the coast mainly from the 3rd and the 4th quadrants and deep water values of significant wave height (Hs) of 8 m and 11 s associated period (T), whereas lesser storms approach from the 2nd quadrant with Hs = 5.5 m and T = 10.5 s.

4.2.4 *TIDES*

The Gulf of Gela is characterized by a microtidal regime, as well-documented by the variations in levels at the tide gauge station located at Porto Empedocle (AG), at NW 40 km from the eastern edge of the Gulf. Since 2010 the tide level has been measuring by a new sensor with millimetre accuracy, the

SIAP+MICROS TLR. The average water level fluctuation computed over the time between 2010 and 2019 was 0.04 m (Fig. 48).

4.3   NATURAL PROTECTION AREAS

Natura 2000 is an ecological network composed of sites designated under the Birds Directive (Special Protection Areas, SPAs) and the Habitats Directive (Sites of Community Importance, SCIs, and Special Areas of Conservation, SACs). The aim is to create breeding and resting sites for rare and threatened species, and to protect some rare natural habitat types. Four Natura 2000 sites fall within the coastal sub-cell n. 4.2 (Fig. 31), three of them are identified as Sites of Community Importance (SCI) and one as Special Protection Area (SPA).
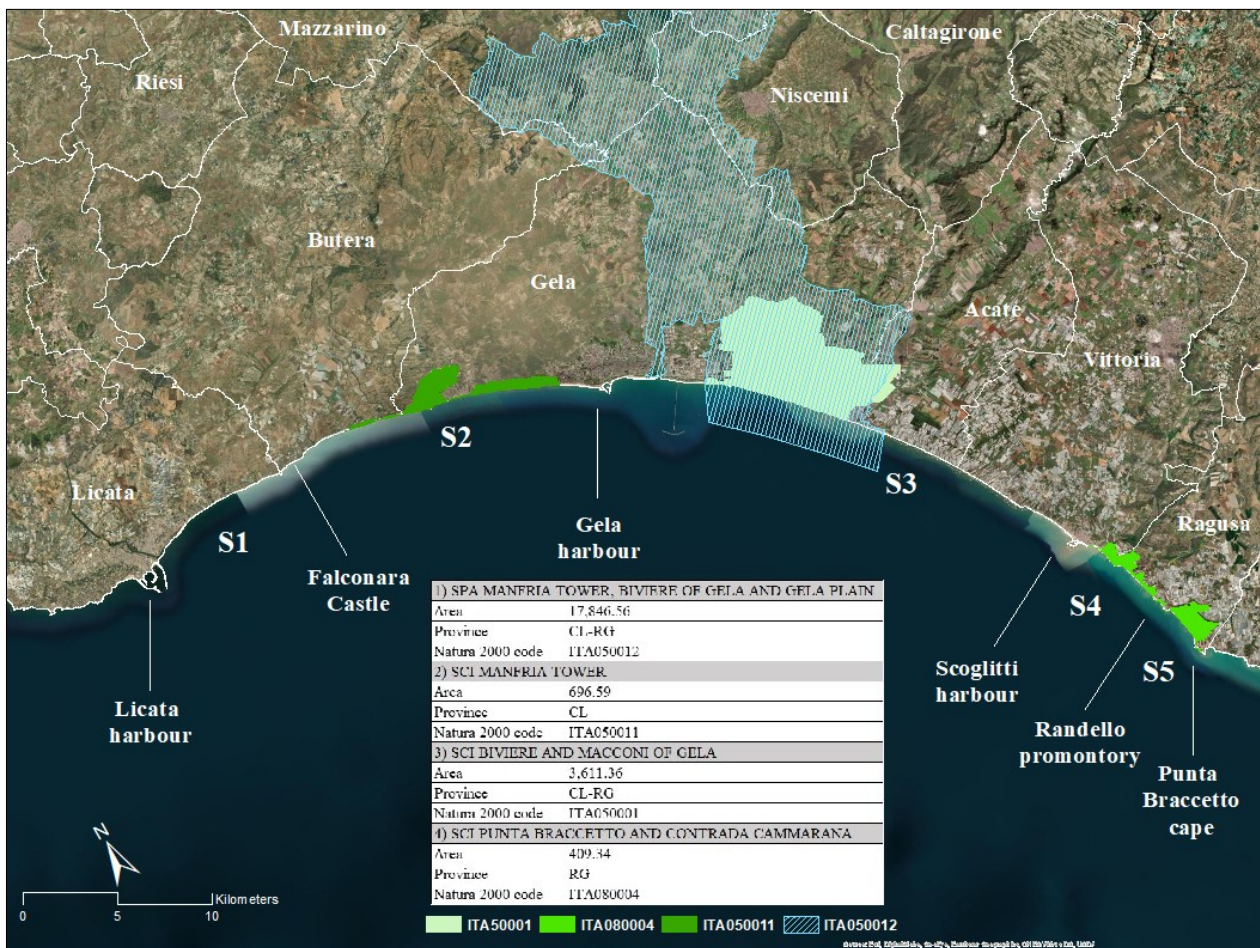
Fig. 31 –Natura 2000 sites within the coastal sub-cell n. 4.2. Table shows technical details for each site.

4.3.1 *THE SPECIAL PROTECTION AREA ITA 050012 – MANFRIA TOWER, BIVIERE OF GELA AND GELA PLAIN*

The Special Protection Zone "Torre Manfria, Biviere di Gela, Piana di Gela" includes a wetland of international importance and it is considered a site of great naturalistic value.

It falls within the sector n.3 n and is 178.46 km² wide, equal to 3.6% of the total area of the regional nature network (Fig. 32).

The strategic geographical position and the hilly morphology of the Gulf of Gela acts as a funnel favoring the crossing of the avifauna coming from North Africa, especially in the spring period. The site contains 71 species in Annex I of the Birds Directive 93 habitual migratory birds, 12 species included in Annex II of the Habitats Directive, 38 regional and Italian endemic species and subspecies, and finally a complex of 109 species included in the Red Lists, in the Annexes of the International Directives and Conventions, etc. The coastal dune belt of the SCI, about 10,000 m long, hosts priority habitats and the target species Muscari gussonei (leopoldia).
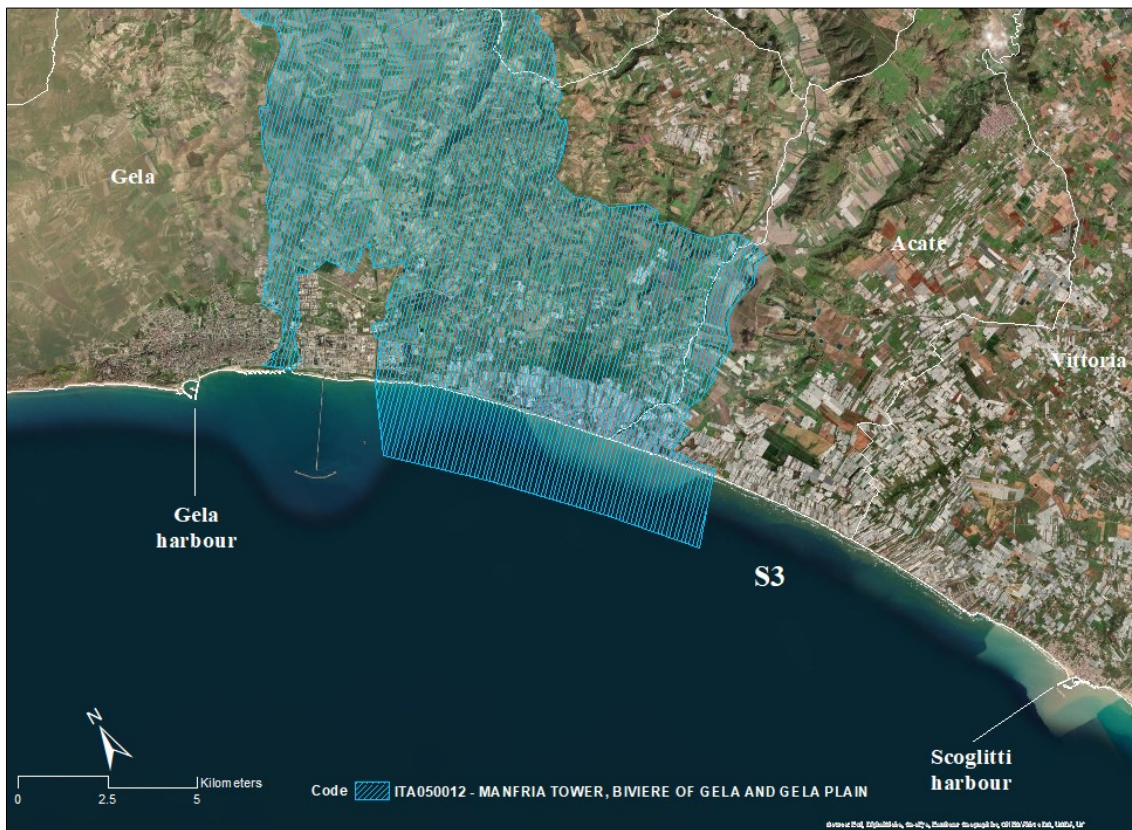
Fig. 32 – The Special Protection Area ITA 050012 – Manfria Tower, Biviere of Gela and Gela Plain that falls within the sector n. 3.

4.3.2 *THE SITE OF COMMUNITY IMPORTANCE ITA 050001 –BIVIERE OF AND MACCONI OF GELA*

The Site of Community Importance ITA 050001 falls within the territory of the municipalities of Gela and Acate, where it covers a total area of ca. 3600 Ha (Fig. 33). It embraces the coastal stretch located south-east of the town of Gela, as well as the area of the Biviere and Macconi, already included within a nature reserve and considered one of the most interesting biotopes of the central-southern side of Sicily.

Based on the bioclimatic classification according to Rivas-Martinez, the territory falls mainly within the thermomediterranean belt, with lower dry shade, tending inwards to the top. The vegetal landscape of the areas is largely dominated by arable crops. In proximity to the coast assumes considerable importance the greenhouses system.
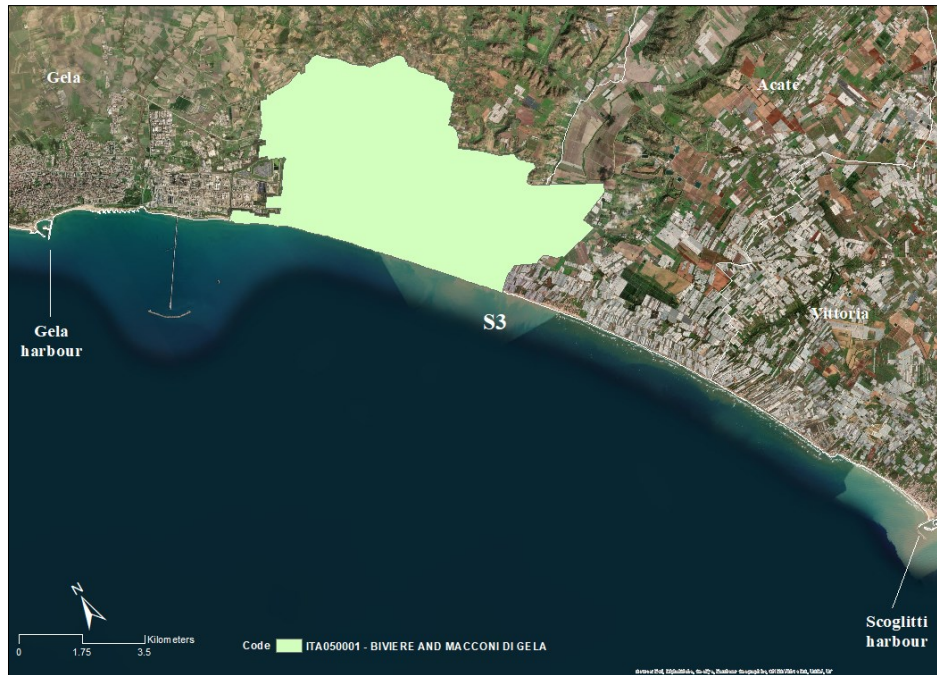
Fig. 33 – The Site of Community Importance ITA 050001 – Biviere and Macconi of Gela that falls within the sector n. 3.

4.3.3 *THE SITE OF COMMUNITY IMPORTANCE ITA 050011 – MANFRIA TOWER*

The SCI Manfria Tower (Fig. 34) is 697 Ha and covers the coastal stretch west of the town of Gela, including the area of Contrada Manfria, considered a biotope of high naturalistic and environmental interest (Brullo et al., 1995; Giusso del Galdo & Sciandrello, 2003).
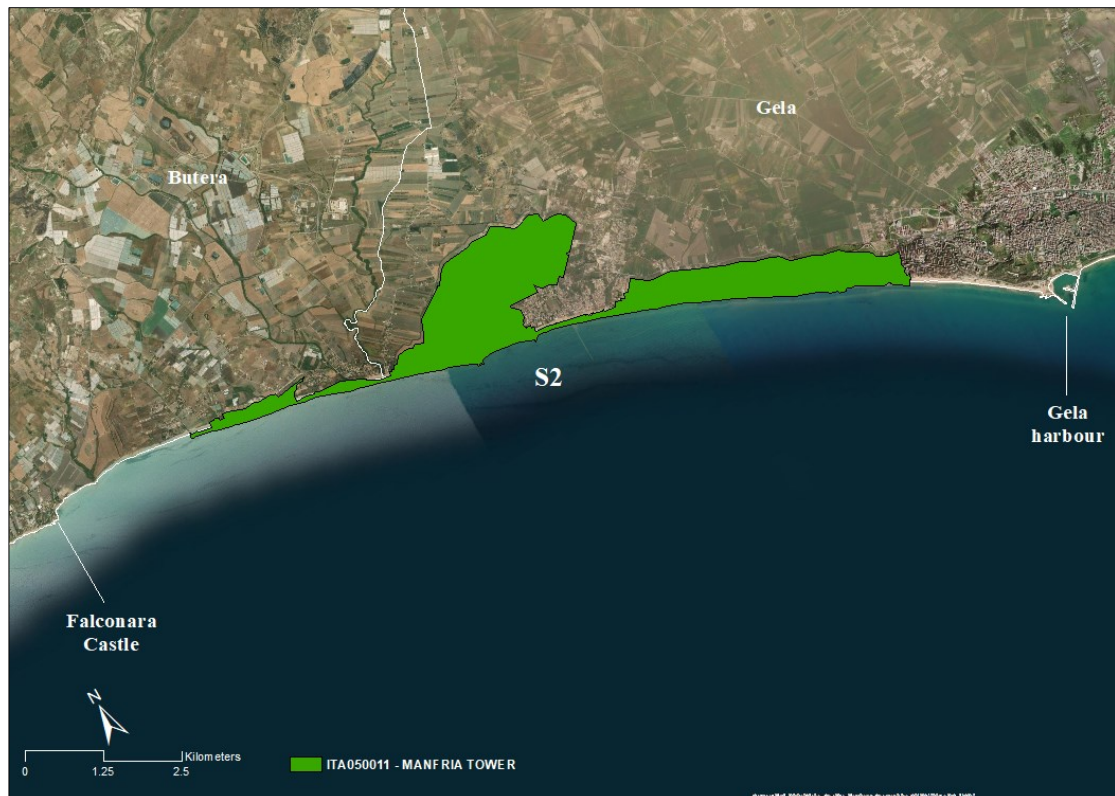
Fig. 34 – The SCI Manfria Tower that falls within the sector n. 2.

Based on the bioclimatic classification of Rivas-Martinez, the area is classified as a thermomediterranean thermotype and a dry ombrotype. The Gela Plain is an essential ecological unit in the Mediterranean area for the migration of many species of avifauna (*Ciconia ciconia, Circaetus gallicus, Falco naumanni, Burhinus oedicnemus, Glareola pratincola, Melanocorypha calandra, Calandrella brachydactyla)* (Campo et al., 2001). Part of the ancient and wider dune system still resist and some scrub strips of *Retama raetam* subsp. *gussonei* are still common in this area (Ilardi et al., 2000). Therefore, this SCI has a high floristic, phytocoenotic and landscape value within the Mediterranean zone. The entire Gela Plain is considerably affected by the agricultural and greenhouses system that have often the need of using herbicides and fungicides. The dune system is largely threatened by the plantation of allochtonous or exotic species and by the increasing agricultural activities (Badalamenti et al., 1988).

4.3.4 *THE SITE OF COMMUNITY IMPORTANCE ITA 080004 – PUNTA BRACCETTO-CONTRADA CAMMARANA*

The Punta Braccetto-Contrada Cammarana SCI (ITA080004) stretches 9 km along the western coastline of the Province of Ragusa, between the suburbs of Cape Punta Braccetto and Scoglitti town (Fig. 35). It mainly consists of extensive coastal dunes, with *psammophilous* vegetation and rocky coastal stretches with a *Limonietum hyblaeid* type of vegetation.
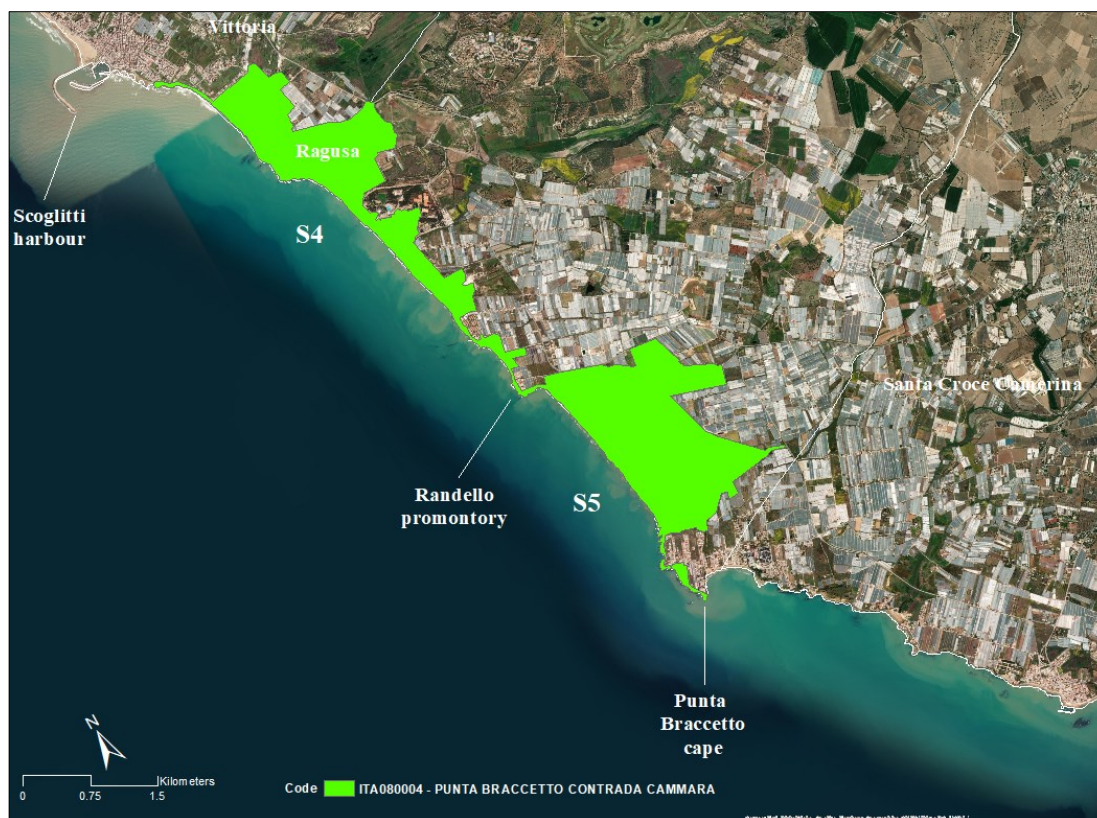
Fig. 35 – The SCI Punta Braccetto-Contrada Cammarana that falls within the sector n. 5.

Most of the area is covered by dune formations with *Juniperus oxycedrus* subsp. *macrocarpa*, *Retama raetam* and *Ephedra fragilis* (Maugeri & Leonardi,1974). However, over the 1950s, most of the dune ridges have been replanted with allochtonous or exotic species, as *Acacia saligna*, *Pinus halepensis* and *Pinus pinea*. High-value plant associations can be found, as *Crucianella rupestris*, shrub formations at *Limoniastrum monopetalum*, associations dominated by *Helichrysum conglobatum* var. *compactum*, dune formations at Malcolmietalia with *Muscari gussonei* (Bartolo et al., 1982; Brullo et al., 1995). In the sea there are submerged prairies at *Cymodocea nodosa*. This site is important for the wide range of animals, mainly invertebrates, whose presence is strictly bound to those dunes typical of some zones of Southern Sicily (Bella et al., 1996; Bella et al., 2001; Bruno, 1970; Turrisi & Vaccaro, 1998; Turrisi & Vaccaro, 2004; Sabella & Sparacio, 2004). The area is heavily populated due to greenhouse cultivation and seaside tourism. This area is extremely altered by greenhouse plantations and beach resorts. The main dangers for the habitats of this area are roads and invasive species, as the *Carpobrotus edulis* (L.).

4.3.5 LIFE LEOPOLDIA PROJECT

From 2012 to 2016, the Life Leopoldia Project has been carrying on along the coastal areas of the Gulf of Gela to reinstate and protect the dune habitats (Natura 2000 habitat codes 2110, 2120, 2210, 2230,

2250*), most suitable for the conservation and spread of the priority species *Leopoldia gussonei* being threatened by excessive pressure from greenhouse agriculture and tourism and by the illegal occupation of the maritime state property (Life Leopoldia Final report, 2016). The project has been implemented in the SCIs and SPA mentioned above and in the Ippari river Valley (Vittoria Pinewood) SCI. The main actions realized were the elimination of allochtonous species, the restoration of the dune ridges, creating new access points and fence off the habitats (Fig. 36), the collection of the germoplasm and monitoring the *Leopoldia gussonei* populations, the promotion of knowledge on natural resources.

Fig. 36 – Boardwalk built on the dune ridge of Punta Braccetto. The picture has taken in 2016.

4.4   PREVIOUS STUDIES ON THE EVOLUTION OF THE GULF OF GELA COASTAL AREA

There are few papers and regional reports that investigated the shoreline change rates and the dynamic evolution of the coast in the study area. Brambati et al. (1992) correlated the variation of coastal dynamic in the Gulf of Gela to the implementation of the harbours and the increasing urbanization. The cartographic dataset used for the shoreline analysis was heterogeneous and counted maps and images of the years 1928, 1931, 1940, 1966, 1982 and 1988. Results showed that the rate of shoreline change was positive over the time span 1928-1940, but it has been reversed in the Sixties. A maximum retreat of 300 m has been detected eastward the Southern Imera river mouth, 60 m at Punta delle Due Rocche and approximately 30 m East of the Gela harbour. Accretion of about 100 m has been observed westward the Gela Harbour, of 110 m between Scoglitti harbour and Punta Braccetto (Fig. 37).
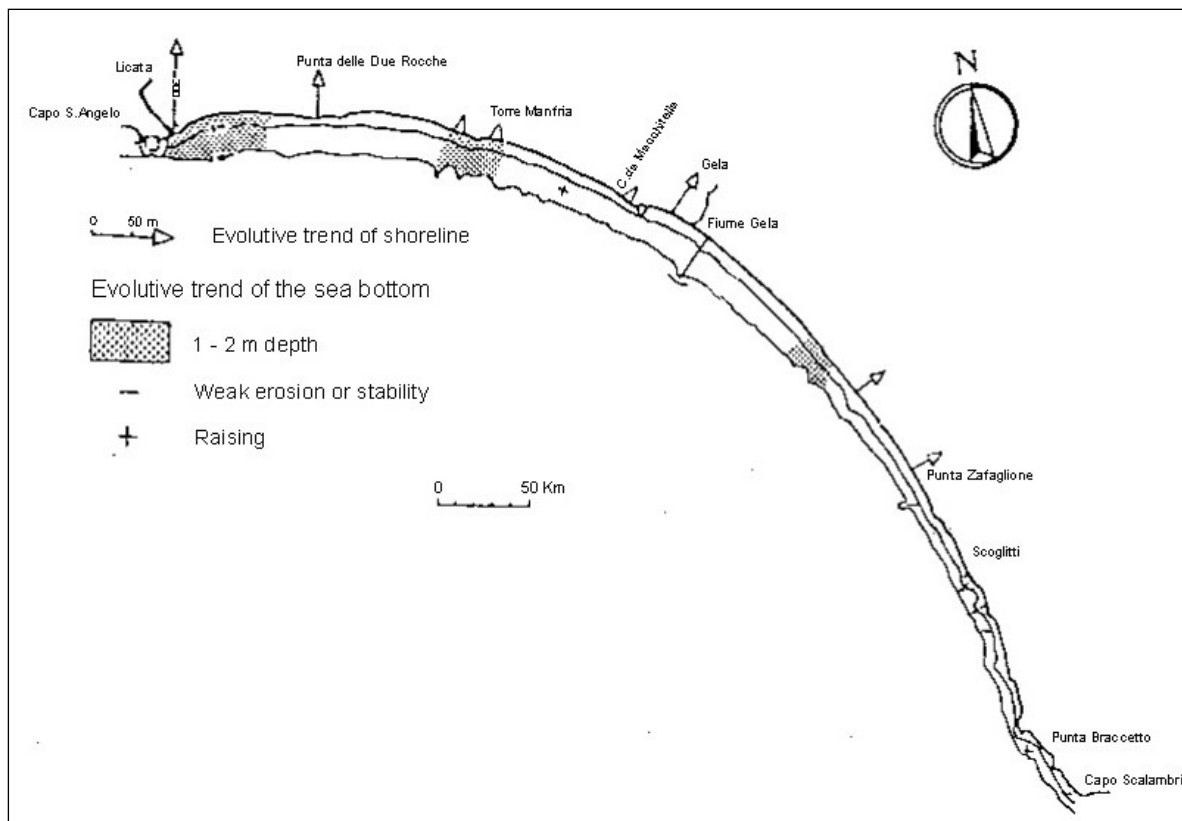
Fig. 37 - Evolutive trend of shoreline and of sea bottom in the Gulf of Gela (as modified from Brambati et al., 1992).

Brambati et al. (1992) identified some critical areas where the erosive phenomena have been extremely intensive, as the Southern Imera river mouth, the beach westward Falconara Castle, the Manfria beach, Macchitella and Contrada Macconi beaches. They related the rapid retreat to the rising development of the intensive greenhouses system, the implementation of the road network and the industrialization of the area of the Gulf. The textural analysis of beach sediment has also been performed. A bimodal curve has been found, values range from 230 to 390 μm and from 165 to 195 μm. The authors interpreted the data as typical of a mixture of alluvial and aeolian deposits. The median values showed a discontinuous trend, higher values have been detected and they were probably ascribed to fluvial origins (Southern Imera, Cantigaglione) or to local coastal erosive processes (Falconara Castle, Manfria, Macchitella beaches etc). The shoreface variations have been partly studied, 1-2 m sea bottom depth has been measured along Licata and Punta delle Due Rocche, between Manfria Tower and Gela harbour 1.5 m depth has been detected and approximately 1 m depth nearby the Dirillo river mouth has been identified.

Based on wave motion analysis, the authors underlined that the regional littoral drift mostly moves eastward for the seas from 240°. The coastal hydrodynamics are characterized by the increase of a

transversal drift to the East and by the contraposition of longitudinal dispersive system eastward for the seas from 240° - 210° and westward for the seas from 180° - 150°.

Considering all the above, the authors finally concluded that (i) the whole littoral along the Gulf of Gela has been retreated both above and below water level, relevant processes have been detected and seemed to be irreversible in some areas; (ii) the eroded sediments range into the fine grain-size values and are generally carried away to the offshore; (iii) there is no relationship between fluvial sediment load and the beaches sediment; (iv) the main source of sediment supply within the system is the cliff and low rocky coast erosion.

Amore et al. (2002) described the temporal evolution of the Salso river mouth, relating to the implementation of the Licata Harbour system. They analysed historical documents, ancient maps and aerial photos that cover a time span of 45 years (1952–1997) and carried out field surveys in order to trace the Salso river mouth evolution. The authors observed that until the 19th century the river mouth continuously changed with significant lateral migrations. In 1823, Schauroth's survey the river channel appeared meandering with subaerial levees and swash bars on both banks and it flew out 460 - 480 m retreated than the present-day coastline and eastern of 140 m than the actual mouth (Fig. 38; Fig. 39). In 1940, the coastline seemed to be stationary west to the Licata harbour and accreting of ca. 220 m at Giummarella bay. Furthermore, the river mouth migrated in parallel to the coastline eastward of 420 m generating a right mouth bar of 70 m. Between 1940 and 1952, the Licata harbour has been implemented was modified with Western Quay, a Northwestern – Southeastern breakwater stretching to stop the eastward sediment longshore transport, and the new Eastern dike at Giummarella bay, between the river mouth and the ruins of the old Castle. In 1952, the distance between the river mouth and the harbour itself was reduced and the coastline became south cuspidate shaped with a wide mouth bar in the middle. In 1960 the river mouth reached its maximum accretion of 770 m with a lateral migration of 400 m towards the southwestern; in the same year a strong accretion occurred along the eastern beach of Licata with the formation of small marshes along the coastal dune belt. Since 1960, the Licata shoreline accretion trend stopped and a retreating rate of 15 – 30 m/year has been computed. In 1967, the river mouth retreated to the same position to that recorded in 1952 but facing south-east, with a right-hand riverbed bar about 40 m wide and stretching for almost 200 m. The authors hypothesized that coastal erosion occurred between 1960s and 1980s was to be imputed to the

implementation of the Eastern dike of the Licata harbour, which blocked the longshore sediment transport, and to the dams built along the drainage of the Southern Imera river. Between 1977 and 1987, the western quay of the harbour has been connected to the old western breakwater. Between 1987 and 1997 further interventions were made to extend the external westward and eastward dikes. From 1980s to the 1997, the final stretch of the Southern Imera river has become totally stabilised and only small alterations may be noted at the river mouth, the enlargement of the right-hand bar recorded in 1987, and of the left-hand one, of about 50 - 125 m. Between 1983 and 1997, no significant modifications have been recorded, except for the flood of the 12th October 1991 and for the retreat of about 110 m along the beach at East of river mouth, between 1983 and 1987, and of about 25 m, between 1988 and 1989.
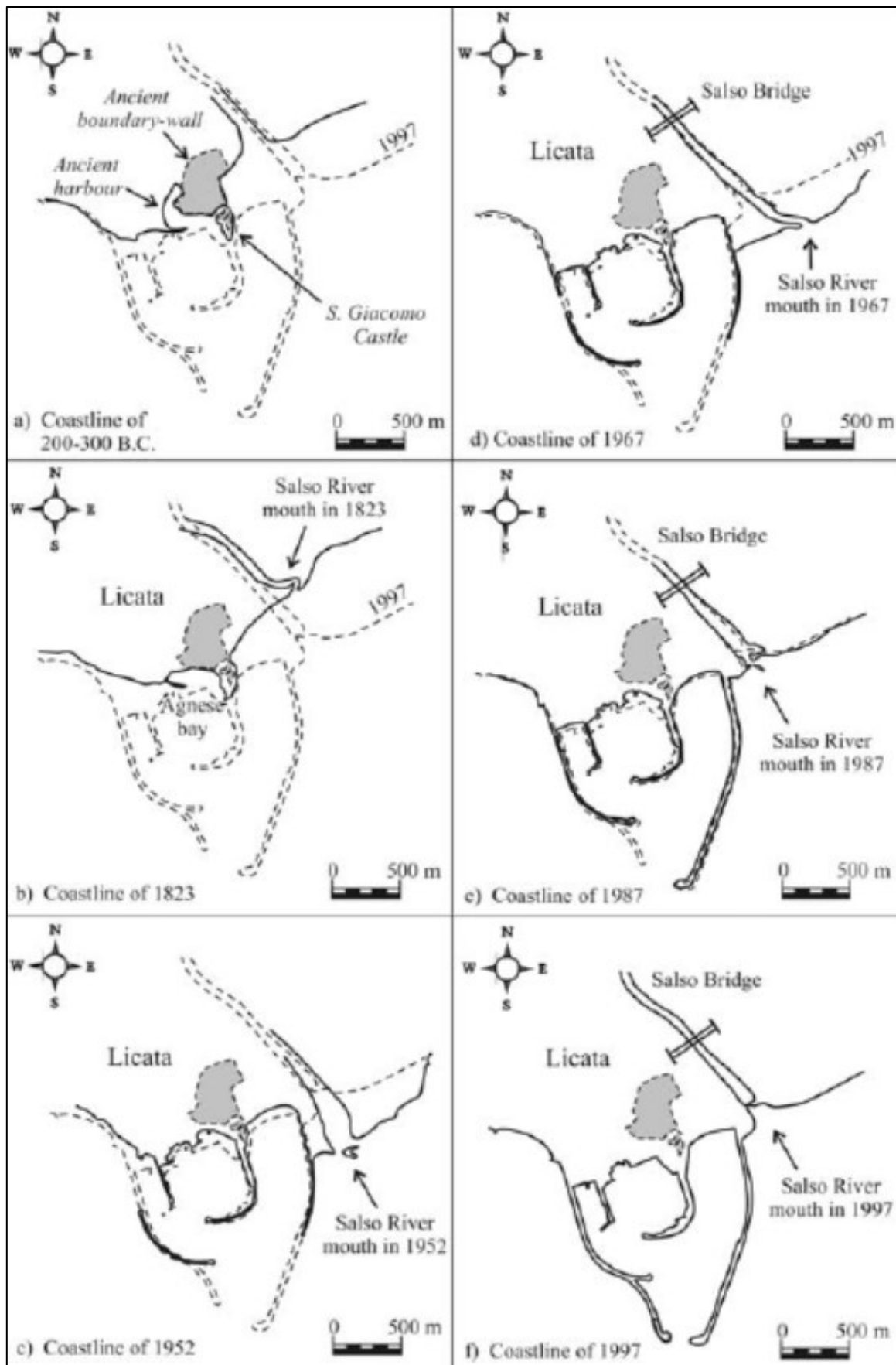
Fig. 38 - Evolution of the Southern Imera river mouth and of the Licata harbour: a) II-III sec b.C.; b) 1823; c) 1952; d) 1967; e) 1987; f) 1997 (from Amore et al., 2002).
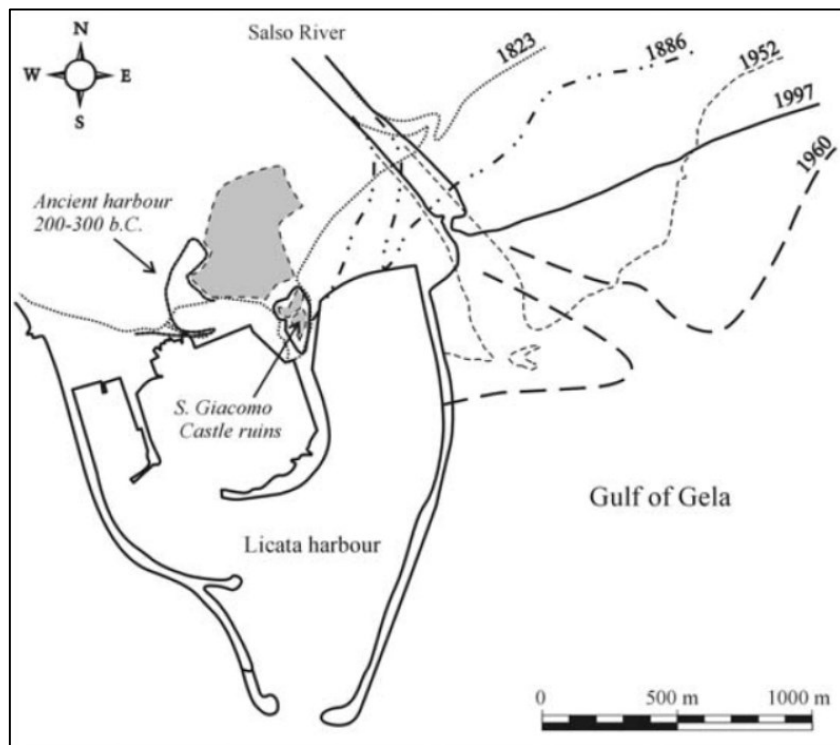
Fig. 39 - Temporal evolution of Southern Imera river mouth from 1823 to 1997 (from Amore et al., 2002).

In 2007, the Department of the Environment and the Territory of the Sicilian Region has published the Hydrogeological Management Plan, which included the reports of the 26 coastal sub-cell of Sicily. The methodology used to analyse the shoreline evolution is described in the General Report of the Hydrogeological Management Plan. The Sicilian Regional Technical Map 1:10.000 of 1997, aerial images of 1994, 1998 and 2003 and the Italian Military Geographical Institute (IGMI) cartography 1:25.000 of 1960 have been used to trace the shorelines. All cartographic data have been georeferenced and the same coordinate system was used. The estimated error for the assessment of the shoreline rate is ca. 2 m, corresponding to the pixel size of the Sicilian Regional Technical Map 1:10.000. The report highlighted that erosive processes affected both high rocky coasts and low sandy beaches. The cliff instability mainly depends on the natural erosive processes and the wave action contributes to erode the soft rocks (calcarenite, clay and marls). Longshore drift and winds move the suspended sediment along the coast and it represents the main supply source of the beaches. The coastal change analysis has shown that 27% of the coast of the coastal sub-cell has been retreating, it includes 17.1 km of beach and 2.5 km of cliff. The main beach erosion trend of the coastal sub-cell has been found in the Gela municipality (ca. 7,575 m); the analysis identified the highest erosion rate in the Butera municipality, 58,8% of the coast has retreated, 1,272 m of collapse cliff

and 3,344 m of beach retreat have been observed. In the coastal sub-cell, the results portrayed that the erosion rate ranges from 0.56 to 6.11 m/y. The shoreline change analysis identified the highest retreat nearby the Southern Imera river mouth, with a rate of 6 m/yr. Scoglitti beach showed 18 m retreat and erosion rate of 2 m/y; an erosion rate of 1,1 m/y has been found in Manfria tower and Federico II di Svevia Promenade beaches, finally, other relevant erosion rates have been found in Marina di Butera, Falconara Castle and Poggio della Guardia, with respectively rate of 2.2 m/y; 1.0 m/y and 0.78 m/y. Following a summary table of the data for each municipalities of the coastal sub-cell, resulting by the shoreline analysis (Table 6).

MUNICIPALITY	Total coastal length (m)	Stable coastline (m)	Collapse cliff (m)	Retreating beach (m)	Erosion (m)	Erosion (%)
Licata (AG)	10,667	8,779	85	1,803	1,888	17.7
Butera (CL)	7,848	3,232	1,272	3,344	4,616	58.8
Gela (CL)	27,364	19,498	291	7,575	7,866	28.7
Acate (RG)	7.38	5,541	0	1,839	1,839	24.9
Ragusa	10,956	9,656	600	700	1.3	11.9
Vittoria (RG)	8.38	6,301	173	1,906	2,079	24.8
TOTAL	**56,851**	**53,007**	**2,421**	**17,167**	**18,289**	**27.0**

Table 6 - Summary table of collapse cliff, retreating beach and erosion rates of each municipality lying in the Coastal sub-cell n. 8 (as modified from Regione Siciliana, 2007).

In 2011, Martino et al. investigated the geomorphological changes and the evolutionary trend of the coastal area that lies within the Butera municipality (Caltanissetta province). The aim of their study was to quantify the erosion rate and to propose efficient tools in order to protect the coastal zones. The analysis was undertaken using a mixed method that consists of (i) shoreline change analysis on a time span of 44 years; (ii) grain-size analysis of the main morphological features of the beach (foreshore, berms, dune); (iii) digitization in situ by GPS of the visible shoreline, as determined by the operator.

The shoreline change analysis was based on orthophotos (1966, 1988, 1994), satellite images (1998, 2000, 2006-2007, 2007-2008, 2009) and the 2010 shoreline digitized in situ by using GPS. Martino et al. (2011) divided the time span into six periods and traced the evolution of the beach, as follow: (i) 1966-1998, the analysis revealed a shoreline retreat of 18,50 m; they even detected the maximum beach width in 1966 (ca. 83) m and the minimum one in 1998 (ca. 65 m); (ii) 1998-2000, all along the coast under examination it has been shown further 27 m retreat, except for the area eastward the Desusino parking, where the erosion is less severe; (iii) 2000-2006, the landward average migration was of 43 m. As the previous time period, the area eastward the Desusino parking has faced the erosion better than the other part of the beach, probably due to the presence of a residual dune system, the change here amounted to 20 m; (iv) 2006-2008, the

erosion rate seems to be decreasing, the shoreline has lost 8 m; (v) 2008-2010, the analysis has shown a 20 m retreat. The image change detection allowed the authors to point out that the Desusino parking started to be partly destroyed by storms since 2008; (vi) 1966-2010, the total average retreat was 76 m.

The grain-size analysis was performed using 25 samples. The authors casted 7 transects, placed from NW to SE in Punta delle Due Rocche (1), Falconara (2-3), Desusino (4), Macconi (5) and Manfria (6-7) (Fig. 40). One sample for each morphological element of the beach (i.e. foreshore, foreshore step, berms and dune foot) has been collected, and the statistical sedimentological indexes in terms of mean (average grain-size), standard deviation (sorting), skewness and kurtosis have been computed.
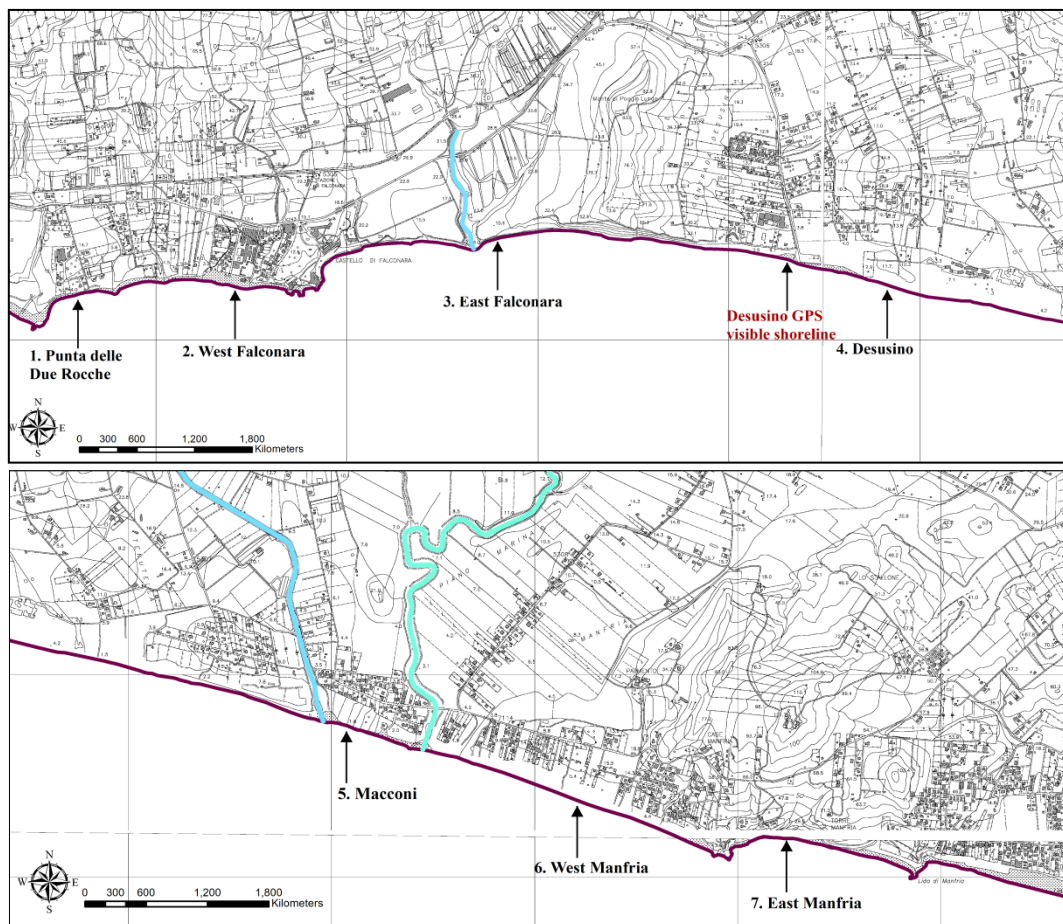
Fig. 40 - a) Four of the seven transects along which the sediment samples have been collected; b) three of the seven transects chosen for the grain-size analysis (modified from Martino C. et al., 2011).

The grain-size analysis results of the Martino et al. (2011) study showed that (i) most of the samples fell within the range of medium sand, except for the foreshore step in Punta delle Due Rocche (1), Falconara (2) and Desusino (4), that showed mean values indicating medium to coarse sand and eastward Falconara transect, where berm samples mean values indicated fine sand; (ii) standard deviation ranged from moderate to well sorted, major values have been observed in foreshore step samples than berms or dune foot ones; (iii)

skewness lies mostly in the range of symmetry, although foreshore step samples of Punta delle Due Rocche, Falconara (2), Desusino, Macconi, Manfria (1) and Manfria (2) had negative values; (iv) kurtosis values depict mainly mesokurtic curve and partly platykurtic.

Most of the berm and foreshore step samples had mean values ranging from medium to coarse sand, standard deviation indicated well sorted particles. These outlines led Martino et al. (2011) to conclude that the data depicted an erosive scenario for the studied area (Dal Cin, 1969; Carobene & Brambati, 1975; Ferrari et al., 2008). They even supposed that the sediment supply decreased moving from Licata to Manfria, reason why the standard deviation increased in this direction.

A landward migration tendency within the Gulf of Gela emerged by the above-mentioned research works and these results and insights will be used as baseline to confirm or reject the data obtained by the present Ph.D. thesis.

5 METHODS AND USED WORKFLOW

5.1 SHORELINE CHANGE ANALYSIS

5.1.1 INPUT DATA

The main constraining factor for diachronic analysis is the availability of data for the specific study site that generally leads the researchers to use different data sources in order to cover the desired time frame (Boak & Turner, 2005). For the purpose of the present Ph.D. thesis, the dataset used for the shoreline evolution detection included different sources that cover a time span of 63 years, from 1955 to 2018. The dataset used for the analysis included (i) *aerial photographs (1955, 1966),* they were bought by the Italian Military Geographical Institute (IGMI), which is the National Cartographic Authority, producing and providing the official high-quality cartography. The photographs are dating back to 1955 and 1966, (ii) *orthophotographs (1989, 2000, 2006, 2012),* consulted at the Consultation Service of the Italian National Geoportal. The Service permits to visualize, navigate, change the display scale, change in the framed area portion or overlay spatial data sets and to display pages information contained in captions and any relevant content of metadata (European Parliament, 2007). This service is implemented using the standard ISO 19128 – Web Map Service (WMS) 1.3.0. The WMS (Web Map Service) provides a map that is the representation of spatial information in the form of a digital image file in PNG, GIF or JPEG, but it cannot be edited by the end-users. The use of image formats that support transparent background allows the superimposition of different maps, which can be requested from different servers. The orthophotos scale is 1:10.000, with spatial resolution ranging from 0.5 to 1 m. The coordinate system is WGS84/UTM 33N. The photographs were taken by flight in 1997, 1998, 1999, 2005 and 2010. The final release has been available after making picture correction. The 1997, 1998 and 1999 photographs are dating as 2000, the 2005 dataset has been released in 2006, the 2010 in 2012, (iii) *Unmanned Aerial Vehicle (UAV) image (2018)* that covered the coastal length of the sector n. 5 and has been acquired the 21st December 2018 by a quadcopter Aeryon Scout™, property of the Biological, Geological and Environmental Science Department of the University of Catania. The drone carried a GoPro Hero 3, 12-megapixel camera (visible spectrum sensor) modified with a rectilinear lens to eliminate the fish-eye effect. The output image coordinate system is the WGS84/UTM 33N. For more information about Calibration, Bundle Block Adjustment, Geolocation, Initial Processing and Point Cloud Densification details consult the Quality Report in Appendix n. 1 (Fig. 41).
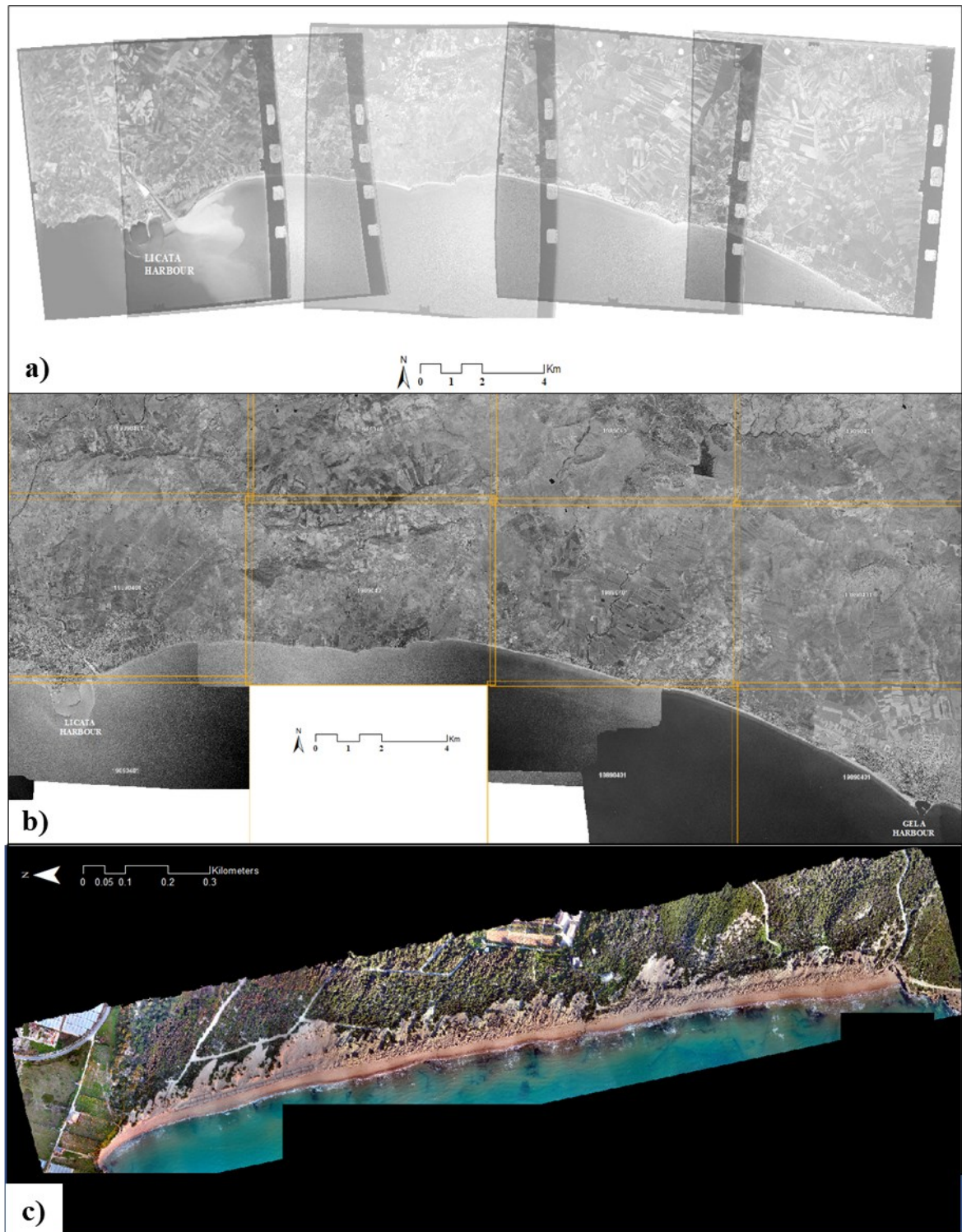
Fig. 41 – a) Overlay of the 1966 aerial photograph sequence of sector n.1 and part of sector n. 2; **b)** 1989 orthophotographs of the Consultation Service of the Italian National Geoportal; **c)** Orthomosaic of the sector n. 5 acquired the 21st December 2018 by UAV.

5.1.2 DIGITAL PHOTOGRAMMETRIC PROCESSING

The *aerial photographs* were processed by ERDAS Imagine 2014 using the Sicilian Regional Technical Map 1:10.000 (ATA 2007/2008) and the LIDAR DTM with a pixel size of 2x2 m downloaded from the Regional Technical Information System website. The coordinate system of both data sources is Monte Mario Italy 2. About 20-30 Ground Control Points (GCPs, Fig. 42) for each time series have been applied to georeference and rectify all aerial images; depending on the number of ground control points, the aerial photographs were rectified with a second- or third-order polynomial transformation. The GCPs were placed homogeneously in the area of interest and easily identifiable in each picture of the time series. They cover road intersections or railroad intersections, river bridges, large low buildings. Natural features are generally not preferred because of their irregular shapes, but it may be necessary to use them in areas lacking suitable cultural features. During such points selection it has to be taken into account that certain boundaries can be subject to variations (forest, water bodies) and may be different on images and maps. The photogrammetric process was completed determining the interior orientation, performed using empirical camera parameters and the fiducial marks of each photograph.
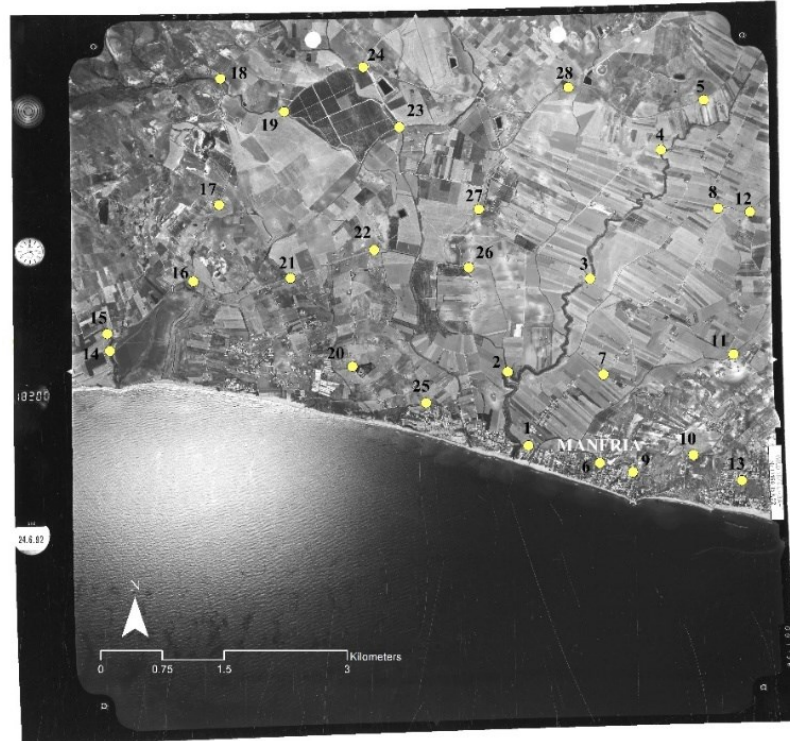
Fig. 42 - Example of Ground Control Points used for the orthorectification process. The below image is an aerial photograph of 1992.

In order to analyse the shoreline changes, all shoreline dataset should be presented in the same coordinate system and overlapped, all the data have been implemented in ArcGIS 10.3 environment and converted to the coordinate system Monte Mario Italy 2.

5.1.3 SHORELINE DETECTION

Once the dataset has been rectified and georeferenced setting a common coordinate system, the next key issue is the selection of an adequate feature that can serve as a shoreline proxy or indicator for the land-water interface, so that it properly reflects real shoreline position and evolution. The local geomorphology of the study area and the kind of dataset are both parameters that can lead the researchers to apply one indicator than another. In this work, the proxy that was chosen to detect the shoreline is *the wet/dry line (*Boak & Turner, 2005). Any available dataset can be used to extract a tidal datum-based indicator; thus, the detection technique should be the manual visual interpretation of a visibly discernible shoreline feature from the aerial photographs, the orthophotographs, and the drone image. Furthermore, the geomorphology of both study areas is heterogeneous, many areas have been strongly modified over time by the human actions and many natural features are not still recognizable (stable vegetation line, dune toe, dune crest). The *wet/dry line* resulted to be the best shoreline indicator because it is easily detectable in all images and representative of the land-water boundary for the dataset (Fig. 43). Moreover, the *wet/dry proxy* is the most commonly found within the shoreline change analysis literature, as a result the uncertainty is described by several authors and can be computed taking into account some precise data.
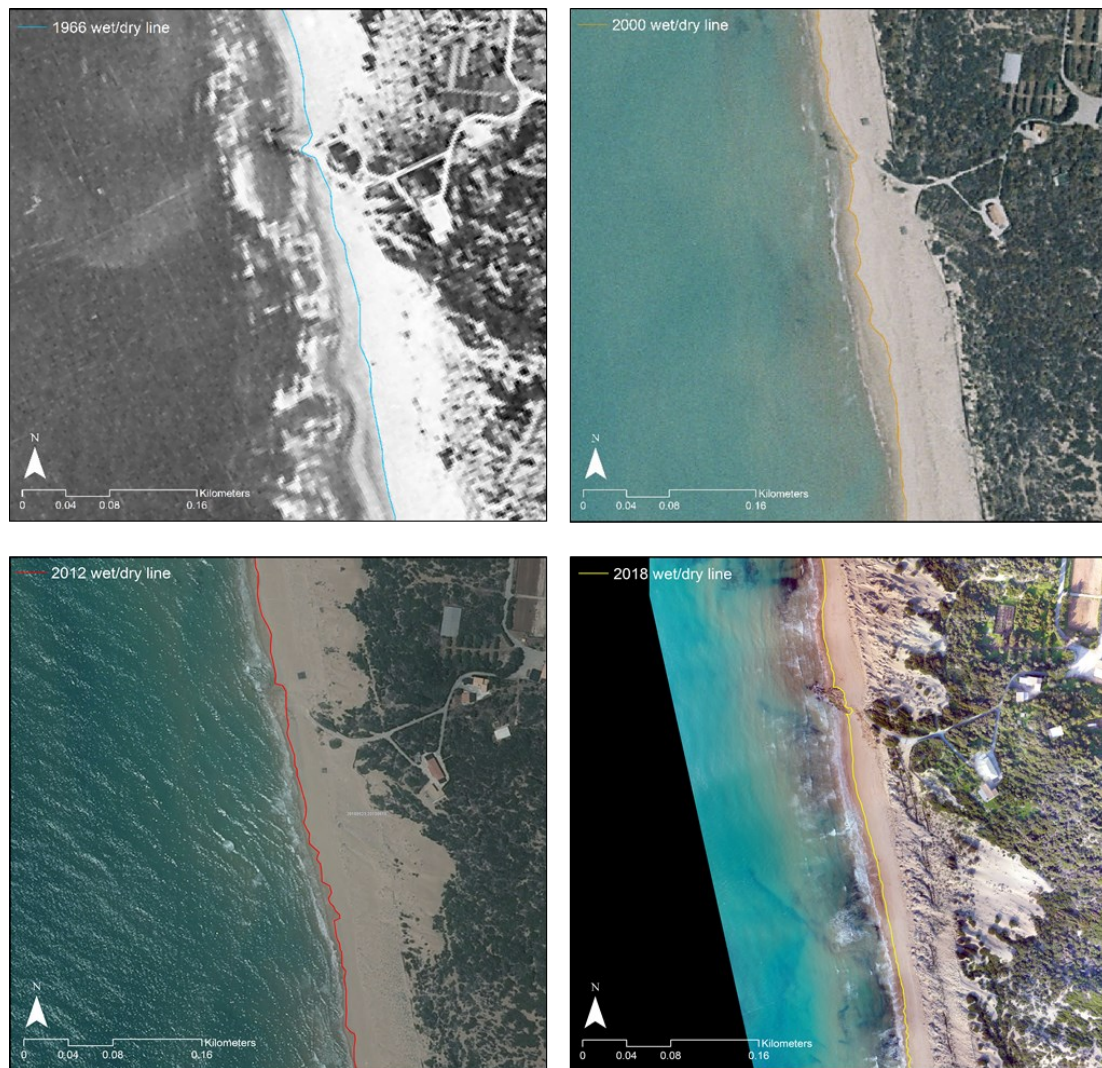
Fig. 43 – The shoreline proxy has been chosen in the present research is the wet/dry lines, as shown in the images. It was extracted from each available image. The 1966 image is an IGMI aerial photograph, the 2000 and the 2012 are Consultation Service of the Italian National Geoportal, the 2018 is the drone image.

5.1.4 DIGITAL SHORELINE ANALYSIS SYSTEM

Once the shorelines have been extracted, they should be used to compute the rate-of-change statistics in ArcGIS environment. The Digital Shoreline Analysis System (DSAS) has been used for the purpose of the calculation rate, it is a freely available software application that works within the Esri Geographic Information System (ArcGIS) software. The DSAS enables the user to calculate rate-of-change statistics from multiple historical shoreline positions. The Digital Shoreline Analysis System provides an automated method for establishing measurement locations, performs rate calculations, computes the statistical data necessary to assess the robustness of the rates (Thieler et al., 2005). Cliff and rocky coasts have not been considered in the statistical computation, because a different approach should be followed to depict the coastal dynamic.

The DSAS works within a personal geodatabase, it serves as the storage location for the program-generated transect feature class and related statistical output tables. The required input data are:

- Shorelines feature class;

- Baseline, used as measurement method to calculate rate-of-change statistics for a time series of shorelines (Clow & Leatherman, 1984).

Each shoreline must also have an attribute table with the following fields:

- OBJECTID, which is generated by the program;

- SHAPE, it is auto-generated as well, it gives information on the geometry of the feature;

- SHAPE_Length, it is computed by the program;

- DATE_, it is created by the user and represents the date of the picture;

- UNCERTAINTY, the calculated rates of change provided by DSAS are only as reliable as the measurement and sampling errors that the user must account for when compiling each shoreline position. Its computation will be lately discussed.

The baseline is the starting point for the transects casting performed by the DSAS application. The line has been established adjacent to the series of shoreline positions, thus the transects have been casted mainly perpendicular to the baseline and intersected the shorelines to establish measurement points. The baseline consists of more segments for the study area 1 and a single line for the second one (Fig. 44). In both cases, the baselines are onshore, never offshore. They were built starting with a new feature class.
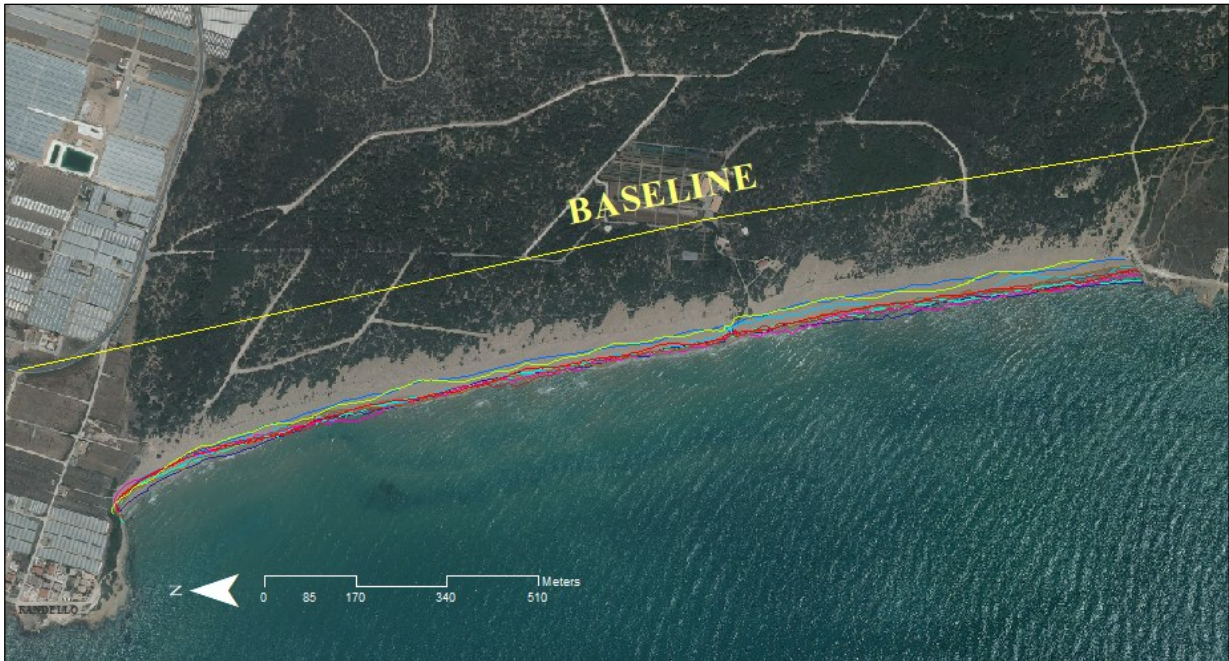
Fig. 44 - Baseline and shorelines of sector n. 5.

The attribute field requirements for the baseline provide necessary information to DSAS about the alongshore order of transects as well as the location of the baseline with respect to the shorelines. This information is incorporated into the calculations so that rate-of-change statistics properly denote erosion as negative and accretion as positive.

The transect-generation process begins by selecting the default settings in the Set Default Parameters window. This window can be accessed from the DSAS toolbar and contains three tabs (Fig. 45):

- Cast Transect Settings, it manages the placement, length, and spacing of the transects used to establish measurement points for rate calculations;

- Shoreline Calculation Settings, specifying the attribute fields containing the date and shoreline uncertainty values;

- Metadata Settings, which includes user and project information.
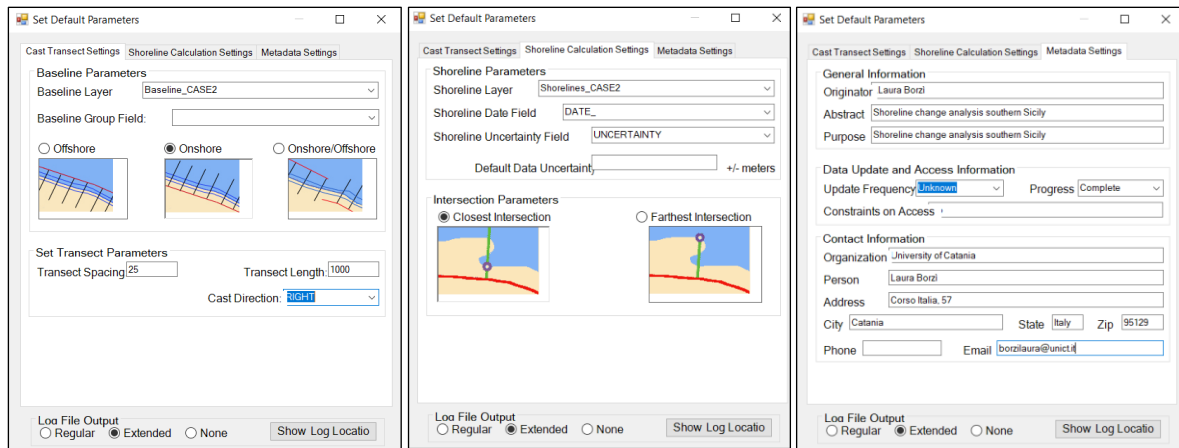
Fig. 45 - Set default parameters tabs.

The chosen spacing distance between transects is 25 m and the transects length is 1000 m for the each sector (Fig. 46). The cast direction is oriented right on the flow of the first baseline segment.
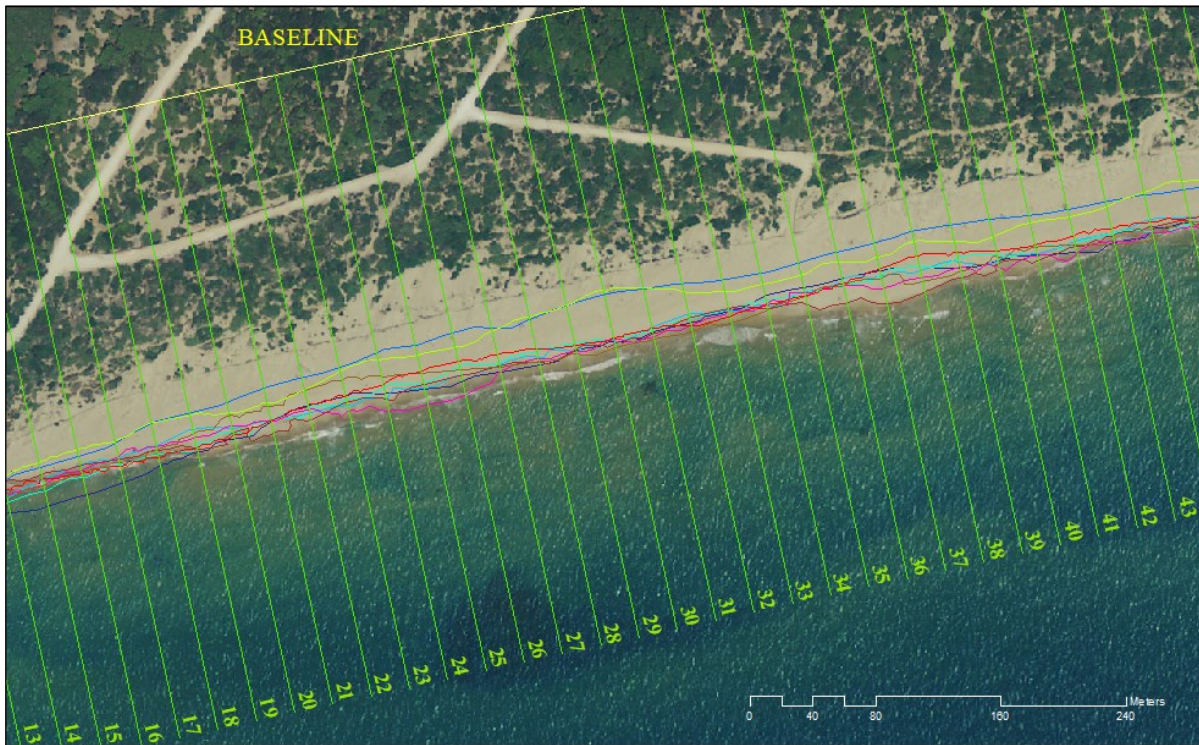
Fig. 46 – Transects casted authomatically by the DSAS, spacing distance set at 25 m.

In the Shoreline Calculation Settings tab, the shoreline layer to be used, the field that stores date and the field storing the positional/measurement uncertainty value must be specified. If there are shoreline segments that do not have a value, a default uncertainty can be chosen. Default Data Uncertainty has not been indicated in this study because each shoreline has its own uncertainty value previously computed.

DSAS automatically generates FGDC-compliant metadata with minimal user input for the transect feature class. Metadata generated by DSAS is structured to meet the Federal Geographic Data Committee (FGDC) Content Standard for Digital Geospatial Metadata (CSDGM) v. 2.0.

After setting the set default parameter, next step is casting transects, made by the Cast Transect tab. It allows to choose the storage parameters and the casting method. The Smoothed Baseline Cast has been selected, to better orient transects along curved sections of the case 1 baseline, with a smoothing distance of 20 m. The Simple Baseline Cast option has been chosen for the case 2 baseline, because it is a short straight line without curved segment.

Once the transect feature class has been created and all updates or modifications have been made, the data can be used to compute change statistics. The DSAS calculate change statistics tab (Fig. 47) allows the user to choose from the list the statistical analysis that can be performed.
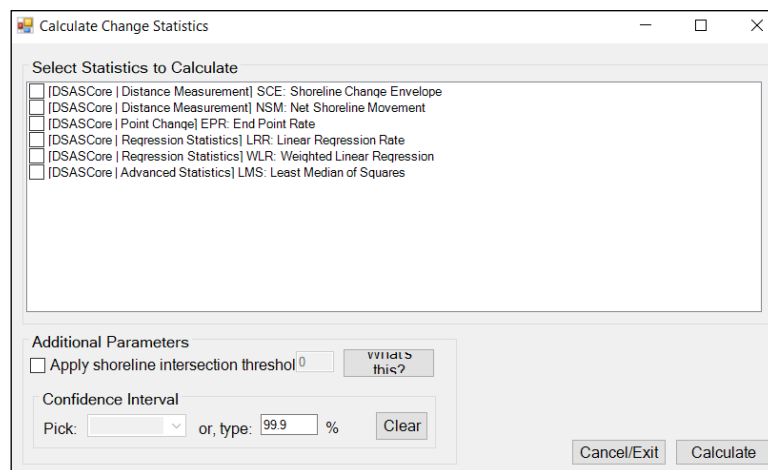
Fig. 47 - DSAS Calculate Change Statistics tab.

The Weighted Linear Regression rate (WLR) and the Linear Regression Rate (LRR) have been computed for each sector. The NSM and the SCE indexes have been computed for sector n. 1, n. 2 and n. 5 over the long-term time span (1955 – 2012 for first sectors, 1955 – 2018 for sector n. 5). The NSM reports the distance between the oldest and the youngest shorelines. The SCE is a measure of the total change in shoreline movement considering all available shoreline positions and reporting their distances, without reference to their specific dates.

As briefly showed in the previous paragraph, the DSAS requires data on the errors that affect the measurement method and the cartographic sources. The reliability of the statistics computed by the system depends mainly on the uncertainty value related to each shoreline dataset. In this Ph.D. thesis, to better estimate rates of change and reduce the effect of short-term variability on long-term analysis, the uncertainties were considered independent, uncorrelated, random and, following Crowell et al. (1991), Fletcher et al. (2003), Genz et al. (2007), Romine et al. (2009) and Virdis et al. (2012), the total positional uncertainty of each dataset has been calculated with the following equation:

$$\sigma_t = \sqrt{\sigma_d^2 + \sigma_p^2 + \sigma_r^2 + \sigma_{td}^2 + \sigma_{wr}^2}$$

The Digitizing Error (σ_d) has been obtained detecting several times the same feature on the same image and calculating the error as the standard deviation of the residual value for that feature.

The Pixel Error (σ_p) was assumed to be equal to the pixel size.

For the Orthorectification Error (σ_r), the RMSE computed for the photogrammetric and polynomial rectification process has been used as error value.

The Tidal Fluctuation Error (σ_{td}) has been considered as the variations in levels at the tide gauge station located at Porto Empedocle (AG), at NW 40 km from the study area. It is set inside the harbour, since 2010 the tide level is measured by a new sensor with millimetre accuracy, the SIAP+MICROS TLR. The min-max tidal range varied from 0.03 m to more than 1 m (October 2017, Fig. 48), but the average water level fluctuation was 0.04 m.
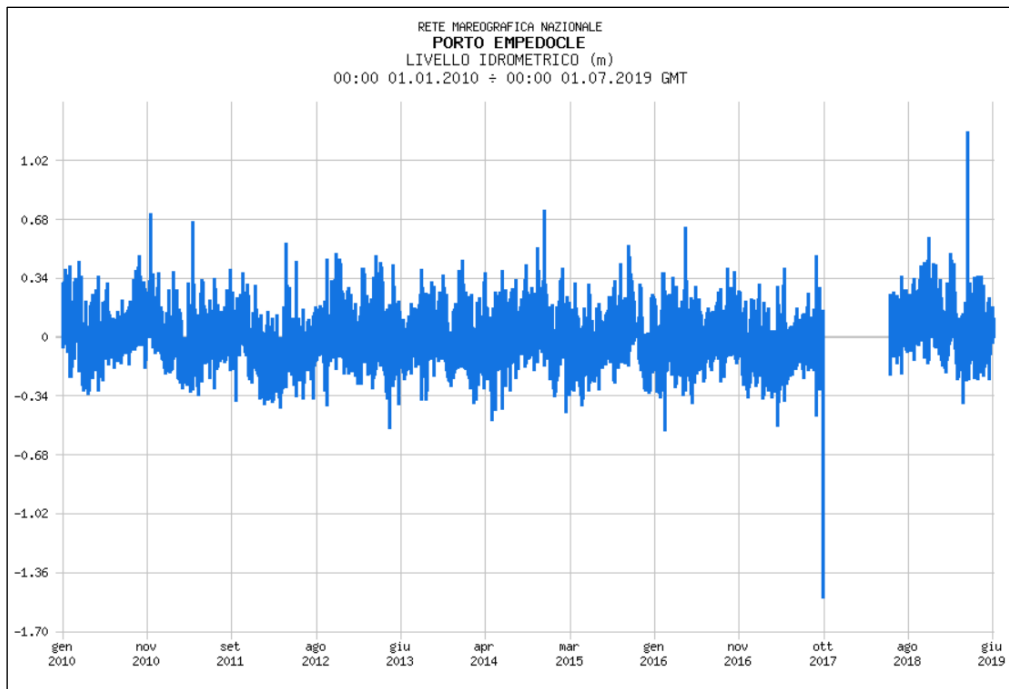
Fig. 48 - Tidal fluctuation detected by the Porto Empedocle (AG) tide gauge station; the time period covered is from the 1st January 2010 to 30th June 2019. There is a gap since the 1st November 2017 to May 2018.

The Wave Runup Error (σ_{wr}) has been estimated thanks to the Copernicus Climate Data Store. The European freely available service provides the fifth generation ECMWF atmospheric reanalysis of the global climate, the ERA5. It combines model data with observations from across the world into a globally complete and consistent dataset using the laws of physics. It also offers a web-based and API-based search and retrieve facilities to access climate data and information (Fig. 49).

```
import cdsapi

c = cdsapi.Client()

c.retrieve(
    'reanalysis-era5-single-levels',
    {
        'product_type':'reanalysis',
        'format':'grib',
        'variable':'peak_wave_period',
        'year':'1989',
        'month':[
            '01','02','03',
            '04','05','06',
            '07','08','09',
            '10','11','12'
        ],
        'day':[
            '01','02','03',
            '04','05','06',
            '07','08','09',
            '10','11','12',
            '13','14','15',
            '16','17','18',
            '19','20','21',
            '22','23','24',
            '25','26','27',
            '28','29','30',
            '31'
        ],
        'time':[
            '00:00','01:00','02:00',
            '03:00','04:00','05:00',
            '06:00','07:00','08:00',
            '09:00','10:00','11:00',
            '12:00','13:00','14:00',
            '15:00','16:00','17:00',
            '18:00','19:00','20:00',
            '21:00','22:00','23:00'
        ]
    },
    'download.grib')
```

Fig. 49 - Example of API-based search tab used to download ocean waves data for the computation of Wave Runup.

The time covered by the ERA5 data is 1979-present day. The Mean Wave Direction, the Significant Height of Combined Wind Waves and Swell, the Peak Wave Period have been downloaded and used to compute the runup elevation for each images by empirical equations (Hunt, 1959; Holman & Sallenger, 1985; Mase, 1988; Hughes, 2006; Nielsen & Hanslow, 1991). An average slope value of 4% for has been extracted from DTM 2 m buffer zone along the whole 2008 shoreline. As mentioned above, there are no ocean data earlier than 1979, thus the runup value obtained for the 1979 has been applied to the 1955 and 1966 pictures.

A sum up table of the errors and the total uncertainty computed for the study area is presented in Table 7.

year	digitizing error (σ_d)	pixel error (σ_p)	orthorectification error (σ_r)	tidal fluctuation (σ_{td})	wave runup (σ_{wr})	UNCERTAINTY (σ_t)
1955	1.60	3.00	1.549	0.04	0.14	3.74
1966	1.85	3.00	1.73	0.04	0.14	3.93
1989	1.01	1.00	1.00	0.04	0.14	1.74
2000	0.92	1.00	1.00	0.04	0.15	1.69
2006	1.32	0.50	0.50	0.04	0.13	1.50
2012	1.33	0.50	0.50	0.04	0.19	1.52

Table 7 - Errors and shoreline uncertainty (*units in meters*).

5.1.6 STATISTICAL OUTPUT AND DATA ELABORATION

When the selected calculations have been processed, results are returned to DSAS provided in a table and automatically added to the ArcMap project. The system generates two new tables, rates and intersects ones. The rate-of-change statistic tables have been exported to Microsoft Excel worksheet. The WLR index has been classified following the methodology proposed by Molina et al. (2019). All values have been normalized and the Gaussian distribution resulted has been used to set the classes limits (Table 8). More than 40% of all data ranged between $\pm$ 0.4 m, it has been assumed as the most recurrent smallest change due to seasonal oscillations and thus classified as *stability state*. Values between -0.4 and -0.7 m and between +0.4 and 0.7 m have been considered as *moderate erosion* and *moderate accretion* respectively, corresponding to 25% of all dataset; the remaining 34% data have been grouped into 4 classes, *high erosion* (<-0.7 m; $\geq$ -1.5 m), *very high erosion* (< -1.5 m), *high accretion* (>0.7 m; $\leq$ 1.5 m) and *very high accretion* (> 1.5 m). The percentage of each beach evolution class has been computed for each sector.

Class	m/year
Very high erosion	<-1.5
High erosion	$\geq$ -1.5 ; < -0.7
Moderate erosion	$\geq$ -0.7 ; < -0.4
Stability	$\geq$ -0.4 ; $\leq$ + 0.4
Moderate accretion	> +0.4 ; $\leq$ +0.7
High accretion	> +0.7 ; $\leq$ +1.5
Very high accretion	> +1.5

Table 8 – Beach evolution classes defined for the present work following the methodology proposed by Molina et al. (2019).

5.2 DUNE FRAGMENTATION INDEX

The dune fragmentation index (F) has been proposed for the first time by Molina et al. (2020). It has been used to assess how the dune systems within the study area have been modified by human action over time. The F index is expressed as the ratio between the length of all breaks (l) identified within a dune system and the whole dune toe length (L):

$$F = \frac{l}{L}$$

Each shorefront dune toe has been divided in 100 m tracts to reduce the importance of dune seaward length and the F index has been calculated for each. The F Index is expressed by three classes that were computed by Molina et al. (2020) using the Natural Breaks Function. The annual level of dune fragmentation of each system has been expressed as the average value of the F index computed for all tracts for each available image. In the present research work, five classes have been used to depict the dune fragmentation evolution over time, the classification has been obtained using the Natural Breaks Function applied to the total value range. The fragmentation level has been thus expressed as Null (F = 0), Low fragmentation (0 < F ≤ 0.05), Medium level of fragmentation (0.05 < F ≤ 0.1), High and Very High/Maximum fragmentation (0.1 < F ≤ 0.4, F > 0.4, respectively).

5.2.1 SAMPLING METHOD AND SEDIMENT ANALYSIS

Grain-size analysis is a measurement of the size distribution of individual particles in a sample and provides important clues to the sediment provenance, transport history and depositional conditions. For this study, the analysis has been performed over three years, during summer- and winter-time in 2017 and 2018, only during winter-time in 2019. The beach model followed in the present thesis is the scheme proposed by the Shore Protection Manual (Coastal Engineering Research Center, 1984) that placed the boundary between the backshore and the foreshore at the first berm, which is produced by the wave erosion to the beach and coincident with the medium high tide level (Howard & Reineck, 1981). This scheme results to be largely accepted in the most common models used for different purposes. The sediments were collected in three different sites and approximately on the same place, where the main beach features (dune, berms and foreshore) are easily detectable (Fig. 50). The sample sites were chosen on the base of their

geomorphological profile, four of them were set closeby the Falconara Castle, where a narrow beach has been identified and summer houses have replaced the dune ridge; three transect were located easterly the Manfria Tower, where there is a wider beach and a small dune ridge still resists. Samples were even collected along one transect within the sector n. 5. In all, one hundred and sixty samples were performed and then analysed in the University of Catania sedimentology laboratory.
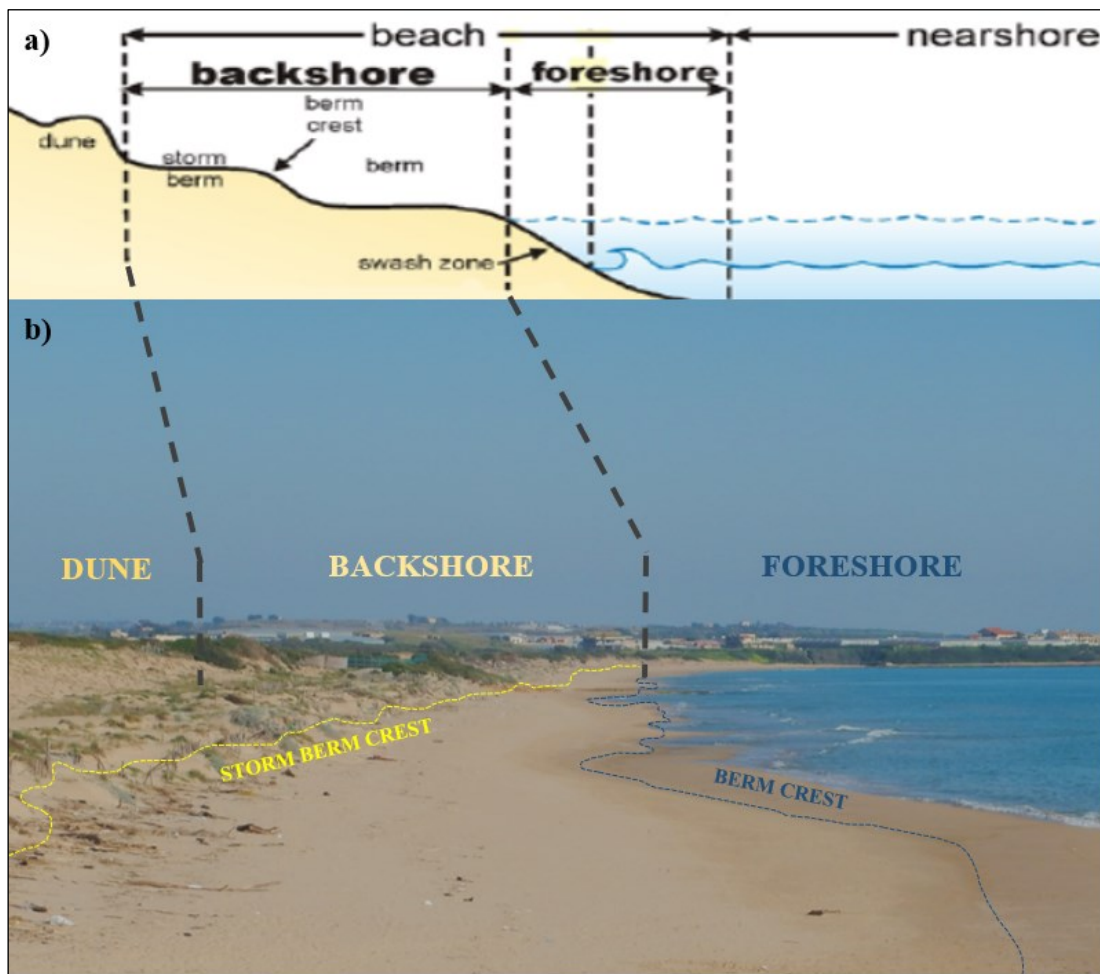
Fig. 50 – a) Scheme of the reference beach model adopted (from Longhitano, 2014) and terms describing a typical beach profile according to the Shore Protection Manual of the Coastal Engineering Research Center (1984); b) Study area 2 and its detectable beach features, where sediment samples have been collected. The lower foreshore limit has not been investigated in this work, thus not specified in the image.

Concurrently samples positioning was conducted by using handled GARMIN GPS 76 and samples were then carefully preserved in polythene bags. In the laboratory, shells were separated from sediments and the mixed saline content was removed from the grains by washing with water. Thus, they were dried at approximately 60°C using a VISMARA Thermotop drying oven and the dry weight has been detected by a Mettler PE 2000 Balance (Fig. 51).

Fig. 51 – a) Garmin GPS 76S used to trace the position where the sediment samples have been collected; b) samples preserved in polythene bags; c) VISMARA Thermotop drying oven; d) dried sediment samples.

After drying and weighing the samples, they were treated with hydrogen peroxide in order to enhance dispersion of aggregates, then they have been washed again and re-dried.

The grain-size distribution was carried out by a mechanical sieve shaker, using ASTM sieve series. The sediments consist mainly of sand; thus, the sieve particle-size range has been working with is from 63 μm to 8 mm. The residual soil under 63 μm has been analysed by the ELZONE 282 PC densimeter. The sediments have been described using the Udden-Wentworth grain-size classification (Wentworth, 1922), it is a widely used scale in scientific literature; *mean grain size* (Mz), *standard deviation* (s), *skewness* (Sk) and *kurtosis* (Kg) have been elaborated for each sample (Folk & Ward, 1957; Friedman, 1961).

5.3   COASTAL ARMOURING ANALYSIS

For this Ph.D. thesis, the coastal structures have been mapped as line segments in ArcGIS environment, different feature classes have been created for each type of armour (Fig. 52).

Fig. 52 - Example of coastal structures mapped as line feature class in ArcMap. The image below is the 2012 orthophoto.

As already mentioned, the *coefficient of technogenous impact K* (Aybulatov & Artyukhin, 1993) has to be used to assess the anthropogenic structure impacts on the study area. It is obtained by dividing the total length of all emerged and visible submerged maritime structures (groins, moles, seawalls, revetments, breakwaters, etc.), l, by the entire length (L) of the coast under consideration. According to this methodology the extent of *technogenous impact* is considered as minimal at K = 0.0001−0.1; averaged when K = 0.11−0.5; maximal at K = 0.51−1.0 and extreme if K > 1.0.

6   RESULTS

6.1   SHORELINE EVOLUTION

Over the mid-term (1989 – 2012) analysis, the normal distribution resulted to be negative skewed, 3 of the 5 sectors mainly experienced a landward migration trend and 2 of them showed stability state. Any sector has been globally found to be significantly accreted.

Sector n. 1 is ca. 10 km long from the Licata harbour to the Falconara Castle. The main coastal human work insisting on the coast is the Licata harbour, set just westerly the Southern Imera river mouth. The port is considered a strategic infrastructure and it has been implemented several times since the Fifties, but last works have been finished in 1997. Easterly the Southern Imera river mouth, eleven breakwaters have been emplaced to block the huge erosional trend here recorded. The 32% of the transects (120) fell within the stability state range, but the erosion classes reached 56% (214 transects) with a maximum negative WLR value of -3,15 m/year registered nearby the Licata harbour. Total accretion classes percentage was 12% (46 transects) and only recorded at the Licata breakwaters shoreline (Fig. 53).
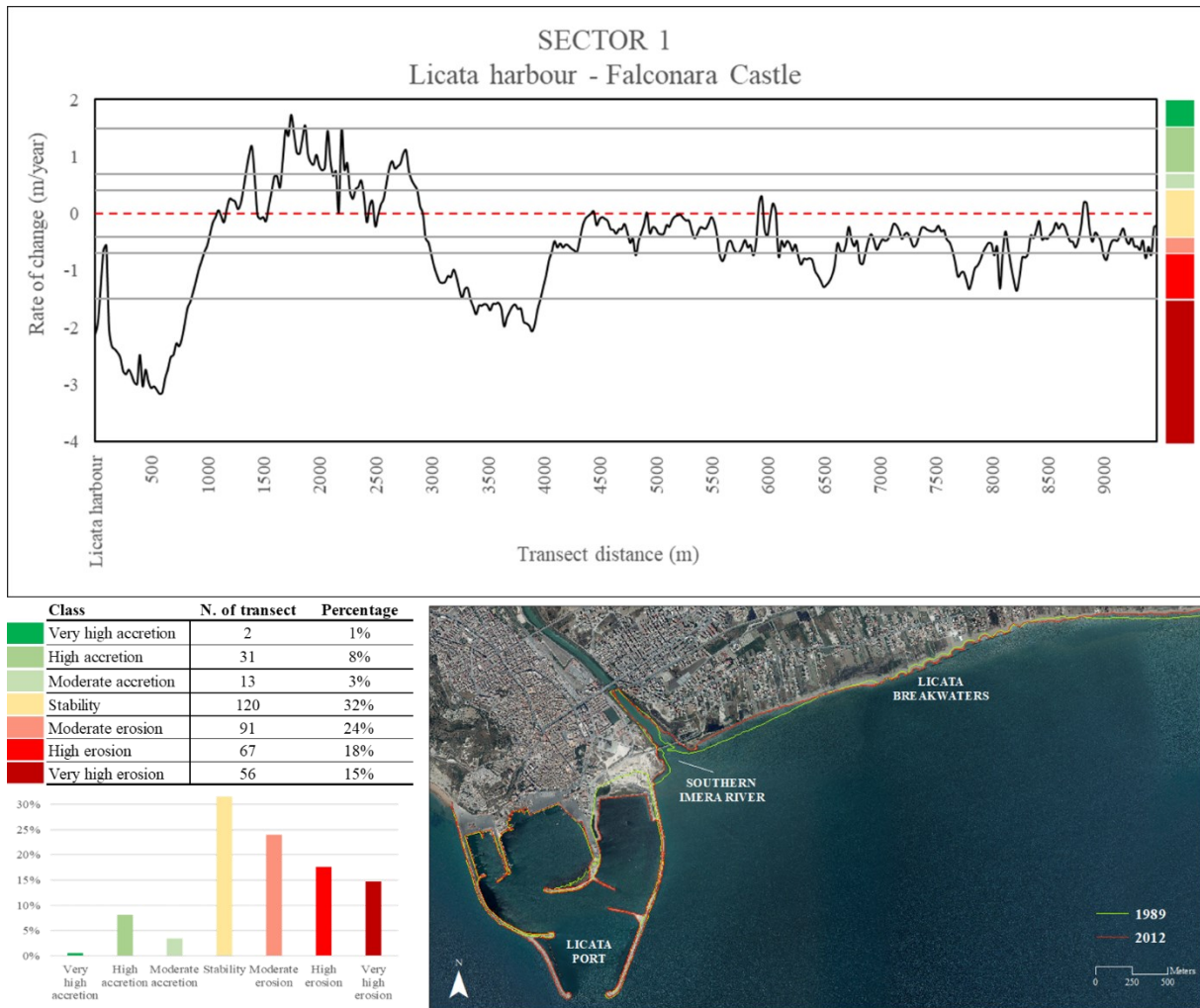
Fig. 53 – Shoreline changes over mid-term period (1989 – 2012) within the sector n. 1. Erosion phenomena (-3,15 m/year) occurred right next to the Southern Imera river mouth, easterly the Licata harbour. Accretional classes have been recorded where 11 breakwaters have been emplaced to block the intense sediment loss.

Sector n. 2 stretches between the Falconara Castle and the Gela harbour. The Site of Community Importance ITA 050011 – Manfria Tower is here set, and easterly the Manfria Tower there is still a small dune ridge. Stability state class represented more than 50% of the data (300 transects), even though landward movements have been recorded mostly at the western part of the sector, where shoreline faced a maximum retreat of -1,98 m/year, and moderate accretion values (ca. 13%) occurred mainly at the eastern part (Fig. 54).
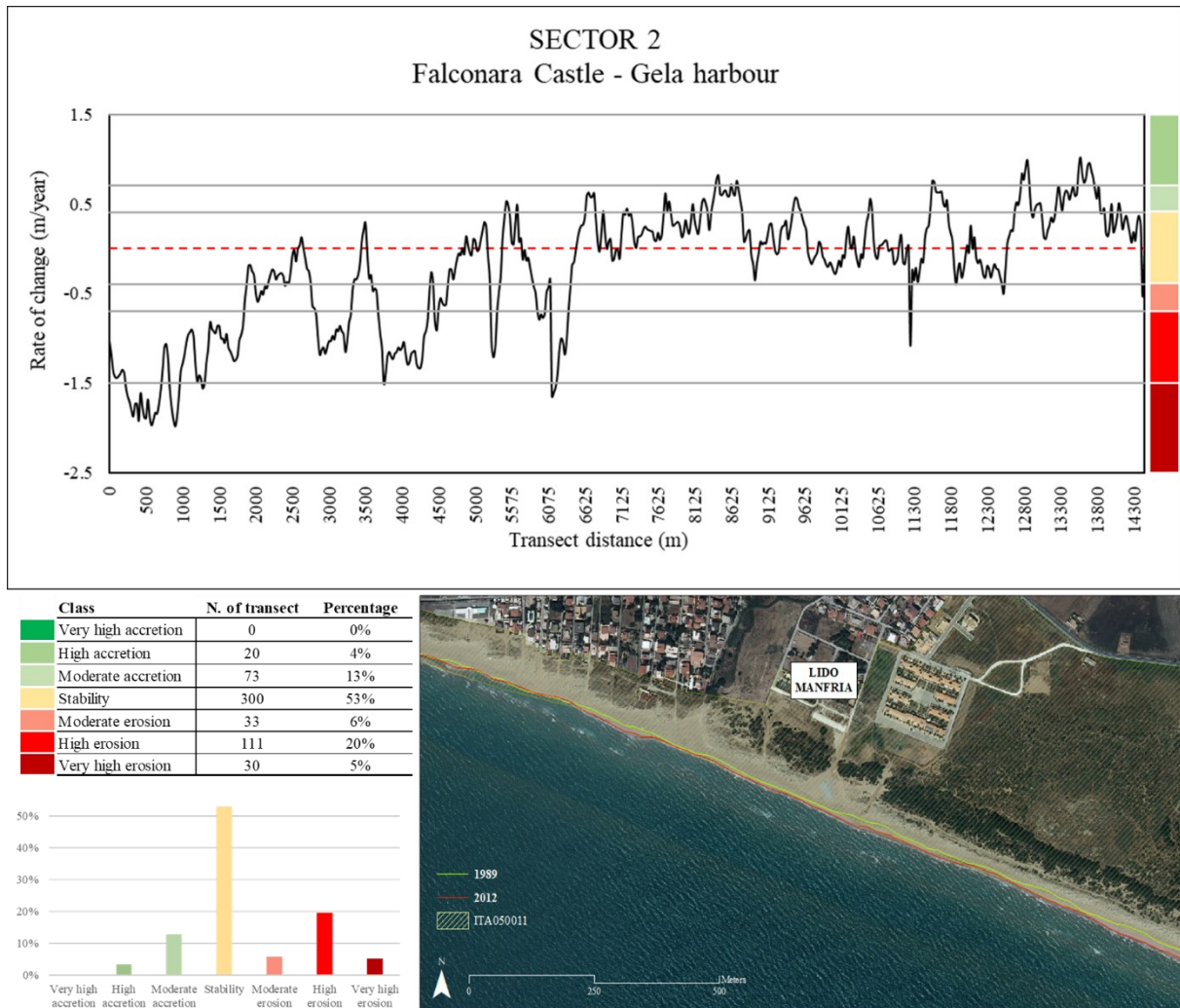
Fig. 54 – Shoreline evolution over the mid-term period (1989 – 2012) within sector n. 2 that mostly showed a stable trend (53%). Sector n. 2 partly concides with the Site of Community Importance ITA 050011 – Manfria Tower, there is a dune ridge of such meters in the easternmost part of the SCI where higher sediment deposition processes have been recorded, 93 transects ranged between moderate and high accretion class.

Within the sector n. 3, the 43% of transects (367) showed values belonging to the erosion classes. It is the longest sector under study (ca. 24 km) and most of the the dune ridges have been here replaced by greenhouses cultivation. However, the 39% (327 transects) of the shoreline maintained a stability state over time and the 18% of the data (153 transects) ranged between the accretion classes. The very high accretion peak (8,31 m/year) has been found at the easternmost edge of the sector, where the northern dike of the Scoglitti harbour was implemented in 2008 and caused high up-drift sediment deposition (Anfuso et al., 2012; Fig. 55).

SECTOR 3
Gela harbour - Scoglitti harbour
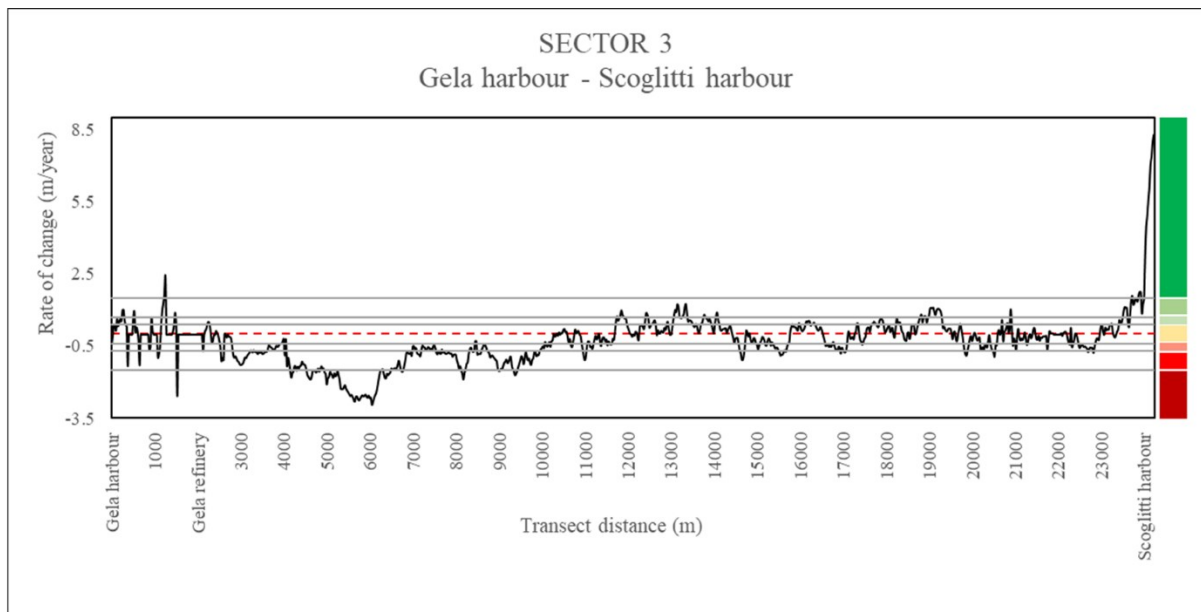
Class	N. of transect	Percentage
Very high accretion	13	2%
High accretion	56	7%
Moderate accretion	84	10%
Stability	327	39%
Moderate erosion	118	14%
High erosion	172	20%
Very high erosion	77	9%

Fig. 55 – Sector n. 3 shoreline changes over the mid-term period (1989 – 2012), it is the longest sector by length (ca. 24 km). It mainly showed a stable trend (39%), as shown the histogram chart, even though it partly faced landward movements with the highest negative WLR value of -2,93 m/year. Very high accretion (8,31 m/year) occurred up-drift the northern dike of the Scoglitti port, finished in 2008, which worked as sediment trap.

Sector n. 4 is ca. 5,5 km long between the Scoglitti harbour and the Randello promontory. More than 60% (79 transects) of the shoreline within sector n. 4 showed mainly a stable trend, but the 38% (49 transects) experienced landward migration, mainly down-drift coastal protection structures (Scoglitti breakwaters). Any significant accretion processes have been detected within this coastal strip (Fig. 56).

Fig. 56 – Sector n. 4 is southeasterly the Scoglitti port and is ca. 5,5 km long. The coastal evolution over the mid-term period (1989 – 2012) has been mainly affected by the port, any significant accretional phenomena have been detected even though 5 breakwaters have been emplaced down-drift the port. However, the stability class is the most representative (61%).

Sector n. 5 is the smallest by length and represented by the beach ca. 2 km long named Punta Braccetto. A wide dune system is here still well-preserved and has been under environmental restrictions since 1967 (Regione Siciliana, 1967). In 1996, a Site of Community Importance has been established due to its environmental value. However, this sector faced from moderate (32%, 22 transects) to high erosion (22%, 15 transects) mainly in the western part, the 44% of the shoreline experienced stability state and any significant sediment deposition occurred over the mid-term period (Fig. 57).
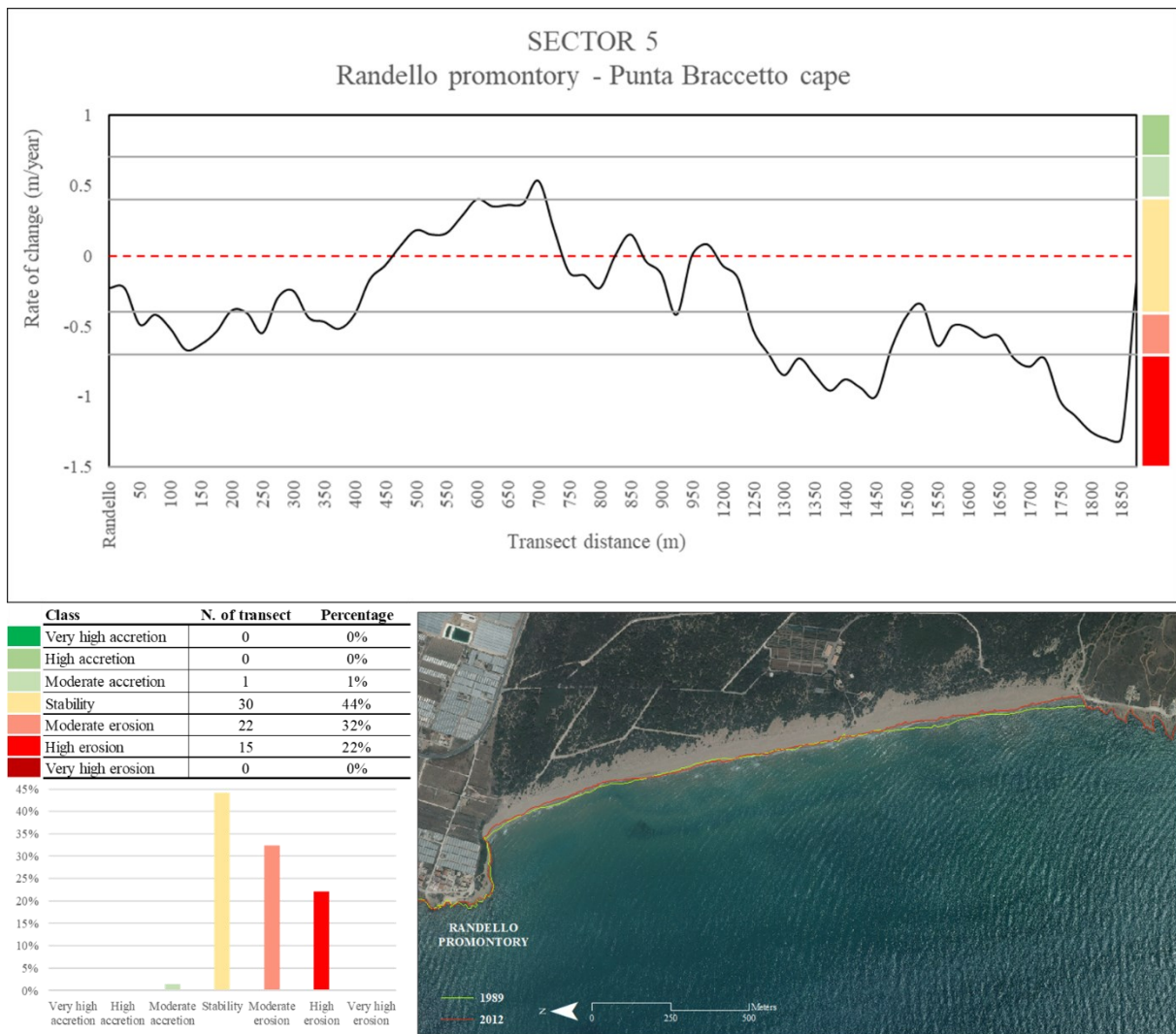
Fig. 57 – Sector n. 5 is characterized by a wide beach-dune system well-preserved over time**.** The shoreline has mainly retreated over the mid-term period (1989 – 2012), the erosion class are the most representative (54%, 37 transects) and the 44% showed a stable trend.

A long-term shoreline change analysis has been even carried out for the coastal sector n. 1 and n. 2, and for sector n. 5. The time span covered 57 years (1955 – 2012) for sectors n. 1 and n. 2, and 63 years (1955 – 2018) for n. 5. Within sector n. 1, the first 35 transects localized nearby the Licata harbour (9%) registered very high erosion level with a maximum WLR negative value of -6.,7 m/yr, and the next 1000 m experienced from moderate (2%, 7 transects) to high (6%, 22 transects) and very high accretion (7%, 28 transects), but the coast between 2,5 and 9,5 km recorded stable trend (63%, 240 transects). The Shoreline Change Envelope index revelead that most of the seaward migration detected nearby the Licata harbour occurred between 1955 and 1966 (Fig. 58).
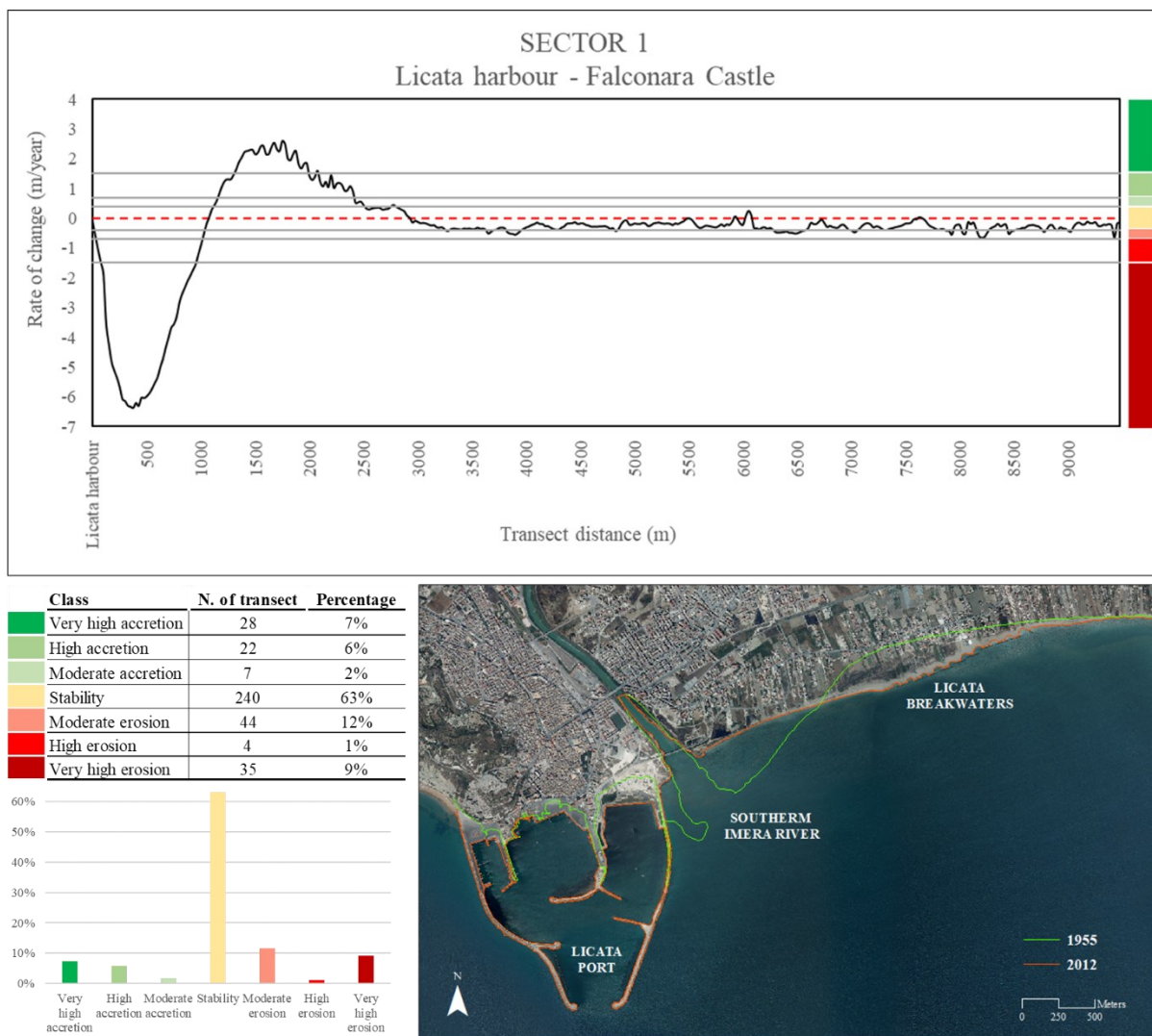
Fig. 58 – Rate of change within sector n. 1 over a long-term period (1955 – 2012). The 63% of the data falls within the stability state range, but the stable trend has been mainly detected from 3 to 10 km. The western portion of the sector (Licata port to 3 km) showed that very high erosion occurred nearby the port, the Southern Imera river mouth retreat with a rate of – 6,37 m/year, but significant sediment deposition has been recorded at 1,5 km, where 11 breakwaters have been emplaced.

Within sector n. 2, the 40% of the data (226 transects) falls within the accretion classes range, although sediment deposition mainly occurred in the eastern portion of the sector. The 30% recorded stable trend, the 14% moderate erosion and 16% high erosion (Fig. 59).
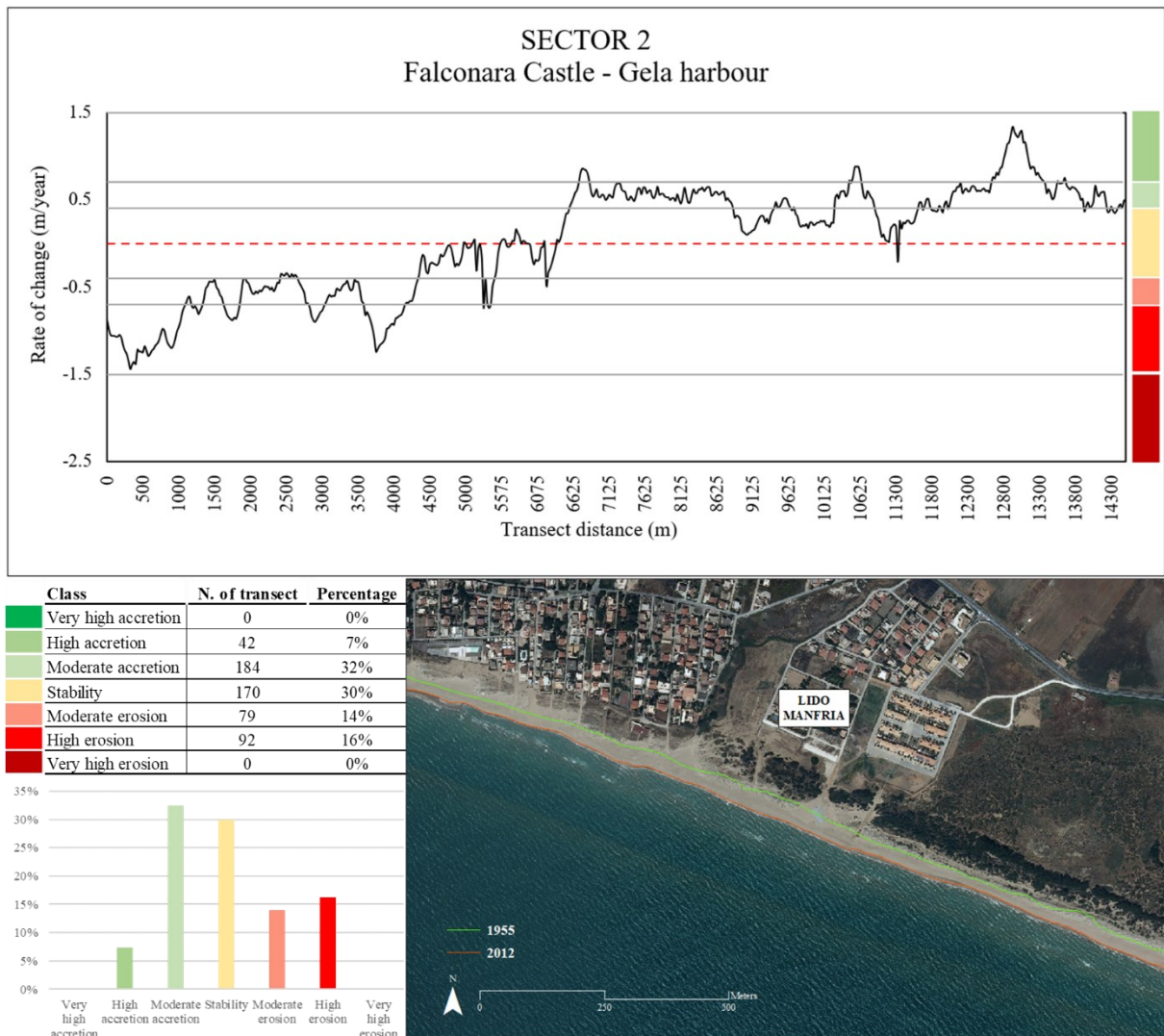
Fig. 59 – Moderate accretion (32%, 184 transects) has been mainly recorded within sector n. 2 over the long-term period (1955 – 2012), followed by stable trend (30%, 170 transects). Significant retreat occurred along the 30% of the sector.

The plot of the WLR of sector n. 5 shows mostly values ranging within the stability state class (90%, 61 transects), the remaining 10% experienced moderate accretion. Any erosion classes data have been recorded within this sector over the long-term period (Fig. 60).
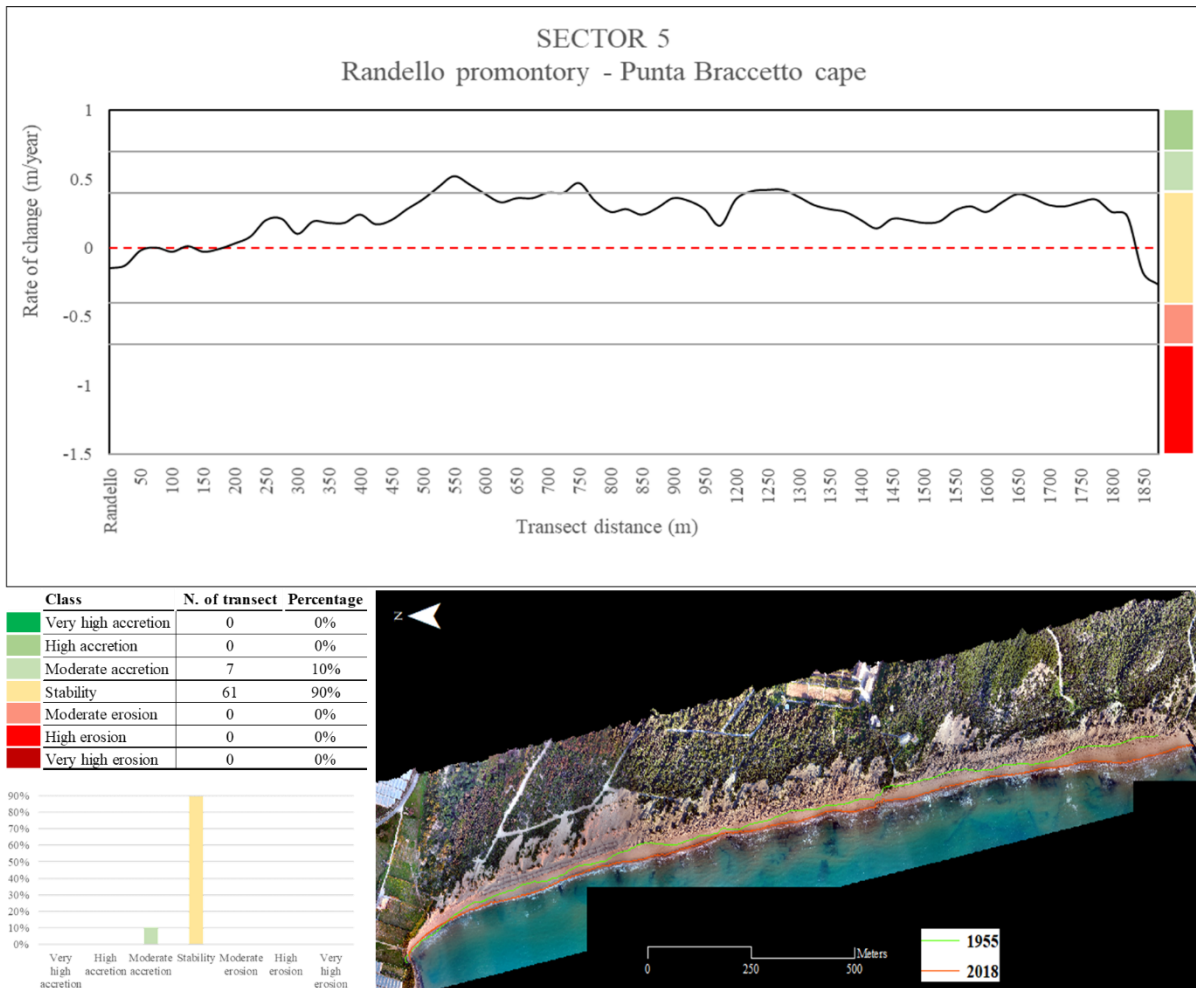
Fig. 60 – Only two classes have been registered within sector n. 5 over the long-term period (1955 – 2018). The sector experienced at 90% stability state and 10% of the data falls within the range of moderate accretion.

6.1.1 DUNE FRAGMENTATION ANALYSIS

The dune system detected in the 1955 and 1966 pictures seemed to be continuous and never stopped by artificial works. The dune fragmentation index computed for these years was obviously null. Over time, the dune system toe length along the Gulf significantly decreased and the seaward vegetation line has been repeatedly interrupted (Fig. 61). The dune system found within sector n. 5, namely known as Punta Braccetto beach, is the only one that has not been fragmented over the time between 1955 and 2012 (Fig. 62).
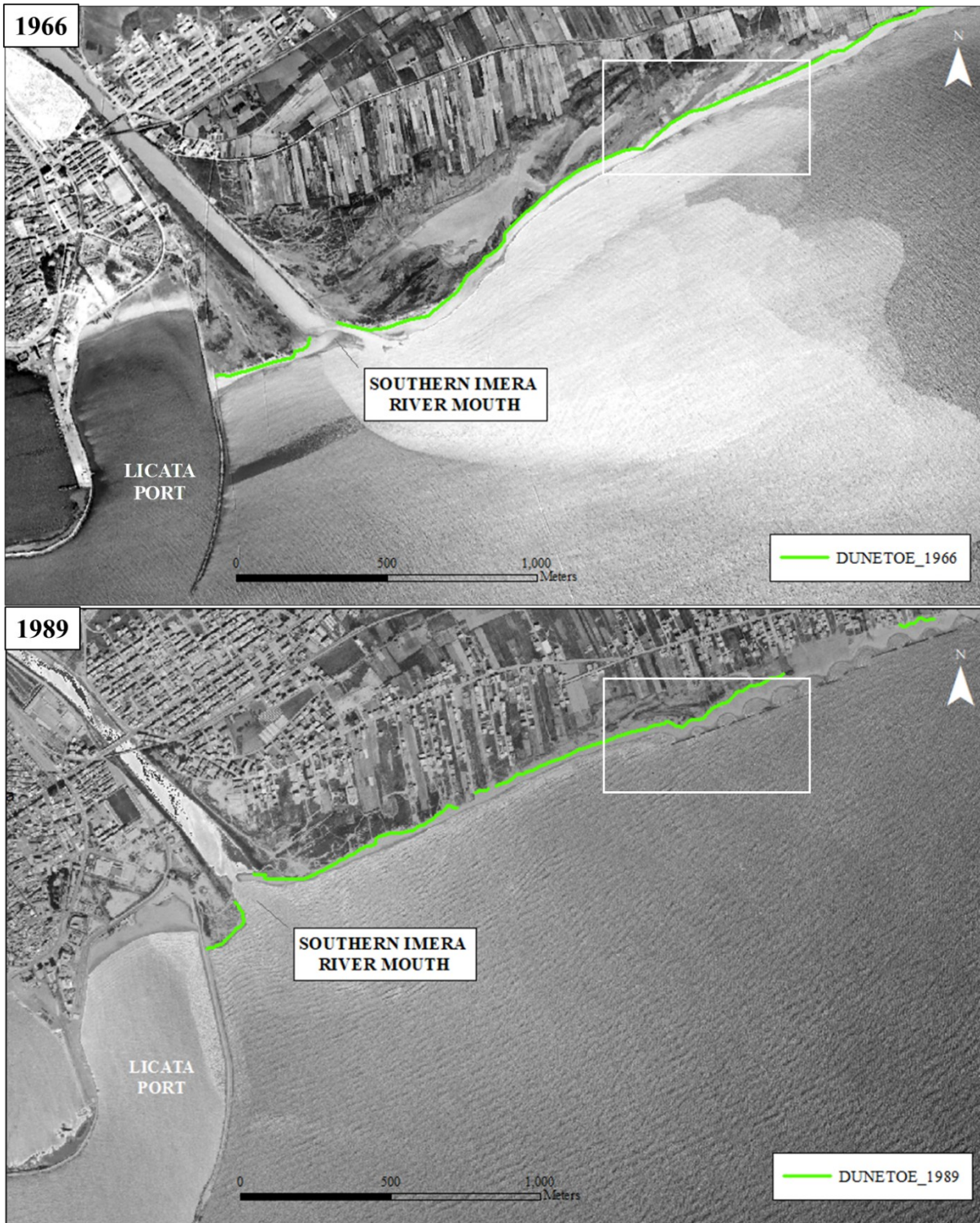
Fig. 61 – Dune toe detected nearby the Licata port on the 1966 aerial image and on the 1989 orthophoto. In 1966, the dune system is several kilometers long and only interrupted by physiographic or natural elements. In 1989, the dune ridge has been significantly retreated (white square) and partly interrupted by manmade works. Green line is the dune toe proxy.
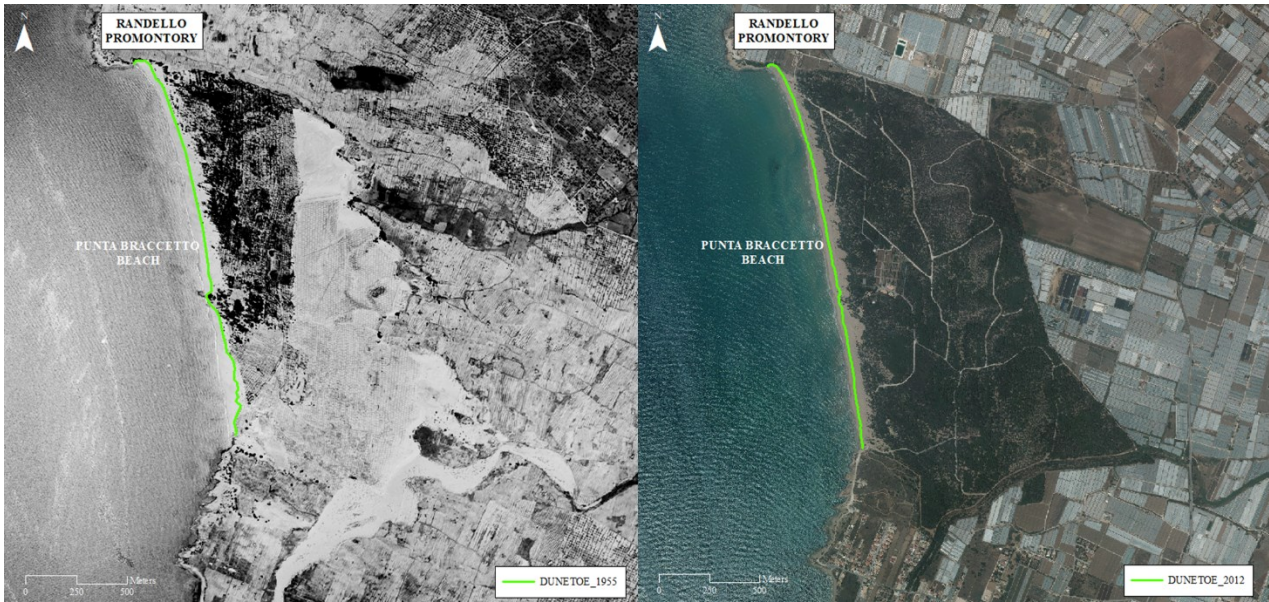
Fig. 62 -Dune system within sector n. 5. This case is the only one that did not experience any changes over the long-term period (1955 – 2012).

Over the period between 1989 and 2012, nineteenth dune systems have been detected and the dune fragmentation index has been computed for each. Only one system totally disappeared over the studied time span (dune system n. 1, F = 1 recorded in 2012, Very High/Maximum class) and only one system registered a decreased in fragmentation level (dune system n. 11, F = 0,1 in 1989, Medium class; F = 0,04 in 2012, Low class). Nine of the nineteenth systems experienced dune fragmentation increasing and eight did not recorded any changes. The highest dune fragmentation increasing occurred within sector n. 3, where the dune system set nearby the town of Gela faced severe modifications, passing from low to high class over the time between 1989 and 2012 (dune system n. 10, F = 0.02 in 1989, F = 0.21 in 2012; Fig. 63).
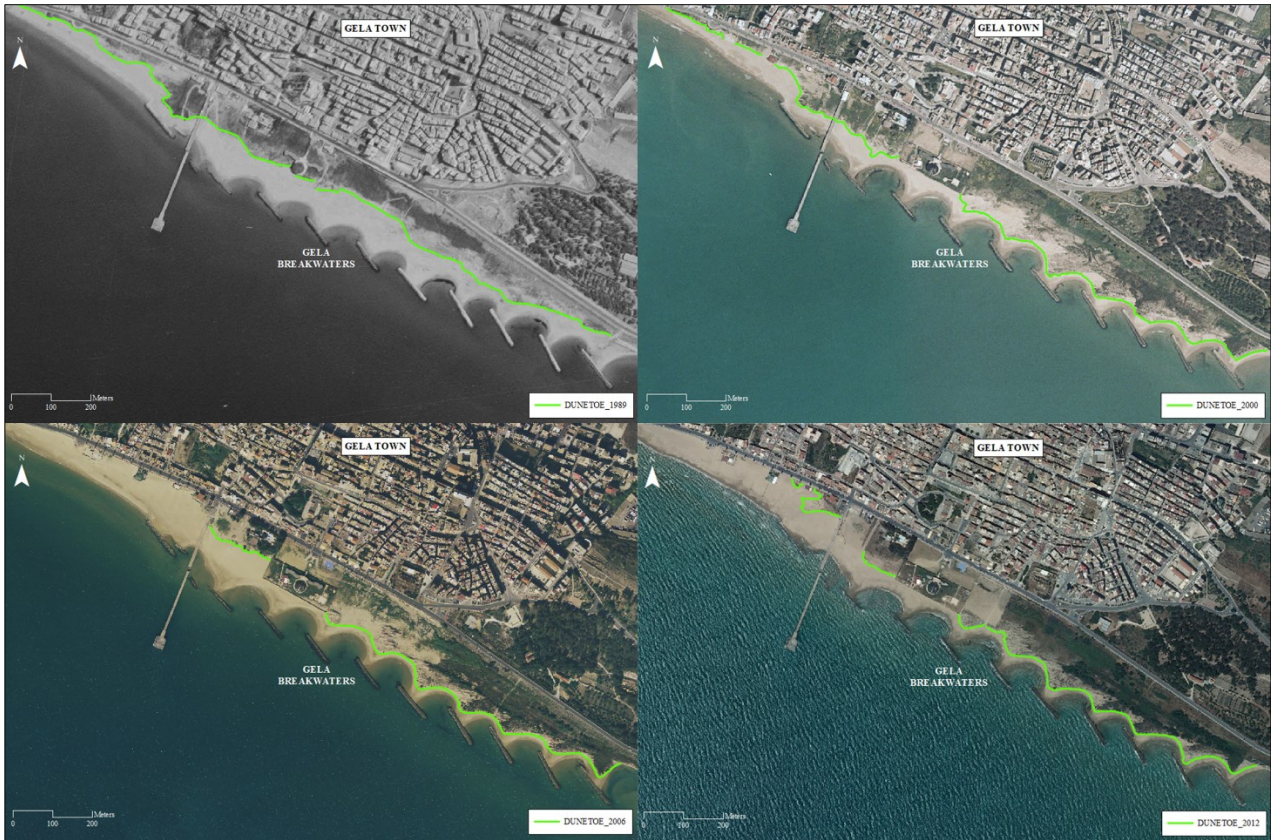
Fig. 63 - Dune toe fragmentation evolution of the dune system n. 11 found at the Gela town beach over the time 1989 – 2012. The eleven breakwaters acted as sediment trap and the dune vegetation line migrated seaward. On the other hand, westward the dock the small dune ridge has been partly damaged, and the dune vegetation significantly decreased or disappeared.

Moreover, the 46% of the dune system were not fragmented at all in 1989 and the 26% were scarsely fragmented (Low class). The tendency has changed after 2006, when the 47% of the dune system turned out to be far higher fragmented than the pass rates for previous years and the Very high/Maximum class first appeared. The medium class varied as well from 5% in 1989 to 21% in 2012 (Fig. 64).
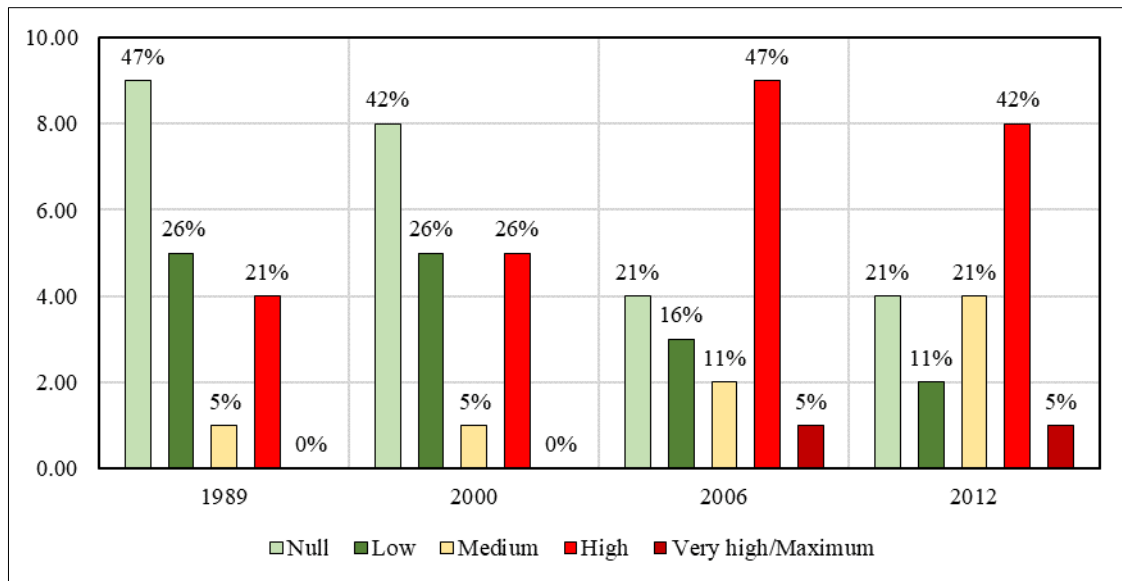
Fig. 64 – Percentage of F index classes per year. In 1989, the most frequent classes are the Null and the Low fragmatation one, Medium fragmentation class is only the 5% and the High 21%, the Very High/Maximum fragmentation class has not been found. In 2012, the tendency has changed and the higher fragmentation classes are the most represented (more than 65%) and Null and the Low one significantly decreased (34%).

6.1.2 COASTAL ARMOURING ANALYSIS

The *coefficient of technogenous impact* (K) was computed to assess the maritime structures impact on the shoreline evolution. This coefficient represents the ratio between the total length of all maritime hydraulic structures (groins, moles, seawalls, dikes, navigational channells and permeable bridges) and total coastal length of the study area (Aybulatov & Artyukhin, 1993). The coefficient can range from 0 to more than 1, and the human impact can be considered as minimal when K = 0 – 0.1; averaged when K = 0.11 – 0.5; maximal at K = 0.51 – 1 and extreme if K > 1.

Table 9 shows the *coefficient of technogenous impact* (K), the total coastal length (L) per year and the total length of maritime structures (l) per year. Over the fifties and sixties, the three harbours nowadays insisting on the coast (Licata, Gela, Scoglitti) were the only maritime infrastructures. The K value has not been computed for sector n. 3 and 4 for the year 1955 and 1966, because of the lack of aerial images for those year. The K value computed for sector n. 1 did not appreciably vary over these years and falls within the maximal range values (0.5 – 0.8). Any coastal structures have been detected in 1955 and 1966 within sector n. 2 and n. 5, thus the K value is 0. Between 1966 and 1989, the total structures length significantly increased, due to the progressive Licata harbour implementation and for breakwaters that have been built eastward the Licata harbour, two were emplaced up-drif and eleven of them down-drift the Gela harbour, and the down-drift the Scoglitti harbour in order to block the strong retreatments occurred over the seventies at

the Gela town beach and six breakwaters are set down-drift the Scoglitti harbour. In 1989, the K value of sector n. 1 resulted to be significantly higher (1.2) reaching the range of extreme class. Sector n. 2 did not register any changes, as sector n. 5. The impact of coastal armouring both within sector n. 3 and n. 4 resulted to be average. Over the time 2000 – 2012, the coefficient K slightly increased within sector n. 1, varying from 1.3 to 1.5 (extreme class); sector n. 2, n. 3 and n. 5 did not change their armouring class (minimal for sector n. 2 and n. 5, average for sector n. 3), the K value of sector n. 4 registered an increase, passing from average to maximal impact (from 0.5 to 0.8 computed for 1989 and 2012 respectively) and the total structures length has seen a 112% increase over the 1955. It should be noticed that the harbours represent most of the maritime structure length over the entire time span, last works have been carried out in 1997 for the Licata harbour and in 2008 for the Scoglitti one.

Year	Sector	Total coastal length (L)	Total structures length (l)	K
1955	1	9825.6	7706.1	0.8
	2	16649.6	0.0	0.0
	3	-	-	-
	4	-	-	-
	5	1898.5	0.0	0.0
1966	1	10134.1	8443.2	0.8
	2	16687.1	0.0	0.0
	3	-	-	-
	4	-	-	-
	5	1898.5	0.0	0.0
1989	1	10215.7	11969.0	1.2
	2	16804.1	388.3	0.0
	3	24112.3	12217.7	0.5
	4	6424.0	3486.0	0.5
	5	1898.5	0.0	0.0
2000	1	10198.4	13639.8	1.3
	2	16810.5	467.0	0.0
	3	26134.1	12310.7	0.5
	4	6181.8	4458.3	0.7
	5	1898.5	0.0	0.0
2006	1	9727.2	13918.2	1.4
	2	16808.5	388.3	0.0
	3	24600.0	13172.2	0.5
	4	6236.3	4458.3	0.7
	5	1974.9	0.0	0.0
2012	1	9732.5	15013.6	1.5
	2	16759.3	388.3	0.0
	3	25017.8	13172.2	0.5
	4	6308.9	5181.5	0.8
	5	1937.3	0.0	0.0

Table 9 – The coefficient of technigenous impact K computed for each sector per year. The Total Coastal Length (L) and the Total Structures Length (l) per year are shown. The coefficient can be expressed by qualitative classes as minimal when K = 0 – 0.1; averaged when K = 0.11 – 0.5; maximal at K = 0.51 – 1 and extreme if K > 1. All measures are expressed in *meter* (m).

One hundred and forty samples have been performed within the coastal sub-cell n. 4.2. Four transects were located within sector n. 1 nearby the Falconara castle (F), three ones easterly the Manfria Tower (M) within the sector n.2 and one was sampled along the Punta Braccetto beach (PB) within sector n. 5. Some morphological beach features were sometimes absent or not easily recognizable. The average value of each statistical parameter for every transect group has been computed. Table 10 summarizes the results obtained for 2017. Data were divided on the base of the season the samples have been collected. In summer-time, the average grain size *(Mz)* falls within the range of medium sand for all samples (minimum = 1.25 in foreshore Manfria group sample; maximum = 1.90 in dune Manfria group sample); even though higher values have been observed in Manfria Tower samples. *Sorting (s)* emerged well sorted to moderately well sorted, with a minimum of 0.36 recorded in dune sample of Manfria Tower group and maximum of 0.66 registered in foreshore sample within Manfria Tower area. *Skewness (Sk)* values having nearly symmetrical to fine skewed (-0.06 observed in Manfria Tower foreshore sample to 0.11 obtained for storm berm Falconara sample). *Kurtosis (Kg)* values depicted mesokurtic to leptokurtic curve, minimum (0.95) observed in Manfria foreshore sample, maximum (1.17) found in storm berm sample in Manfria. During winter-time, the *Mean (Mz)* falls within medium sand range in all survey sites. In Falconara castle site, sediments were well sorted to moderately well sorted, while they ranged from very well sorted to well sorted in Manfria site. *Kurtosis (Kg)* ranged from mesokurtic (0.98) to leptokurtic (1.35).

SITE	STATISTICS	SUMMER				WINTER			
		Foreshore	Storm berm	Tide berm	Dune	Foreshore	Storm berm	Tide berm	Dune
F	*Mean (Mz)*	1.37	1.48	1.38	-	0.95	1.48	-	-
	Sorting (s)	0.40	0.43	0.42	-	0.59	0.43	-	-
	Skewness (Sk)	0.05	0.11	0.08	-	0.19	0.16	-	-
	Kurtosis (Kg)	1.14	1.01	1.18	-	1.35	1.04	-	-
M	*Mean (Mz)*	1.25	1.80	1.63	1.90	1.30	1.46	-	1.83
	Sorting (s)	0.66	0.39	0.38	0.36	0.36	0.42	-	0.33
	Skewness (Sk)	-0.06	0.02	0.05	0.12	0.11	0.14	-	0.16
	Kurtosis (Kg)	0.95	1.17	1.11	0.94	1.07	0.98	-	1.03

Table 10 – Statistical parameters of the 2017 summer and winter surveys. F means Falconara castle transect group, M means Manfria Tower transect group.

In Table 11, summer and winter 2018 results were summed up. In summer, no significant mean size changes have been registered, sediment samples were classified as belonging to medium sand range (minimum = 1.43, in Falconara foreshore; maximum = 1.82, in Manfria dune). Both transect groups values conquered that moderately well sorted to well sorted. The negative skewness values indicate coarse-skewed

material, whereas the positive value (0.02, storm berm of Falconara group) represented more material in fine skewed. *Kurtosis (Kg)* occurred from mesokurtic to leptokurtic, with a minimum value of 0.97 and a maximum value of 1.25. In winter 2018, mean size indicated medium sand sediments, most of the samples emerged as well sorted, except for the foreshore sample of Falconara, which was moderately well sorted (0.51). *Skewness (Sk)* is nearly symmetrical and *Kurtosis (Kg)* values described mesokurtic to leptokurtic curve.

SITE	STATISTICS	SUMMER				WINTER			
		Foreshore	Storm berm	Tide berm	Dune	Foreshore	Storm berm	Tide berm	Dune
F	Mean (Mz)	1.43	1.60	1.63	-	1.35	1.64	-	-
	Sorting (s)	0.57	0.42	0.45	-	0.51	0.40	-	-
	Skewness (Sk)	-0.11	0.02	-0.05	-	-0.08	0.02	-	-
	Kurtosis (Kg)	1.05	0.97	1.13	-	1.17	1.20	-	-
M	Mean (Mz)	1.50	1.51	1.73	1.82	1.51	1.69	-	1.76
	Sorting (s)	0.56	0.43	0.48	0.39	0.46	0.44	-	0.44
	Skewness (Sk)	-0.19	-0.03	-0.04	-0.01	0.07	0.02	-	0.00
	Kurtosis (Kg)	1.25	1.05	1.09	1.03	1.02	1.08	-	1.19

Table 11 - Statistical parameters of the 2018 summer and winter surveys. F means Falconara castle transect group, M means Manfria Tower transect group.

In 2019, surveys could be performed only over winter-time (Table 12). *Mean (Mz)* values indicated medium sand sediments and *Sorting (s)* varied from well sorted to moderately well sorted. Samples showed a symmetrical curve and range from mesokurtic to leptokurtic.

SITE	STATISTICS	WINTER			
		Foreshore	Storm berm	Tide berm	Dune
F	Mean (Mz)	1.01	1.43	-	-
	Sorting (s)	0.54	0.42	-	-
	Skewness (Sk)	-0.02	0.08	-	-
	Kurtosis (Kg)	1.05	1.07	-	-
M	Mean (Mz)	1.34	1.61	-	1.75
	Sorting (s)	0.48	0.46	-	0.43
	Skewness (Sk)	0.04	-0.02	-	-0.02
	Kurtosis (Kg)	1.06	1.06	-	1.17

Table 12 - Statistical parameters of the 2019 summer and winter surveys. F means Falconara castle transect group, M means Manfria Tower transect group.

Within sector n. 5, medium (1.89) to fine sand values have been recorded in summer 2017; samples appeared mainly well sorted and moderately well sorted in the tide berm site. The curve showed coarse (-0.25, tide berm) to fine skewed trends, with maximum value of 0.12. *Kurtosis (Kg)* intervals fluctuated from mesokurtic (0.96) to leptokurtic (1.28). Over winter-time, the sediments mean size ranged between medium (1.98, foreshore) and fine sand. *Sorting (s)* emerged very well sorted (0.25 to 0.33) and sediments consist essentially of positive skewness. *Kurtosis (Kg)* varied from mesokurtic with a minimum value of 1.10

registered in dune sample to leptokurtic with a maximum of 1.32 observed in storm berm samples (Table 13).

SITE	STATISTICS	SUMMER				WINTER			
		Foreshore	Storm berm	Tide berm	Dune	Foreshore	Storm berm	Tide berm	Dune
PB	*Mean (Mz)*	1.89	2.10	2.01	2.17	1.98	2.24	-	2.30
	Sorting (s)	0.37	0.38	0.52	0.36	0.31	0.33	-	0.25
	Skewness (Sk)	0.12	-0.02	-0.25	-0.09	0.13	0.05	-	0.16
	Kurtosis (Kg)	1.11	0.96	1.11	1.28	1.27	1.32	-	1.10

Table 13 - Statistical parameters of the 2017 summer and winter surveys. PB states for Punta Braccetto beach.

Results of 2018 surveys are shown in Table 14. In summer, the average *Mean (Mz)* went from medium to fine sand values, *Sorting (s)* indicated very well sorted (0.30) to moderately sorted (0.75) sediment. Negative skewness has been detected and mesokurtic to leptokurtic curve have been depicted. Winter samples seemed to be made of finer sediment than summer ones, mainly well sorted and nearly symmetrical. The curve resulted to be positive skewed. *Kurtosis (Kg)* was platykurtic (0.85, foreshore) to leptokurtic (1.36, storm berm).

SITE	STATISTICS	SUMMER				WINTER			
		Foreshore	Storm berm	Tide berm	Dune	Foreshore	Storm berm	Tide berm	Dune
PB	*Mean (Mz)*	1.76	2.04	1.99	2.23	2.03	2.15	-	2.25
	Sorting (s)	0.75	0.44	0.51	0.30	0.41	0.35	-	0.24
	Skewness (Sk)	-0.24	-0.09	-0.23	-0.02	0.06	0.03	-	0.10
	Kurtosis (Kg)	0.94	1.02	1.08	1.36	0.85	1.36	-	1.13

Table 14 - Statistical parameters of the 2018 summer and winter surveys. PB states for Punta Braccetto beach.

Winter samples performed over 2019 have been characterized as ranging from medium to fine sand. Well sorted sediments were predominant, along tide and storm berm and foreshore samples symmetrical curve emerged and fine skewed only in dune sample. *Kurtosis (Kg)* values depicted mesokurtic to leptokurtic curves (Table 15).

SITE	STATISTICS	WINTER			
		Foreshore	Storm berm	Tide berm	Dune
PB	*Mean (Mz)*	1.94	2.30	-	2.30
	Sorting (s)	0.35	0.35	-	0.24
	Skewness (Sk)	0.10	0.06	-	0.19
	Kurtosis (Kg)	1.13	1.36	-	1.13

Table 15 - Statistical parameters of the 2019 summer and winter surveys. PB states for Punta Braccetto beach.

7   DISCUSSION

7.1   SHORELINE AND ENVIRONMENTAL CHANGES OF THE COAST OF THE GULF OF GELA

The coastline under analysis has been split into 5 sectors and coastal structures and main promontories have been chosen to be their edge limits. The shoreline change analysis has been performed using aerial photographs (1955, 1966), orthophotographs (1989, 2000, 2006 and 2012) and Unmanned Aerial Vehicle (UAV) image (2018) and the rates-of-change have been elaborated for each sector. The results showed that the coastal sub-cell mainly faced erosional phenomena over the mid-term period (1989 – 2012), even though different behaviour have been detected within the 5 sectors. The maximum negative WLR value has been recorded within sector n. 1 nearby the Licata harbour (-3,15 m/year). This sector experienced severe landward migration (56% of data falls into the erosion classes range), on the other hand, the total accretion classes percentage was recorded at the Licata breakwaters shoreline. The dune fragmentation analysis showed that the highest fragmentation occurred within the coastal sector n. 1, even though it is not the biggest one by length and only two dune systems have been here identified. The Licata harbour and eleven breakwaters insist on the coast of the sector and the coefficient of technogenous impact ranges between maximal to extreme classes impact (Fig. 65).
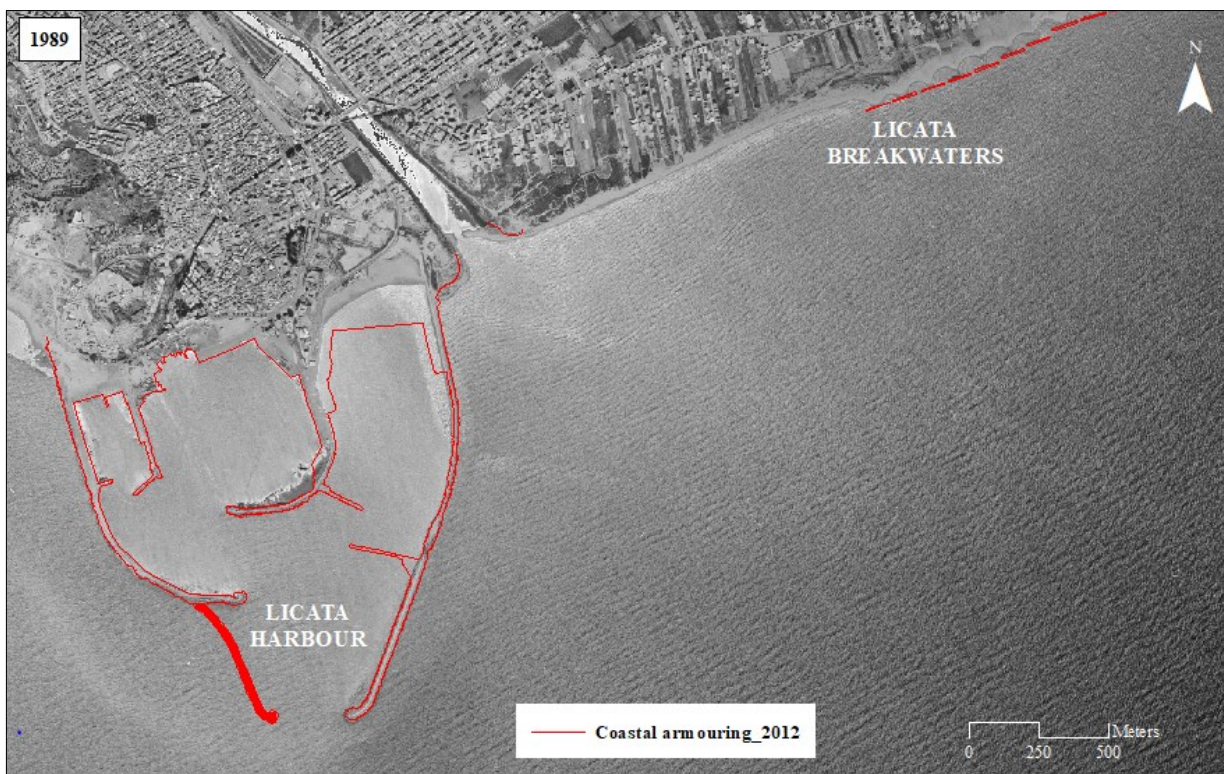
Fig. 65 – The Licata harbour and the eleven breakwaters set easterly the Southern Imera river mouth. The red line is the coastal armouring line detected for the year 2012, the western dike of the harbour has been finished in 1997 and not visible in the 1989 orthophoto.

128

The long-term period analysis confirmed that the area nearby the Licata harbour registered the most significant shoreline changes, where the first 35 transects (9%) registered very high erosion level with a maximum WLR negative value of -6,7 m/year, and the next 1000 m recorded seaward movement (15%). In line with the insights of Brambati et al. (1992) and Amore et al. (2002), the western part of sector n. 1, corresponding to the coastal strip between the Licata harbour and the Licata breakwaters, where the Southern Imera river flows, can be identified as an area of critical concern. The river mouth has significantly retreated as most of the coastal tract easterly the port, where some buildings have been compromised by the intense landward movement (Fig. 66).

Fig. 66 – The area easterly the Southern Imera river mouth faced severe coastal erosion, holidays houses were compromised and partly submerged by sea water, as shown by the white squares that framed a house partly swallowed up by the sea.

The Shoreline Change Envelope index revealed that high accretion occurred between 1955 and 1966, but shoreline began retreating after 1966 (Fig. 67). On one hand, these results might suggest that the sediment river load significantly decreased over next decades, the artificial reservoirs built (Villarosa, Olivo, Gibbesi) over the decade 1960-70 blocked the Southern Imera river course to satisfy the huge increase in irrigation water demands, formed sediment traps and reduce peak floodflows, thereby decreasing the sediment supply to the coast; on the other hand, the landward migration could be also imputed to the expansion of the eastern dike and of the western quay of the Licata harbour that have been built over the

129

seventies and ended in the eighties. This kind of work generally (i) modifiy the amount of wave energy being dissipated by the beach material, resulting in an increase in the rate of sediment loss, and (ii) impound littoral material, interrupting the longshore sediment transport (Griggs, 2005; Dugan et al., 2011; Molina et al., 2019).
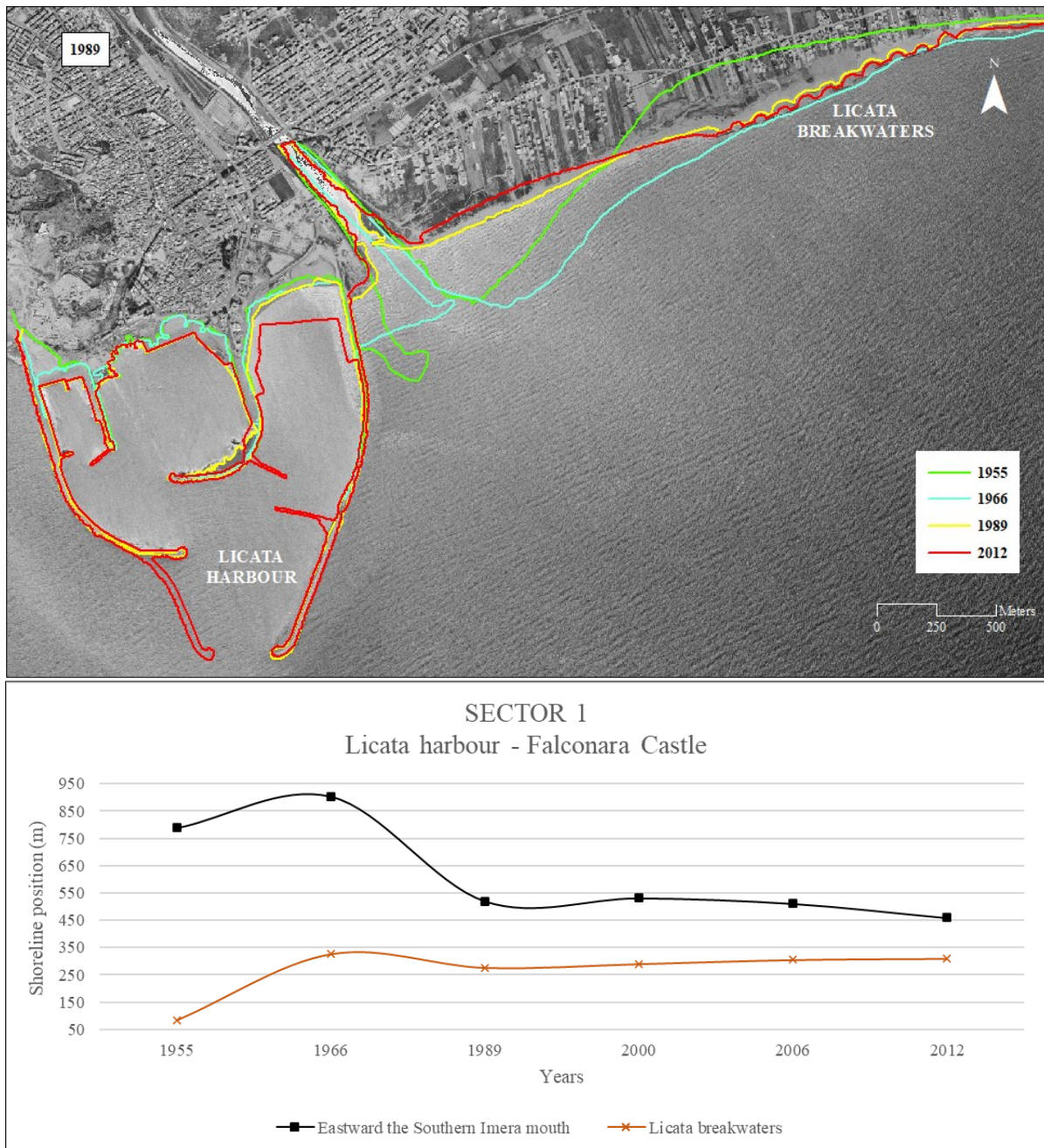
Fig. 67 – The shoreline evolution of the Southern Imera river mouth and the area easterly the mouth. The trend seemed to be positive between 1955 and 2012, but the Shoreline Change Envelope and the shoreline change position chart revealed that significant accretion has been recorded between 1955 and 1966, and very high erosion has been registered between 1966 and 1989. The green line is the 1955 shoreline, the blue line is the 1966 one, the yellow line is the 1989 one and the red line is the 2012 shoreline. Thus, landward movements occurred between 1966 and 1989 just nearby the Southern Imera river mouth, but shoreline has been accreting between 1989 and 2012 where breakwaters have been emplaced, as shown by the shoreline change position chart.

The coastal sectors from n. 2 to 5 mainly showed stable trend, but the data distribution appeared negative skewed though. Very high erosion class has been recorded within sector n. 2 and n. 3 (5% and 9% of the data, respectively), generally detected down-drift coastal works (ports, breakwaters); on the other hand, the highest WLR value (8,31 m/year) has been found up-drift the Scoglitti harbour, where last implementation works have been finished in 2008. The shoreline change analysis over both mid- and long-term period outlined same behaviour within sector n.2, (i) the western part mainly faced erosional phenomena, as well-documented by Martino et al. (2011); (ii) the eastern part experienced stability state or moderate accretion (up to 1,4 m/year). The exposed rocks of the headlands and the wide dune ridge of Manfria (Site of Community Importance ITA 050011 – Manfria Tower) set within the eastern portion of sector n. 2 probably protected the coastline, providing sediment reservoirs to the shore; and acting as barriers to prevent waves and high water from moving inland. The dune fragmentation index resulted to be here null and very low in 1989, but it turned into medium-high classes in 2012. Only two coastal breakwaters have been detected within sector n. 2, which have emplaced up-drift the Gela harbour to enhance the sediment deposition processes.

Sector n. 3 is the longest one that has been analysed. It is ca. 24 km long and a narrow but long dune ridge has been here found. Nearby the Gela refinery, significant landward migration has been detected and the dune fragmentation index saw an increase from low-medium classes to medium-high ones (Fig. 68). The coefficient of technogenous impact did not register noticeable variations; however, this sector has been strongly modified by human actions and the long and wide dune ridge has been replaced by greenhouses.

Fig. 68 – Significant shoreline and seafront dune ridge retreating between 1989 and 2012 are shown; within the two white squares manmade structures are framed, in 1989 they were on land, in 2012 they have been progressively swallowed up by the sea. Moreover, greenhouses and crop cultivations damage or destroyed the dune system whose fragmentation constantly increased over time.

Within sector n. 4 any dune system has been found, except for a residual dune ridge damaged and blocked by the provincial road 102, which could not be considered (Fig. 69). The second highest coefficient of techonogenous impact has been here found. The coast seemed to be stable over the mid-term period, even though erosion has been recorded down-drift the harbour.

Fig. 69 – Within sector n. 4 any seaward dune ridge has been detected, even though a residual dune system can be found southerly the Scoglitti town, but its seafront is limited by the provincial road n. 102.

Over the long-term period (1955 – 2018), sector n. 5 did not face any retreating phenomena and showed low accretion level and high stability state (90% of the data), but over the medium time span (1989 – 2018) this sector faced from moderate (32%, 22 transects) to high erosion (22%, 15 transects) and only the 44% of the shoreline experienced stability state and any significant sediment deposition has been observed. The Shoreline Change Envelope index confirmed this insight, revealing that accretion mainly occurred between 1955 and 1989, and landward migration has been registered later than 2000. Any changes of the seaward vegetation line have been recorded and the coefficient of technogenous impact was not computed because any coastal structure have been found within this coastal sector (Fig. 70). The Life Leopoldia project has been here carrying on between 2012 and 2016 to restore the dune habitats, putting in place short length fence, placed perpendicular to the shoreline to increase trapping aeolian sediment rates. Despite this works and the existence of a well-preserved wide dune system protected since 1967, the shoreline of sector n. 5 showed slightly landward movements over the mid-term period. It could be probably assumed that the Scoglitti harbour reduced the sediment load by the longshore drift, causing huge updrift accretion and significant downdrift retreatments (Anfuso et al., 2012).
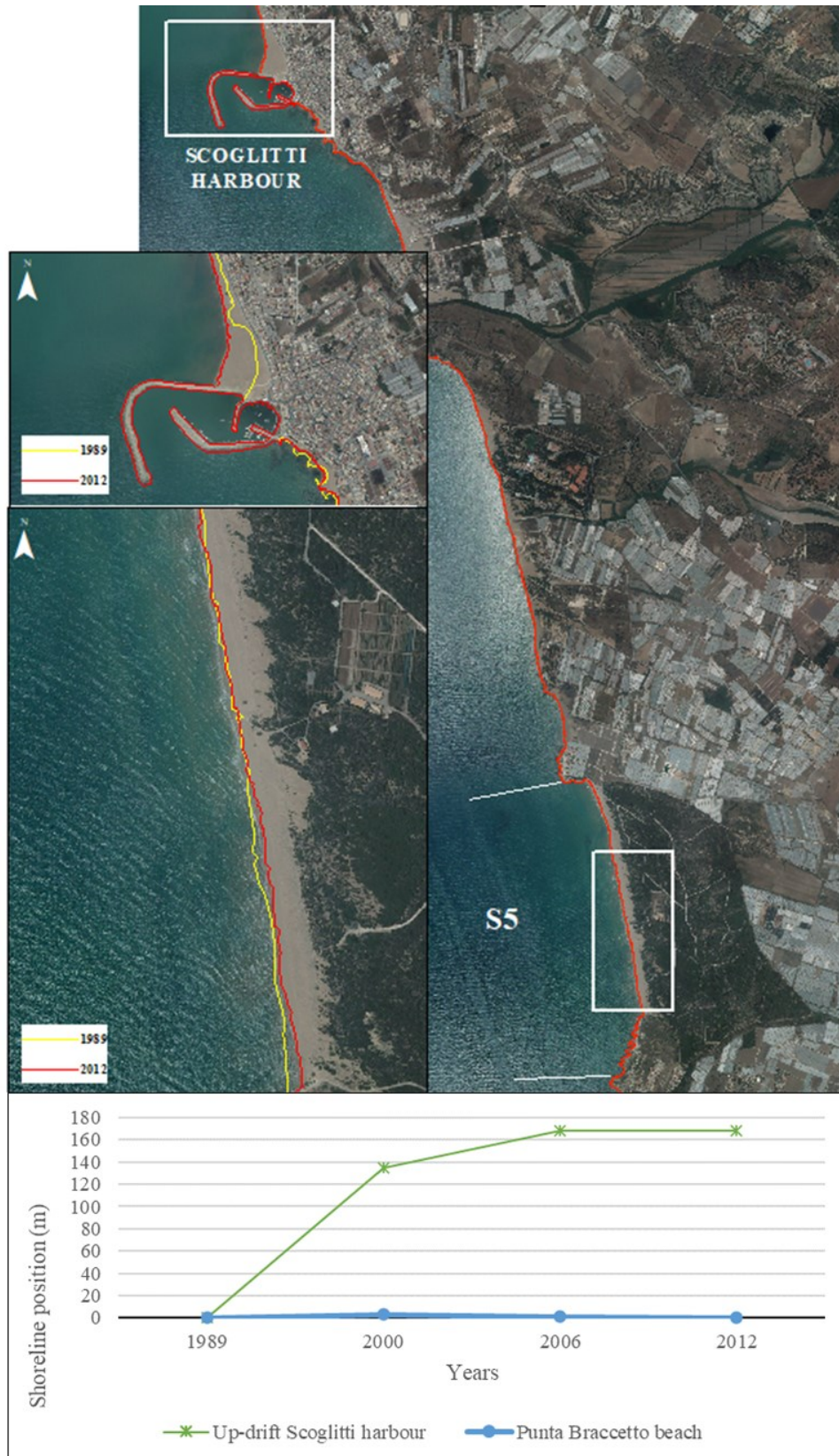
Fig. 70 – Sector n. 5 experienced mainly stability state and moderate accretion over the long-term period, but any accretion or erosion tendency has been observed between 1989 and 2012. The Scoglitti harbour is set within sector n. 4, ca. 6 km northern sector n. 5 and the northern dike has been first implemented in 1987 and finished in 2008. High accretion rate has been recorded up-drift the harbour that probably trapped sediment by the longshore drift and changing the shoreline dynamic within sector n. 5. The below chart showed the significant accretion registered up-drift the northern dike of the Scoglitti harbour and any accretion within Punta Braccetto beach.

7.2   INSIGHTS FROM GRAIN-SIZE AND TEXTURAL ANALYSIS

The grain-size analysis has been performed in summer- and winter-time over 2017 and 2018, but in winter over 2019. Sediments were collected where the main beach features (foreshore, dune and storm berm and tide berm) can visibly recognizable. Thus, the four moments of the grain-size distribution curve (*Mean grain size*, *standard deviation*, *skewness* and *kurtosis)* were computed for each sample (Folk & Ward, 1957; Friedman, 1961).

All samples performed along the transects within the Falconara and Manfria transects fell within the range of medium sands. Moreover, it should be noted that (i) summer foreshore samples were generally moderately well sorted and the curve resulted to be mainly negative skewed; winter Falconara foreshore samples were all moderately well sorted, whereas Manfria foreshore samples are all well sorted; most of the winter foreshore samples showed a symmetrical curve; (ii) both summer and winter bermlines samples resulted to be all well sorted and s*kewness* (Sk) was generally nearly symmetrical; (iii) dune sediments were well sorted, even though most of them seemed to reach the limit between the well sorted and very well sorted classes; positively skewed samples have been found along Manfria transects in 2017 over summer and winter time, but it turned to symmetrical tendency in 2018 and 2019.

Slightly sedimentological differences have been traced between Falconara and Manfria survey sites over summer and winter time. Falconara foreshore samples resulted to be all moderately well sorted and negatively skewed, Manfria ones were better sorted in winter than in summer with symmetrical sorting; all bermlines samples showed same characteristics, they were all well sorted and symmetrical. Any dune samples have been collected along Falconara transects, because the dune ridge has been totally replaced by summer holidays homes (Fig. 71). Positive skewness and high well sorting have been found in Manfria dune samples in 2017 and symmetrical curve emerged in 2018 and 2019. Dune samples generally appeared better sorted and positively skewed while beach sands are mostly negatively skewed; negative skewness and coarser sediments can be related to the intensity and duration of high energy environment that tend to easily disperse fine material (Folk & Ward, 1957; Mason & Folk, 1958; Friedman, 1961). If those fine sediments are not replaced by longshore sediment supply, the shoreline starts to move landward (Friedman, 1961; Dal Cin, 1969). The picture depicted for Falconara sites roughly corresponds with the model of an eroding beach (negative skewness and moderately well sorting), Manfria beach morphology emerged to be modelled by

less intensive phenomena, with (i) foreshore samples showing better sorting and more positive skewness than Falconara beach and (ii) dune samples having curves that are fine-skewed and sediments well sorted.

What has been said so far fits with the data obtained by the grain-size analysis of Martino et al. (2011), which observed that most of the bermline and foreshore samples of Desusino survey site (Butera municipality, CL) had mean values ranging from medium to coarse sand, and standard deviation indicating well sorted particles.

Fig. 71 – Both images show summer holidays houses in Falconara castle sites, built right next to the beach modifying the beach morphology and reducing or destroying the dune ridge.

The grain-size analysis performed along the transect within sector n.5 showed that (i) foreshore samples belonged all to the medium sand range, except for 2018 winter sample that belonged to the fine sands class, samples were generally positively skewed, but the 2018 sample resulted to be slightly negative skewed; (ii) in bermline samples, fine sands with moderately well sorted and well sorted sediments have been found, summer samples appeared coarse-skewed, whereas winter samples were nearly symmetrical; (iii) dune samples were made of fine sand with very well sorted sediments and mainly fine skewed curve.

8 CONCLUSION

Coastal areas are the most productive and valued ecosystem on Earth. They are subject to changes that vary greatly in geographic scale, timing and duration and that combine to create dynamic and biologically productive coastal systems vulnerable to additional pressures resulting from human activities. It's becoming increasingly important for councils and governments to start managing coastlines in order to protect them from increasing coastal erosion and flooding, thus large-scale studies on shoreline evolution became key issue for Nation governments to identify the scope of the problems and the areas of critical concern (Stauble, 2003).

The Southern coast of Sicily (Italy) plays a key role in the economic strategies of the regional management. The area includes such long and wide sandy beaches that enhanced the development of leisure activities and infrastructures; greenhouse-crop systems are here quite widespread thanks to mild weather conditions, on the coast of Gela town stands one of the largest petrol-chemical poles in Europe that has been recently converted in biorefinery (Gela refinery; Fig. 22), and some of the coastal regional strategic infrastructures insist on this wide coastal sector.

The Southern coast of Sicily is identified as a coastal sub-cell of I-order by the Regional Plain against Coastal Erosion (Regione Siciliana, 2020). This cell has been split into II and III-order sub-cells and the coastal sub-cell n. 4.2 has been studied in this work due to its peculiar characteristics. The Southern Imera river basin is the second largest drainage basin by size in Sicily and severe modifications of the river mouth have been observed (Amore & Randazzo, 2002). Most of the strategic economic activities above mentioned are here set, but significant well-documented coastal erosional phenomena have threatening holiday houses or human works (Brambati et al., 1992; Amore & Randazzo, 2002; Martino et al., 2011; Anfuso et al., 2012). However, previous studies focused only on parts of the sub-cell and not on the entire coastal length and most of them used a single methodology. The present work aim was to study main coastal changes of the Gulf of Gela using for the first time a modern and combined methodology, thus the shoreline evolution of the sub-cell n. 4.2 over mid- and long-term period has been investigated, both computing statistical indexes thanks to the ESRI ArcGIS© Digital Shoreline Analysis System, and examining the local environmental changes, as the progressive damage of the dune ridges and the increasing impact of coastal armouring.

A negative coastline evolution trend has been mainly found within the Gulf of Gela. The shoreline change analysis showed that sector n. 1, between the Licata harbour and the Falconara Castle, has experienced the most significant variations. Significant erosion phenomena have been detected nearby the Licata harbour, at the western edge of the sector, where the Southern Imera river mouth has profoundly changed, retreating up to hundreds of meters. Eastward the river mouth, such shoreline accretion has been observed both over long- and mid-term period, but the Shoreline Change Envelope index revealed that the main seaward movements occurred over the decade 1955 – 1966, and landward migration started after 1966 and has gone on till 2012. However, the eleven breakwaters set at 1 km eastward the river mouth stopped the erosion phenomena and slight accretion has been here recorded between 1989 and 2012. The Licata harbour has been implemented several times and the coefficient of technogenous impact (K) increased of 19% over 1989 and 2012, varying from the maximal to the extreme class, due to the works to extend the western dike of the Licata harbour. The dune fragmentation has increased as well, the continuous dune ridge detected in 1955 has been progressively damaged by manmade works and the F index changed from null fragmentation class to the high one. Stable trend has been registered within the eastern portion of sector n. 1 over mid- and long-term period. These findings demonstrates that the huge retreats registered within the western part of sector n. 1 could be imputed to the Licata harbour implementation works, which changed the amount of wave energy being dissipated by the beach material and acted as sediment trap, interrupting the longshore sediment transport and increasing the rate of sediment loss.

The stability state is also the most frequent class found within the 4 sectors; some exceptions have been found though. Two different tendencies have been observed within sector n. 2, the easternmost part has gradually moved forward. The headlands of Manfria Tower and a wide and well-preserved dune ridges have been here detected and probably worked as sediment reservoir for the coast. A minimal coastal armouring level and a lower dune fragmentation index has been observed, as such the Site of Community Importance ITA 050011 "Manfria Tower", here established in 1995, has acted as constraining factor to human pressure on this area. Sector n. 3 is the longest one and heterogeneous that has been studied, it is more than 20 km long, from the Gela harbour to the Scoglitti harbour. The highest dune fragmentation index was here found, the dune system found at the Gela town beach has been repeatedly interrupted by manmade works. The

eleven breakwaters here set acted as sediment trap and the dune vegetation line gradually migrated seaward, but it has been damaged by human works and the dune vegetation disappeared or significantly decreased. The F index computed for the 1989 lies mainly in the range of low class, the dune toe seemed continuous, but the dune system is quite straight. Most of the greenhouse cultivation of the Gulf are here set and the plastic-covered structure have been built on the residual dune ridge that gradually retreated and disappeared, as such the dune fragmentation index gradually increased over the next years reaching high level. The highest accretion has been found up-drift the Scoglitti harbour, at the southernmost part of sector n. 3. The port has been repeatedly implemented since the eighties and last work on the northern dike have been finished in 2008. The northern dike has modified the longshore drift, trapping sediments up-drift but causing severe erosion downdrift the harbour. Sector n. 5 is the only one that did not experience any significant environmental changes over time. The dune fragmentation index was null over the time between 1955 and 2012 and any coastal structures has been implemented within this sector. The wide dune system has been under environmental restrictions since 1967 and the Site of Community Importance (ITA 080004 "Punta Braccetto Contrada Cammarana") has been established in 1996 due to its environmental value. The Life Leopoldia project has been here carrying on between 2012 and 2016 to restore the dune habitats, putting in place short length fence, placed perpendicular to the shoreline to increase trapping aeolian sediment rates. The long-term shoreline change analyses showed that any erosion phenomena occurred within this sector and the beach mostly experienced stability state and moderate. Against all odds, the mid-term analysis and the SCE index revealed that the area faced consistently erosion between 1989 and 2018. Although the Scoglitti harbour is set 6 km far from sector n. 5, it could be assumed that the northern dike implementation could negatively affect the shoreline evolution of sector n. 5.

The grain-size and textural analysis depicted unstable beach profile within the areas where the shoreline change analysis showed an erosional trend, thus confirming the data obtained by statistical computation and demonstrating that the negative tendency observed within the Gulf has been probably continuing till present day.

The present Ph.D. work improved the knowledge on the shoreline evolution of the Gulf of Gela and on the environmental status of the coast. The combined methodology allowed to investigate and relate the detected shoreline changes to the main coastal modification. It was useful to consider both mid- and long-

term period and compute more than one statistical index, to better understand and depict the evolution trend. The Weighted Linear Regression rate shows the main shoreline change tendency within the study area, but the data should be integrated and compared with the Shoreline Change index, which is the measure of the total change in shoreline movement without reference to their specific dates and revealed when the trend of shoreline change reversed. This was the case of the westernmost part of sector n. 1 and for the sector n. 5. The dune fragmentation index is a useful tool to assess the human pressure on dune systems, but it would be better improving this analysis considering the entire dune systems distribution and evolution. The submerged beach grain-size and textural parameters as well as the bathymetry can be investigated to improve the study on the evolution of the Gulf of Gela and to describe the equilibrium between the sediment supply and the reworking processes, which involves the interdependence between the emerged and submerged beach.

REFERENCES

Aarninkhof, S.G.J., Caljouw, M., & Stive, M.J.F. (2001). Video-based, Quantitative assessment of intertidal beach variability. In: B.L. Edge (Ed.), Proceedings of 27th International Conference on Coastal Engineering (ICCE 2000), 4, 3291-3304.

Agostino, I., Patané, G., La Delfa, S. (2009). Correlation between the dynamics of the Hyblean Foreland and Etnean volcanism. Journal of Geodynamics, 47, 96–106.

Ainsworth, R.B. (2003). Sequence stratigraphic-based analysis of depositional connectivity using 3-D reservoir modelling techniques. Ph.D. thesis, University of Liverpool, United Kingdom, 310 pp.

Ainsworth, R.B., Flint, S., & Howell, J. (2008). Predicting coastal depositional style: Influence of basin morphology and accommodation to sediment supply ratio within a sequence stratigraphic framework. In: Hampson, G.J,.Steel, R.J, Burgess, P.M., & Dalrymple, R.W., eds., Recent advances in models of shallow-marine stratigraphy: SEPM Special Publication 90, 237–263.

Ainsworth, R.B., Vakarelov, B.K., & Nanson, R.A. (2011). Dynamic spatial and temporal prediction of changes in depositional processes on clastic shorelines: toward improved subsurface uncertainty reduction and management. AAPG bulletin, 95(2), 267-297.

Allan, J.C., Komar, P.D., & Priest, G.R. (2003). Shoreline variability on the high-energy Oregon coast and its usefulness in erosion-hazard assessments. Journal of Coastal Research, SI 38, 83-105.

Allen, J.R.L. (1970). Physical processes of sedimentation. An Introduction. American Elsevier Pub. Co. 248 pp.

Amodio Morelli, L., Bonardi, G., Colonna, V., Dietrich, D., Giunta, G., Ippolito, F., ... & Piccarreta, G. (1976). L'arco calabro-peloritano nell'orogene appenninico-maghrebide. Memorie della Società Geologica Italiana, 17, 1-60.

Amore, C., & Randazzo, G. (1997). First data on the coastal dynamics and the sedimentary characteristics of the area influenced by the River Irminio basin (SE Sicily). Catena, 30(4), 357-368.

Amore, C., Geremia, F., & Randazzo, G. (2002). Historical evolution of the Salso River mouth with respect to the Licata harbour system (Southern Sicily, Italy). In: Littoral 2002, The Changing Coast. EUROCOAST / EUCC, Porto – Portugal, 253-260.

Anders, F.J., & Byrnes, M.R. (1991). Accuracy of shoreline change rates as determined from maps and aerial photographs. Shore and Beach, 59(1), 17-26.

Anfuso, G. (1999). Il litorale ragusano compreso tra Cava d'Aliga e la foce del fiume Dirillo. Bollettino Accademia Gioenia Scienze Naturali, 31(355), 287-301.

Anfuso, G., & Martínez del Pozo, J.Á. (2005). Towards management of coastal erosion problems and human structure impacts using GIS tools: case study in Ragusa Province, Southern Sicily, Italy. Environmental Geology, 48(4), 646-659.

Anfuso, G., Martínez del Pozo, J.Á., & Rangel-Buitrago, N. (2012). Bad practice in erosion management: The southern Sicily case study. In: J.A.G. Cooper and O.H. Pilkey (eds.), Pitfalls of Shoreline Stabilization: Selected Case Studies, Coastal Research Library, 3, 215-233.

Argnani, A.J. (1989). The Gela nappe: evidence of accretionary mélange in the Maghrebian foredeep of Sicily. Memorie della Società Geologica Italiana, 38, 419–428.

Aybulatov, N. A., & Artyukhin, Y. V. (1993). Geo-ecology of the World Ocean's Shelf and Coasts. Hydrometeo Publishing, Leningrad, 304 pp.

Badalamenti, F., Chemello, R., Gristina, M., Piraino, S., Riggio, S., & Toccaceli, M. (1988). Notes on the biocoenoses of a polluted coastal area in southern Sicily: the gulf of Gela. Rapp. Comm. Int. Mer Medit., 32 pp.

Bartlett, D., Devoy, R., McCall, S., & O'Connor, I. (1997). A dynamically segmented linear data model of the coast. Marine Geodesy, 20, 137-151.

Bartolo, G., Brullo, S., & Marcenò, C. (1982). La vegetazione costiera della Sicilia sud-orientale: contributo alla interpretazione delle fasce di vegetazione delle coste mediterranee. In: Quaderni C.N.R., P.F. Promozione Qualità dell'Ambiente. Serie AQ/1/226, 49 pp.

Battjes, J.A. (1974). Computation of set-up, longshore currents, run-up and overtopping due to wind-generated waves. Delft Univ. of Tech., Report n. 74–2, 466-480.

Bella, S., Russo, P., & Parenzan, P. (1996). Contributi alla conoscenza della lepidotterofauna siciliana. III. Bombici e Sfingi. - Phytophaga, 6, 85-109.

Bella, S., Duchi, A., Galletti, I., & Turrisi, G.F. (2001). Contributo alla conoscenza della fauna di Cava Randello. Quad. Biol. Amb. Appl, 12, 109-116.

Bellomo, D., Pajak, M.J., & Sparks, J. (1999). Coastal flood hazards and the national flood insurance program. Journal of Coastal Research, 28, 21-26.

Bellon, H., Coulon, C., & Edel, J. (1977). Le deplacement de la Sardaigne: Synthese de domées, geochronologiques, magmatiques et paleomagnetiques, Bull. Soc. Geol. Fr., 19(7), 825-831.

Benassai, G. (2006). Introduction to coastal dynamics and shoreline protection. WIT Press, Southampton, UK, 331 pp.

Ben-Avraham, Z., & Grasso, M. (1991). Crustal structure variations and transcurrent faulting at the eastern and western margins of the eastern Mediterranean. Tectonophysics, 196, 269-277.

Beneo, E. (1958). Sull'olistostroma quaternario di Gela (Sicilia meridionale). Bollettino Servizio Geologico d'Italia, 79, 5-15.

Besse, J., Pozzi, J.P., Mascle, G., & Feinberg, H. (1984). Paleomagnetic study of Sicily: consequences for the deformation of Italian and African margins over the last 100 million years. Earth and Planetary Science Letters, 67(3), 377-390.

Bianchi, F., Carbone, S., Grasso, M., Invernizi, G., Lentini, F., Longaretti, G., Merlini, S. & Mostardini, F. (1989). Sicilia orientale: profilo geologico Nebrodi – Iblei. Memorie della Società Geologica Italiana, 38, 429-458.

Bird, E.C.F. (1993). Submerging coasts: the effects of a rising sea level on coastal environments. Wiley & Sons (NY), 184 pp.

Boak, E.H., & Turner, I.L. (2005). Shoreline definition and detection: a review. Journal of coastal research, 21(21), 688-703.

Bonardi, G., Giunta, G., Perrone, V., Russo, M., & Zuppetta, A.C.G. (1980). Osservazioni sull'evoluzione miocenica dell'Arco Calabro-Peloritano nel Miocene Inferiore: la Formazione di Stilo-Capo d'Orlando. Bollettino della Società Geologica Italiana, 99, 365-393.

Brambati A., Amore C., Giuffrida E. & Randazzo G. (1992). Relationship between the port structures and coastal dynamics in the Gulf of Gela (Sicily-Italy). In: Proceedings of the International Coastal Congress ICC - Kiel 1992, 773-793.

Brown, D.G., & Arbogast, A.F. (1999). Digital photogrammetric change analysis as applied to active coastal dunes in Michigan. Photogrammetric Engineering and Remote Sensing, 65, 467-474.

Brullo, S., Minissale, P., & Spampinato, G. (1995). Considerazioni fitogeografiche sulla flora della Sicilia. Ecologia mediterranea, 21(1), 99-117.

Bruno, S. (1970). Anfibi e rettili di Sicilia. Atti Accademia Gioenia Scienze Naturali, 7(2), 185-326.

Burrollet, P.F., Mugniot, G.M., & Sweeney, P. (1978). The geology of the Pelagian Block: the margins and basins of Southern Tunisia and Tripolitania. In: Narin, A., Kanes, W., & Stelhi, F.G. (eds). The Ocean basins and Margins, Plenum Press (NY), 331-339.

Byrnes, M.R., Gingerich, K.J., Kimball, SM., & Thomas, G.R. (1989). Temporal and spatial variations in shoreline migration rates, Metompkin Island, Virginia. In: Lang, P. (ed.), Proceedings of Coastal Zone '89 (ASCE), 78-92.

Byrnes, M.R., McBride, R.A., & Hiland, M.W. (1991). Accuracy standards and development of a national shoreline change data base. In: Kraus, N.C. (ed.), Coastal Sediments '91 (ASCE), 1027-1042.

Cadkin, J. (2002). Understanding Dynamic Segmentation. ArcUser Magazine October-December 2002. ESRI Press, Redlands, California, 40-43.

Campo, G., Collura, P., Giudice, E., Puleo, G., Andreotti, A., & Ientile, R. (2001). Osservazioni sulla migrazione primaverile di uccelli acquatici nel Golfo di Gela. Avocetta-Parma, 25(1), 185-185.

Carobene, L. & Brambati, A. (1975). Metodo per l'analisi morfologica quantitativa delle spiagge. Bollettino della Società Geologica Italiana, 94, 479-493.

Carr, A.P. (1962). Cartographie Record and Historical Accuracy. Geography, 47(2), 135-144.

Carr, A.P. (1980). The significance of cartographic sources in determining coastal change. In: Cullingford, R. A.; Davidson, D. A., and Lewin, J. (eds.), Timescales in Geomorphology, 69–78.

Catalão, J., Catita, C., Miranda, J., & Dias, J. (2002). Photogrammetric analysis of the coastal erosion in the Algarve (Portugal)/Analyse photogrammétrique de l'érosion côtiere en Algarve (Portugal). Geomorphologie-relief Processus Environnement - Geomorphologie, 8(2), 119-126.

Catalano, R., & D'Argenio, B. (1978). An essay of palinspastic restoration across western Sicily. Geologica Romana, 17, 145-159.

Catalano, R., Di Stefano, P., & Vitale, F.P. (1995). Structural trends and palaeogeography of the central and western Sicily belt: new insights. Terra Nova, 7(2), 189-199.

Catalano, R., Franchino, A., Merlini, S., & Sulli, A. (2000). Central western Sicily structural setting interpreted from seismic reflection profiles. Memorie della Società Geologica Italiana, 55, 5-16.

Catalano, R., Doglioni, C., & Merlini, S. (2001). On the mesozoic Ionian basin. Geophysical Journal International, 144(1), 49-64.

Catalano, R., Agate, M., Albanese, C., Avellone, G., Basilone, L., Gasparo Morticelli, M., ... & Pierini, S. (2013). Walking along a crustal profile across the Sicily fold and thrust belt. Geological Field Trips, 5.

Chamot-Rooke, N., Rangin, C., & Le Pichon, X., Dotmed working group. (2005). DOTMED - Deep Offshore Tectonics of the Eastern Mediterranean: A Synthesis of Deep Marine Data in the Eastern Mediterranean: the Ionian Basin and Margins, the Calabria Wedge and the Mediterranean Ridge. Mémoire de la Société géologique de France & American Association of 18 Petroleum Geologists, Special number, 177, 64 pp.

Channell, J.E.T., D'Argenio, B., & Horvath, F. (1979). Adria, the African promontory, in Mesozoic Mediterranean palaeogeography. Earth-Science Reviews, 15(3), 213-292.

Charlier, R.H., Chaineux, M.C.P., & Morcos, S. (2005). Panorama of the history of coastal protection. Journal of Coastal Research, 21(1), 79-111.

Chrzastowski, M.J. (2004). History of the uniquely designed groins along the Chicago lakeshore. Journal of Coastal Research, SI 33, 19-38.

Cifelli, F., Mattei, M., & Rossetti, F. (2007). Tectonic evolution of arcuate mountain belts on top of a retreating subduction slab: The example of the Calabrian Arc. Journal of Geophysical Research: Solid Earth, 112(B9), 1-20.

Clow, J.B., & Leatherman, S.P. (1984). Metric mapping: An automated technique of shoreline mapping. In: Proceedings of the 44th American Congress on Surveying and Mapping. Falls Church, Virginia: American Society of Photogrammetry, 309-318.

Coastal Engineering Research Center (1984). Shore Protection Manual. US Army Corps of Engineers, Washington, DC.

Coastal Engineering Research Center (1995). Coastal Engineering Manual (CEM). US Army Corps of Engineers, Washington, DC.

Coastal Engineering Research Center (2001). Coastal Engineering Manual (CEM). Chapter V-3: Shore Protection Projects. US Army Corps of Engineers, Washington, DC.

Cogan, J., Rigo, L., Grasso, M., & Lerche, I. (1989). Flexural tectonics of south-eastern Sicily. Journal of Geodynamics, 11(3), 189-204.

Coyne, M.A., Fletcher, C.H., & Richmond, B.M. (1999). Mapping coastal erosion hazard areas in Hawaii: Observations and errors. Journal of Coastal Research, 28(28), 171-184.

Cracknell, A.P. (1999). Remote sensing techniques in estuaries and coastal zones an update. International Journal of Remote Sensing, 20(3), 485-496.

Crossland, C.J., Kremer, H.H., Lindeboom, H., Crossland, J.I.M., & Le Tissier, M.D. (2005). Coastal fluxes in the Anthropocene: the land-ocean interactions in the coastal zone project of the International Geosphere-Biosphere Programme. Series: Global Change - The IGBP Series, 232 pp.

Crowell, M., Leatherman, S.P., & Buckley, M.K. (1991). Historical shoreline change: error analysis and mapping accuracy. Journal of coastal research, 7(3), 839-852.

Crowell, M., Leatherman, S.P., & Buckley, M.K. (1993). Shoreline change rate analysis: long term versus short term data. Shore and Beach, 61(2), 13-20.

Crowell, M., Douglas, B.C., & Leatherman, S.P. (1997). On forecasting future US shoreline positions: a test of algorithms. Journal of Coastal Research, 13, 1245-1255.

Crowell, M., Honeycutt, M., & Hatheway, D. (1999). Coastal erosion hazards study: phase one mapping. Journal of Coastal Research, SI 28, 10-20.

Dabrio, C.J. (1990). Fan-delta facies associations in late Neogene and Quaternary basins of southeastern Spain. In: Coarse-grained deltas. Spec. Publ. Int. Ass. Sediment, 10, 91-112.

Dal Cin, R. (1969). Distinzione tra spiagge in erosione ed in avanzamento mediante metodo granulometrico. Edizione Scientifiche Italiane, 4, 227-233.

Dally, W.R., & Dean, R.G. (1984). Suspended sediment transport and beach profile evolution. Journal of waterway, port, coastal, and ocean engineering, 110(1), 15-33.

Davies, J.L. (1964). A morphogenic approach to world shorelines. Zeitschrift fur Geomorphologie, 8, 127-142.

Dean, R.G., & Malakar, S. B. (1999). Projected flood hazard zones in Florida. Journal of Coastal Research, SI 28, 85-94.

DeCelles, P.G., & Giles, K.A. (1996). Foreland basin systems. Basin research, 8(2), 105-123.

Del Rio, L., & Gracia, F.J. (2013). Error determination in the photogrammetric assessment of shoreline changes. Natural hazards, 65(3), 2385-2397.

Dercourt, J., Zonenshain, L.P., Ricou, L.E., Kazmin, V.G., Le Pichon, X., Knipper, A.L., ... & Pechersky, D.H. (1986). Geological evolution of the Tethys belt from the Atlantic to the Pamirs since the Lias. Tectonophysics, 123(1-4), 241-315.

Dewey, J.F. (1988). Extensional collapse of orogens. Tectonics, 7(6), 1123-1139.

Di Geronimo, I., Ghisetti, F., Lentini, F., & Vezzani, L. (1978). Lineamenti neotettonici della Sicilia orientale. Mem. Soc. Geol. It., 19, 543-549.

Di Stefano, A., De Pietro, R., Monaco, C., & Zanini, A. (2013). Anthropogenic influence on coastal evolution: A case history from the Catania Gulf shoreline (eastern Sicily, Italy). Ocean & coastal management, 80, 133-148.

Distefano, S., Gamberi, F., & Di Stefano, A. (2019). Stratigraphic and structural reconstruction of an offshore sector of the Hyblean Foreland ramp (southern Italy). Italian Journal of Geosciences. 138. 1-14.

European Parliament. (2007). Directive, I. N. S. P. I. R. E (2007/2/EC): Infrastructure for Spatial Information in the European Community (INSPIRE). Published in the official Journal on the 25th April.

Dolan, R., Hayden, B., & Heywood, J. (1978). A new photogrammetric method for determining shoreline erosion. Coastal Engineering, 2, 21-39.

Dolan, R., Hayden, B.P., May, P., & May, S. (1980). The reliability of shoreline change measurements from aerial photographs. Shore and beach, 48(4), 22-29.

Dolan, R., Fenster, M.S., & Holme, S.J. (1991). Temporal analysis of shoreline recession and accretion. Journal of coastal research, 7(3), 723-744.

Douglas, B.C., Crowell, M., & Leatherman, S.P. (1998). Considerations for shoreline position prediction. Journal of Coastal Research, 14(3), 1025-1033.

Douglas, B.C., & Crowell, M. (2000). Long-term shoreline position prediction and error propagation. Journal of Coastal Research, 16(1), 145-152.

Duée, G. (1969). Etude géologique des Monts Nebrodi. Thése Fac. Sc., Paris, 424 pp.

Dugan, J., Airoldi, L., Chapman, M., Walker, S., Schlacher, T., Wolanski, E., McLusky, D. (2011). Estuarine and coastal structures: Environmental effects, a focus on shore and nearshore structures. In Treatise on Estuarine and Coastal Science; Wolanski, E., McLusky, D.S., Eds.; Academic Press: Waltham, MA, USA, 2011; Volume 8, pp. 17–41.

Elter, P., Grasso, M., Parotto, M., Vezzani, L. (2003) Structural setting of the Apennine-Maghrebian thrust belt. Episodes, 26(3), 205-211.

Evenden, G.I. (1990). Cartographic projection procedures for the UNIX environment: A user's manual. United States Geological Survey, 64 pp.

Evenden, G.I. (1991). Notes on a method to transform digitized coordinates to geographic coordinates. United States Department of The Interior Geological Survey, Open-file Report, 7 pp.

Fenster, M.S., Dolan, R., & Elder, J.F. (1993). A new method for predicting shoreline positions from historical data. Journal of Coastal Research, 9(1), 147-171.

Fenster, M., & Dolan, R. (1994). Large-scale reversals in shoreline trends along the US mid-Atlantic coast. Geology, 22(6), 543-546.

Fenster, M.S., Dolan, R., & Morton, R.A. (2001). Coastal storms and shoreline change: signal or noise? Journal of Coastal Research, 17(3), 714-720.

Ferrari, M., Balduzzi, I., Bozzano, A., & Artom, C. (2008). Valutazione dello stato erosivo delle spiagge liguri: applicazione di un sistema informativo geografico. In: Atti della 12a Conferenza Nazionale ASITA, L'Aquila (AQ), 21-24.

Finetti, I.R., Lentini, F., Carbone, S., Del Ben, A., Di Stefano, A., Forlin, E., ... & Prizzon, A. (2005a). Geological outline of Sicily and lithospheric tectono-dynamics of its Tyrrhenian margin from new CROP seismic data. CROP Project: deep seismic exploration of the central Mediterranean and Italy. Atlases in Geoscience, 1, 75-155.

Finetti, I.R., Lentini F., Carbone, S., Del Ben, A., Di Stefano, A., Guarnieri, P., Pipan, M., Prizzon, A. (2005b). Crustal tectonostratigraphy and geodynamics of the Southern Apennines from CROP and

other integrating seismic and geological data. In: Finetti, I.R. (ed), CROP Deep Seismic exploration of the Mediterranean Region, Elsevier, 225-261.

Fletcher, C., Rooney, J., Barbee, M., Lim, S.C., & Richmond, B. (2003). Mapping shoreline change using digital orthophotogrammetry on Maui, Hawaii. Journal of Coastal Research, SI 38, 106-124.

Folk, R.L., & Ward, W.C. (1957). Brazos River bar [Texas]; a study in the significance of grain size parameters. Journal of Sedimentary Research, 27(1), 3-26.

Folk, R.L. (1968). Petrology of sedimentary rocks: Hemphill's. Austin, Texas, 1-170.

Foster, E.R., & Savage, R.J. (1989). Methods of historical shoreline analysis. In: Proceedings of Coastal Zone '89, ASCE, 5, 4434-4448.

Foti, E., Musumeci, R.E., Leanza, S., & Cavallaro, L. (2010). Feasibility of an offshore wind farm in the gulf of Gela: Marine and structural issues. Wind Engineering, 34(1), 65-84.

Friedman, G.M. (1961). Distinction between dune, beach, and river sands from their textural characteristics. Journal of Sedimentary Research, 31(4), 514-529.

Galgano, F.A., Douglas, B.C., & Leatherman, S.P. (1998). Trends and variability of shoreline position. Journal of Coastal Research, SI 26, 282-291.

Galgano, F.A., & Douglas, B.C. (2000). Shoreline position prediction: methods and errors. Environmental Geosciences, 7(1), 23-31.

Garcia, T., Ferreira, Ó., Matias, A., & Dias, J.A. (2010). Overwash vulnerability assessment based on long-term washover evolution. Natural hazards, 54(2), 225-244.

Gasparini, G.P., Smeed, D.A., Alderson, S., Sparnocchia, S., Vetrano, A., & Mazzola, S. (2004). Tidal and subtidal currents in the Strait of Sicily. Journal of Geophysical Research (Oceans), 109(C2), 1-19.

Genz, A.S., Fletcher, C.H., Dunn, R.A., Frazer, L.N., & Rooney, J.J. (2007). The predictive accuracy of shoreline change rate methods and alongshore beach variation on Maui, Hawaii. Journal of Coastal Research, 23(1), 87-105.

Ghielmi, M., Amore, M.R., Bolla, E.M., Carubelli, P., Knezaurek, G., & Serraino, C. (2012). The Pliocene to Pleistocene succession of the Hyblean foredeep (Sicily, Italy). In AAPG Internat. Conf. Exhib. Milan, Italy, October, 23-26.

Giunta, G., Bellomo, D., Carnemolla, S., Pisano, A., Profeta, R., & Runfola, P. (1989). La "Linea di Taormina": residuo epidermico di una paleostruttura crostale del fronte cinematico maghrebide. In: Atti dell'8° Convegno G.N.G.T.S., Esagrafica (Roma), 1197-1213.

Giusso Del Galdo, G., & Sciandrello, S. (2003). Contributo alla flora dei dintorni di Gela (Sicilia meridionale). In: 98o Congresso della Società Botanica Italiana, riassunti, 235.

Goldsmith, V. & Oertel, G. (1978). Beach profiling. In: Tanner, W.F. (ed.), Standards for Measuring Shoreline Changes: Proceedings of a Workshop. Tallahassee, Florida: Geology Department, Florida State University, 37–41.

Gorman, L., Morang, A., & Larson, R. (1998). Monitoring the coastal environment; part IV: mapping, shoreline changes, and bathymetric analysis. Journal of Coastal Research, 14(1), 61-92.

Grasso, M. (2001). The Apenninic-Maghrebian orogen in southern Italy, Sicily and adjacent areas. In: Vai, G.B, & Martini, I.P. (eds), Anatomy of an Orogen: The Apennines and Adjacent Mediterranean Basins, Springer (Netherlands), 343, 255-286.

Grasso, M., & La Manna, F. (1993). Lineamenti stratigrafici e strutturali del fronte della falda di Gela affiorante a NW del Plateau Ibleo (Sicilia Sud-Orientale). Geologica Romana, 29, 55-72.

Graybill, F.A., & Iyer, H.K. (1994). MINITAB Laboratory Manual to Accompany Regression Analysis: Concepts and Applications. Brooks/Cole Pub Co, 1732 pp.

Griggs, G.B. (2005). The impacts of coastal armoring. Shore and beach, 73(1), 13-22.

Hansen, J.B., & Svendsen, I.A. (1984). A theoretical and experimental study of undertow. Coastal Engineering Proceedings, 1(19), 2246-2262.

Hanson, H., Gravens, M.B., & Kraus, N.C. (1989). Prototype applications of a generalized shoreline change numerical model. In: 21st International Conference on Coastal Engineering 1988, 1265-1279.

Hapke, C., & Richmond, B. (2000). Monitoring beach morphology changes using small-format aerial photography and digital softcopy photogrammetry. Environmental Geosciences, 7(1), 32-37.

Hayes, M.O. (1979). Barrier Island Morphology as a Function of Tidal and Wave Regime. In: Leatherman, S.P. (ed.), Barrier Island from the Gulf of St. Lawrence to the Gulf of Mexico, Academic Press, New York, Chapter I, 29 pp.

Heward, A.P. (1981). A review of wave-dominated clastic shoreline deposits. Earth-Science Reviews, 17(3), 223-276.

Hill, K.C., & Hayward, A.B. (1988). Structural constraints on the Tertiary plate tectonic evolution of Italy. Marine and Petroleum Geology, 5(1), 2-16.

Himmelstoss, E.A., Henderson, R.E., Kratzmann, M.G., & Farris, A.S. (2018). Digital Shoreline Analysis System (DSAS) version 5.0 user guide. U.S. Geological Survey Open-File Report 2018–1179, 110 pp.

Holland, KT., Holman, R. A., Lippmann, T.C., Stanley, J., & Plant, N. (1997). Practical use of video imagery in nearshore oceanographic field studies. IEEE Journal of oceanic engineering, 22(1), 81-92.

Holman, R.A., & Sallenger, A.H. (1985). Setup and swash on a natural beach. Journal of Geophysical Research: Oceans, 90(C1), 945-953.

Holman, R.A. (1986). Extreme value statistics for wave run-up on a natural beach. Coastal Engineering, 9(6), 527-544.

Holman, R.A., Sallenger, A.H., Lippmann, T.C., & Haines, J.W. (1993). The application of video image processing to the study of nearshore processes. Oceanography, 6(3), 78-85.

Honeycutt, M.G., Crowell, M., & Douglas, B.C. (2001). Shoreline-position forecasting: impact of storms, rate-calculation methodologies, and temporal scales. Journal of Coastal Research, 17(3), 721-730.

Howard, J.D., & Reineck, H.E. (1981). Depositional facies of high-energy beach-to-offshore sequence: comparison with low-energy sequence. AAPG Bulletin, 65(5), 807-830.

Hsü, K.J., Cita, M.B., & Ryan, W.B.F. (1973). The origin of the Mediterranean evaporites. Initial Report of the Deep Sea Project 13, U.S. Government Printing Office, Washington D.C., 1203–1231.

Hsü, K.J., Montadert, L., Bernoulli, D., Cita, M.B., Erickson, A., Garrison, R.E., Kidd, R.B., Melieres, F., Müller, C., & Wright, R.C. (1977). History of the Mediterranean salinity crisis. Nature, 267, 399–403.

Hughes, M.L., McDowell, P.F., & Marcus, W.A. (2006). Accuracy assessment of georectified aerial photographs: implications for measuring lateral channel movement in a GIS. Geomorphology, 74(1), 1-16.

Hughes, M. (2016). Coastal waves, water levels, beach dynamics and climate change. Coast Adapt, National Climate Change Adaptation Research Facility, Gold Coast, 21 pp.

Hunt, I.A. (1959). Design of sea-walls and breakwaters. Transactions of the American Society of Civil Engineers, 126(4), 542-570.

Ilardi, V., Spadaro, V., & Angelini, A. (2000). Biodiversità vegetale e livelli di naturalità in un'area sensibile della costa meridionale della Sicilia sottoposta ad elevato impatto ambientale. Quad. Bot. ambientale appl, 9(1998), 175-206.

Inman, D.L. (1952). Measures for describing the size distribution of sediments. Journal of Sedimentary Research, 22(3), 125-145.

Kamphuis, J.W. (2010). Introduction to coastal engineering and management: 2nd edition. Advanced Series on Ocean Engineering, 30, 1-562.

Keller, J.B. (1961). Tsunamis: water waves produced by earthquakes. In: Proceedings of the Conference on Tsunami Hydrodynamics, 24, 154-166 pp.

Kinsman, B. (1965). Wind Waves. Their Generation and Propagation on the Ocean Surface. Englewood Cliffs, NJ: Prentice-Hall, 23 pp.

Kleinbaum, D.G., Kupper, L. L., Muller, K. E., & Nizam, A. (1988). Applied regression analysis and other multivariable methods. Belmont, CA: Duxbury Press, 601, 188-208.

Knowles, S.C., & Gorman, L.T. (1991). Historical coastal morphodynamics at St. Marys entrance and vicinity, Florida, USA. In: Proceedings of Coastal Sediments, ASCE, 1447-1461.

Komar, P.D. (1976). The transport of cohesionless sediments on continental shelves. In: Stanley, D.J., & Swift, D.J.P. (eds), Marine Sediment Transport and Environmental Management, 107–125.

Komar, P.D. (1983). Beach Processes and Erosion — an Introduction. CRC handbook of Coastal Processes and Erosion. CRC Series in Marine Science, CRC Press, 48 pp.

Komar, P.D. (1998). Beach Processes and Sedimentation, Second Edition, Upper Saddle River, New Jersey: Prentice Hall, 544 pp.

Kvale, E.P. (2006). The origin of neap–spring tidal cycles. Marine geology, 235(1), 5-18.

Lanza, S., & Randazzo, G. (2011). Improvements to a Coastal Management Plan in Sicily (Italy) New Approaches to borrow sediment management. Journal of Coastal Research, SI 64, 1357-1361.

Leatherman, S.P. (1983). Historical and projected shoreline mapping. In: Coastal Zone '83: Proceedings of the Symposium on Coastal and Ocean Management, ASCE, 2902-2910.

Leatherman, S.P. (2001). Social and economic costs of sea level rise. International Geophysics, 75, 181-223.

Lehmbeck, D.R., & Urbach, J.C. (2004). Image quality for scanning. In: Marshall, G.F. (ed.) Handbook of optical and laser scanning. Taylor and Francis (NY), 154–300.

Lentini, F., Grasso, M., & Carbone, S. (1987). Introduzione alla geologia della Sicilia e Guida all'escursione. Società Geologica Italiana, Convegno "Giornate in memoria di Leo Ogniben", Naxos, 6-8 Giugno 1991, 60 pp.

Lentini, F., Carbone,, S., Catala,no S., Grasso M., Monaco, C. (1990) Principali elementi strutturali del Thrust belt Appenninico-Maghrebide in Sicilia centro-orientale. Mem Soc. Geol. It., 45, 295-502.

Lentini, F., Carbone, S., Catalano, S., (1994) Main structural domain of the central Mediterranean region and their tectonic evolution. Boll. Geofis. Teor. Appl., 36, 103-125.

Lentini, F., Catalano, S., & Carbone, S. (1996). Discussion on: The external thrust system in southern Italy; a target for petroleum exploration. Petroleum Geoscience, 3(3), 285.

Lentini, F., & Carbone, S. (2014). Geologia della Sicilia, con i contributi di Branca S. (vulcanico) e Messina A. (basamenti cristallini). ISPRA. Memorie descrittive della carta geologica d'Italia, 95, 7-414.

Lickorish, W.H., Grasso, M., Butler, R.W., Argnani, A., & Maniscalco, R. (1999). Structural styles and regional tectonic setting of the "Gela Nappe" and frontal part of the Maghrebian thrust belt in Sicily. Tectonics, 18(4), 655-668.

Longhitano, S.G. (2014). Short-term assessment of retreating vs. advancing microtidal beaches based on the backshore/foreshore length ratio: Examples from the Basilicata Coasts (southern Italy). Open Journal of Marine Science, 5(1), 123.

Maffione, M., Speranza, F., Cascella, A., Longhitano, S.G., & Chiarella, D. (2013). A~ 125 post-early Serravallian counterclockwise rotation of the Gorgoglione Formation (Southern Apennines, Italy): New constraints for the formation of the Calabrian Arc. Tectonophysics, 590, 24-37.

Manzi, V., Lugli, S., Roveri, M., & Schreiber, C.B. (2009). A new facies model for the Upper Gypsum of Sicily (Italy): chronological and palaeoenvironmental constraints for the Messinian salinity crisis in the Mediterranean. Sedimentology, 56(7), 1937-1960.

Martino, C., Curcuruto, E., Di Stefano, A., Monaco, C., & Zanini, A. (2011). Fenomeni erosivi lungo il litorale di Marina di Butera (CL), Sicilia centro-meridionale. Geologi di Sicilia, 3, 4-15.

Mascle, G. (1979). Etude géologique des monts Sicani (Sicile) Riv It. Paleont. Strat., Milano, XVI, 1-430.

Mase, H. (1988). Spectral characteristics of random wave run-up. Coastal Engineering, 12(2), 175-189.

Mason, C.C., & Folk, R.L. (1958). Differentiation of beach, dune, and aeolian flat environments by size analysis, Mustang Island, Texas. Journal of Sedimentary Research, 28(2), 211-226.

Maugeri, G., & Leonardi, S. (1974). Esempio di macchia a Ginepro e Lentisco nella Sicilia meridionale. Arch. Bot. Biogeogr. Ital., 50, 51-59

May, V.J., & Hansom, J.D. (2003). Coastal Geomorphology of Great Britain. Geological Conservation Review Series No. 28, Peterborough. Joint Nature Conservation Committee, 739 pp.

McBeth, F.H. (1956). A method of shoreline delineation. Photogrammetric Engineering, 22(2), 400–405.

McBride, R.A. (1989). Accurate computer mapping of coastal change: Bayou Lafourche shoreline, Louisiana, USA. In: Magoono, T. (ed.), Proceedings of Coastal Zone '89, ASCE, 707-719.

McCave, I.N. (2008). Size sorting during transport and deposition of fine sediments: sortable silt and flow speed. Developments in Sedimentology, 60, 121-142.

Miche, M. (1951). Le pouvoir réfléchissant des ouvrages maritimes exposés à l'action de la houle. Annales de Ponts et Chaussées, 121, 285-319.

Milliman, J.D., & Meade, R.H. (1983). World-wide delivery of river sediment to the oceans. The Journal of Geology, 91(1), 1-21.

Molina, R., Anfuso, G., Manno, G., & Gracia Prieto, F. J. (2019). The Mediterranean coast of andalusia (Spain): Medium-term evolution and impacts of coastal structures. Sustainability, 11(13), 3539, 24 pp.

Molina, R., Manno, G., Lo Re, C., & Anfuso, G. (2020). Dune Systems' Characterization and Evolution in the Andalusia Mediterranean Coast (Spain). Water, 12(8), 2094, 23 pp.

Moore, L.J. (2000). Shoreline mapping techniques. Journal of coastal research, 16(1), 111-124.

Moore, L.J., & Griggs, G.B. (2002). Long-term cliff retreat and erosion hotspots along the central shores of the Monterey Bay National Marine Sanctuary. Marine Geology, 181(1-3), 265-283.

Moore, L.J., Ruggiero, P., & List, J.H. (2006). Comparing mean high water and high water line shorelines: should proxy-datum offsets be incorporated into shoreline change analysis?. Journal of Coastal Research, 22(4), 894-905.

Morton, R.A. (1991). Accurate shoreline mapping: past, present, and future. In: Coastal sediments '91, ASCE, 1, 997-1010.

Morton, R.A., Leach, M.P., Paine, J.G., & Cardoza, M.A. (1993). Monitoring beach changes using GPS surveying techniques. Journal of Coastal Research, 9(3), 702-720.

Morton, R.A., & Speed, F.M. (1998). Evaluation of shorelines and legal boundaries controlled by water levels on sandy beaches. Journal of Coastal Research, 14(4), 1373-1384.

Morton, R.A., & Peterson, R.L. (2003). West-central Florida coastal classification maps, Anclote Key to Venice Inlet. USGS Open File Report 03-227, Version 1.1.

Morton, R.A., Miller, T.L., & Moore, L.J. (2004). National assessment of shoreline change: Part 1 - Historical shoreline changes and associated coastal land loss along the US Gulf of Mexico. USGS Open-File Report 04-1043.

National Research Council (US). Committee on Coastal Erosion Zone Management. (1990). Managing coastal erosion. National Academies Press, 204 pp.

Nicholls, R.J., Wong, P.P., Burkett, V., Codignotto, J., Hay, J., McLean, R., ... & Brown, B. (2007). Coastal systems and low-lying areas. In: Parry, M.L., Canziani, O..F, Palutikof, J..P, Van der Linden, P.J., & Hanson, C.E. (eds), Climate change 2007: impacts, adaptation and vulnerability. Contribution of Working Group II to the fourth assessment report of the Intergovernmental Panel on Climate Change, Cambridge, UK, Cambridge University Press, 2007, 315-356.

Nielsen, P., & Hanslow, D.J. (1991). Wave runup distributions on natural beaches. Journal of Coastal Research, 7(4), 1139-1152.

Nordstrom, K.F. (1977). The use of grain size statistics to distinguish between high-and moderate-energy beach environments. Journal of Sedimentary Research, 47(3), 1287-1294.

Ogniben, L. (1969). Schema introduttivo alla geologia del confine calabro-lucano. Mem. Soc. Geol. It., 8, 453-763.

Oldow, J.S., Channell, J.E.T., Catalano, R., & D'argenio, B. (1990). Contemporaneous thrusting and large-scale rotations in the western Sicilian fold and thrust belt. Tectonics, 9(4), 661-681.

Overton, M.F. & Fisher, J.S. (1996). Shoreline analysis using digital photogrammetry. In: Proceedings of the 25th International Conference on Coastal Engineering (Orlando, Florida), 3750–3761.

Overton, M.F., Grenier, R.R., Judge, E.K., & Fisher, J.S. (1999). Identification and analysis of coastal erosion hazard areas: Dare and Brunswick Counties, North Carolina. Journal of Coastal Research, SI 28, 69-84.

Pajak, M.J., & Leatherman, S. (2002). The high water line as shoreline indicator. Journal of Coastal Research, 18(2), 329-337.

Patacca, E., Scandone, P., Giunta, G., & Liguori, V. (1979). Mesozoic paleotectonic evolution of the Ragusa zone (SE Sicily). Geologica Romana, 18, 331-369.

Pieri, M. (1967). Caratteristiche sedimentologiche del limite Cretacico Terziario nella zona di Monterosso Almo, Monti Iblei, Sicilia sudorientale. Riv. It. Paleont. Strat., 73, 1259-1294.

Pinet, P.R. (2006). Invitation to Oceanography, 4th ed., Jones and Bartlett Publ., Sudbury, Mass, 196 pp.

Polonia, A., Torelli, L., Mussoni, P., Gasperini, L., Artoni, A., & Klaeschen, D. (2011). The Calabrian Arc subduction complex in the Ionian Sea: Regional architecture, active deformation, and seismic hazard. Tectonics, 30(5).

Reading, H.G. (1996). Sedimentary Environments: Processes, Facies and Stratigraphy, Wiley & Sons (NY), 704 pp.

Regione Siciliana – Assessorato per i Beni Culturali ed Ambientali e per la Pubblica Istruzione. (1987). D.A. pubblicato nella Gazzetta Ufficiale della Regione Siciliana del 28 Febbraio 1987, Parte I n. 9.

Regione Siciliana (1967). – D.A. n. 2067 pubblicato nella Gazzetta Ufficiale della Regione Siciliana del 3 giugno 1967. n. 25.

Regione Siciliana - Assessorato Territorio e Ambiente, Dipartimento Territorio e Ambiente, Servizio 4 "Assetto del territorio e difesa del suolo". (2007). Piano Stralcio di Bacino per l'Assetto Idrogeologico (P.A.I.). UNITA' FISIOGRAFICA N° 8 - PUNTA BRACCETTO – PORTO DI LICATA.

Regione Siciliana - Assessorato Territorio e Ambiente, Dipartimento Territorio e Ambiente, Servizio 4 "Assetto del territorio e difesa del suolo". (2008). Piano Stralcio di Bacino per l'Assetto Idrogeologico (P.A.I.). Bacino Idrografico del F. Imera Meridionale (072) Area territoriale tra il Bacino Idrografico del F. Palma e il Bacino Idrografico del F. Imera Meridionale (071).

Regione Siciliana – Ufficio del Commissario di Governo contro il Dissesto Idrogeologico nella Regione Siciliana. (2020). Piano Regionale contro l'Erosione Costiera, versione 1.0, 1527 pp.

Richards, J.A. and Jia, X. (1999). Remote Sensing Digital Image Analysis. An Introduction. Springer (NY), 363 pp.

Robinson, A.R., Sellschopp, J., Warn-Varnas, A., Leslie, W.G., Lozano, C.J., Haley, P.J., ... & Lermusiaux, P.F.J. (1999). The Atlantic Ionian Stream. Journal of Marine Systems, 20(1-4), 129-156.

Romine, B.M., Fletcher, C.H., Frazer, L.N., Genz, A.S., Barbee, M.M., & Lim, S.C. (2009). Historical shoreline change, southeast Oahu, Hawaii; applying polynomial models to calculate shoreline change rates. Journal of Coastal Research, 25(6), 1236-1253.

Romine, B.M., & Fletcher, C.H. (2012). Armoring on eroding coasts leads to beach narrowing and loss on Oahu, Hawaii. In Pitfalls of Shoreline Stabilization. Springer, Dordrecht, 141-164.

Ross, D.A. (1995). Introduction to Oceanography. HarperCollins College Publishers (NY), 236–242.

Roure, F., Howell, D.G., Müller, C., & Moretti, I. (1990). Late Cenozoic subduction complex of Sicily. Journal of Structural Geology, 12(2), 259-266.

Rousseeuw, P.J., & Leroy, A.M. (1987). Robust Regression and Outlier Detection. Wiley & Sons (NY), 329 pp.

Ruggiero, P., Komar, P.D., McDougal, W.G., Marra, J.J., & Beach, R.A. (2001). Wave runup, extreme water levels and the erosion of properties backing beaches. Journal of Coastal Research, 17(2), 407-419.

Sabella, G., & Sparacio, I. (2004). Il ruolo dei parchi siciliani nella conservazione di taxa di insetti di particolare interesse naturalistico (Insecta Coleoptera et Lepidoptera Rhopalocera). Naturalista siciliano, 28(1), 477-508.

Salman, A., Lombardo, S., & Doody, P. (2004). Living with coastal erosion in Europe: Sediment and Space for Sustainability. In: Hydraulic Engineering Reports, Eurosion project. EUCC, 21 pp.

Savage, R.P. (1958). Wave Run-up Roughed and Permeable Slope. Journal of the Waterways and Harbors Division, 84(3), 1-38.

Saville, T. (1956). Wave run-up on shore structures. Journal of the Waterways and Harbors Division, 82(2), 1-14.

Schwarzer, K., Diesing, M., Larson, M., Niedermeyer, R.O., Schumacher, W., & Furmanczyk, K. (2003). Coastline evolution at different time scales–examples from the Pomeranian Bight, southern Baltic Sea. Marine Geology, 194(1-2), 79-101.

Short, A.D. (1982). Cliff erosion. In: Beaches and Coastal Geology. Encyclopedia of Earth Science. Springer, Boston, MA.

Shoshany, M., Golik, A., Degani, A., Lavee, H., & Gvirtzman, G. (1996). New evidence for sand transport direction along the coastline of Israel. Journal of Coastal Research, 12(1), 311-325.

Smith, G.L., & Zarillo, G.A. (1990). Calculating long-term shoreline recession rates using aerial photographic and beach profiling techniques. Journal of Coastal Research, 6(1), 111-120.

Smith, A.W.S., & Jackson, L.A. (1992). The variability in width of the visible beach. Shore and Beach, 60(2), 7-14.

Snyder, J.P. (1987). Map projections: A working manual. U.S. Government Printing Office, USGS Numbered Series, 1395, 385 pp.

Speranza, F., Maniscalco, R., Mattei, M., Di Stefano, A., Butler R.W.H., Funiciello, R. (1999). Timing and magnitude of rotations in the frontal thrust systems of southern Sicily. Tectonics, 18(6), 1178-1197.

Stafford, D.B., & Langfelder, J. (1971). Air photo survey of coastal erosion. Photogrammetric engineering, 37(6), 565-575.

Stancheva, M., & Marinski, J. (2007). Coastal defense activities along the Bulgarian black sea coast– methods for protection or degradation?. In: Coastal Structures 2007 - 5th Coastal Structures International Conference, CST07, 480-489.

Stauble, D. K. (2003). The use of shoreline change mapping in coastal engineering project assessment. Journal of Coastal Research, SI 38, 178-206.

Stive, M.J.F., & Wind, H.G. (1986). Cross-shore mean flow in the surf zone. Coastal Engineering, 10(4), 325-340.

Stockdon, H.F., Sallenger, A.H., List, J H., & Holman, R.A. (2002). Estimation of shoreline position and change using airborne topographic lidar data. Journal of Coastal Research, 18(3), 502-513.

Stockdon, H.F., Holman, R.A., Howd, P.A., & Sallenger, A. H. (2006). Empirical parameterization of setup, swash, and runup. Coastal engineering, 53(7), 573-588.

Summerfield, M.A. (1991). Tectonic geomorphology. Progress in Physical Geography, 15(2), 193-205.

Svendsen, I.A., Schäffer, H.A., & Hansen, J.B. (1987). The interaction between the undertow and the boundary layer flow on a beach. Journal of Geophysical Research (Oceans), 92(C11), 11845-11856.

Thieler, E.R., & Danforth, W.W. (1994). Historical shoreline mapping (II): application of the digital shoreline mapping and analysis systems (DSMS/DSAS) to shoreline change mapping in Puerto Rico. Journal of Coastal Research, 10(3), 600-620.

Thieler, E.R., Rodriguez, R.W., & Carlo, M. (1995). Beach erosion and coastal development at Rincón, Puerto Rico. Shore and Beach, 63(4), 18-28.

Thieler, E.R., Himmelstoss, E.A., Zichichi, J.L., & Miller, T.L. (2005). Handbook: Digital Shoreline Analysis System (DSAS) Version 3.0: an Arcgis extension for calculating shoreline change. United States Geological Survey.

Thieler, E.R.; Himmelstoss, E.A.; Zichichi, J.L., and Ergul, A., (2009). Digital Shoreline Analysis System (DSAS) version 4.0—An ArcGIS Extension for Calculating Shoreline Change. U.S.G.S. Open-File Report 2008-1278.

Thurman, H.V. (1991). Introductory Oceanography. Macmillan, New York, 526 pp.

Trask, P.D. (1950). Applied sedimentation. Wiley & Sons, 70(2), 161 pp.

Turrisi, G.F., & Vaccaro, A. (1998). Contributo alla conoscenza degli Anfibi e dei Rettili di Sicilia. Bollettino Accademia Gioenia Scienze Naturali, 30, 5-88.

Turrisi, G.F., & Vaccaro, A. (2004). Status and conservation of herpetofauna from the Iblean area (south eastern Sicily). Italian Journal of Zoology, 71(S2), 185-189.

Valenti, V. (2010). Shallow structures at the outer Calabrian accretionary wedge (NW Ionian Sea): new insights from recently migrated reflection data. Terra Nova, 22(6), 453-462.

Valenti, V. (2011). New insights from recently migrated CROP multichannel seismic data at the outermost Calabrian arc accretionary wedge (Ionian Sea). Italian Journal of Geosciences, 130(3), 330-342.

Van Rijn, L.C. (2013). Design of hard coastal structures against erosion. Website: www.leovanrijn-sediment.com

Vanderstraete, T., Goosens, R., Ghabour, T.K. (2003) Remote sensing as a tool for bathymetric mapping of coral reefs in the Red Sea (Hurghada—Egypt). BELGEO, 3, 257–267.

Virdis, S.G., Oggiano, G., & Disperati, L. (2012). A geomatics approach to multitemporal shoreline analysis in Western Mediterranean: the case of Platamona-Maritza beach (northwest Sardinia, Italy). Journal of Coastal Research, 28(3), 624-640.

Visser, P.J. (1991). Laboratory measurements of uniform longshore currents. Coastal Engineering, 15(5), 563-593.

Vousdoukas, M.I., Velegrakis, A.F., Dimou, K., Zervakis, V., & Conley, D.C. (2009). Wave run-up observations in microtidal, sediment-starved pocket beaches of the Eastern Mediterranean. Journal of Marine Systems, 78, S37-S47.

Walton, T.L., Aherns, J.P., Truitt, C.L., & Dean, R.G. (1989). Criteria for evaluating coastal flood-protection structures. Coastal Engineering Research Center, Vicksburg Ms. Technical Report Cerc-89-15, 165 pp.

Walton, T.L. (1992). Interim guidance for prediction of wave run-up on beaches. Ocean engineering, 19(2), 199-207.

Weeks, A.R. (1996). Fundamentals of electronic image processing. Bellingham: SPIE Optical Engineering Press, 570 pp.

Wentworth, C.K. (1922). A scale of grade and class terms for clastic sediments. The Journal of Geology, 30(5), 377-392.

Wolf, P.R., & Dewitt, B.A. (2000). Elements of photogrammetry: with applications in GIS. McGraw-Hill (NY).

Wright, L.D., Chappell, J., Thom, B.G., Bradshaw, M.P., & Cowell, P. (1979). Morphodynamics of reflective and dissipative beach and inshore systems: Southeastern Australia. Marine Geology, 32(1-2), 105-140.

Wright, L.D., & Short, A.D. (1984). Morphodynamic variability of surf zones and beaches: a synthesis. Marine geology, 56(1-4), 93-118.

Yu, J., & Slinn, D.N. (2003). Effects of wave-current interaction on rip currents. Journal of Geophysical Research (Oceans), 108(C3), 3088.

Zhang, K., Douglas, B., & Leatherman, S. (2002). Do storms cause long-term beach erosion along the US East Barrier Coast?. The journal of Geology, 110(4), 493-502.

Zviely, D., & Klein, M. (2004). Coastal cliff retreat rates at Beit-Yannay, Israel, in the 20th century. Earth Surface Processes and Landforms, 29(2), 175-184.

APPENDIX 1

Quality Report

⚠ **Important:** Click on the different icons for:

  ⓘ Help to analyze the results in the Quality Report

  ⓘ Additional information about the sections

💡 Click here for additional tips to analyze the Quality Report

Summary ⓘ

Project	Punta_bracetto_Comp
Processed	2019-02-18 18:15:43
Camera Model Name(s)	FC330_3.6_4000x3000 (RGB)(1), FC330_3.6_4000x3000 (RGB)(2), FC330_3.6_4000x3000 (RGB)(3)
Average Ground Sampling Distance (GSD)	4.41 cm / 1.74 in
Area Covered	0.959 km² / 95.8984 ha / 0.37 sq. mi. / 237.0926 acres

Quality Check ⓘ

ⓘ Images	median of 41673 keypoints per image	✓
ⓘ Dataset	674 out of 739 images calibrated (91%), all images enabled	⚠
ⓘ Camera Optimization	4.88% relative difference between initial and optimized internal camera parameters	✓
ⓘ Matching	median of 20870.6 matches per calibrated image	✓
ⓘ Georeferencing	yes, 28 GCPs (28 3D), mean RMS error = 2.399 m	⚠

ⓘ Preview ⓘ
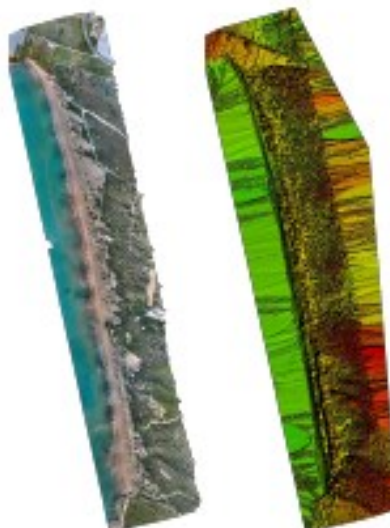
Figure 1: Orthomosaic and the corresponding sparse Digital Surface Model (DSM) before densification.

162

Calibration Details

Number of Calibrated Images	674 out of 739
Number of Geolocated Images	739 out of 739

⑦ Initial Image Positions
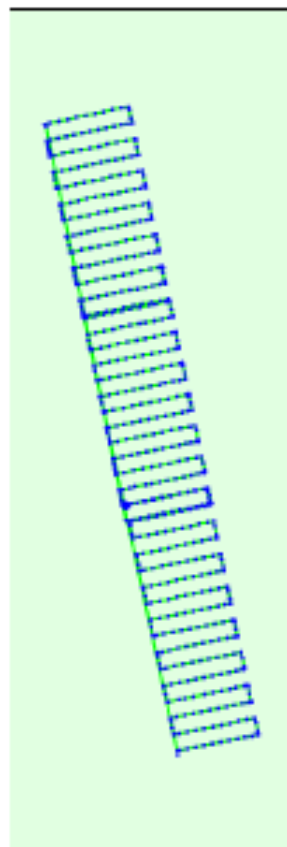
Figure 2: Top view of the initial image position. The green line follows the position of the images in time starting from the large blue dot.

⑦ Computed Image/GCPs/Manual Tie Points Positions
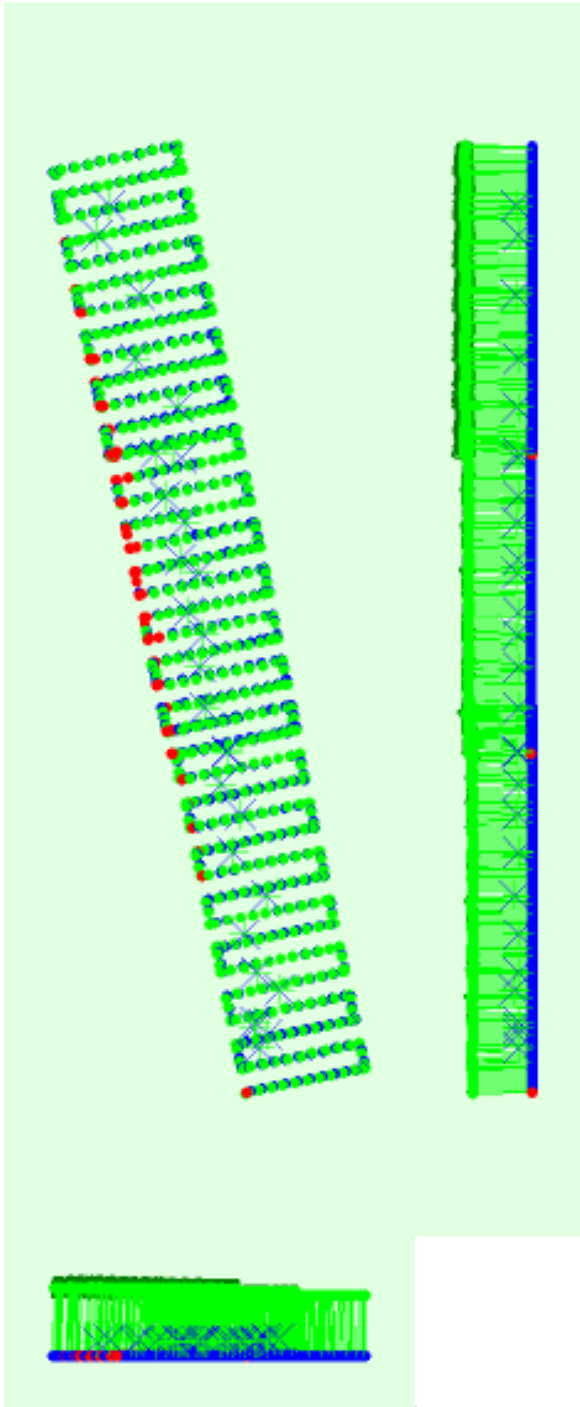
Uncertainty ellipses 100x magnified

Figure 3: Offset between initial (blue dots) and computed (green dots) image positions as well as the offset between the GCPs initial positions (blue crosses) and their computed positions (green crosses) in the top-view (XY plane), front-view (XZ plane), and side-view (YZ plane). Red dots indicate disabled or uncalibrated images. Dark green ellipses indicate the absolute position uncertainty of the bundle block adjustment result.

164

	X[m]	Y[m]	Z[m]	Omega [degree]	Phi [degree]	Kappa [degree]
Mean	0.033	0.026	0.128	0.011	0.016	0.006
Sigma	0.011	0.013	0.049	0.005	0.004	0.004

Overlap

Number of overlapping images: 1 2 3 4 5+
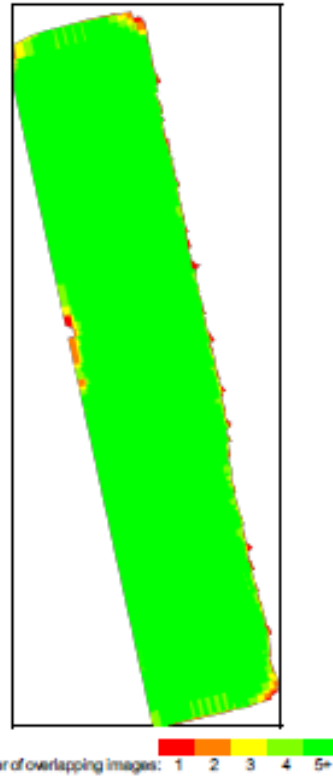
Figure 4: Number of overlapping images computed for each pixel of the orthomosaic.
Red and yellow areas indicate low overlap for which poor results may be generated. Green areas indicate an overlap of over 5 images for every pixel. Good
quality results will be generated as long as the number of keypoint matches is also sufficient for these areas (see Figure 5 for keypoint matches).

Bundle Block Adjustment Details

Number of 2D Keypoint Observations for Bundle Block Adjustment	13259161
Number of 3D Points for Bundle Block Adjustment	4388530
Mean Reprojection Error [pixels]	0.217

Internal Camera Parameters

FC330_3.6_4000x3000 (RGB)(1). Sensor Dimensions: 6.317 [mm] x 4.738 [mm]

EXIF ID: FC330_3.6_4000x3000

	Focal Length	Principal Point x	Principal Point y	R1	R2	R3	T1	T2

	Focal Length	Principal Point x	Principal Point y	R1	R2	R3	T1	T2
Initial Values	2285.722 [pixel] 3.610 [mm]	2000.006 [pixel] 3.159 [mm]	1500.003 [pixel] 2.369 [mm]	-0.001	-0.002	0.000	-0.001	-0.001
Optimized Values	2261.603 [pixel] 3.572 [mm]	2021.646 [pixel] 3.193 [mm]	1449.629 [pixel] 2.290 [mm]	-0.004	0.003	-0.002	-0.001	-0.000
Uncertainties (Sigma)	2.138 [pixel] 0.003 [mm]	0.118 [pixel] 0.000 [mm]	0.103 [pixel] 0.000 [mm]	0.000	0.000	0.000	0.000	0.000

The correlation between camera internal parameters determined by the bundle adjustment. White indicates a full correlation between the parameters, ie. any change in one can be fully compensated by the other. Black indicates that the parameter is completely independent, and is not affected by other parameters.

The number of Automatic Tie Points (ATPs) per pixel, averaged over all images of the camera model, is color coded between black and white. White indicates that, on average, more than 16 ATPs have been extracted at the pixel location. Black indicates that, on average, 0 ATPs have been extracted at the pixel location. Click on the image to the see the average direction and magnitude of the re-projection error for each pixel. Note that the vectors are scaled for better visualization. The scale bar indicates the magnitude of 1 pixel error.
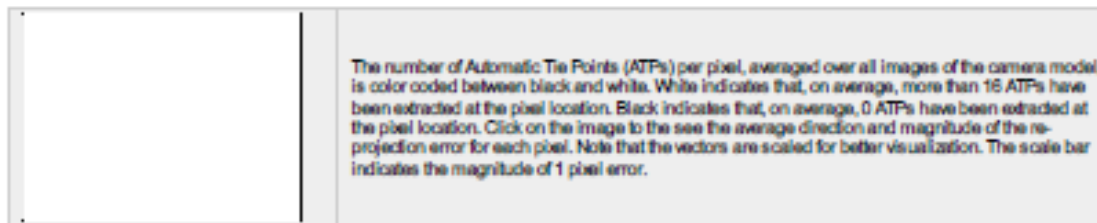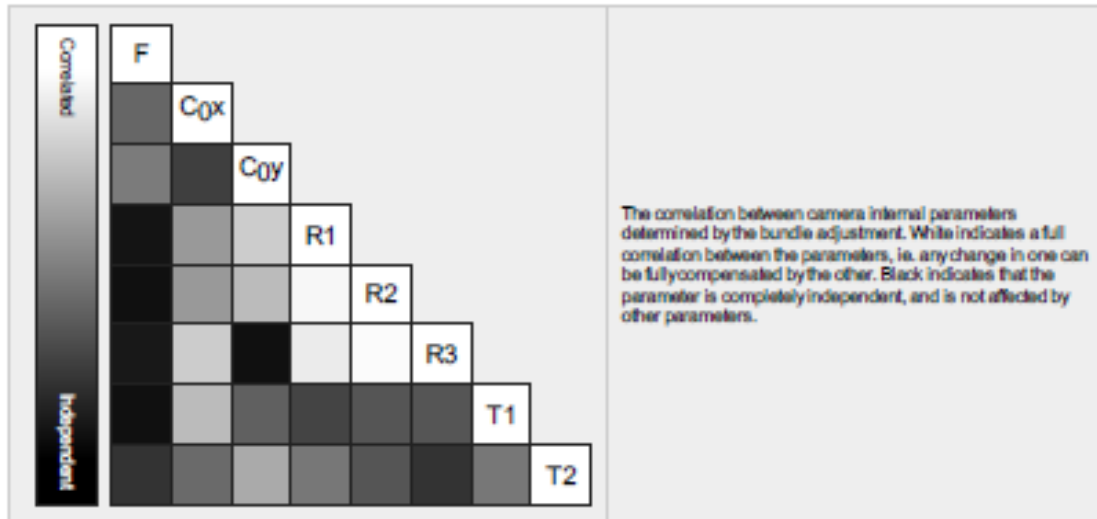
Internal Camera Parameters

FC330_3.6_4000x3000 (RGB)(2). Sensor Dimensions: 6.317 [mm] x 4.738 [mm]

EXIF ID: FC330_3.6_4000x3000

	Focal Length	Principal Point x	Principal Point y	R1	R2	R3	T1	T2
Initial Values	2285.722 [pixel] 3.610 [mm]	2000.006 [pixel] 3.159 [mm]	1500.003 [pixel] 2.369 [mm]	-0.001	-0.002	0.000	-0.001	-0.001
Optimized Values	2402.456 [pixel] 3.794 [mm]	2022.093 [pixel] 3.194 [mm]	1450.412 [pixel] 2.291 [mm]	-0.005	0.003	-0.002	-0.001	-0.000
Uncertainties (Sigma)	2.430 [pixel] 0.004 [mm]	0.166 [pixel] 0.000 [mm]	0.144 [pixel] 0.000 [mm]	0.000	0.000	0.000	0.000	0.000

The correlation between camera internal parameters determined by the bundle adjustment. White indicates a full correlation between the parameters, ie. any change in one can be fully compensated by the other. Black indicates that the parameter is completely independent, and is not affected by other parameters.

The number of Automatic Tie Points (ATPs) per pixel, averaged over all images of the camera model, is color coded between black and white. White indicates that, on average, more than 16 ATPs have been extracted at the pixel location. Black indicates that, on average, 0 ATPs have been extracted at the pixel location. Click on the image to see the average direction and magnitude of the re-projection error for each pixel. Note that the vectors are scaled for better visualization. The scale bar indicates the magnitude of 1 pixel error.
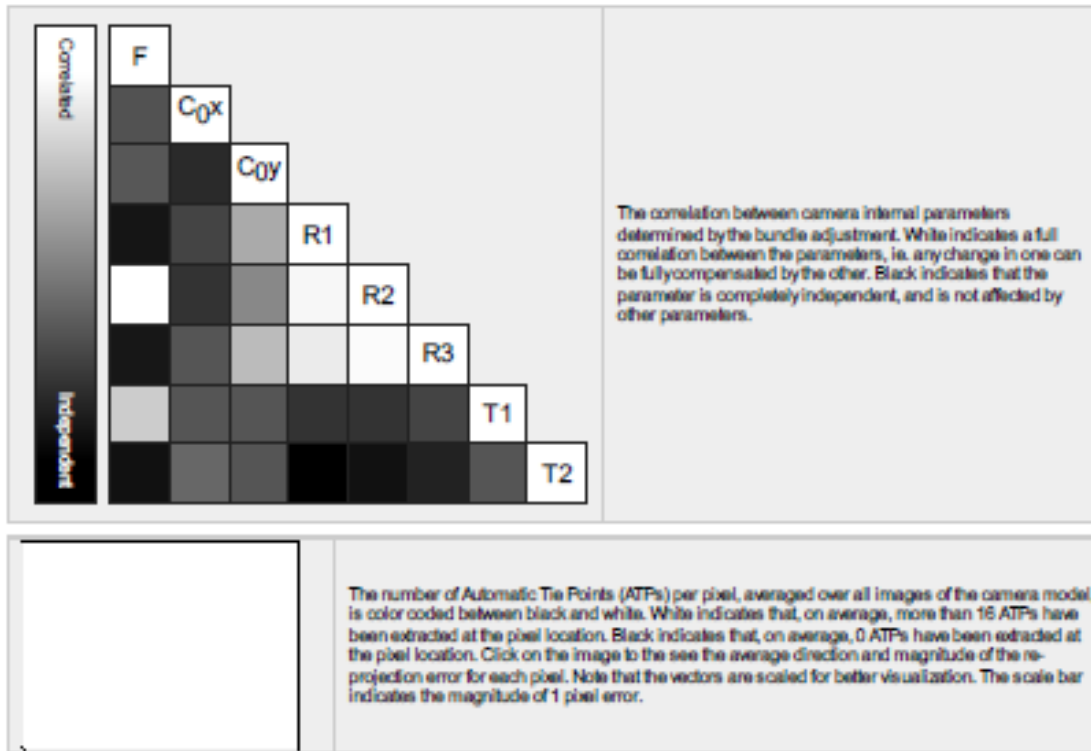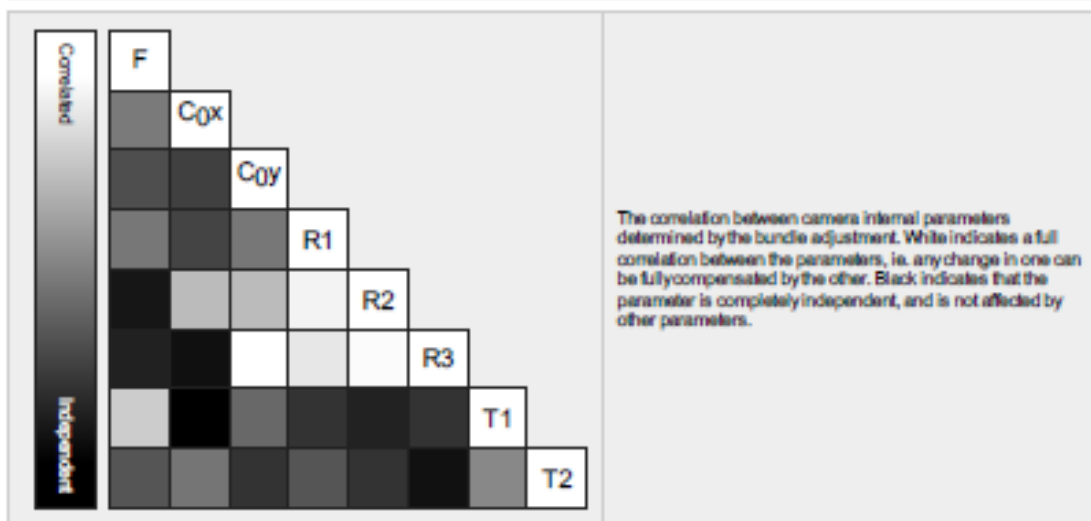
Internal Camera Parameters

FC330_3.6_4000x3000 (RGB)(3). Sensor Dimensions: 6.317 [mm] x 4.738 [mm]

EXIF ID: FC330_3.6_4000x3000

	Focal Length	Principal Point x	Principal Point y	R1	R2	R3	T1	T2
Initial Values	2285.722 [pixel] 3.610 [mm]	2000.006 [pixel] 3.159 [mm]	1500.003 [pixel] 2.369 [mm]	-0.001	-0.002	0.000	-0.001	-0.001
Optimized Values	2480.098 [pixel] 3.917 [mm]	2015.279 [pixel] 3.183 [mm]	1451.471 [pixel] 2.292 [mm]	-0.004	0.004	-0.003	-0.000	-0.000
Uncertainties (Sigma)	4.418 [pixel] 0.007 [mm]	0.207 [pixel] 0.000 [mm]	0.157 [pixel] 0.000 [mm]	0.000	0.000	0.000	0.000	0.000

The correlation between camera internal parameters determined by the bundle adjustment. White indicates a full correlation between the parameters, ie. any change in one can be fully compensated by the other. Black indicates that the parameter is completely independent, and is not affected by other parameters.

The number of Automatic Tie Points (ATPs) per pixel, averaged over all images of the camera model, is color coded between black and white. White indicates that, on average, more than 16 ATPs have been extracted at the pixel location. Black indicates that, on average, 0 ATPs have been extracted at the pixel location. Click on the image to the see the average direction and magnitude of the re-projection error for each pixel. Note that the vectors are scaled for better visualization. The scale bar indicates the magnitude of 1 pixel error.

ⓘ 2D Keypoints Table

	Number of 2D Keypoints per Image	Number of Matched 2D Keypoints per Image
Median	41673	20871
Min	17871	64
Max	68703	48135
Mean	39290	19672

2D Keypoints Table for Camera FC330_3.6_4000x3000 (RGB)(1)

	Number of 2D Keypoints per Image	Number of Matched 2D Keypoints per Image
Median	45867	22910
Min	17871	123
Max	68703	48135
Mean	41888	20591

2D Keypoints Table for Camera FC330_3.6_4000x3000 (RGB)(2)

	Number of 2D Keypoints per Image	Number of Matched 2D Keypoints per Image
Median	42418	22264
Min	18279	64
Max	62505	46235
Mean	39294	20249

2D Keypoints Table for Camera FC330_3.6_4000x3000 (RGB)(3)

	Number of 2D Keypoints per Image	Number of Matched 2D Keypoints per Image
Median	37797	17507
Min	18927	94
Max	67510	44676
Mean	36184	18041

Median / 75% / Maximal Number of Matches Between Camera Models

	FC330_3.6_40...(RGB)(1)	FC330_3.6_40...(RGB)(2)	FC330_3.6_40...(RGB)(3)
FC330_3.6_4000x3000 (RGB)(1)	299 / 1310 / 38051	1 / 1 / 3	
FC330_3.6_4000x3000 (RGB)(2)		366 / 1522 / 35321	1 / 1 / 1
FC330_3.6_4000x3000 (RGB)(3)			225 / 879 / 35204

ⓘ 3D Points from 2D Keypoint Matches

	Number of 3D Points Observed
In 2 Images	2675761
In 3 Images	836990
In 4 Images	372896
In 5 Images	172079
In 6 Images	84229
In 7 Images	55471
In 8 Images	41346
In 9 Images	32823

In 10 images	25243
In 11 images	19864
In 12 images	17140
In 13 images	14714
In 14 images	11415
In 15 images	8370
In 16 images	5013
In 17 images	4122
In 18 images	3510
In 19 images	2615
In 20 images	1706
In 21 images	1039
In 22 images	689
In 23 images	493
In 24 images	330
In 25 images	234
In 26 images	159
In 27 images	92
In 28 images	81
In 29 images	53
In 30 images	40
In 31 images	18
In 32 images	3
In 33 images	1
In 35 images	1

2D Keypoint Matches

Uncertainty ellipses 100x magnified

Number of matches

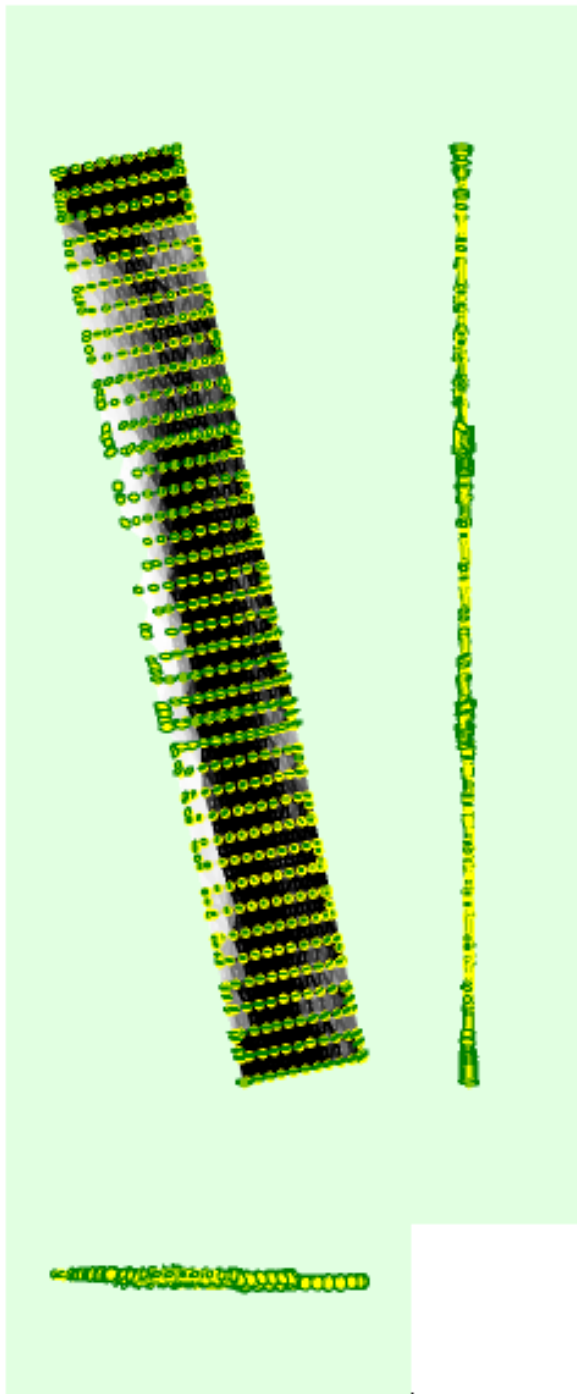25 222 444 666 888 1111 1333 1555 1777 2000

Figure 5: Computed image positions with links between matched images. The darkness of the links indicates the number of matched 2D keypoints between the images. Bright links indicate weak links and require manual tie points or more images. Dark green ellipses indicate the relative camera position uncertainty of the bundle block adjustment result.

	X [m]	Y [m]	Z [m]	Omega [degree]	Phi [degree]	Kappa [degree]
Mean	0.085	0.051	0.102	0.032	0.035	0.017
Sigma	0.031	0.021	0.044	0.012	0.011	0.004

Geolocation Details ⓘ

⑦ Ground Control Points ⓘ

GCP Name	Accuracy XY/Z [m]	Error X [m]	Error Y [m]	Error Z [m]	Projection Error [pixel]	Verified/Marked
101 (3D)	0.020/0.020	-0.060	-0.004	0.027	0.713	19 / 20
114 (3D)	0.020/0.020	0.006	-0.014	0.015	0.683	19 / 19
115 (3D)	0.020/0.020	0.038	0.079	-0.027	0.611	19 / 19
116 (3D)	0.020/0.020	-0.040	-0.048	-0.087	0.597	15 / 15
117 (3D)	0.020/0.020	-0.022	-0.045	0.050	0.492	14 / 14
102 (3D)	0.020/0.020	-0.044	0.086	0.069	0.547	25 / 25
103 (3D)	0.020/0.020	0.145	-0.072	-0.064	1.142	21 / 21
104 (3D)	0.020/0.020	0.032	0.010	-0.099	0.897	21 / 22
105 (3D)	0.020/0.020	-0.062	-0.055	-0.000	1.031	13 / 13
106 (3D)	0.020/0.020	0.010	-0.022	0.002	0.482	21 / 21
107 (3D)	0.020/0.020	0.030	0.011	0.006	0.619	25 / 25
108 (3D)	0.020/0.020	-0.107	0.037	0.033	0.631	12 / 12
109 (3D)	0.020/0.020	0.060	-0.009	-0.029	0.678	20 / 20
110 (3D)	0.020/0.020	0.026	-0.010	-0.172	0.377	14 / 14
111 (3D)	0.020/0.020	0.005	0.003	0.042	0.662	25 / 25
112 (3D)	0.020/0.020	-0.038	0.032	-0.029	0.521	11 / 11
113 (3D)	0.020/0.020	0.012	-0.006	0.045	0.469	10 / 10
118 (3D)	0.020/0.020	-0.051	-0.028	0.065	0.804	18 / 18
119 (3D)	0.020/0.020	0.080	0.024	-0.036	0.655	19 / 19
120 (3D)	0.020/0.020	-0.035	0.022	-0.016	0.658	13 / 13
121 (3D)	0.020/0.020	-0.001	0.007	0.004	0.632	15 / 15
122 (3D)	0.020/0.020	16.786	-19.438	1.112	0.757	13 / 13
123 (3D)	0.020/0.020	-0.110	0.127	1.837	0.369	14 / 14
124 (3D)	0.020/0.020	-0.306	0.016	1.466	0.447	20 / 20
125 (3D)	0.020/0.020	0.023	-0.011	-0.008	0.555	29 / 29
126 (3D)	0.020/0.020	-0.061	-0.025	-0.048	0.901	16 / 16
127 (3D)	0.020/0.020	0.076	0.004	0.048	0.619	23 / 23
128 (3D)	0.020/0.020	-0.071	0.030	-0.085	0.900	14 / 14
Mean [m]		0.582910	-0.689297	0.147173		
Sigma [m]		3.119325	3.608484	0.471869		
RMS Error [m]		3.173322	3.673729	0.494287		

Localisation accuracy per GCP and mean errors in the three coordinate directions. The last column counts the number of calibrated images where the GCP has been automatically verified vs. manually marked.

⑦ Absolute Geolocation Variance ⓘ

Min Error [m]	Max Error [m]	Geolocation Error X [%]	Geolocation Error Y [%]	Geolocation Error Z [%]
-	-15.00	0.00	0.00	0.00
-15.00	-12.00	0.00	0.00	0.15
-12.00	-9.00	0.00	0.00	16.77

-9.00	-6.00	0.89	0.00	15.13
-6.00	-3.00	8.75	4.01	0.15
-3.00	0.00	49.70	46.88	17.06
0.00	3.00	24.63	47.33	12.46
3.00	6.00	10.39	1.63	1.63
6.00	9.00	5.64	0.00	26.56
9.00	12.00	0.00	0.15	10.09
12.00	15.00	0.00	0.00	0.00
15.00	-	0.00	0.00	0.00
Mean [m]		-0.830237	1.466304	-136.806758
Sigma [m]		2.967790	1.665352	7.300561
RMS Error [m]		3.081732	2.218884	137.001413

Min Error and Max Error represent geolocation error intervals between -1.5 and 1.5 times the maximum accuracy of all the images. Columns X, Y, Z show the percentage of images with geolocation errors within the predefined error intervals. The geolocation error is the difference between the initial and computed image positions. Note that the image geolocation errors do not correspond to the accuracy of the observed 3D points.

Geolocation Bias	X	Y	Z
Translation [m]	-0.830237	1.466304	-136.806758

Bias between image initial and computed geolocation given in output coordinate system.

Relative Geolocation Variance

Relative Geolocation Error	Images X [%]	Images Y [%]	Images Z [%]
[-1.00, 1.00]	90.21	99.85	87.24
[-2.00, 2.00]	100.00	99.85	100.00
[-3.00, 3.00]	100.00	100.00	100.00
Mean of Geolocation Accuracy [m]	5.000000	5.000000	10.000000
Sigma of Geolocation Accuracy [m]	0.000000	0.000000	0.000000

Images X, Y, Z represent the percentage of images with a relative geolocation error in X, Y, Z.

Geolocation Orientational Variance	RMS [degree]
Omega	0.892
Phi	0.909
Kappa	4.065

Geolocation RMS error of the orientation angles given by the difference between the initial and computed image orientation angles.

Initial Processing Details

System Information

Hardware	CPU: Intel(R) Core(TM) i7-7700 CPU @ 3.60GHz RAM 32GB GPU: NVIDIA GeForce GTX 1060 6GB (Driver: 23.21.13.8813)
Operating System	Windows 10 Pro, 64-bit

Coordinate Systems

Image Coordinate System	WGS84 (egm2008)
Ground Control Point (GCP) Coordinate System	WGS 84 / UTM zone 33N (egm2008)
Output Coordinate System	WGS 84 / UTM zone 33N (egm2008)

Processing Options

Detected Template	⊖ 3D Maps
Keypoints Image Scale	Full, Image Scale: 1
Advanced: Matching Image Pairs	Aerial Grid or Corridor
Advanced: Matching Strategy	Use Geometrically Verified Matching: no
Advanced: Keypoint Extraction	Targeted Number of Keypoints: Automatic
Advanced: Calibration	Calibration Method: Standard Internal Parameters Optimization: All External Parameters Optimization: All Rematch: Auto, yes

Point Cloud Densification details

Processing Options

Image Scale	multiscale, 1/2 (Half image size, Default)
Point Density	Optimal
Minimum Number of Matches	3
3D Textured Mesh Generation	yes
3D Textured Mesh Settings:	Resolution: Medium Resolution (default) Color Balancing: no
LOD	Generated: no
Advanced: 3D Textured Mesh Settings	Sample Density Divider: 1
Advanced: Image Groups	group1
Advanced: Use Processing Area	yes
Advanced: Use Annotations	yes
Time for Point Cloud Densification	01h:19m:39s
Time for Point Cloud Classification	NA
Time for 3D Textured Mesh Generation	09m:23s

Results

Number of Generated Tiles	3
Number of 3D Densified Points	37613782
Average Density (per m³)	38.99

DSM, Orthomosaic and Index Details

Processing Options

DSM and Orthomosaic Resolution	1 x GSD (4.41 [cm/pixel])
DSM Filters	Noise Filtering: yes Surface Smoothing: yes, Type: Sharp
Raster DSM	Generated: yes Method: Inverse Distance Weighting Merge Tiles: yes
Orthomosaic	Generated: yes Merge Tiles: yes GeoTIFF Without Transparency: no Google Maps Tiles and KML: no
Time for DSM Generation	40m:15s
Time for Orthomosaic Generation	43m:46s
Time for DTM Generation	00s
Time for Contour Lines Generation	00s
Time for Reflectance Map Generation	00s
Time for Index Map Generation	00s